UNCERTAINTY AND STATE ESTIMATION OF POWER SYSTEMS

A Thesis submitted to The University of Manchester for the degree of

Doctor of Philosophy

In the Faculty of Engineering and Physical Sciences

2012

by

Gustavo Adolfo Valverde Mora

School of Electrical and Electronic Engineering

List of Content

Final count: 54 152 words.

List of Figures

List of Tables

Abstract

The University of Manchester
Faculty of Engineering and Physical Sciences

PhD Thesis
Uncertainty and State Estimation of Power Systems

Gustavo A. Valverde Mora
April, 2012.

The evolving complexity of electric power systems with higher levels of uncertainties is a new challenge faced by system operators. Therefore, new methods for power system prediction, monitoring and state estimation are relevant for the efficient exploitation of renewable energy sources and the secure operation of network assets.

In order to estimate all possible operating conditions of power systems, this Thesis proposes the use of Gaussian mixture models to represent non-Gaussian correlated input variables, such as wind power output or aggregated load demands in the probabilistic load flow problem. The formulation, based on multiple Weighted Least Square runs, is also extended to monitor distribution radial networks where the uncertainty of these networks is aggravated by the lack of sufficient real-time measurements.

This research also explores reduction techniques to limit the computational demands of the probabilistic load flow and it assesses the impact of the reductions on the resulting probability density functions of power flows and bus voltages.

The development of synchronised measurement technology to support monitoring of electric power systems in real-time is also studied in this work. The Thesis presents and compares different formulations for incorporating conventional and synchronised measurements in the state estimation problem. As a result of the study, a new hybrid constrained state estimator is proposed. This constrained formulation makes it possible to take advantage of the information from synchronised phasor measurements of branch currents and bus voltages in polar form.

Additionally, the study is extended to assess the advantages of PMU measurements in multi-area state estimators and it explores a new algorithm that minimises the data exchange between local area state estimators.

Finally, this research work also presents the advantages of dynamic state estimators supported by Synchronised Measurement Technology. The dynamic state estimator is compared with the static approach in terms of accuracy and performance during sudden changes of states and the presence of bad data. All formulations presented in this Thesis were validated in different IEEE test systems.

Declaration

No portion of the work referred to in the thesis has been submitted in support of an application for another degree or qualification of this or any other university or other institute of learning.

Copyright Statement

To my wife Rebeca and my parents

Acknowledgements

I want to thank God for giving me the opportunity to complete my studies and for all the blessings I have received so far. I also want to thank my supervisor Prof. Vladimir Terzija for his help during my PhD studies.

Special thanks to the Engineering and Physical Science Research Council (EPSRC) in the UK and the University of Costa Rica (UCR) for their financial support during my PhD studies. I am very pleased to be part of the School of Electrical Engineering in the UCR.

I want to express my gratitude to *Dr. Elias Kyriakides*, *Dr. Saikat Chakrabarti*, *Prof. Gerald Heydt* and *Prof. Andrija Saric* for their helpful comments and guidance during my research work.

Thanks to my friends and family in Costa Rica for their support and all my friends in Manchester for making my life easier and funnier, particularly to Miguel, Ricardo, Manuel, Gary, Deyu, Pawel, Jairo, Angel, Nando and Helge.

Special thanks to my parents *Grettel Mora* and *Humberto Valverde* for their support, love and comprehension. You guys understood that I had a dream that today becomes true… I am sure you are very proud about it.

Finally, I want to express my gratitude to my beloved wife *Rebeca* for being there always next to me. Thanks for your comprehension and support during stressful moments of my studies. I have no way to pay you back. Remember that this is also your PhD Thesis.

Chapter 1 Introduction

The systematic interconnection of power systems that took place in the second half of the twentieth century, as an attempt to strengthen the networks and to facilitate the transmission of electricity, brought new operation challenges that could not be faced by power engineers unless the state of the network was properly monitored in real-time [1].

The blackout of 1965 in the northeast region of the US encouraged power engineers to develop sophisticated tools to collect, transmit and process measurements from all over the network for the supervision and control of the system. This was a step before today's Energy Management Systems (EMS) of modern power networks. These EMS are in charge of the data acquisition, state estimation, load flow analysis, economic dispatch, voltage-frequency control and security assessment of the system, among other sophisticated features.

For many years, these tools were very effective to monitor and control power networks made of conventional generation and uncongested transmission corridors. Today, the panorama has changed:

- There is a need to reduce CO_2 emissions of existing power plants which must be gradually replaced by renewable generation, e.g. wind farms or solar panels.
- This renewable generation is variable, difficult to predict and no longer centralised but distributed.
- The networks follow a deregulated structure to incentivise investment and efficiency in electricity utilisation. Based on this,
- The networks operate closer to their stability limits and transmission corridors are stressed due to the restrictions on the building of new transmission lines.

In order to cope with the challenges faced by intermittent generation, congested transmission corridors and massive exchange of power between areas, it is necessary to improve the current practice to monitor the power networks in real-time and to explore new tools that can be used to analyse the network operation over a range of possible conditions imposed by the uncertainty of intermittent generation and demand.

1.1 Research Background

The following subsections present an introduction of previous work related to the topics covered in this PhD Thesis. Further literature review is presented at the beginning of each Chapter.

1.1.1 Probabilistic Load Flows

The Probabilistic Load Flow (PLF) studies are typically run for network planning purposes and they analyse the performance of the power network over most of its working operation conditions. The studies determine the likelihood of overstressed transmission corridors and unacceptable bus voltage magnitudes and they can assess the impact of intermittent generation in power networks [2].

The PLF takes into account the random nature of generation and demand, represented by probability density functions, to determine the probability density of output variables such as bus voltages and power flows. It was firstly proposed in [3] by *Borkowska* in 1974, and it can be solved either numerically (e.g. Monte Carlo simulations) or analytically by mathematical developments as an alternative to reduce the computational demands of the Monte Carlo simulations [4].

Among the first analytical methods, *Allan et al.* solved the probabilistic load flow by linear approximations of the power flow equations [5]. Here, the probability densities of the power flows were approximated by convolution techniques.

In 1990, *da Silva* and *Arienti* combined the Monte Carlo Simulations and a multi-linearised load flow equations in [6]. In addition, the Weighted Least Square (WLS) method was used in

[7] to solve the PLF problem where all of the input variables were treated as Gaussian random variables.

Recently in 2005, the Point Estimate method was implemented in probabilistic power flows [8]. The method calculates a set of deterministic points to capture the first moments of the input random variables. These points are later evaluated in the power flow problem to obtain the mean and standard deviation of any power system variable.

An extension of the capabilities of the Point Estimate method was later presented in [9]. Normal and Binomial distributions were used to model the input variables. The authors compared four Hong's Point Estimate methods whose differences are the required number of deterministic points. They found that for a large number of input random variables m, the creation of $2m+1$ points provides the best performance i.e. closer to the Monte Carlo simulation results.

During the last few decades, the PLF studies were used to study the variability of aggregated loads modelled by Gaussian distributions. With the increased penetration of intermittent generation, the probabilistic studies have gained more attention due to the need for modelling the intermittent power output as random variables that are typically non-Gaussian distributed [10, 11].

Because of the proliferation of these renewable sources, the representation of these non-Gaussian PDFs is an open field of research. Different approximations have been developed to model non-Gaussian input random variables in power systems. For instance, in order to model the variability of wind power output, an indirect algorithm based on the *Beta* distribution was proposed in [12] and later considered in [10].

The probability distribution of the wind speed is typically non-Gaussian and it has been modelled by the *Gamma*, *Weibull* or the *Rayleigh* distributions [4]. The *Weibull* distribution has demonstrated better results because of its two flexible parameters k and c [13]. Nonetheless, since the wind speed PDF cannot be always approximated as a *Weibull* distribution, a mixed *Gamma-Weibull* distribution and a mixed truncated *Normal* distribution were introduced in [13].

The PDFs of power demands of aggregated loads can be also non-Gaussian distributed. For example, the *Normal*, *log-normal* and *Beta* distributions were used to evaluate their effectiveness to model the load uncertainty [14]. Because of its flexibility to adapt to the skewness of the distribution, the *Beta* distribution was found to be the most appropriate. This distribution was also used in [15] to model the variability of load demand.

Recently, a more accurate approximation of the marginal distribution of any power demand was introduced in [16]. As the PDF of load demands cannot be represented by a specific distribution, the authors proposed the use of the Gaussian mixture distribution. Although the work in [16] concentrates on the probability distribution of power demands, Gaussian mixtures can be used to represent the variability of any other non-Gaussian variable in electric power systems, e.g. renewable energy sources.

The present research work starts from the latter affirmation: it assumes that the marginal distribution of any wind farm power output, wind speed or power demands can be represented by Gaussian mixtures and this will be the input of the PLF analysis.

1.1.2 State Estimation

State Estimation is the process of assigning a value to an unknown system state variable based on measurements collected from the network [17]. The state variables are the bus voltage magnitudes and their phase angles and they are typically estimated by the WLS formulation.

The process involves redundant imperfect measurements that are processed to obtain the best estimate of the system state. The state estimator acts as a filter block between the raw measurements received from all over the network and the EMS applications that require very accurate and reliable information about the actual state of the network [18].

The typical sources of errors that affect the performance of modern state estimators are: topology errors (undetected by the operator); gross errors in measurements and transducers; parameter errors in the data base and the unsynchronised nature of conventional measurements. However, the development of synchronised measurements units has opened new opportunities to better monitor the power networks. The development of new strategies for incorporating these synchronised measurements in current state estimators is one of the main objectives of this Thesis.

1.1.3 Synchronised Measurements

A Phasor Measurement Unit (PMU) is a piece of equipment able to measure phasors of voltage and currents, usually called synchrophasors. They were firstly introduced in the early 1980s and they originally served as disturbance recorders [19].

The PMUs are the base line of wide-area monitoring systems that collect and process synchronised measurements across the network to monitor power oscillations during large disturbances and to monitor power flows and bus voltages during normal steady state conditions [20].

In 2005, the IEEE published the Standard C.37.118-2005 to establish the data exchange requirements in order to facilitate the compatibility of equipment between different vendors [21]. Standard C.37.118-2005 also defines a list of steady state performance requirements including range of signal frequency, phase angle, and harmonic distortion, among others [22]. The performance of PMUs with dynamic measurements was not included in C.37.118-2005 but it will be included in an updated version of C.37.118.

Since the PMUs can measure phasors of bus voltages, the state can be measured directly. This is an advantage that could not be achieved by conventional unsynchronised measurements of power flows. Additionally, as phasors of current can be measured, it is possible to extend the voltage measurements to buses where no PMUs are installed.

To date, the process of introducing PMUs in power systems is costly and it requires more time to see the full benefits of wide area monitoring systems. In the meanwhile, the studies must concentrate on making the most of the information provided by few installed PMUs until the gradual insertion of PMUs will make the system fully observable.

1.1.4 Hybrid State Estimators

The use of synchrophasors improves the capability to monitor the condition of the system in real-time. The inclusion of PMU measurements in existing state estimators increases the redundancy levels for better bad data detection, helps to determine the actual topology of the network and improves the accuracy of the estimation as synchronised measurements are substantially more accurate than conventional measurements [23-26].

If a system becomes fully observable with only PMU measurements, a linear (non-iterative) WLS can be used as direct measurements of voltage and current phasors are available. However, the high cost of installing hundreds of PMUs in large interconnected power systems makes this option unfeasible in the short term. As a consequence, a mixture of existing conventional measurements and synchronised measurements is the most practical and feasible option to gradually incorporate these synchronised measurements in existing estimators.

An example of this transition is the state estimator proposed in [26]. This state estimator consists of a two-step state estimator: a conventional state estimator corrected by a linear state estimator that uses synchronised measurements only. The main advantage of this estimator is that there is no need to replace the existing conventional state estimator.

An alternative hybrid state estimator was later proposed in [27]. Unlike the two-step hybrid estimator, the authors combined both the conventional and synchronised measurements in a non-linear state estimator.

Recent studies also proposed new formulations for including synchrophasors in Multi-Area State Estimators (MASE). It was found that synchrophasors can be used to improve bad data processing around boundary buses [28], and to measure the phase shift between the slack buses of different areas [29, 30].

This Thesis, as extension of the work presented above, explores new methods for combining conventional and synchronised measurements in modern state estimators, and assesses the impact of the dispersed PMU measurements in single-area and multi-area state estimation. It also explores the use of synchrophasors in dynamic state estimation.

1.2 Objectives

- To provide a step forward on probabilistic studies to estimate the operating conditions of electric power systems in the presence of uncertain input variables such as power demand and intermittent generation.

- To improve state estimation practice, enabling it to cope with the uncertainty of the system to achieve a better network monitoring by making use of available technology based on synchronised measurements.

- To propose and explore different formulations for including synchronised phasor measurements in state estimation, including static and dynamic state estimators.

1.3 Thesis Structure

Chapter 1 – Introduction

This is the introduction of the Thesis. This chapter presents a brief explanation of the importance and relevance of this research work. In addition, the Chapter presents the objectives and the contribution of this PhD Thesis.

Chapter 2 – Classical State Estimation in Power Systems

The Chapter presents an overview of power system state estimation theory including the details of the WLS formulation, observability analysis, redundancy analysis and bad data processing. It also introduces the equations of power flows and power injections that are used in the WLS formulation. The theory presented in this Chapter is later implemented in the following Chapters of the Thesis.

Chapter 3 – Estimation of Probabilistic Load Flows: Theory and Modelling

This Chapter extends the Gaussian Component Combination Method (GCCM), originally introduced in [31] as an alternative to Monte Carlo simulations, to estimate probability density functions of power flows and bus voltages in the presence of non-Gaussian correlated random input variables (papers 4 and 5 in Appendix H). Additionally, the use of Gaussian mixture reduction techniques to limit the computational demand of the GCCM is proposed (Paper 9 in Appendix H).

Chapter 4 – Estimation of Probabilistic Load Flows: Simulations

The probabilistic load flow study introduced in Chapter 3 is implemented in three representative test systems. The study includes the impact of the correlation between input variables in power flow studies of transmission networks and state estimation of distribution networks (Papers 4 and 5 in Appendix H).

Chapter 5 – Synchronised Measurements in State Estimation

This Chapter explores different methods to include synchronised measurements in state estimation based on the WLS formulation. The study focuses on how the PMU measurements of currents can be used to improve the accuracy of hybrid state estimators.

Based on the inability to include current measurements in polar form, this study proposes the use of a Hybrid Constrained State Estimator (HCSE) that avoids the propagation of measurement uncertainties because it does not use any transformation of measurements. A comparison with other hybrid state estimators is included in the analysis (Paper 2 in Appendix H).

Chapter 6 – Multi-Area State Estimation

This Chapter deals with the problem of state estimation in multi-area power systems. The study proposes a Multi-Area State Estimator (MASE) based on wide area synchronised measurements to estimate the angle difference between reference buses and to improve the estimation accuracy in boundary buses.

The main objective of the proposed MASE is to reduce the data exchange between local area and the coordination state estimators, and consequently to reduce the number of estimated states of the coordination level. The impact of the proposed simplified MASE is also assessed in terms of accuracy in a 300 bus test system (paper 6 in Appendix H).

Chapter 7 – Dynamic State Estimation

Due to the possibility to process scans of measurements with higher sampling rates, this Chapter explores the use of power system dynamic state estimators supported by synchronised measurements. In addition, this study explores the use of the Unscented Kalman Filter (UKF) as an alternative to the Extended Kalman Filter (EKF) to cope with the non-linearities of the measurement equations used in dynamic state estimators.

Finally, this Chapter compares the performance of dynamic and static estimators under normal conditions, the presence of bad data and sudden changes of states. This study was implemented in two test systems (paper 1 in Appendix H).

Chapter 8 – Conclusions and Future Work

This Chapter summarises the conclusions drawn from the tests executed in Chapters 3 through 7. Furthermore, it discusses the limitations of the presented work and presents new ideas for future work as consequence of this research.

Figure 1.1 presents a diagram with the structure of the PhD Thesis to summarise the organisation of the research work.

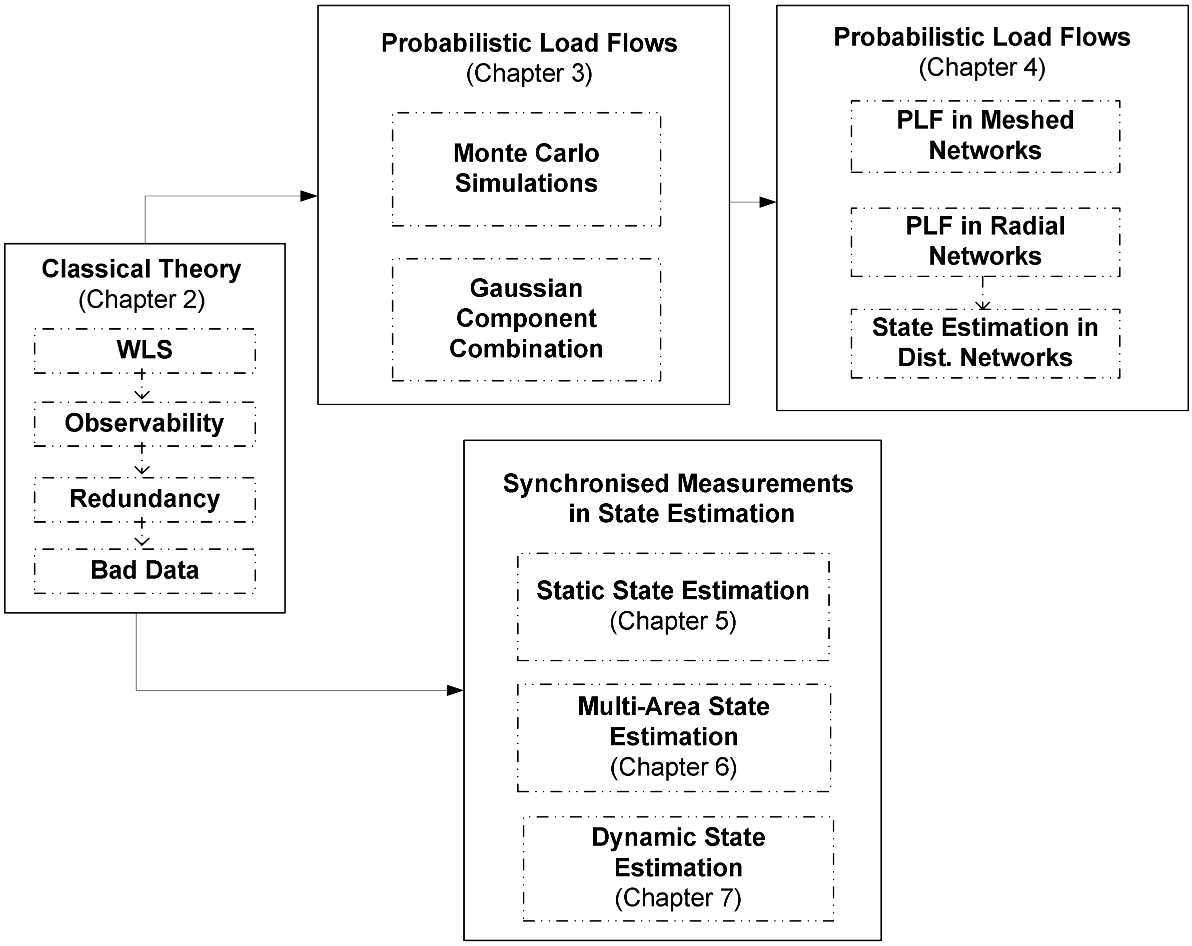

Figure 1.1: PhD Thesis Structure

1.4 Contribution of this Research

In order of appearance, the main contributions of this Thesis are:

- Proposal of a probabilistic load flow to estimate power flows and bus voltages in the presence of non-Gaussian correlated input variables (demand and intermittent generation). The proposed method uses the actual probability density functions as input variables – represented as Gaussian mixtures.

- Development of a methodology to run Monte Carlo simulations with Gaussian mixture models as input variables.
- Simplification of Gaussian mixture models (with fewer components) to reduce the computational demands of the proposed probabilistic load flow (and state estimator).
- Evaluation of the impact of including (or neglecting) the correlation between input variables on the estimated probability densities of voltages and power flows of transmission and distribution networks.
- Proposal of a state estimator for distribution networks that uses few real real-time measurements and pseudo-measurements of power injections expressed by probability densities. This state estimator not only provides the estimated mean values of any variable but also calculates the corresponding density function of voltages, power flows and power injections of poorly monitored areas.
- Assessment of the impact of the reduced models in the calculation of the probability densities in both the probabilistic load flow and the state estimator.
- Proposal of a hybrid constrained state estimator that uses synchronised measurements in polar form. This method avoids the propagation of measurement uncertainties as no transformation of measurements is required.
- Application of the Unscented Transformation to calculate the propagation of measurement uncertainties when synchronised measurements are transformed (from polar to rectangular form or as pseudo-measurements of voltages).
- Proposal of a multi-area state estimator, supported by synchronised measurements, which requires minimum data exchange between the local and coordination estimators.
- Assessment of the impact of not including power injection measurements of boundary buses in two-level multi-area state estimators.
- Implementation of the Unscented Kalman filter in power system dynamic state estimation supported by synchronised measurements.
- Comparison of dynamic versus static state estimators in the presence of bad data and after sudden changes of states.

A list of the publications achieved as a result of the research carried out during this PhD project has been included in Appendix H.

Chapter 2 Classical State Estimation in Power Systems

Power system State Estimation (SE) is one of the most critical on-line applications necessary for efficient Energy Management System (EMS) applications. The solution of a state estimator is used as input for optimal power flow studies and contingency analysis and it is also used for real-time security assessment to determine, and subsequently correct, unacceptable voltage and power flow levels, to determine network losses, to alert network topology changes and to monitor transferred power flows between areas.

The state estimator provides the best estimate of the system states (voltage angles and magnitudes) commonly using the non-linear Weighted Least Square (WLS) technique based on available measurements in the network.

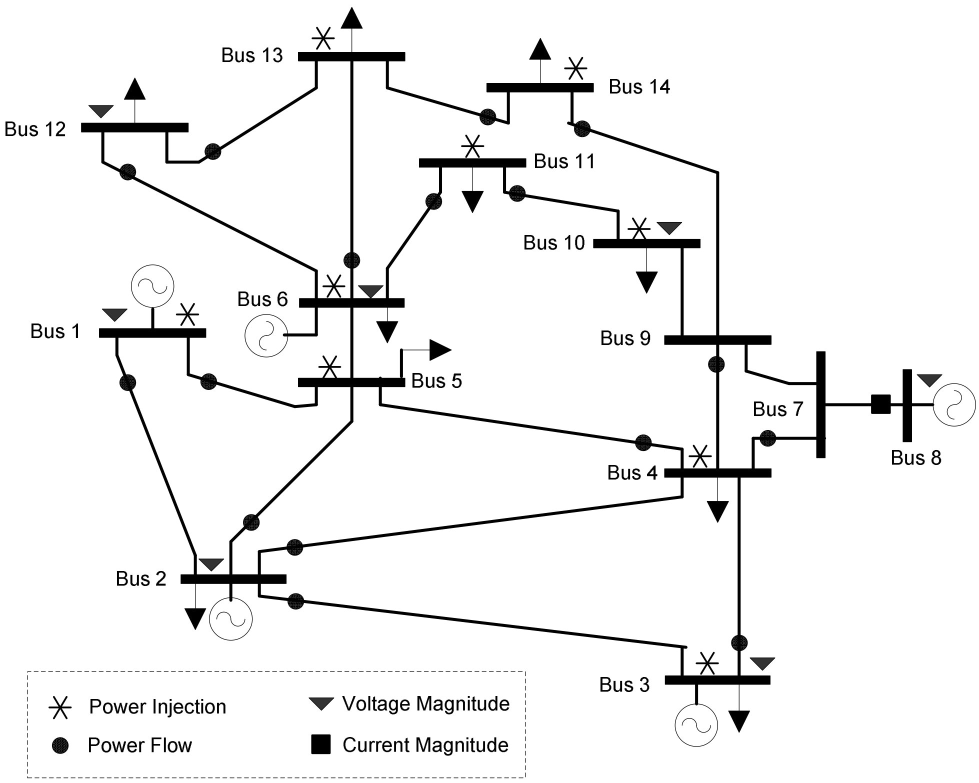

Figure 2.1: 14-bus system with conventional set of measurements

Figure 2.1 presents an example of a small power system with dispersed conventional measurements across the system which are commonly collected and transmitted through a Supervisory Control and Data Acquisition (SCADA) system. These conventional measurements and the set of virtual measurements (extended in Section 2.1.2.) are processed to obtain the best estimate of voltages, power injections and power flows of directly and non-directly monitored buses and transmission lines. The inclusion of more sophisticated, reliable and synchronised measurements is presented in Chapters 5 to 7.

Figure 2.2 presents the functions of a SE [1]. In the pre-filtering step, the operator corrects and eliminates measurements that are clearly wrong. The topology processor is implemented to estimate the physical layout of substations and the connectivity between buses based on information of Circuit Breaker (CB) status and available measurements.

The observability analysis is carried out to determine if the system state can be obtained from the available set of measurements. In case the system is not fully observable, the SE determines the unobservable zones/branches and the required set of measurements to make the system fully observable.

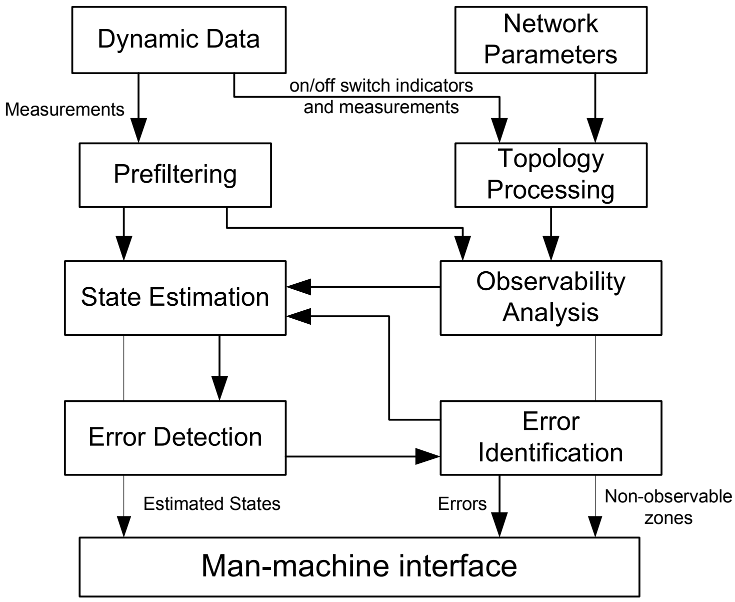

Figure 2.2: Building block of a state estimator

The estimated states are obtained from the WLS method and it performs quite well under quasi-steady state conditions. However, the good performance of the state estimator depends on measurement accuracy and redundancy levels. Therefore, bad data detection and elimination constitutes an important part of the state estimator.

The following sections present an overview of classical power system state estimation analysis including the WLS formulation, observability analysis, redundancy analysis and bad data processing. All the theory presented in this Chapter is later implemented in the following Chapters of this Thesis.

2.1 WLS Formulation

The classical approach of state estimation in power systems consists of the application of the Weighted Least Square (WLS) methodology, in which a set of measurements $\mathbf{z}$ can be represented as [18]:

$$\mathbf{z} = \mathbf{h}(\mathbf{x}) + \mathbf{e} \tag{2.1}$$

where $\mathbf{h}(\mathbf{x})$ is the set of equations relating the error free measurements with the state variables $\mathbf{x}$ and $\mathbf{e}$ is the vector of uncorrelated measurement errors with mean value $E[\mathbf{e}] = \mathbf{0}$. The n×1 state vector $\mathbf{x}$ is defined as the set of bus voltage magnitudes and angles. For instance, for an N-bus system with reference at bus 1:

$$\mathbf{x} = [\theta_2, \theta_3, \cdots, \theta_N, V_1, V_2, \cdots, V_N]^T \tag{2.2}$$

Now let $\mathbf{r} = \mathbf{z} - \mathbf{h}(\mathbf{x})$ be a vector of residuals. The best estimate of $\mathbf{x}$ is the vector $\hat{\mathbf{x}}$ that minimises the weighted sum of the squares of the measurement residuals $\mathbf{r}$:

$$J(\mathbf{x}) = [\mathbf{z} - \mathbf{h}(\mathbf{x})]^T \mathbf{R}^{-1} [\mathbf{z} - \mathbf{h}(\mathbf{x})] \tag{2.3}$$

where $\mathbf{R} = E[\mathbf{e} \cdot \mathbf{e}^T] = diag\{\sigma_1^2, \sigma_2^2, \ldots, \sigma_m^2\}$ is the error covariance matrix and σ_i^2 is the i-th variance for the i = 1, 2,…, m measurements. The solution of (2.3) is obtained when the first derivative of J ($\mathbf{x}$), evaluated at the optimum state vector $\hat{\mathbf{x}}$, gives a zero value.

$$\frac{\partial J(\hat{\mathbf{x}})}{\partial \mathbf{x}} = 0 \tag{2.4}$$

As the problem is non-linear, an iterative procedure is necessary to find the optimal vector $\hat{\mathbf{x}}$. See Appendix A.1 for further details. At iteration *k*, the following holds:

$$\mathbf{G}(\mathbf{x}^k)\Delta\mathbf{x}^k = \mathbf{H}^T(\mathbf{x}^k)\,\mathbf{R}^{-1}[\mathbf{z} - \mathbf{h}(\mathbf{x}^k)] \tag{2.5}$$

where $\mathbf{H}(\mathbf{x}^k) = \partial\mathbf{h}(\mathbf{x}^k)/\partial\mathbf{x}$ is the $m \times n$ Jacobian matrix and $\mathbf{G}(\mathbf{x}^k) = \mathbf{H}^T(\mathbf{x}^k)\,\mathbf{R}^{-1}\mathbf{H}(\mathbf{x}^k)$ is the $n \times n$ *Gain* matrix. The iteration procedure finishes when $\Delta\mathbf{x}^k = \mathbf{x}^{k+1} - \mathbf{x}^k$ is smaller than a pre-defined value. The result is the state estimate $\hat{\mathbf{x}}$.

Since the set of measurements in electric networks are obtained from bus voltages, power flows and injected powers, the set of equations $\mathbf{h}(\mathbf{x})$ must relate the error free measurements with the state variables. In the case of voltage measurements, there is a linear relation between the state variable (voltage magnitude) and the measurement itself. In the case of injected and transferred powers, the non-linear equations are:

$$P_i = V_i \sum_{j=1}^{N} V_j (G_{ij}\cos\theta_{ij} + B_{ij}\sin\theta_{ij}) \tag{2.6}$$

$$Q_i = V_i \sum_{j=1}^{N} V_j (G_{ij}\sin\theta_{ij} - B_{ij}\cos\theta_{ij}) \tag{2.7}$$

And the transferred power relationships are given as:

$$P_{ij} = \frac{V_i^2}{a_{ij}^2}(g_{si} + g_{ij}) - \frac{V_i V_j}{a_{ij}}(g_{ij}\cos\theta_{ij} + b_{ij}\sin\theta_{ij}) \tag{2.8}$$

$$Q_{ij} = -\frac{V_i^2}{a_{ij}^2}(b_{si} + b_{ij}) - \frac{V_i V_j}{a_{ij}}(g_{ij}\sin\theta_{ij} - b_{ij}\cos\theta_{ij}) \tag{2.9}$$

$$P_{ji} = V_j^2(g_{sj} + g_{ij}) - \frac{V_j V_i}{a_{ij}}(g_{ij}\cos\theta_{ji} + b_{ij}\sin\theta_{ji}) \tag{2.10}$$

$$Q_{ji} = -V_j^2(b_{sj} + b_{ij}) - \frac{V_j V_i}{a_{ij}}(g_{ij}\sin\theta_{ji} - b_{ij}\cos\theta_{ji}) \tag{2.11}$$

Here $G_{ij}+jB_{ij}$ is the *ij*-term of the power network admittance matrix and $g_{si}+jb_{si}$ corresponds to the admittance of the shunt branch connected to bus *i*, as presented in Figure 2.3.

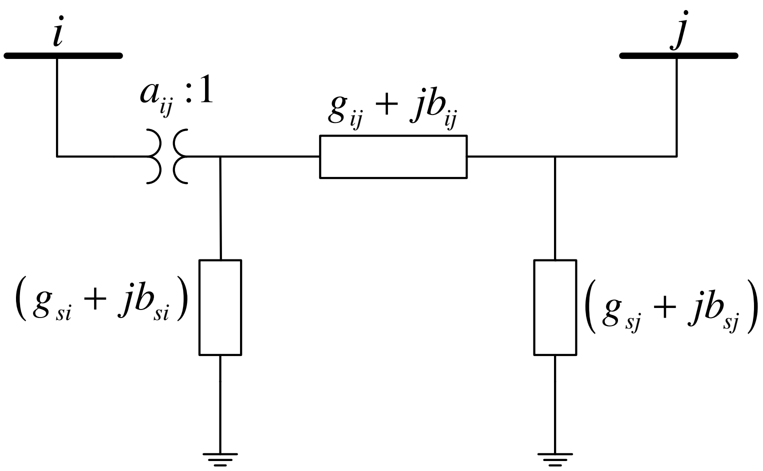

Figure 2.3: Pi-model of network branch including tap modelling

Also, a_{ij} is the off-nominal tap position of transformer connected to buses i and j. In case that branch ij is a transmission line, $a_{ij} = 1$.

2.1.1 Jacobian Elements

The elements of the *Jacobian* matrix **H**(**x**) correspond to the partial derivatives of equations (2.6) – (2.11) with respect to the state variables **x**, as presented in Tables 2.1 and 2.2. In addition, the partial derivatives of the bus voltage magnitude with respect to the state variables are presented in Table 2.3. Other types of measurements including synchronised and current magnitude measurements will be presented in Chapter 5. The way how these measurements are included and expressed in the SE is a key part of this work.

Table 2.1: Elements of H corresponding to power injections

$\frac{\partial P_i}{\partial \theta_i} = -V_i \sum_{j=1}^{N} V_j (G_{ij}\sin\theta_{ij} - B_{ij}\cos\theta_{ij}) - V_i^2 B_{ii}$	$\frac{\partial P_i}{\partial V_i} = \sum_{j=1}^{N} V_j (G_{ij}\cos\theta_{ij} + B_{ij}\sin\theta_{ij}) + V_i G_{ii}$
$\frac{\partial P_i}{\partial \theta_j} = V_i V_j (G_{ij}\sin\theta_{ij} - B_{ij}\cos\theta_{ij})$	$\frac{\partial P_i}{\partial V_j} = V_i (G_{ij}\cos\theta_{ij} + B_{ij}\sin\theta_{ij})$
$\frac{\partial Q_i}{\partial \theta_i} = V_i \sum_{j=1}^{N} V_j (G_{ij}\cos\theta_{ij} + B_{ij}\sin\theta_{ij}) - V_i^2 G_{ii}$	$\frac{\partial Q_i}{\partial V_i} = \sum_{j=1}^{N} V_j (G_{ij}\sin\theta_{ij} - B_{ij}\cos\theta_{ij}) - V_i B_{ii}$
$\frac{\partial Q_i}{\partial \theta_j} = -V_i V_j (G_{ij}\cos\theta_{ij} + B_{ij}\sin\theta_{ij})$	$\frac{\partial Q_i}{\partial V_j} = V_i (G_{ij}\sin\theta_{ij} - B_{ij}\cos\theta_{ij})$

Table 2.2: Elements of H corresponding to line power flows

$\frac{\partial P_{ij}}{\partial \theta_i} = -\frac{V_i V_j}{a_{ij}}(-g_{ij}\sin\theta_{ij} + b_{ij}\cos\theta_{ij})$	$\frac{\partial P_{ij}}{\partial V_i} = 2\frac{V_i}{a_{ij}^2}(g_{si} + g_{ij}) - \frac{V_j}{a_{ij}}(g_{ij}\cos\theta_{ij} + b_{ij}\sin\theta_{ij})$
$\frac{\partial P_{ij}}{\partial \theta_j} = -\frac{V_i V_j}{a_{ij}}(g_{ij}\sin\theta_{ij} - b_{ij}\cos\theta_{ij})$	$\frac{\partial P_{ij}}{\partial V_j} = -\frac{V_i}{a_{ij}}(g_{ij}\cos\theta_{ij} + b_{ij}\sin\theta_{ij})$
$\frac{\partial P_{ji}}{\partial \theta_i} = -\frac{V_j V_i}{a_{ij}}(g_{ij}\sin\theta_{ji} - b_{ij}\cos\theta_{ji})$	$\frac{\partial P_{ji}}{\partial V_i} = -\frac{V_j}{a_{ij}}(g_{ij}\cos\theta_{ji} + b_{ij}\sin\theta_{ji})$
$\frac{\partial P_{ji}}{\partial \theta_j} = -\frac{V_j V_i}{a_{ij}}(-g_{ij}\sin\theta_{ji} + b_{ij}\cos\theta_{ji})$	$\frac{\partial P_{ji}}{\partial V_j} = 2V_j(g_{sj} + g_{ij}) - \frac{V_i}{a_{ij}}(g_{ij}\cos\theta_{ji} + b_{ij}\sin\theta_{ji})$
$\frac{\partial Q_{ij}}{\partial \theta_i} = -\frac{V_i V_j}{a_{ij}}(g_{ij}\cos\theta_{ij} + b_{ij}\sin\theta_{ij})$	$\frac{\partial Q_{ij}}{\partial V_i} = -2\frac{V_i}{a_{ij}^2}(b_{si} + b_{ij}) - \frac{V_j}{a_{ij}}(g_{ij}\sin\theta_{ij} - b_{ij}\cos\theta_{ij})$
$\frac{\partial Q_{ij}}{\partial \theta_j} = \frac{V_i V_j}{a_{ij}}(g_{ij}\cos\theta_{ij} + b_{ij}\sin\theta_{ij})$	$\frac{\partial Q_{ij}}{\partial V_j} = -\frac{V_i}{a_{ij}}(g_{ij}\sin\theta_{ij} - b_{ij}\cos\theta_{ij})$
$\frac{\partial Q_{ji}}{\partial \theta_i} = \frac{V_j V_i}{a_{ij}}(g_{ij}\cos\theta_{ji} + b_{ij}\sin\theta_{ji})$	$\frac{\partial Q_{ji}}{\partial V_i} = -\frac{V_j}{a_{ij}}(g_{ij}\sin\theta_{ji} - b_{ij}\cos\theta_{ji})$
$\frac{\partial Q_{ji}}{\partial \theta_j} = -\frac{V_j V_i}{a_{ij}}(g_{ij}\cos\theta_{ji} + b_{ij}\sin\theta_{ji})$	$\frac{\partial Q_{ji}}{\partial V_j} = -2V_j(b_{sj} + b_{ij}) - \frac{V_i}{a_{ij}}(g_{ij}\sin\theta_{ji} - b_{ij}\cos\theta_{ji})$

Table 2.3: Elements of H for bus voltages

$\frac{\partial V_i}{\partial \theta_i} = 0$	$\frac{\partial V_i}{\partial V_i} = 1$
$\frac{\partial V_i}{\partial \theta_j} = 0$	$\frac{\partial V_i}{\partial V_j} = 0$

2.1.2 Equality Constrained WLS

Even when the classical WLS method for state estimation provides reasonable results of power injections at all buses, it may not provide a zero value for null power injections (no load or generation connected). In order to improve the accuracy of the estimations, particularly around the null power injection buses, a set of virtual measurements with mean value equal to zero and small variance can be included in the formulation. However, the presence of very small variances (large weights) in some measurements may lead to ill-conditioned *Gain Matrix* [18].

Alternatively, a set of constraints can be included in the formulation to guarantee zero power injections in those buses but also to avoid large weights in $\mathbf{R}^{-1}$, which is one source of ill-conditioning the *Gain Matrix* [18].

The minimization problem stated in equation (2.3) is now extended to meet a set of constraints $\mathbf{c}(\mathbf{x}) = \mathbf{0}$. The Lagrange multipliers are used to account for the equality constraints as follows [32, 33]:

$$L(\mathbf{x}, \boldsymbol{\lambda}_c) = [\mathbf{z} - \mathbf{h}(\mathbf{x})]^T \mathbf{R}^{-1} [\mathbf{z} - \mathbf{h}(\mathbf{x})] - \boldsymbol{\lambda}_c^T \mathbf{c}(\mathbf{x}) \tag{2.12}$$

where $\boldsymbol{\lambda}_c$ is the vector of Lagrange multipliers. Thus, partial derivatives of $L(\mathbf{x}, \boldsymbol{\lambda}_c)$ with respect to $\mathbf{x}$ and $\boldsymbol{\lambda}_c$ are obtained to minimise this function, see Appendix A.2 for details. Solving for $\Delta\mathbf{x}$ and $\boldsymbol{\lambda}_c$, it is possible to establish the iterative procedure to find the vector $\hat{\mathbf{x}}$ that minimises $L(\mathbf{x}, \boldsymbol{\lambda}_c)$:

$$\begin{bmatrix} \mathbf{H}^T(\mathbf{x}^k)\,\mathbf{R}^{-1}\mathbf{H} & -\mathbf{C}^T(\mathbf{x}^k) \\ -\mathbf{C}(\mathbf{x}^k) & \mathbf{0} \end{bmatrix} \begin{bmatrix} \Delta\mathbf{x}^k \\ \boldsymbol{\lambda}_c^{k+1} \end{bmatrix} = \begin{bmatrix} \mathbf{H}^T(\mathbf{x}^k)\,\mathbf{R}^{-1}[\mathbf{z} - \mathbf{h}(\mathbf{x}^k)] \\ \mathbf{c}(\mathbf{x}^k) \end{bmatrix} \tag{2.13}$$

where $\mathbf{C}(\mathbf{x}^k) = \partial\mathbf{c}(\mathbf{x}^k)/\partial\mathbf{x}$.

As seen from equation (2.13), the state vector is extended with a set of Lagrange multipliers. Also, the Jacobian matrix is partitioned into a block corresponding to constraints and another block related to all measurements in the system [33].

2.2 Observability Analysis

A power system is observable if the number of linearly independent measurements is equal or larger than the number of states [1] . It means that for each state variable there must be at least one measurement “observing” it. Reference [34] indicates in a simple way that a system is observable if there are sufficient measurements to run a state estimator.

If one or more states are unobserved, the *Gain Matrix* **G** defined in (2.5) would become singular, i.e. non invertible, and equation (2.5) could not be solved. Because of this, the system is said to be unobservable due to insufficient number of measurements in the system.

Two different concepts of observability are found in the literature [35]: *Topological Observability and Numerical Observability*. The first one is based on *Graph Theory*, and the second one is based on linear algebra formulation [36]. This research work focuses and applies *Numerical Observability* as it also implies *Topological Observability*.

2.2.1 Numerical Observability

A system is said to be numerically observable if the *Jacobian* matrix is of full rank i.e. the *Gain Matrix* is non-singular which is the condition for the state estimator to have a unique solution.

A decoupled Jacobian matrix can be used to simplify the problem. The decoupling is based on the fact that under normal operating conditions, changes of active powers are weakly related to variations of magnitudes of bus voltages. In a similar way, changes of reactive powers are weakly related to changes of bus angles [34].

The Jacobian matrix is approximated as:

$$\mathbf{H} = \begin{bmatrix} \mathbf{H}_{P\theta} & 0 \\ 0 & \mathbf{H}_{QV} \end{bmatrix} \tag{2.14}$$

where $\mathbf{H}_{P\theta} = \dfrac{\partial \mathbf{h}_P(\mathbf{V},\boldsymbol{\theta})}{\partial \boldsymbol{\theta}}$ and $\mathbf{H}_{QV} = \dfrac{\partial \mathbf{h}_Q(\mathbf{V},\boldsymbol{\theta})}{\partial \mathbf{V}}$. The subscripts P and Q refer to active and reactive power equations, respectively. And the *Gain Matrix* will be:

$$\mathbf{G} = \begin{bmatrix} \mathbf{G}_{\theta} & \mathbf{0} \\ \mathbf{0} & \mathbf{G}_{V} \end{bmatrix} \tag{2.15}$$

where $\mathbf{G}_{\theta} = \mathbf{H}_{P\theta}^T \mathbf{R}_P^{-1} \mathbf{H}_{P\theta}$ and $\mathbf{G}_V = \mathbf{H}_{QV}^T \mathbf{R}_Q^{-1} \mathbf{H}_{QV}$. In other words, the observability of the system can be obtained separately.

A power system with N buses is said to be P-θ numerically observable if the rank of $\mathbf{G}_{\theta}$, the maximum number of linearly independent equations, is "N-1". Also, the system is said to be Q-V numerically observable if the rank of $\mathbf{G}_V$ is "N" [37] . If the system is found to be P-θ

numerically observable, it will be assumed to be *Q-V* numerically observable considering that power measurements are obtained in pairs (active and reactive) and the existing of at least one voltage magnitude measurement [38].

A linear model of the power measurements simplifies even more the problem to obtain the factorization of the *Gain Matrix* $\mathbf{G}_\theta$. Since the numerical observability is independent of the branch parameters and the operating state of the system, the voltage magnitudes at all buses and the reactances at all branches are assumed to be *1 p.u.*. Based on the previous assumptions, the active power flow from bus *i* to *j* can be modelled as [39]:

$$P_{ij} = \theta_i - \theta_j \tag{2.16}$$

And the linear Jacobian matrix becomes:

$$\mathbf{H}_{P\theta} = \begin{array}{c} \\ \vdots \\ P_{ij} \\ \vdots \\ \vdots \end{array} \begin{array}{c} \begin{array}{ccccc} & \theta_i & & \theta_j & \end{array} \\ \begin{bmatrix} \cdots & \cdots & \cdots & \cdots & \cdots \\ 0 & 1 & \cdots & -1 & 0 \\ \vdots & \vdots & \vdots & \vdots & \vdots \\ \vdots & \cdots & \cdots & \cdots & \vdots \end{bmatrix} \end{array} \tag{2.17}$$

Here, the reference angle is also included in the set of states. Then, the *Gain Matrix* $\mathbf{G}_\theta$ can be easily decomposed using *triangular factorization* to obtain the new matrix $\overline{\mathbf{G}}_\theta$. In case a zero pivot is found during the factorization, it will be necessary to make permutation of rows in $\mathbf{G}_\theta$ and then continue with the decomposition.

If the system is not fully observable, more than one element will be zero in the diagonal of $\overline{\mathbf{G}}_\theta$. Otherwise, under full network observability, the last diagonal element of $\overline{\mathbf{G}}_\theta$ will be zero and the rank of $\mathbf{G}_\theta$ will be *N-1*. Note that, if one determines that the system is numerically observable with the simplified linear model, one also ensures that the system is topologically observable.

2.2.2 Identification of Observable Islands

Based on a linear *P-θ* measurement model with unitary covariance matrix, the solution of the estimated states, starting from (2.5), is:

$$\mathbf{G}_\theta \hat{\boldsymbol{\theta}} = \mathbf{H}_P \mathbf{z}_P \tag{2.18}$$

where $\mathbf{z}_P$ is the set of active power measurements. Consider the case where all the measurements are all set to zero:

$$\mathbf{G}_\theta \hat{\boldsymbol{\theta}} = \mathbf{0} \tag{2.19}$$

Under full network observability conditions, the estimated active powers obtained from (2.16) should be also equal to zero. Any other value different from zero would imply that such branch is not being observed with the available measurements.

From the decomposed matrix $\overline{\mathbf{G}}_\theta$, it is possible to determine which branches are unobserved and need measurement allocation. The algorithm is as follows [40]:

1. Initialize the measurement set with available measurements
2. Create the new gain matrix $\mathbf{G}_\theta$
3. Perform triangular factorization of $\mathbf{G}_\theta$ (called $\overline{\mathbf{G}}_\theta$). A θ pseudo measurement is introduced whenever a zero pivot is encountered. If only one zero pivot occurs (necessary at the end), stop. Otherwise:
4. Solve the DC estimator from equation (2.18), considering all the measured values equal to zero, except for the θ pseudo-measurements, that assume the values $\theta_k = 0, 1, 2 \ldots$
5. Evaluate the branch flows from equation (2.16).
6. Update the power network by removing all branches with $P_{ij} \neq 0$. These are unobservable branches.

7. Update the measurements set of interest by removing power injection measurements from buses adjacent to at least one of the branches removed in Step 6. These are irrelevant measurements.
8. Return to Step 2.

The iteration is required because the sub networks identified can only be theoretically classified as candidate for observable islands [34]. Once all the unobserved branches are removed, it is possible to identify all observable islands in the system. Allocation of new measurements will be necessary to unify the observable islands and make the system fully observable.

On the other hand, reference [41] uses a non-iterative numerical method to remove the non-observable branches. From the decomposition of matrix $\mathbf{G}_\theta$, it is obtained the factors **L** (non-singular unitary lower triangular matrix), and **U** (upper triangular matrix) such that $\mathbf{G}_\theta = \mathbf{LU}$. The decomposition is based on Gaussian elimination by using the Peters and Wilkinson method explained in [42], see Appendix B.1.

Later, a singular diagonal matrix **D** is built up from $\mathbf{D} = \mathbf{L}^{-1}\mathbf{G}_\theta\mathbf{L}^{-T}$ containing zero diagonal elements in those rows corresponding to the zero pivots found during the factorization of $\mathbf{G}_\theta$. By taking the inverse of **L**, and keeping the rows of $\mathbf{L}^{-1}$ corresponding to the zero diagonals of **D**, it is obtained a *Test Matrix* **W**.

Finally, compute **C** matrix from the branch-bus incidence matrix **A** and matrix **W**:

$$\mathbf{C} = \mathbf{A}\mathbf{W}^T \tag{2.20}$$

where the entry A_{ij} is 1 (-1) if the sending (receiving) end of branch i connects to bus j, or zero otherwise. If at least one element in a row of **C** is non-zero, then the corresponding branch is unobservable. The observable islands are found once these branches are removed.

2.3 Redundancy Analysis

In power system state estimation, a measurement can be classified as either critical or redundant [39]. Redundant measurements can be removed from the system without causing loss of observability. However, the removal of a critical measurement makes the system unobservable. This is equivalent to say that the removal of a critical measurement decreases (by one) the rank of the Jacobian Matrix **H**. The row of the Jacobian matrix corresponding to a critical measurement is linearly independent of the other rows (other measurements) of **H** [43]**.**

The residual $r_i = z_i - h_i(\hat{\mathbf{x}})$ of any critical measurements i, is always zero (irrespective of good or bad data) which means that any error in a critical measurement can not be detected, affecting the performance of the state estimator [18].

A critical pair is a set of two measurements that when removed make the system unobservable, a critical trio is a set of three measurements that when removed makes the system unobservable and so on. An optimal placement of measurements can eliminate any critical measurement and improve local redundancy levels (can eliminate critical pairs or trios).

Similar to *Observability Analysis*, the decoupled Jacobian matrix, based on a linear model of the power measurements, is enough to identify critical measurements and redundancy levels.

The first step consists on the decomposition of the Jacobian matrix by using *LU decomposition*. The set of measurements in the Jacobian matrix will include only the linear model of all available real power measurements. The set of states are the bus phase angles but excluding the reference bus.

After decomposition of $\mathbf{H}_{P\theta}$ (and possible needed exchange of rows), the equivalent matrix becomes [39]:

$$\tilde{\mathbf{H}}_{m\times(N\text{-}1)} = \begin{bmatrix} \mathbf{I}_{(N-1)} \\ \mathbf{K}_{red} \end{bmatrix} \tag{2.21}$$

where,

$\mathbf{I}_{(N\text{-}1)}$ is the identity matrix of dimension (N-1) and $\mathbf{K}_{red}$ is the equivalent sub-matrix with all the redundant measurements.

The columns of $\tilde{\mathbf{H}}$ represent the bus angles and the rows of $\tilde{\mathbf{H}}$ correspond to the available measurements. Matrix $\mathbf{I}_{(N\text{-}1)}$ represents the basic set of measurements which makes the system fully observable whereas the measurements grouped in $\mathbf{K}_{red}$ are the redundant measurements [38]. In case that all elements in a column of $\mathbf{K}_{red}$ are all zero, the corresponding measurement in $\mathbf{I}_{(N\text{-}1)}$ is identified as a critical measurement.

The non-zero elements that appear in each column of $\tilde{\mathbf{H}}$, identify the measurements that contain information about the state corresponding to that column. From here, one can identify critical pairs or critical trios formed by only one basic measurement. Of course, there can be critical sets with more than one basic measurement. These critical sets can be identified based on the method proposed in [38] .

Elimination of critical measurements or critical sets can be carried out by including new measurements into the Jacobian matrix and then check if the column of interest has a new non-zero element in the row corresponding to the new measurement. Once critical measurements are eliminated, and local redundancy is improved, it is possible to rely on bad data processing techniques.

2.4 Bad Data Processing

Measurement readings are exposed to errors due to failure of communications, wrong wiring, inaccuracy of measurement transformers, transducers, etc. There are other causes of bad data which are related to topology and line parameter errors [44] but they are not considered in this work.

The first task in Bad Data Processing (BDP) consists of detecting the presence of wrong measurements which can be carried out using statistical procedures. Once the system operator knows that bad data are present in the set of measurements, it is necessary to eliminate it or correct the bad data from other available information.

2.4.1 Chi square Distribution Test

Consider a set of independent random variables grouped in a vector **v**. If each element v_i follows a normal standard distribution $N(0,1)$, the chi square distribution χ^2_m, with *m* degrees of freedom, is the distribution of the random variable *y* defined as [18], [45]:

$$y = \sum_{i=1}^{m} v_i^2 \tag{2.22}$$

The degrees of freedom *m* represent the number of independent variables in the sum of squares. This value will decrease if any of the variables v_i form a linearly dependent subset.

Figure 2.4 presents the Probability Density Function (PDF) for a chi square distribution with 20 degrees of freedom. As the number of degrees of freedom *m* increases, the PDF of χ^2 will tend to a normal distribution [45].

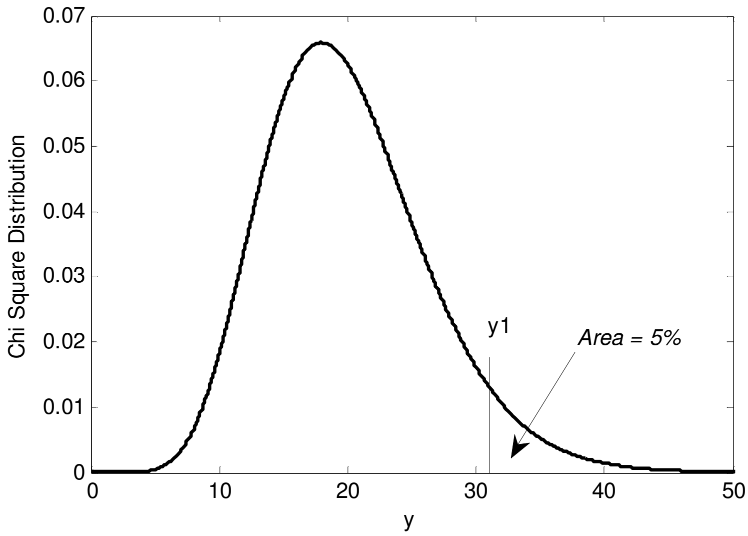

Figure 2.4: Chi Square PDF for 20 degrees of freedom

The larger area under the PDF of Figure 2.4 represents the probability of finding a value of *y* smaller than a threshold y^1. Figure 2.4 shows that the probability of finding *y* smaller than 31.4

is 95%. This probability calculation can be used to detect presence of bad data in the set of measurements.

If there is no bad data in the set of power system measurements and the m measurement errors e_i (i=1, 2, …, m) have normal distribution $N(0,\sigma_i^2)$, the performance index $J(\hat{\mathbf{x}})$, defined in equation (2.3), will follow a chi-square distribution $\chi^2_{m\text{-}n}$. Here, m is the number of measurements, n is the number of states and vector $\hat{\mathbf{x}}$ refers to the estimated states [46]. The degrees of freedom must be constrained to m-n because it is considered that there are at the most m-n linearly independent equations.

One can determine that $J(\hat{\mathbf{x}})$ follows a chi square distribution, i.e. free of bad data, if $J(\hat{\mathbf{x}})$ is smaller than a threshold y[1] at a certain level of confidence α. This level of confidence α is usually specified at 95% but may change depending on the system or application. Using the example of Figure 2.4, if the estimated $J(\hat{\mathbf{x}})$ for a given system with 20 degrees of freedom is smaller than 31.4, bad data will not be suspected with a confidence level of 95%.

2.4.2 Measurement Residuals

This section introduces the identification of bad data based on the *measurement residuals approach* [18]. Consider the linearized measurement equation around the estimated point $\mathbf{x}_0$:

$$\Delta\mathbf{z} = \mathbf{H}\Delta\mathbf{x} + \mathbf{e} \tag{2.23}$$

where $\Delta\mathbf{z} = \mathbf{z}\text{-}\mathbf{h}(\mathbf{x}_0)$ is the mismatch between the measurement vector and its calculated value at an estimate $\mathbf{x}_0$. Also $\Delta\mathbf{x} = \mathbf{x}\text{-}\mathbf{x}_0$, $\mathbf{H} = \partial\mathbf{h}(\mathbf{x}_0)/\partial\mathbf{x}$ and $\mathbf{e}$ is the set of uncorrelated measurement errors with Gaussian distribution and covariance matrix $\mathbf{R}$. Similar to (2.5), the WLS estimation solution of the linearized state vector will be:

$$\Delta\hat{\mathbf{x}} = (\mathbf{H}^T\mathbf{R}^{-1}\mathbf{H})^{-1}\mathbf{H}^T\mathbf{R}^{-1}\Delta\mathbf{z} \tag{2.24}$$

$$\Delta\hat{\mathbf{x}} = \mathbf{G}^{-1}\mathbf{H}^T\mathbf{R}^{-1}\Delta\mathbf{z} \tag{2.25}$$

And the estimated value of $\Delta\mathbf{z}$ will be:

$$\Delta\hat{\mathbf{z}} = \mathbf{H}\Delta\hat{\mathbf{x}} = \mathbf{K}\Delta\mathbf{z} \tag{2.26}$$

where $\mathbf{K} = \mathbf{H}\mathbf{G}^{-1}\mathbf{H}^{T}\mathbf{R}^{-1}$.

For a set of m measurements, the $m \times 1$ vector of measurement residual will be denoted as:

$$\mathbf{r} = \Delta\mathbf{z} - \Delta\hat{\mathbf{z}} \tag{2.27}$$

$$\mathbf{r} = (\mathbf{I} - \mathbf{K})\Delta\mathbf{z} \tag{2.28}$$

where $\mathbf{I}$ is the *Identity Matrix*. By substitution of equation (2.23) into (2.28) it is obtained:

$$\mathbf{r} = (\mathbf{I} - \mathbf{K})(\mathbf{H}\Delta\mathbf{x} + \mathbf{e}) \tag{2.29}$$

Based on the property that $(\mathbf{I}\text{-}\mathbf{K})\mathbf{H} = \mathbf{0}$, equation (2.29) can be expressed as [18], [44] :

$$\mathbf{r} = (\mathbf{I} - \mathbf{K})\mathbf{e} \tag{2.30}$$

$$\mathbf{r} = \mathbf{S}\mathbf{e} \tag{2.31}$$

Matrix $\mathbf{S}$ is called the *Residual Sensitivity Matrix*. Based on the relation above, it is possible to calculate the probability distribution of the measurement residuals as follows:

$$E(\mathbf{r}) = E(\mathbf{S}\mathbf{e}) = \mathbf{S}E(\mathbf{e}) = 0 \tag{2.32}$$

$$\mathbf{\Omega} = \mathrm{cov}(\mathbf{r}) = E[\mathbf{r}\mathbf{r}^{T}] \tag{2.33}$$

$$\mathbf{\Omega} = \mathbf{S}E[\mathbf{e}\mathbf{e}^{T}]\mathbf{S}^{T} \tag{2.34}$$

$$\mathbf{\Omega} = \mathbf{S}\mathbf{R}\mathbf{S}^{T} = \mathbf{S}\mathbf{R} \tag{2.35}$$

The off diagonal elements of the $m \times m$ matrix $\mathbf{\Omega}$ identify strong versus weakly interacting measurements. The higher the element Ω_{ij}, the stronger the interaction between measurements i and j.

The covariance matrix $\mathbf{\Omega}$ is also used to calculate the normalized residuals to identify and reject any bad data in the set of measurements.

2.4.3 Normalized Residual Test

Once the state estimation is obtained using WLS, the residual vector is calculated as the difference between each measurement and the corresponding function $\mathbf{h}(\hat{\mathbf{x}})$:

$$\mathbf{r} = \mathbf{z} - \mathbf{h}(\hat{\mathbf{x}}) \tag{2.36}$$

The normalized residuals are obtained by dividing its absolute value by the corresponding diagonal entry in the residual covariance matrix $\mathbf{\Omega}$ [45], [46]:

$$r_i^N = \frac{|r_i|}{\sqrt{\Omega_{ii}}} \tag{2.37}$$

Once the normalized residuals are obtained for all the measurements, the largest normalized residual is compared with a pre-defined threshold. If this value is larger than the threshold, the corresponding data will be removed and a new estimation is performed. This procedure is repeated until the largest normalized residual is lower than the threshold previously established.

If the value of the threshold is too small, the program would filter data that may not be wrong, reducing redundancy, and it may lead to unobservable conditions. However, if the threshold is large, it is possible that wrong data is still present. Generally, a threshold value of 3.0 is enough to reject gross errors in the set of measurements.

There is a different approach where the bad data is not rejected at all but it is corrected instead. This is achieved by subtracting the estimated error from the identified bad measurement. However, this method may not be accurate enough for large errors [45]. The measurement residual of the identified bad measurement is:

$$r_i^{\text{bad}} = z_i^{\text{bad}} - h(\hat{\mathbf{x}}) \approx S_{ii} e_i \tag{2.38}$$

By solving for e_i:

$$e_i \approx \frac{1}{S_{ii}} r_i^{bad} \tag{2.39}$$

And subtracting this estimated error from the identified bad measurements yields:

$$z_i \approx z_i^{bad} - \frac{1}{S_{ii}} r_i^{bad} \tag{2.40}$$

The normalized residual approach is generally very effective but its main limitations are listed below:

- It can not identify errors in critical measurements because the corresponding column in **S** is zero. So, an error in that measurement could not be detected since it will have no effect on the measurement residual [47] . Here the importance of having high redundant systems.
- It may fail to identify erroneous measurements when two interacting measurements have errors that are in agreement (multiple interacting and conforming bad data) [18].

2.5 Summary

This chapter introduced the classical techniques applied to state estimation, redundancy analysis, observability analysis and bad data detection and elimination. The chapter also presented the equations of power flow and power injection as function of the state variables that are used in the WLS formulation. The following chapters will make reference to the equations and formulations presented in Chapter 2.

Chapter 3 Estimation of Probabilistic Load Flows: Theory and Modelling

The insertion of intermittent wind power generation at the transmission level has increased the level of uncertainty of the power networks. Distributed generation and emerging technologies such as storage devices will also increase the uncertainty of the aggregated loads. This leads to running stochastic/probabilistic studies where the input variables can no longer be treated as deterministic values, but as stochastic ones [48].

Probabilistic load flow studies take into account the random nature of generation and demand for a certain period. The information obtained from the probabilistic load flows can be used for planning purposes when power engineers need to make decisions in terms of investment or for operation purposes when it is needed to determine all the possible operating conditions of the power system for a short period [49]. These studies provide valuable information about the likelihood that certain bus voltage or power flow/injection will remain within some acceptable limits.

Most of the work mentioned in Section 1.1.1 was concentrated on the uncertainty of power injections, which were usually assumed to be Gaussian distributed with 5% to 10% of variability. Recent studies have shown that the marginal distribution of wind power production has larger variability and it is non-Gaussian distributed [4, 10].

Reference [31] uses a weighted sum of Gaussian distributions to model any non-Gaussian distribution. The method uses multiple WLS runs to deal with the Gaussian components for each non-correlated input variable.

To date, little attention has been paid to non-Gaussian correlated input variables. This is, however, the most general and realistic scenario to be considered in probabilistic load flows studies. Examples of non-Gaussian correlated variables are power demands of aggregated loads with similar consumption patterns or wind/solar generation in the same geographic area.

References [2, 50] introduced non-Gaussian correlated variables to represent the stochastic power output of wind farms in probabilistic power flows studies. The statistical moments were estimated using the Point Estimate method and the Probability Density Functions (PDFs) were approximated with the Cornish–Fisher expansion series.

In this work, the non-Gaussian PDFs are approximated by the Gaussian Mixture Model (GMM), which is able to model any marginal distribution (standard or not) with a finite number of components.

The contribution of this work is to extend the Gaussian Component Combination Method (GCCM) introduced in [31] to estimate the PDF of power flows in presence of non-Gaussian correlated random input variables.

The advantage of this approach is that it does not need any expansion series to approximate the resulting PDF of the system variables. The resulting PDF of any electrical variable is made of Gaussian components extracted from multiple WLS runs. As the number of WLS runs depends only on the number of Gaussian components of the input variables, a Gaussian mixture reduction technique is also proposed to limit the number of WLS runs.

The first part of this chapter introduces the Gaussian mixture distribution and the Gaussian Mixture Model (GMM) to represent non-Gaussian random variables. Section 3.2 explains a methodology to reduce the number of Gaussian components to simplify the GMMs. Subsequently, Section 3.3 presents the Monte Carlo simulations and the Gaussian Component Combination Method (GCCM) for probabilistic load flow studies in the presence of non-Gaussian correlated variables, whereas Section 3.4 presents the summary of the Chapter.

3.1 Gaussian Mixture Distribution

A Gaussian mixture distribution is the mixture of L Gaussian distribution components. For a one-dimensional random variable Y, the probability density function $f_Y(y)$ is defined as [31]:

$$f_Y(y) = \sum_{i=1}^{L} \omega_i f_{N(\mu_i,\sigma_i^2)}(y) \tag{3.1}$$

where ω_i, μ_i and σ_i^2 are the proportion, mean, and variance of the i-th component of the Gaussian mixture, respectively. In order to maintain the characteristics of a probability distribution, the proportions parameters are constrained to be:

$$0 < \omega_i \le 1 \quad \text{and} \quad \sum_{i=1}^{L} \omega_i = 1 \tag{3.2}$$

In addition, the distribution of the i-th Gaussian component is [51]:

$$f_{N(\mu_i,\sigma_i^2)}(y) = \frac{1}{\sqrt{2\pi\sigma_i^2}} e^{\frac{-(y-\mu_i)^2}{2\sigma_i^2}} . \tag{3.3}$$

The mean and variance of the random variable are respectively [52]:

$$\mu_Y = \sum_{i=1}^{L} \omega_i \mu_i \tag{3.4}$$

$$\sigma_Y^2 = \sum_{i=1}^{L} \omega_i \left(\sigma_i^2 + (\mu_i - \mu_Y)^2 \right) \tag{3.5}$$

The probability density of the Gaussian Mixture is obtained by evaluating $f_Y(y)$ for $-\infty < y < \infty$. For example, consider a Gaussian mixture distribution ($L = 7$) with the parameters given in Table 3.1:

Table 3.1: Parameters of a Gaussian mixture distribution with seven components

Component	i=1	i=2	i=3	i=4	i=5	i=6	i=7
ω_i	0.20	0.20	0.20	0.20	0.10	0.05	0.05
μ_i	43.0	50.0	52.0	58.0	62.0	72.0	80.0
σ_i^2	9.0	16.0	9.0	64.0	4.0	4.0	25.0

Figure 3.1 presents the probability density of the variable Y modelled by the Gaussian mixture parameters of Table 3.1. The sum of the individual weighted Gaussian components creates the Gaussian mixture distribution. This variable Y represents any random variable such as power demands, generation power outputs, or bus voltage magnitudes for a certain period. From Figure 3.1, it can be concluded that the PDF of the variable Y is non-Gaussian and that it does not fit any other typical marginal distribution.

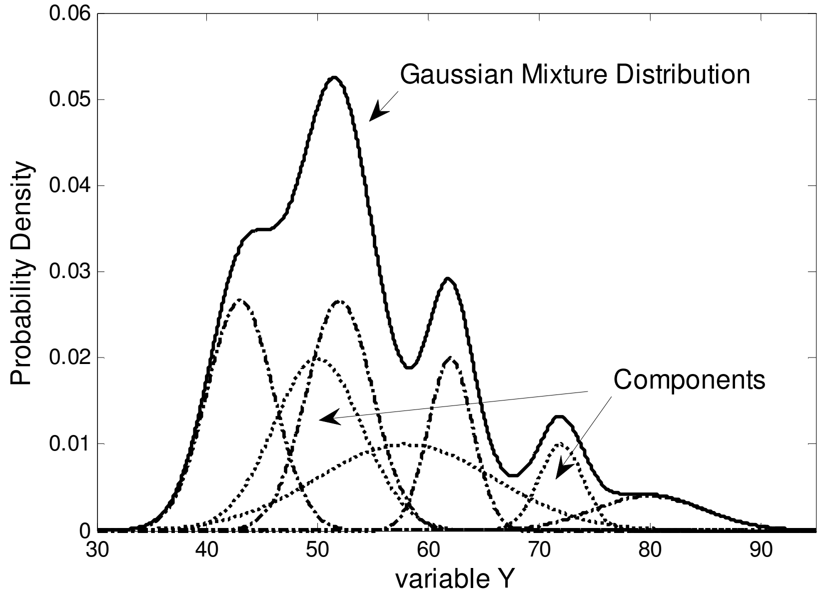

Figure 3.1: Gaussian mixture distribution with 7 Gaussian components

The Cumulative Distribution Function (CDF) of the random variable is the probability that Y assumes a value in the range $-\infty < Y \leq y$ [51]:

$$F_Y(y) = \text{Prob}(Y \leq y) = \int_{-\infty}^{y} f_Y(u)du \tag{3.6}$$

Figure 3.2 presents the CDF of the seven components Gaussian mixture with the parameters listed in Table 3.1. The values of $F_Y(y)$ represent probabilities and they lie in the range 0 to 1. This is particularly important when creating Gaussian mixture random variables for Monte Carlo simulations.

The main advantage of the Gaussian Mixture distribution is that it can approximate any PDF with a finite number of components. This is of particular interest when the distribution of the random variable does not fit the typical distributions (e.g. Gaussian, Uniform, Gamma, etc). The higher the number of components of the Gaussian Mixture Model (GMM), the more accurate the approximation becomes.

The most effective methodology to determine the GMM that best approximates the distribution of the samples of Y is the Expectation Maximisation (EM) algorithm. For example, reference

[16] uses the EM algorithm to determine the parameters of the GMM to model PDFs of power demands.

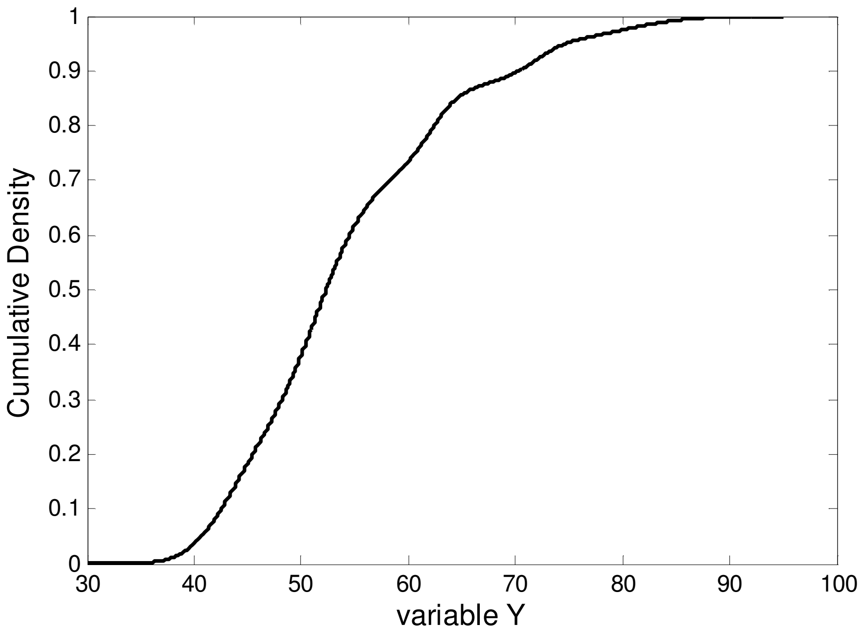

Figure 3.2: CDF for Gaussian mixture with seven components

The input of the EM algorithm is the set of samples $\gamma = [y_1, y_2, \ldots, y_s]$ of the random variable Y and the desired number of Gaussian components of the GMM. Given γ and the initial (or updated) Gaussian mixture parameters η, the algorithm computes the expectation of the log-likelihood of the complete data with respect to the unknown samples. Later, η is updated to maximise the log-likelihood expectation found before. This procedure is iteratively executed until convergence is achieved. The Statistics Toolbox of MATLAB offers the function *gmdistribution.fit* to estimate η using the EM algorithm given the samples γ and the desired number of Gaussian components [53].

Figure 3.3 presents the GMM of a Uniform random variable approximated by 10 components using the EM algorithm. In fact, the Uniform distribution is one of the most difficult distributions to approximate with a GMM. The approximation can be improved with a higher number of Gaussian components.

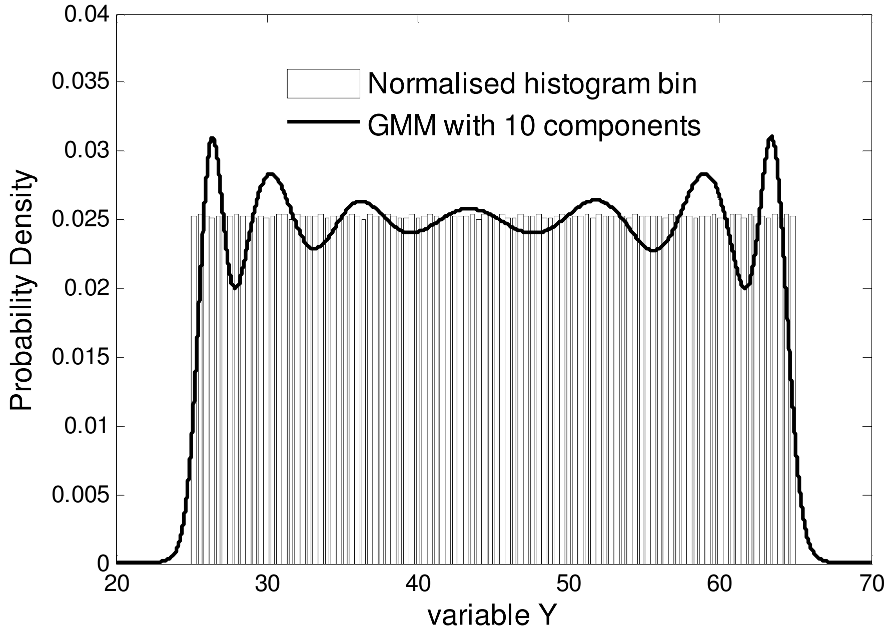

Figure 3.3: Uniform distributed random variable modelled by GMM

Figure 3.4 presents the GMM approximation of a Gamma distributed random variable with 10 components. In this case, the mismatch between the GMM and the random variable density is negligible.

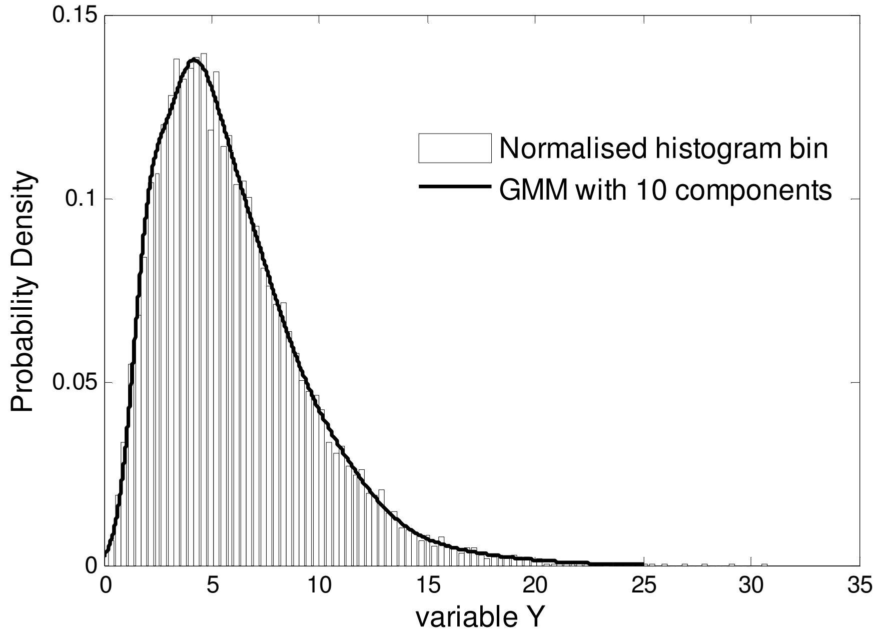

Figure 3.4: Gamma distributed random variable modelled by GMM

The number of components needed to approximate any probability density function depends on the degree of required accuracy. Although adding an extra component to the GMM will always improve the approximation, the number of components is sufficient when adding an extra component produces a negligible improvement in the approximation. The Chi-Square goodness of fit test can be used to quantify the degree of fitness of the set of samples and the GMM [16]. By using a pre-defined threshold, it is possible to determine the number of components of the GMM.

3.2 Reduction of Gaussian Mixtures

The number of components may be a limitation when dealing with simulations that involve a large number of GMM at the same time. Based on this, it is very useful to decrease the number of components of the mixtures in order to reduce the computation demands while keeping a good level of accuracy of the original GMMs.

If one starts from the simplest GMM to represent a non-Gaussian variable and then increases the number of components, it would be necessary to run the Expectation Maximisation (EM) (fitting) technique each time it is desired to improve the accuracy of the GMM. This is both time consuming and impractical. The proposed reduction method no longer requires the use of the raw data (observations). Instead, it starts from the actual accurate model parameters of the GMM and then reduces one component at a time.

The idea of the Gaussian mixture components reduction is to approximate the original GMM in (3.1) as a new GMM with fewer components:

$$g_Y(y) = \sum_{j=1}^{M} \tilde{\omega}_j f_{N(\tilde{\mu}_j, \tilde{\sigma}_j^2)}(y) \tag{3.7}$$

where $M < L$ and $\tilde{\omega}_j$, $\tilde{\mu}_j$ and $\tilde{\sigma}_j^2$ are the proportion, mean, and variance of the j-th component, respectively.

Different reduction algorithms have been presented in recent years. The main requirements of a good reduction algorithm can be summarised as [52]:

- The algorithm should be efficient and easy to execute.
- The algorithm should maintain the mean and variance of the original mixture. If not, the deviation should be negligible.
- The resulting GMM should maintain, within some acceptable limits, the structure of the original mixture.

These requirements may not all be achieved with one single algorithm but it is possible to choose one algorithm or a mixture of algorithms that can achieve most of the requirements listed above.

The approach based on merging pairs of components is the simplest method to reduce Gaussian mixture components. The algorithm starts with $g_Y(y) = f_Y(y)$. The merging is applied to the pair of components of $g_Y(y)$ that when merged produce the minimum discrepancy between $f_Y(y)$ and $g_Y(y)$ [54], [55].

Once the pair of components i and j are identified, they are merged together to obtain a new resulting component ij with the following component parameters [55]:

$$\tilde{\omega}_{ij} = \tilde{\omega}_i + \tilde{\omega}_j \tag{3.8}$$

The mean and variance of the new Gaussian component is:

$$\tilde{\mu}_{ij} = \frac{1}{\tilde{\omega}_i + \tilde{\omega}_j}\left(\tilde{\omega}_i\tilde{\mu}_i + \tilde{\omega}_j\tilde{\mu}_j\right) \tag{3.9}$$

$$\tilde{\sigma}_{ij}^2 = \frac{1}{\tilde{\omega}_i + \tilde{\omega}_j}\left(\tilde{\omega}_i\tilde{\sigma}_i^2 + \tilde{\omega}_j\tilde{\sigma}_j^2 + \frac{\tilde{\omega}_i\tilde{\omega}_j}{\tilde{\omega}_i + \tilde{\omega}_j}(\tilde{\mu}_i - \tilde{\mu}_j)^2\right) \tag{3.10}$$

The new component ij replaces the i-th and j-th components previously identified. Consequently, $g_Y(y)$ loses one component but keeps the mean and variance of the original mixture. This procedure is repeated until the desired number of components is reached.

The identification of the i-th and j-th components of $g_Y(y)$ depends on the selection criteria. The Salmond method identifies the pair of components i and j that produce the minimum increase of the first summand in (3.5) [56]. The increase of the first summand in (3.5) is related to the Square Distance (SD) measure:

$$d_{ij}^2 = \frac{\tilde{\omega}_i \tilde{\omega}_j}{\tilde{\omega}_i + \tilde{\omega}_j} \cdot \frac{(\tilde{\mu}_i - \tilde{\mu}_j)^2}{\sigma_Y^2} \tag{3.11}$$

The smallest squared distance identifies the merged components i and j that produce the minimum value of the cost function. The main disadvantage of this methodology is that it merges the pair of components with the closest means even if their variances are very different [55].

The Williams method identifies the pair of components to be merged that produce the minimum difference between the original $f_Y(y)$ and the reduced Gaussian mixture $g_Y(y)$. In order to evaluate this difference, the Integral Square Difference (ISD) between the original and the reduced mixture is introduced [54]:

$$J_s = \int \left(f_Y(y) - g_Y(y) \right)^2 dy\,. \tag{3.12}$$

The ISD is calculated for all combinations of pairs of components of $g_Y(y)$. The minimum J_s identifies the components i and j to be merged. This procedure is repeated until $g_Y(y)$ is reduced to the desire number of components. The ISD defined in (3.12) can be extended as:

$$J_s = \int f_Y(y)^2 dy - 2\int f_Y(y) \cdot g_Y(y) dy + \int g_Y(y)^2 dy\,, \tag{3.13}$$

or in more compact form,

$$J_s = J_{sff} - 2 \cdot J_{sfg} + J_{sgg}\,, \tag{3.14}$$

with,

$$J_{sff} = \int f_Y(y)^2 dy\,;\; J_{sfg} = \int f_Y(y) \cdot g_Y(y) dy\,;\; J_{sgg} = \int g_Y(y)^2 dy\,. \tag{3.15}$$

By using (3.1) and (3.7) in (3.15) one obtains:

$$J_{sff} = \sum_{i=1}^{L} \sum_{j=1}^{L} \omega_i \omega_j \int f_{N(\mu_i, \sigma_i^2)}(y) \cdot f_{N(\mu_j, \sigma_j^2)}(y) dy\,, \tag{3.16}$$

$$J_{sfg} = \sum_{i=1}^{L} \sum_{j=1}^{M} \omega_i \tilde{\omega}_j \int f_{N(\mu_i, \sigma_i^2)}(y) \cdot f_{N(\tilde{\mu}_j, \tilde{\sigma}_j^2)}(y) dy\,, \tag{3.17}$$

$$J_{sgg} = \sum_{i=1}^{M} \sum_{j=1}^{M} \tilde{\omega}_i \tilde{\omega}_j \int f_{N(\tilde{\mu}_i, \tilde{\sigma}_i^2)}(y) \cdot f_{N(\tilde{\mu}_j, \tilde{\sigma}_j^2)}(y) dy\,. \tag{3.18}$$

The problem is now reduced to evaluate the integrals of the products of two Gaussian densities. As presented in [54], the product of two Gaussian densities $f_{N(\mu_1,\sigma_1^2)}(y)$ and $f_{N(\mu_2,\sigma_2^2)}(y)$ is a Gaussian density $f_{N(\mu_3,\sigma_3^2)}(y)$ multiplied by a scale factor α:

$$f_{N(\mu_1,\sigma_1^2)}(y)\cdot f_{N(\mu_2,\sigma_2^2)}(y)=\alpha\cdot f_{N(\mu_3,\sigma_3^2)}(y) \tag{3.19}$$

where,

$$\alpha=f_{N(\mu_2,\sigma_1^2+\sigma_2^2)}(\mu_1)\,, \tag{3.20}$$

$$\sigma_3^2=(1/\sigma_1^2+1/\sigma_2^2)^{-1}\,, \tag{3.21}$$

$$\mu_3=\sigma_3^2(\mu_1/\sigma_1^2+\mu_2/\sigma_2^2)\,, \tag{3.22}$$

Applying (3.19) in each of the integrals in (3.16)-(3.18), and knowing that the integral of the resulting Gaussian density is unity, the ISD terms become:

$$J_{sff}=\sum_{i=1}^{L}\sum_{j=1}^{L}\omega_i\omega_j f_{N(\mu_j,\sigma_i^2+\sigma_j^2)}(\mu_i)\,, \tag{3.23}$$

$$J_{sfg}=\sum_{i=1}^{L}\sum_{j=1}^{M}\omega_i\tilde{\omega}_j f_{N(\tilde{\mu}_j,\sigma_i^2+\tilde{\sigma}_j^2)}(\mu_i)\,, \tag{3.24}$$

$$J_{sgg}=\sum_{i=1}^{M}\sum_{j=1}^{M}\tilde{\omega}_i\tilde{\omega}_j f_{N(\tilde{\mu}_j,\tilde{\sigma}_i^2+\tilde{\sigma}_j^2)}(\tilde{\mu}_i)\,. \tag{3.25}$$

The ISD selection method takes into account the entire Gaussian mixture to decide which components to merge. However, it is more time consuming than the Salmond method, as more calculations are required.

An alternative measure of similarity between two probability densities $f_1(y)$ and $f_2(y)$ is the Kullback-Leibler (KL) divergence $D(f_1 \| f_2)$ [55] :

$$D(f_1\|f_2)=\int f_1(y)\log\frac{f_1(y)}{f_2(y)}dy \tag{3.26}$$

Contrary to the ISD measure, there is no closed form expression for the KL divergence measure when $f_1(y)$ and $f_2(y)$ are Gaussian mixtures. Because of this limitation, an upper bound on the discrepancy of the reduced mixture from the mixture before the merge was proposed in [55]. The upper bound measure of discrepancy is:

$$B_{ij} = \frac{\tilde{\omega}_i + \tilde{\omega}_j}{2} \cdot \log\left[\tilde{\omega}_{i|ij} \left(\frac{\tilde{\sigma}_i^2}{\tilde{\sigma}_j^2} \right)^{\tilde{\omega}_{j|ij}} + \tilde{\omega}_{j|ij} \left(\frac{\tilde{\sigma}_j^2}{\tilde{\sigma}_i^2} \right)^{\tilde{\omega}_{i|ij}} + \tilde{\omega}_{i|ij} \cdot \tilde{\omega}_{j|ij} \frac{(\tilde{\mu}_i - \tilde{\mu}_j)^2}{\tilde{\sigma}_i^{2\tilde{\omega}_{i|ij}} \tilde{\sigma}_j^{2\tilde{\omega}_{j|ij}}} \right] \tag{3.27}$$

where

$$\tilde{\omega}_{i|ij} = \frac{\tilde{\omega}_i}{\tilde{\omega}_i + \tilde{\omega}_j}; \quad \tilde{\omega}_{j|ij} = \frac{\tilde{\omega}_j}{\tilde{\omega}_i + \tilde{\omega}_j}. \tag{3.28}$$

This KL based selection method identifies the merged components i and j that produce the minimum upper bound discrepancy between the mixture after the merge and the mixture before the merge. Equation (3.27) takes into account the means, weights, and variances of the Gaussian components. In addition, it requires fewer computations than the ISD based method.

In order to demonstrate the performance of the reduction methods presented above, the seven-component Gaussian mixture in Figure 3.1 is approximated by five, four, and three component mixtures, as presented in Figures 3.5, 3.6, and 3.7, respectively. The merged components were selected from the SD, the ISD, and the KL upper bound measures.

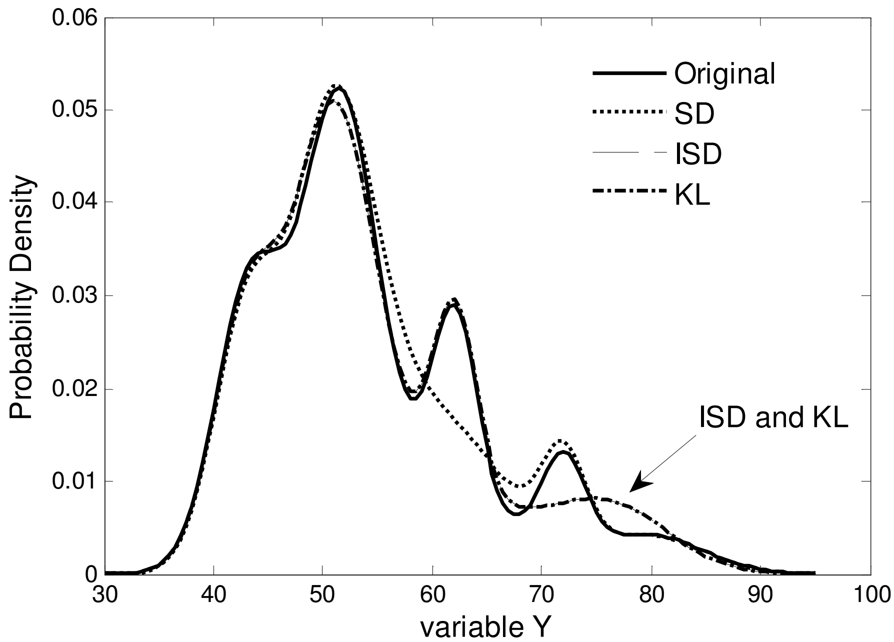

Figure 3.5: GMM reduction using five components

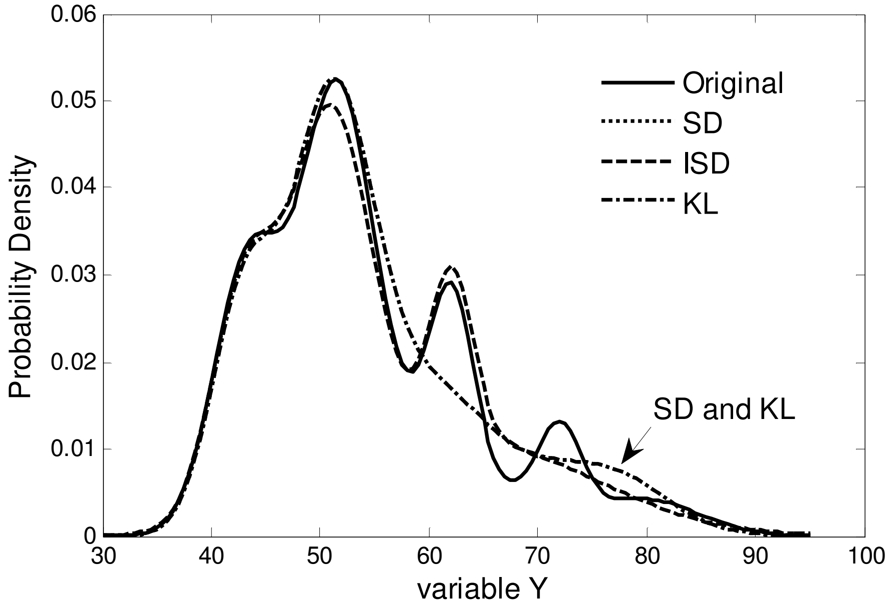

Figure 3.6: GMM reduction using four components

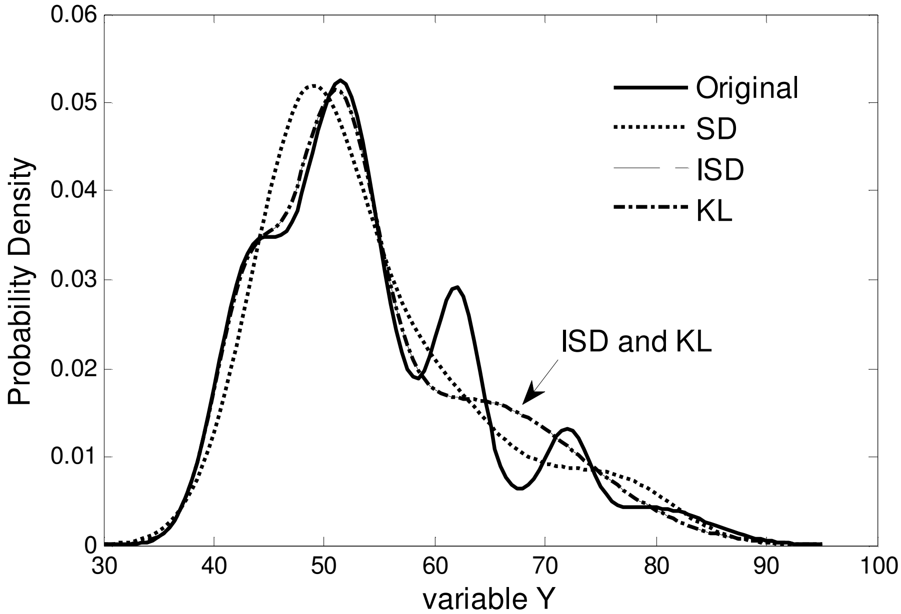

Figure 3.7: GMM reduction using three components

As it is presented in Figure 3.5, the reduced Gaussian mixture obtained from the ISD measure is the same as the resulting Gaussian mixture obtained from the KL upper bound measure. If the original Gaussian mixture is approximated by four Gaussian components, as presented in Figure 3.6, the SD and the KL upper bound selection methods obtained the same reduced distribution.

As it is presented in Figure 3.7, the reduced mixture obtained from the ISD and the KL upper bound discrimination methods are the same. Although it is possible to visualise the resulting Gaussian mixtures from Figures 3.5 to 3.7, the methods have not been quantitatively compared against each other. The ISD is now used to compare the accuracy of the approximations. For comparison purposes, it is convenient to normalise J_s into $0 \leq J_s^N \leq 1$, as follows [57]:

$$J_s^N = \frac{\int \left(f_Y(y) - g_Y(y) \right)^2 dy}{\int f_Y(y)^2 dy + \int g_Y(y)^2 dy}. \tag{3.29}$$

Equations (3.23) to (3.25) are used to evaluate J_s^N. A value of $J_s^N = 0$ means that the reduced Gaussian mixture density perfectly matches the original density whereas $J_s^N = 1$ indicates zero overlapping of the densities.

Table 3.2 presents the comparison of the J_s^N for reduced components with M components obtained by merging pairs of components based on the SD, ISD, and KL upper bound measures. When fewer components are used to model the original density $f_Y(y)$, the approximation becomes less accurate and J_s^N becomes closer to 1.

Table 3.2: J_s^N for resulting $g_Y(y)$ and the original mixture $f_Y(y)$

Method	$M = 6$	$M = 5$	$M = 4$	$M = 3$	$M = 2$	$M = 1$
SD	6.93E-04	0.0094	0.0106	0.0201	0.0231	0.0589
ISD	***6.93E-04***	***0.0027***	***0.0039***	***0.0118***	***0.0231***	***0.0589***
KL	6.93E-04	0.0027	0.0106	0.0118	0.0231	0.0589

As it is presented in Table 3.2, the minimum J_s^N is always obtained when the ISD discrimination measured is used. It is important to mention that the KL upper bound measure selected the same pair of components to merge as the ISD measure did, but excepted when $M = 4$.

Table 3.3 presents the computation times required by the three algorithms. For all the reductions, the KL upper bound discrimination method required less time to find the pair of components to merge, which is the opposite of the ISD method.

The higher processing times of the ISD measure can be a constraint if the number of components is large e.g. 100 components reduced into 25 components. In this case, the KL upper bound algorithm will be much more efficient.

Table 3.3: Comparison of computer time requirements

Method	$M = 6$	$M = 5$	$M = 4$	$M = 3$	$M = 2$	$M = 1$
SD	1.72E-02	0.021953	0.021861	0.020796	0.020154	0.021869
ISD	*4.63E-02*	*0.070542*	*0.079429*	*0.085214*	*0.087209*	*0.090478*
KL	**1.14E-02**	**0.014359**	**0.014363**	**0.014214**	**0.013905**	**0.013639**

Although pair-merging algorithms are very easy to execute and they always maintain the mean and variance of the original mixture, the structure of the resulting mixture may be different with respect to the original density. Furthermore, the resulting component parameters are not necessarily the optimum parameters that best fit the original mixture.

3.2.1 Fine Tuning of GMM Reductions

The resulting parameters obtained from pair-merging methods can be fine tuned to better approximate the original Gaussian mixture [58]. The objective is to correct the set of parameters η of $g_Y(y)$ such that it minimises the ISD cost function, defined in (3.12), as a function of η:

$$J_s(y,\eta) = \int \left(f_Y(y) - g_Y(y,\eta) \right)^2 dy \tag{3.30}$$

where,

$$g_Y(y,\eta) = \sum_{j=1}^{M} \tilde{\omega}_j^2 f_{N(\tilde{\mu}_j, \tilde{\sigma}_j^2)}(y) \tag{3.31}$$

$$\eta = \begin{bmatrix} \eta_1^T & \eta_2^T & \cdots & \eta_M^T \end{bmatrix}^T \tag{3.32}$$

$$\eta_j = \begin{bmatrix} \tilde{\omega}_j & \tilde{\mu}_j & \tilde{\sigma}_j \end{bmatrix}^T \quad \forall\ j = 1,\ldots,M \tag{3.33}$$

The squared term $\tilde{\omega}_j^2$ in (3.31) is used to guarantee positive proportion components [59] . This is, $0 < \tilde{\omega}_j^2 \le 1$. By perturbing $\eta = \overline{\eta} + \Delta\eta$ around the initial point $\overline{\eta}$ and considering only the linear term of the Taylor's series [58]:

$$J_s(y,\eta) = \int \left(f_Y(y) - g_Y(y,\overline{\eta}) - \left(\frac{\partial g_Y(y,\overline{\eta})}{\partial \eta} \right)^T (\eta - \overline{\eta}) \right)^2 dy\,, \tag{3.34}$$

it is possible to find the optimal set of parameters η when the first derivative of (3.34) with respect to η is equal to zero:

$$\underbrace{\int \left(f_Y(y) - g_Y(y,\overline{\eta})\right)\frac{\partial g_Y(y,\overline{\eta})}{\partial \eta}dy}_{\mathbf{h}(\overline{\eta})} = \underbrace{\int \frac{\partial g_Y(y,\overline{\eta})}{\partial \eta}\left(\frac{\partial g_Y(y,\overline{\eta})}{\partial \eta}\right)^T dy}_{\mathbf{P}(\overline{\eta})} \cdot \underbrace{(\eta - \overline{\eta})}_{\Delta\eta} \tag{3.35}$$

Or in more compact form:

$$\mathbf{h}(\overline{\eta}) = \mathbf{P}(\overline{\eta})\Delta\eta\,. \tag{3.36}$$

The gradient vector $\mathbf{h}(\cdot)$ contains M sub-vectors. Each 3x1 sub-vector $\mathbf{h}_j(\cdot)$ corresponds to one η_j, as follows:

$$\mathbf{h}_j(\overline{\eta}) = \int \left(f_Y(y) - g_Y(y,\overline{\eta})\right)\frac{\partial g_Y(y,\overline{\eta})}{\partial \eta_j}dy\,. \tag{3.37}$$

After the partial derivative calculation, the sub-vector $\mathbf{h}_j(\cdot)$ can be expressed by [59]:

$$\mathbf{h}_j(\overline{\eta}) = \int \left(f_Y(y) - g_Y(y,\overline{\eta})\right)\cdot g_j(y,\overline{\eta}_j)\begin{bmatrix} \dfrac{2}{\tilde{\omega}_j} \\ \dfrac{y-\tilde{\mu}_j}{\tilde{\sigma}_j^2} \\ \dfrac{(y-\tilde{\mu}_j)^2 - \tilde{\sigma}_j^2}{\tilde{\sigma}_j^3} \end{bmatrix} dy, \tag{3.38}$$

with $g_j(y,\overline{\eta}_j) = \tilde{\omega}_j^2 \cdot f_{N(\tilde{\mu}_j,\tilde{\sigma}_j^2)}(y)$. The closed form solution of (3.38) is presented in Appendix C.1.

Returning to the linear equation in (3.36), matrix $\mathbf{P}(\cdot)$ is:

$$\mathbf{P}(\overline{\eta}) = \begin{bmatrix} \mathbf{P}^{(1,1)} & \cdots & \mathbf{P}^{(1,M)} \\ \vdots & \ddots & \vdots \\ \mathbf{P}^{(M,1)} & \cdots & \mathbf{P}^{(M,M)} \end{bmatrix} \tag{3.39}$$

Each sub-matrix $\mathbf{P}^{(i,j)}$ in (3.39) is defined by:

$$\mathbf{P}^{(i,j)} = \tilde{\omega}_i\tilde{\omega}_j f_{N(\tilde{\mu}_j,\tilde{\sigma}_i^2+\tilde{\sigma}_j^2)}(\tilde{\mu}_i)\begin{bmatrix} \mathbf{P}_{1,1}^{(i,j)} & \mathbf{P}_{1,2}^{(i,j)} & \mathbf{P}_{1,3}^{(i,j)} \\ \mathbf{P}_{2,1}^{(i,j)} & \mathbf{P}_{2,2}^{(i,j)} & \mathbf{P}_{2,3}^{(i,j)} \\ \mathbf{P}_{3,1}^{(i,j)} & \mathbf{P}_{3,2}^{(i,j)} & \mathbf{P}_{3,3}^{(i,j)} \end{bmatrix}, \tag{3.40}$$

and each of the elements in (3.40) is presented in the Appendix C.2.

The set of linear equations in (3.36) is solved by LU decomposition of $\mathbf{P}$ and $\Delta\eta$ is solved using forward and backward substitution. At the *k*-th iteration, the new set of parameters is obtained by:

$$\eta^{k+1} = \eta^k + \Delta\eta \tag{3.41}$$

The iterations stop when $\Delta\eta$ is lower than a pre-defined threshold. The weights of the resulting optimised $g_Y(y)$ are corrected to ensure the characteristics presented in (3.2):

$$\tilde{\omega}_j^{2'} = \tilde{\omega}_j^2 \Big/ \sum_{j=1}^{M} \tilde{\omega}_j^2 \tag{3.42}$$

If the initial set of parameters η^0 is not close to the optimal solution, the iterative procedure may converge to a local minimum or may not converge at all. A good initial guess is the solution obtained from the pair merging algorithms presented above in Section 3.2.

The optimisation method always improves the approximations obtained from the pair merging methods but it is not possible to guarantee that the solution corresponds to the global minimum.

Figure 3.8 presents the optimal based reduction method compared to the original GMM. The ISD reduction method was used to calculate the initial set of parameters η^0. The new reduction is more accurate and therefore closer to the original GMM.

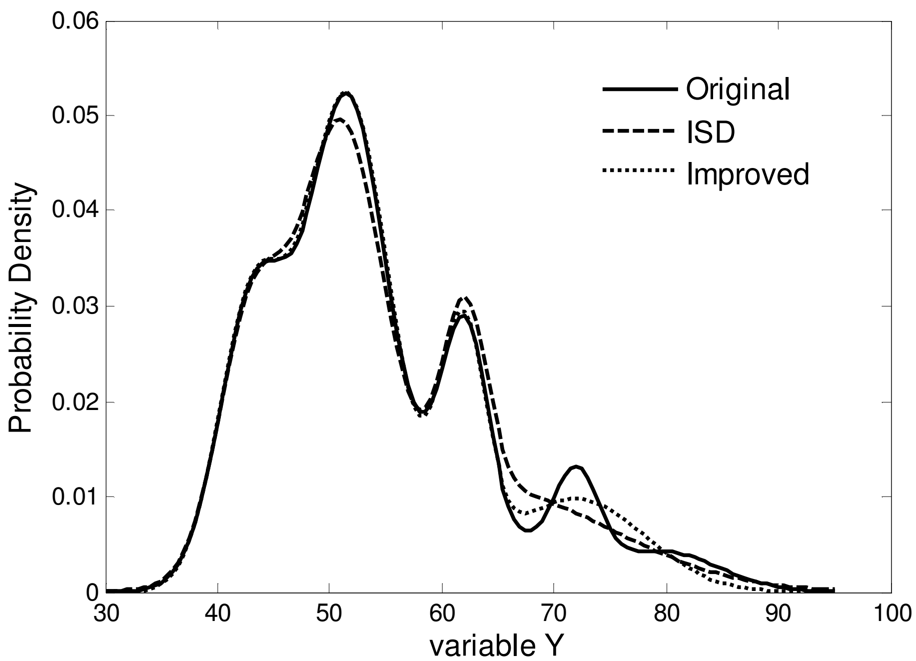

Figure 3.8: Original GMM reduced to four components using the optimal based method

Table 3.4 presents the J_s^N before and after the fine tuning of the Gaussian mixture reduction.

Table 3.4: J_s^N for the resulting improved $g_Y(y)$ and the original mixture $f_Y(y)$

Method	$M = 6$	$M = 5$	$M = 4$	$M = 3$	$M = 2$	$M = 1$
ISD	*6.93E-04*	*0.0027*	*0.0039*	*0.0118*	*0.0231*	*0.0589*
Improved	8.59E-07	**0.0011**	**0.0011**	0.0085	0.0187	0.0321

For all reductions, the approximation was improved. In the case where $M = 5$, the optimisation method reduced M to four components. Such elimination is performed when the ratio $\tilde{\omega}_j^2 / \tilde{\sigma}_j^2$ of component j tends to zero [59]. This is the reason why J_s^N for $M = 5$ and $M = 4$ are the same.

3.3 Probabilistic Load Flows

The inputs of probabilistic load flows studies are the PDFs of:

1. Active and reactive power injections in PQ buses,
2. Active power injection and voltage magnitude in PV buses, and
3. Voltage magnitude in the slack bus.

A typical Probabilistic Load Flow (PLF) problem is represented in Figure 3.9. Given the PDFs of power injections and voltage magnitudes, the operating points of all bus voltages and power flows in all transmission lines are determined by means of statistical studies. As explained before, the GMM density function can be used to approximate any non-Gaussian PDF.

This Section presents two methodologies to run probabilistic studies. The first is based on Monte Carlo Simulations (MCS), which is considered a benchmark method for probabilistic studies. The second is an alternative formulation able to reduce the computational demands of the MCS.

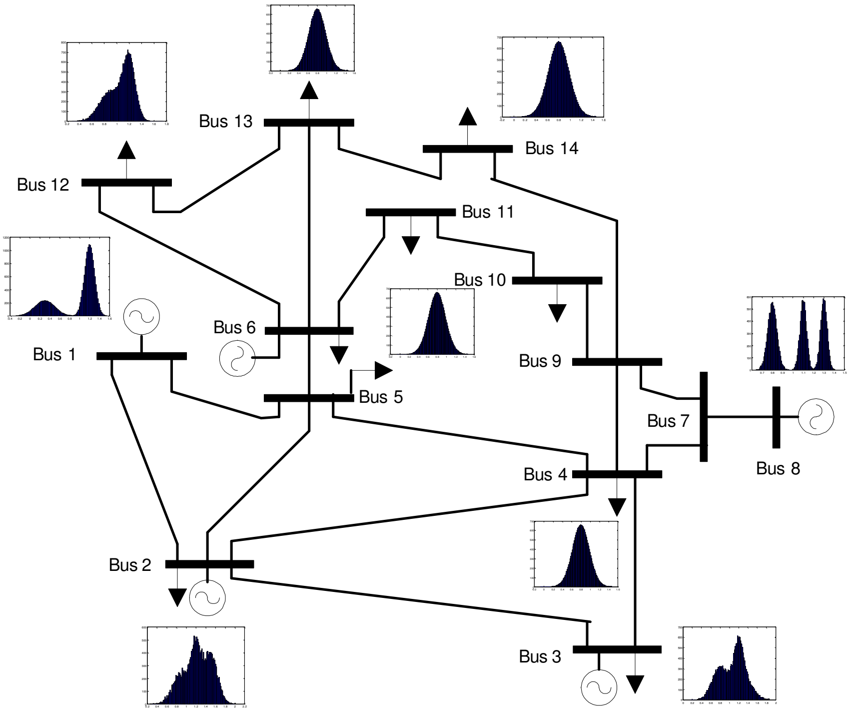

Figure 3.9: PLF problem with non-Gaussian PDFs

3.3.1 PLF using Monte Carlo Simulations

In order to run Monte Carlo simulations, it is necessary to generate samples of each random variable for each Monte Carlo trial.

Well distributed samples of Uniform random variables can be obtained from quasi-random sequence generators, such as the *Niederreiter*, the *Halton,* and the *Sobol* generators [60], [61]. Better distributed samples of random variables make it possible to reduce the number of trials of the Monte Carlo simulations.

3.3.1.1 Generation of Samples from Correlated Variables

The correlation coefficient between pairs of input variables must be known *a priori* from the original set of observations. For each pair of variables Y_1 and Y_2, the correlation coefficient is obtained from [51]:

$$\rho_{Y_1,Y_2} = \mathrm{corr}(Y_1, Y_2) = \frac{\mathrm{cov}(Y_1, Y_2)}{\sigma_{Y1}\sigma_{Y2}} = \frac{E\left[(Y_1 - \mu_{Y_1})(Y_2 - \mu_{Y_2})\right]}{\sigma_{Y1}\sigma_{Y2}}, \tag{3.43}$$

where μ_{Yi} and σ_{Yi} are the mean and standard deviation of variable Y_i and E is the expectation operator.

Since the quasi-random sequence generator creates N_s samples of non-correlated Uniform random variables, it is necessary to transform them into a set of variables with correlation coefficients determined using (3.43). This transformation is carried out in the Gaussian domain.

The N_s samples for each of the d Uniform variables are grouped into the set of vectors $\mathbf{u} = [\mathbf{u}_1, \dots, \mathbf{u}_i, \dots, \mathbf{u}_d]$ and they are converted into Gaussian random samples by using the inverse of the CDF of the Gaussian distribution [2], [62]:

$$\mathbf{v}_i = F_v^{-1}(\mathbf{u}_i), \quad i = 1, \dots, d, \tag{3.44}$$

where F_v stands for the CDF of the Standard Normal distribution. This results in N_s samples for each of the d Gaussian variables $\mathbf{v} = [\mathbf{v}_1, \dots, \mathbf{v}_i, \dots, \mathbf{v}_d]$, which are still not correlated.

The desired correlation matrix $\mathbf{\Sigma}$ must be corrected to account for the transformation from Gaussian to Uniform distributions. Each non-diagonal element of the $d \times d$ correlation matrix $\mathbf{\Sigma}$ is corrected by [62]:

$$\rho_{ij}^N = 2\sin\left(\frac{\pi}{6}\rho_{ij}\right), \tag{3.45}$$

where ρ_{ij} is the desired correlation coefficient between variables i and j and ρ_{ij}^N is the adjusted coefficient to account for the transformation. This creates a new $d \times d$ correlation matrix $\mathbf{\Sigma}^N$. The correlated Gaussian variables are then obtained through the Cholesky decomposition of $\mathbf{\Sigma}^N$ [2]:

$$\mathbf{v}^{corr} = \mathbf{v}\ \mathrm{chol}(\mathbf{\Sigma}^N) \tag{3.46}$$

where $\mathrm{chol}(\mathbf{\Sigma}^N)$ is the upper triangular matrix obtained from the decomposition of $\mathbf{\Sigma}^N$. The samples of the correlated Gaussian variables are transformed back into Uniform samples by using the CDF of the Gaussian distribution:

$$\mathbf{u}_i^{corr} = F_v(\mathbf{v}_i^{corr}), \quad i = 1, \dots, d. \tag{3.47}$$

Finally, the samples of correlated variables with any marginal distribution are obtained from the inverse CDF of the corresponding distribution:

$$\mathbf{y}_i^{corr} = F_Y^{-1}(\mathbf{u}_i^{corr}), \quad i = 1, ..., d. \tag{3.48}$$

where F_Y is the CDF of the GMM, as stated in (3.6). Some deviations from the desired correlation matrix are caused by the non-linear transformation of samples to different distributions.

Consider the case where it is necessary to create N_s=5000 samples from $d = 4$ GMMs that represent the active power consumptions at four different buses. Their parameters are presented in Table 3.5.

Table 3.5: GMM parameters of variables to be correlated

	GMM1				GMM2		
	ω_i	μ_i	σ_i^2		ω_i	μ_i	σ_i^2
i=1	0.7	0.5	0.05	*i*=1	0.5	0.9	0.03
i=2	0.3	1	0.07	*i*=2	0.5	1.2	0.01
	GMM3				GMM4		
	ω_i	μ_i	σ_i^2		ω_i	μ_i	σ_i^2
i=1	0.4	0.8	0.02	*i*=1	0.3	0.9	0.03
i=2	0.3	1.1	0.01	*i*=2	0.3	1.2	0.01
i=3	0.3	1.3	0.01	*i*=3	0.4	1.5	0.02

The correlation matrix of the active power injections at those buses is:

$$\Sigma = \begin{bmatrix} 1.0 & 0.7 & 0.4 & 0.6 \\ 0.7 & 1.0 & 0.8 & 0.5 \\ 0.4 & 0.8 & 1.0 & 0.1 \\ 0.6 & 0.5 & 0.1 & 1.0 \end{bmatrix}.$$

The first step is to create the N_s samples of four Uniform random variables. These samples are transformed into samples of Gaussian variables through the inverse CDF. At this point, the samples are uncorrelated and the correlation matrix of the new Gaussian variables is the Identity matrix.

Due to the transformation of samples, the desired correlation matrix $\mathbf{\Sigma}$ is updated by the correction factor given in (3.45):

$$\Sigma^N = \begin{bmatrix} 1.0000 & 0.7331 & 0.4320 & 0.6360 \\ 0.7331 & 1.0000 & 0.8263 & 0.5355 \\ 0.4320 & 0.8263 & 1.0000 & 0.1096 \\ 0.6360 & 0.5355 & 0.1096 & 1.0000 \end{bmatrix}.$$

The samples of Gaussian variables are obtained using (3.46). The resulting correlation matrix for these new variables is:

$$\Sigma^N_{obtained} = \begin{bmatrix} 1.0000 & 0.7330 & 0.4318 & 0.6364 \\ 0.7330 & 1.0000 & 0.8263 & 0.5365 \\ 0.4318 & 0.8263 & 1.0000 & 0.1109 \\ 0.6364 & 0.5365 & 0.1109 & 1.0000 \end{bmatrix}.$$

Subsequently, these samples are transformed back to Uniform distributions using (3.47). The correlation matrix of the Uniform variables is:

$$\Sigma_U = \begin{bmatrix} 1.0000 & 0.7170 & 0.4157 & 0.6176 \\ 0.7170 & 1.0000 & 0.8132 & 0.5180 \\ 0.4157 & 0.8132 & 1.0000 & 0.1048 \\ 0.6176 & 0.5180 & 0.1048 & 1.0000 \end{bmatrix}$$

Finally, the samples of the GMMs are obtained using (3.48). The resulting correlation matrix of the GMM variables is:

$$\Sigma_{GMM} = \begin{bmatrix} 1.0000 & 0.7074 & 0.4225 & 0.6248 \\ 0.7074 & 1.0000 & 0.8171 & 0.5282 \\ 0.4225 & 0.8171 & 1.0000 & 0.1085 \\ 0.6248 & 0.5282 & 0.1085 & 1.0000 \end{bmatrix}$$

Some corrections, valid for certain conditions, can be executed to reduce the errors in the resulting correlation matrix [2], [63].

Figure 3.10 presents the scatter plots of the variables for N_s= 5000 samples. The generated samples are such that the correlation matrix is Σ_{GMM} .

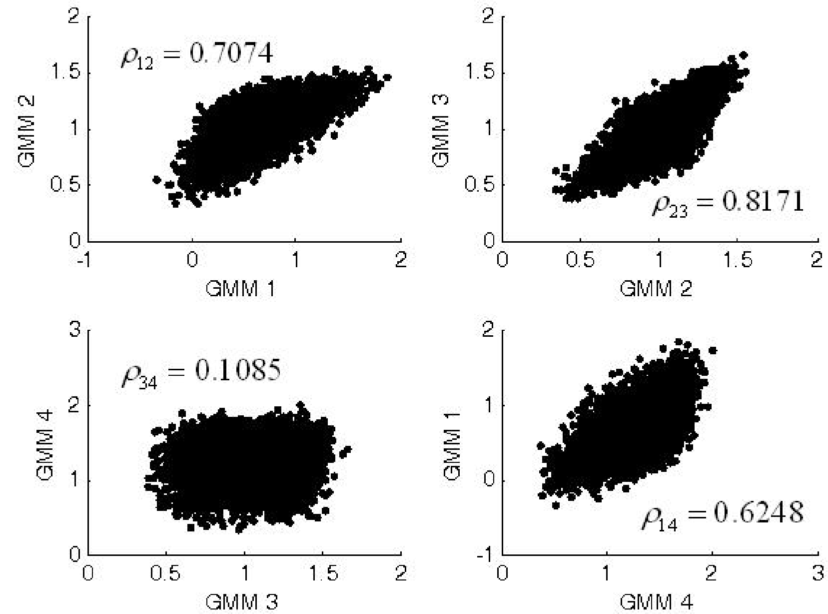

Figure 3.10: Scatter plot of resulting samples

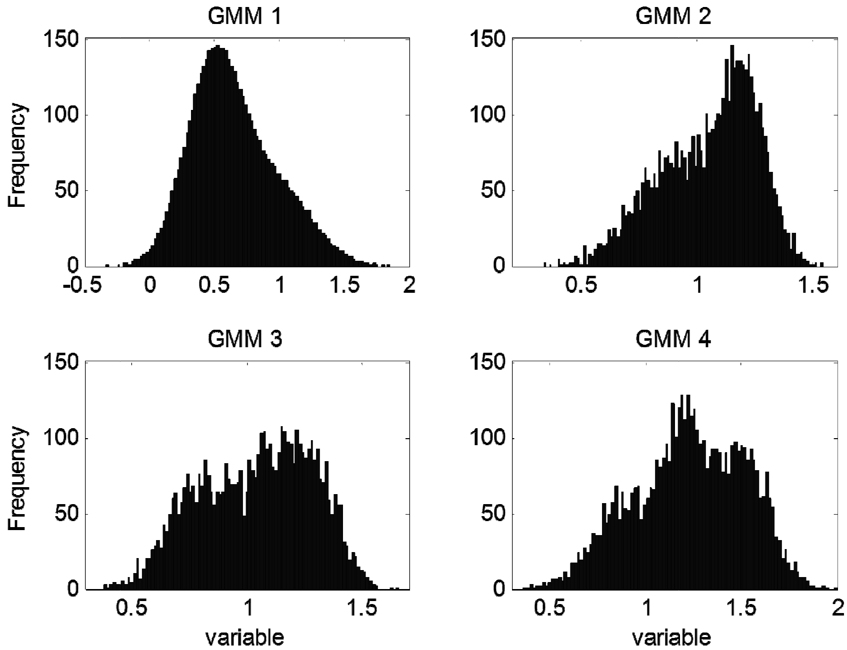

Figure 3.11: Histogram of resulting samples

Figure 3.11 presents the histogram for the correlated variables with 5000 samples. The histograms of GMM 2, 3, and 4 are significantly irregular compared to the GMM 1 that is not affected by the transformation of samples. However, these irregularities are reduced by increasing the number of samples for each GMM.

For comparison purposes, Table 3.6 presents the estimated GMM parameters from the generated samples (using the *EM* algorithm). From these results, it is concluded that the generated correlated samples follow the distribution of the desired GMM presented in Table 3.5.

Table 3.6: Estimated GMM parameters of correlated variables

GMM1				GMM2			
	ω_i	μ_i	σ_i^2		ω_i	μ_i	σ_i^2
i=1	0.68	0.49	0.049	i=1	0.5	0.9	0.03
i=2	0.32	0.98	0.073	i=2	0.5	1.2	0.01
GMM3				GMM4			
	ω_i	μ_i	σ_i^2		ω_i	μ_i	σ_i^2
i=1	0.38	0.79	0.019	i=1	0.31	0.91	0.031
i=2	0.35	1.10	0.012	i=2	0.30	1.20	0.010
i=3	0.27	1.31	0.010	i=3	0.39	1.50	0.020

The above methodology is extended to consider all the random input variables of PQ and PV buses in the network. The correlation and marginal distributions of these variables should be determined based on previous statistical studies.

Once the samples of active/reactive power and bus voltage magnitudes are generated, a power flow run is executed for each set of samples, as presented in Figure 3.12. The number of power flows trials is equal to the number of samples (N_s) of the input variables.

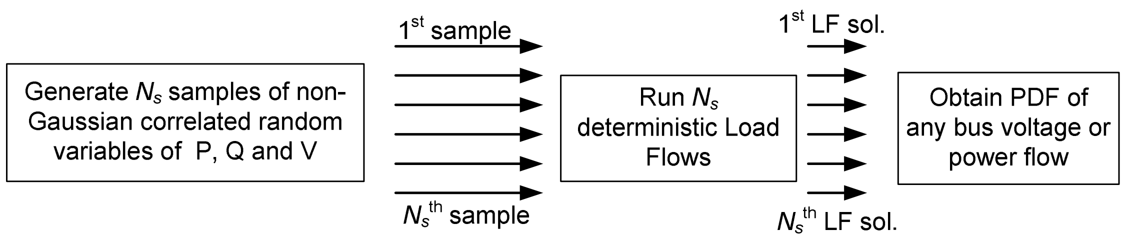

Figure 3.12: Diagram of probabilistic load flows using MCS

The resulting PDFs of bus voltages, power flows, and power injections can be used to determine means, variances, and other higher statistical moments.

3.3.2 PLF using Gaussian Component Combinations

Taking into consideration that any PDF can be approximated by GMMs, the probabilistic load flow problem can be solved by executing multiple WLS runs. Each WLS run takes a combination of Gaussian components of the GMMs used to model the PDFs of the random input variables. The total number of WLS runs is:

$$N_r = \prod_{i=1}^{N_{PDF}} L_i \,. \tag{3.49}$$

where N_{PDF} stands for the number of PDFs and L_i is the number of Gaussian components of the i-th GMM. If the PDFs were all modelled by Gaussian distributions, i.e. $L_i = 1$ for $i = 1, \ldots, N_{PDF}$, only one WLS run would be necessary to solve the problem, as originally proposed in [7].

Figure 3.13 presents an example of the first possible combination of Gaussian components when the load demands and generator outputs are modelled by GMMs in the 14-bus test system shown in Figure 3.9.

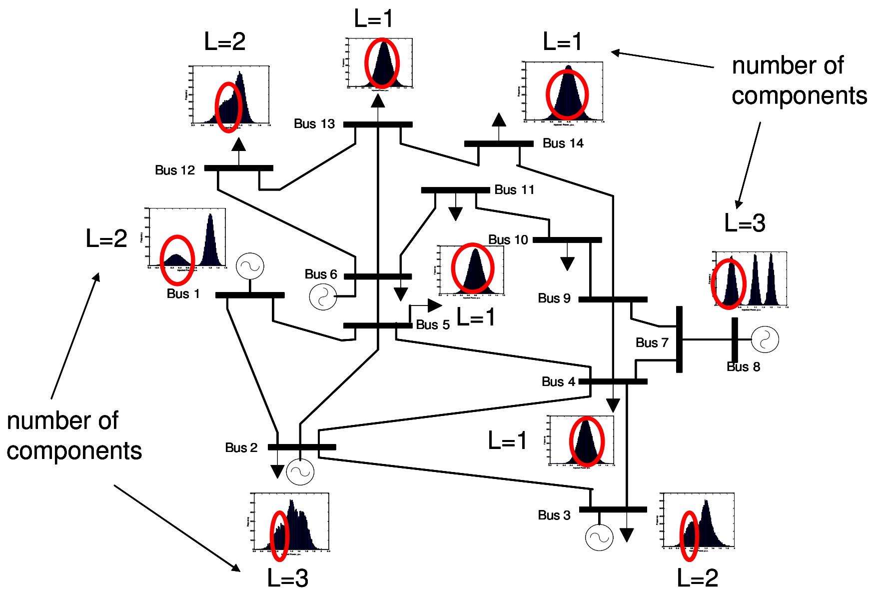

Figure 3.13: Example of a combination of Gaussian components in the GCCM

Let us consider a single combination of Gaussian components extracted from all the GMMs (one Gaussian component for each input variable). The WLS problem is solved iteratively using (2.5). Similarly, as defined in Section 2.1, **x** is the state vector composed by the set of bus voltage magnitudes and angles, $\mathbf{z}$ is the set of input variables, $\mathbf{h}(\mathbf{x})$ is the set of nonlinear equations relating the power system measurements to the state variables, and $\mathbf{R}$ is the error covariance matrix of the input variables $\mathbf{z}$.

The elements of the input set $\mathbf{z}$ and the diagonal elements of matrix $\mathbf{R}$ correspond to the mean values and variances of the Gaussian components used in this combination. The correlation between the input variables is included in the off-diagonal elements of $\mathbf{R}$.

In this formulation, it is assumed that the correlation between Gaussian components that belong to two particular Gaussian mixtures is the same as the correlation between those Gaussian mixtures. Therefore, the off-diagonal element $\mathbf{R}\,(i, j)$ becomes:

$$\mathbf{R}(i, j) = \rho_{ij}\sigma_i\sigma_j \,. \tag{3.50}$$

where $\rho_{ij}\sigma_i\sigma_j$ is the covariance between the i-th and j-th input variables. In addition, $-1 \le \rho \le 1$ and σ stand for correlation coefficient and standard deviation, respectively. This correlation coefficient approximation remains constant for all the WLS runs.

The resulting state vector solution of the WLS run allows the calculation of the voltage, power flow, or power injection of any bus within the system. The inverse of the *Gain Matrix* is the covariance matrix $\mathbf{C}_s$ of the state vector:

$$\mathbf{C}_s = \mathbf{G}(\mathbf{x})^{-1} = \left[\mathbf{H}^T(\mathbf{x})\mathbf{R}^{-1}\mathbf{H}(\mathbf{x})\right]^{-1}, \tag{3.51}$$

and the covariance matrix of the power flows or power injections can be approximated as:

$$\mathbf{C}_{pq} = \mathbf{H}_{pq}(\mathbf{x})\mathbf{C}_s\mathbf{H}_{pq}(\mathbf{x})^T \,, \tag{3.52}$$

where $\mathbf{H}_{pq}$ contains the partial derivatives of transferred powers and power injections with respect to the state vector $\mathbf{x}$. The diagonal elements of the covariance matrices are stored to reconstruct the desired PDFs.

The WLS procedure is repeated for the N_r combinations of Gaussian components. The solution of the i-th WLS run becomes the i-th mean value $\hat{\mu}_i$ of the bus voltages, power flows and power injections. The i-th variance $\hat{\sigma}_i^2$ is obtained from the diagonal elements of (3.51) and (3.52). Finally, the weight of the i-th Gaussian component is the product of all the weights of the Gaussian components involved in the i-th combination:

$$\hat{\omega}_i = \prod_{j=1}^{N_{PDF}} \omega_j \,. \tag{3.53}$$

Therefore, the PDF of any voltage magnitude, voltage angle or power flow is build up by:

$$PDF_{desired} = \sum_{i=1}^{N_r} \hat{\omega}_i f_{N(\hat{\mu}_i, \hat{\sigma}_i^2)}(y) \,, \tag{3.54}$$

with $\sum_{i=1}^{N_r} \hat{\omega}_i = 1$.

The proposed GCCM is summarised as follows:

1. Take one combination of Gaussian mixtures (one Gaussian component for each input variable). The mean value of each Gaussian component corresponds to one element in **z** and the variance of each Gaussian component corresponds to one diagonal element in **R**. If the input variables are correlated, adjust **R** as defined in (3.50).
2. Run the WLS and obtain bus voltages, power flows, and power injections values. Save the diagonal elements of the covariance matrices resulting from (3.51) and (3.52).
3. Calculate the weight of the combination using (3.53).
4. Repeat steps 1 to 3 for all the possible combinations of Gaussian components belonging to different input variables. Finally, build up any PDFs using the N_r Gaussian components, as presented in (3.54).

If the number of combinations N_r is too large, one of the reduction methods presented in Section 3.2 is used to reduce the number of Gaussian components of one or some input variables. This consequently reduces the number of combinations.

3.4 Summary

The variability of renewable generation sources is well-known to be time dependent. Hence, probabilistic load flows are the most suitable studies to take into account the intermittency of renewable generation and the uncertainty of power system demands.

This Chapter presented how the Gaussian Mixture Models (GMM) can be used to represent non-Gaussian input variables with certain degree of correlation between variables. The Chapter also presented two methodologies to run probabilistic load flows: One is based on Monte Carlo simulations and the other is based on multiple WLS runs (GCCM). Both formulations start from the non-Gaussian PDFs of correlated input variables and they obtain the PDFs of any voltage, power flow, or power injection in any bus of the system.

The main advantage of the GCCM with respect to previous methodologies, such as Point Estimate based methods, is that it uses the actual PDFs of the input variables rather than only the first statistical moments. Another feature of this methodology is the inclusion of correlated variables.

The proposed methodology is less computationally demanding than Monte Carlo simulations and it has the advantage that the number of WLS runs can be reduced if fewer components are used to approximate the non-Gaussian PDFs.

Chapter 4 presents simulation tests to validate the accuracy of the proposed method with respect to the Monte Carlo simulations and it also discusses the advantages and limitations of the proposed method for meshed and radial networks.

Chapter 4 Estimation of Probabilistic Load Flows: Simulations

This Chapter compares the Gaussian Component Combination Method (GCCM) with the Monte Carlo Simulations (MCS) to run load flows in the presence of uncertain inputs modelled as non-Gaussian correlated variables represented by Gaussian Mixture Models (GMMs), as introduced in Chapter 3. The comparison of the methods is carried out using two meshed networks (14-buses and 57-buses) and one radial network with 69 buses.

This Chapter is organised as follows: Section 4.1 presents the simulation results for two meshed networks. In this Section, different covariance matrices and Gaussian mixtures are used. The first test system considers non-Gaussian Probability Density Functions (PDFs) of loads whereas in the second test system, it is assumed that all the loads are modelled as Gaussian distributions but the non-Gaussian distributions of the wind farm power outputs are modelled as GMMs. Section 4.2 presents the application of the proposed probabilistic load flow in radial networks. Later, the methodology is extended to solve the state estimation problem in radial distribution networks where only few real-time measurements are available to determine the actual condition of radial networks. Finally, a discussion of results and the Chapter summary are presented in Sections 4.3 and 4.4, respectively.

4.1 Meshed Networks

4.1.1 14-bus IEEE Test System

The 14-bus IEEE test system was used to test the performance of the proposed method. The network configuration, line parameters, and base case solution were taken from [64] and they are listed in Appendix G.1.

Table 4.1 presents the GMM parameters used to model the non-Gaussian PDFs of active power injections (P). Note that only two or three components were used to model the PDFs.

Table 4.1: GMM parameters of the non-Gaussian PDFs of active power injections (*P*) in p.u.

	μ_1	μ_2	μ_3	σ_1	σ_2	σ_3	ω_1	ω_2	ω_3	CV
P2	0.163	0.190	0.210	0.015	0.021	0.025	0.5	0.3	0.2	15%
P3	–0.942	–0.800	–	0.065	0.049	–	0.7	0.3	–	10%
P6	–0.095	–0.110	–	0.003	0.003	–	0.6	0.4	–	8%
P9	–0.250	–0.280	–	0.020	0.030	–	0.5	0.5	–	11%
P13	–0.140	–0.160	–0.130	0.010	0.010	0.007	0.4	0.3	0.3	11%
P14	–0.150	–0.170	–	0.010	0.020	–	0.6	0.4	–	11%

The term *CV* in Table 4.1 stands for the Coefficient of Variation in percentage, defined as the ratio between the standard deviation and the mean value of the random variable [65]. A constant power factor is assumed for *Buses 5*, *9* up to *14*; these values were calculated from [64]. Furthermore, the generation and demand of the remaining buses (not presented in Table 4.1) are assumed to be Gaussian random variables with mean values listed in [64] and $CV = 10$ %.

When applying the Monte Carlo simulations, the number of trials was $N_s = 5000$. This number was found to be sufficient to produce minimum variation of results. In the case of the GCCM, the number of Weighted Least Square (WLS) runs was $N_r = 144$. In this test system, the Gaussian mixture reductions described in Section 3.2 are not considered because the number of components of each GMM is small.

4.1.1.1 Case 1 in 14-bus system

The correlation coefficient between pairs of input variables must be obtained *a priori* using (3.43) with the original set of observations. In this work, the correlation coefficient between variables is assumed to be known as follows:

Due to the assumption of a constant power factor for *Buses 5*, *9* up to *14*, the reactive powers *Q5*, *Q9-Q14* are completely correlated ($\rho = 1.0$) with the active power consumption (*P*) at the same bus. The correlation coefficient between the active power demands *P10*, *P11* and *P12* is $\rho = 0.8$ (Group 1). In addition, the correlation between *P5* and *P6* is $\rho = 0.9$ (Group 2) and the correlation coefficient between Group 1 and Group 2 is $\rho = 0.4$. All other input variables are assumed to be uncorrelated.

The correlated random variables are generated using the Cholesky decomposition of $\mathbf{\Sigma}^N$ for the Monte Carlo Simulations (MCS), see (3.46)-(3.48). In the proposed GCCM, the correlation between input variables at different buses is taken into account in the covariance matrix **R** as presented in (3.50).

The correlation coefficient between P and Q at the same bus is also considered in **R** and it is kept constant for all the combinations of Gaussian components. In addition, when the load power factor is assumed to be constant, the mean and standard deviation of the Gaussian component, representing the reactive power demand, are respectively:

$$\mu_Q = \mu_P \tan(\phi) \tag{4.1}$$

$$\sigma_Q = \sigma_P \tan(\phi) \tag{4.2}$$

where μ_P is the mean value and σ_P is the standard deviation of the Gaussian component of active power and ϕ is the power factor angle.

Figures 4.1-4.2 present the PDFs of active and reactive power flows from *Bus 2* to *Bus 3*. The resulting PDFs are clearly non-Gaussian and they cannot be represented by any other typical marginal distribution.

From the resulting PDFs for all buses and power flows, it is concluded that the GCCM approximates very well the results of 5000 Monte Carlo trials but with only 144 WLS runs. The assumption of using the same correlation coefficient for all the Gaussian component combinations is valid in this case.

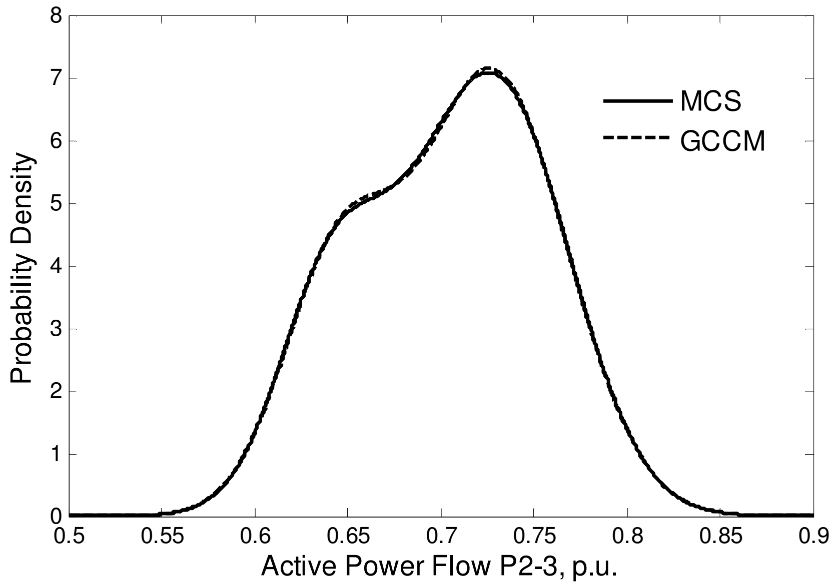

Figure 4.1: PDF of active power flow from Bus 2 to Bus 3 (case 1).

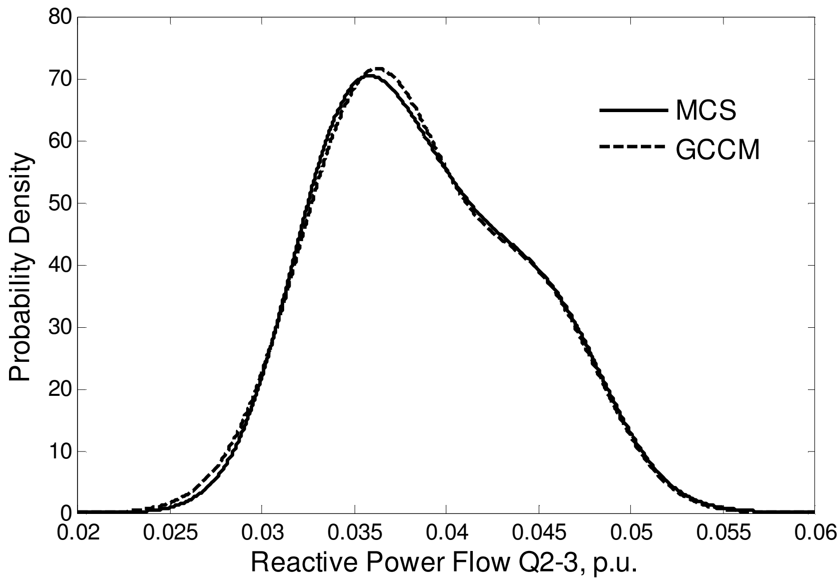

Figure 4.2: PDF of reactive power flow from Bus 2 to Bus 3 (case 1).

Figures 4.3 and 4.4 present the PDFs of the active and reactive power flows from *Bus 9* to *Bus 14*. Similar as before, the PDFs obtained from the GCCM approximate very well the PDFs obtained from the Monte Carlo simulations.

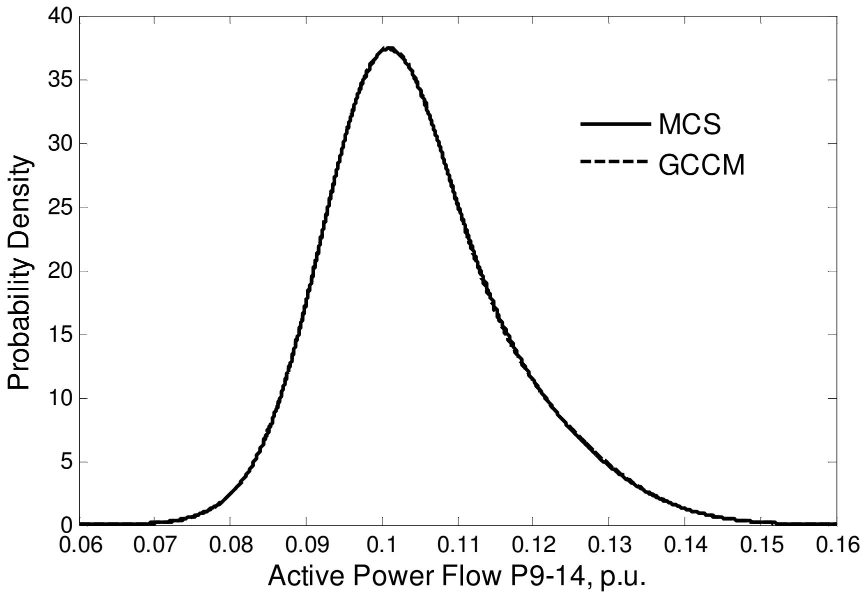

Figure 4.3: PDF of active power flow from Bus 9 to Bus 14 (case 1).

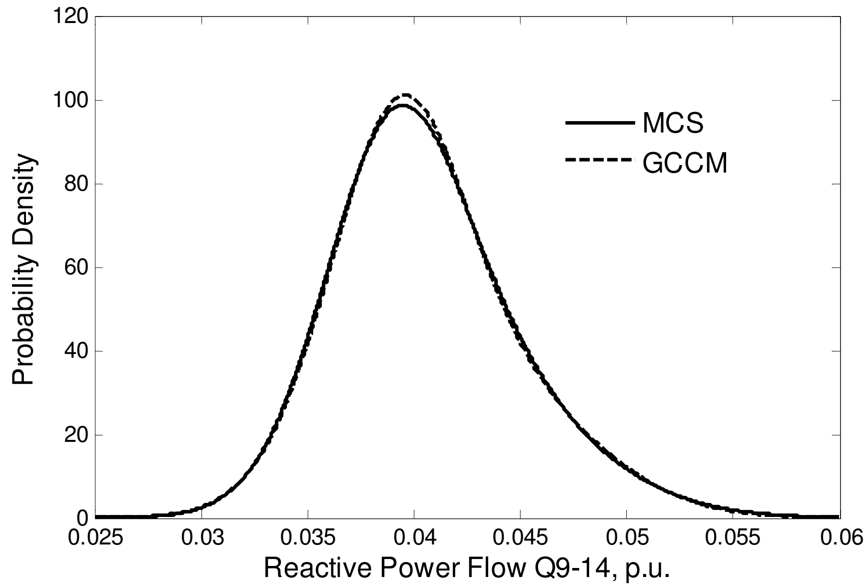

Figure 4.4: PDF of reactive power flow from Bus 9 to Bus 14 (case 1).

It is also interesting to verify the estimated PDFs of bus voltages. For example, the bus voltage at *Bus 13* is presented in Figure 4.5. Here, the difference between PDFs from the GCCM and the MCS is negligible.

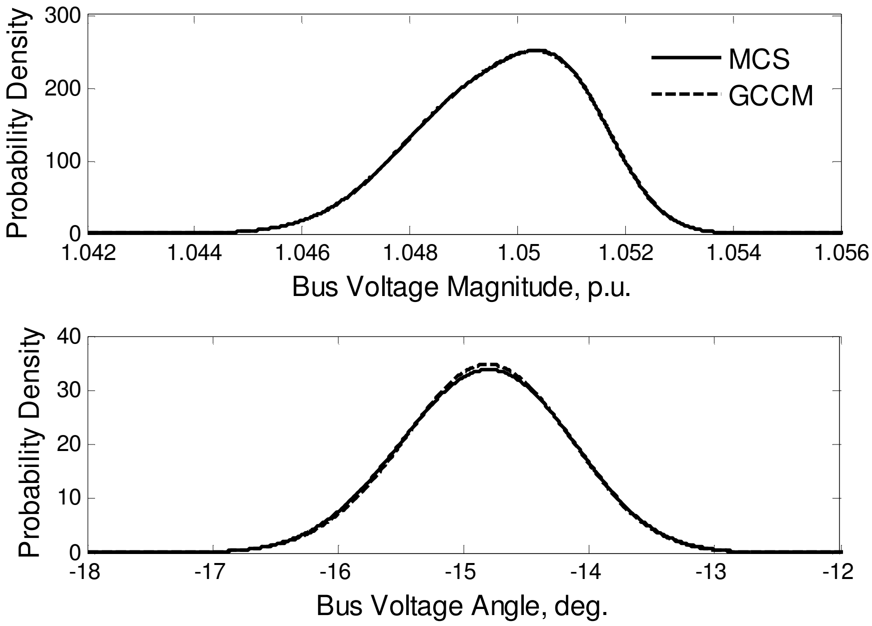

Figure 4.5: PDF of voltage magnitude and angle at Bus 13 (case 1).

Table 4.2 presents the average of percentage errors for *Case 1*. Here, the sub-indices *i* and *t* stand for injected and transmitted powers, respectively. These errors are calculated as percentages of the values obtained from the MCS. The average values of the mean (μ) and standard deviation (σ) errors of power flows and power injections are no larger than 0.68%. This confirms the good accuracy of the proposed method for this scenario.

Table 4.2: Average value of percentage errors Case 1.

	θ	V	P_i	Q_i	P_t	Q_t
μ	0.01	0.00	0.01	0.12	0.01	0.21
σ	1.04	0.27	0.08	0.22	0.85	0.68

4.1.1.2 Case 2 in 14-bus system

In this test scenario, more variables are assumed to be correlated. The correlation coefficient between the active power demands *P10*, *P11*, *P12*, *P13* and *P14* is $\rho = 0.8$ (Group 1). The correlation between *P9* and *P10* is $\rho = 0.9$ (Group 2), the correlation between *P5* and *P6* is $\rho = 0.9$. (Group 3), and the power demands from different groups have a correlation coefficient of $\rho = 0.4$. Similar to *Case 1*, the reactive power injections (Q) at *Buses 5*, *9* up to *14* are completely correlated to their respective active power injections (P).

The particular difference of *Case 2* with respect to *Case 1* is that more non-Gaussian variables are assumed to be correlated with the other variables at different buses (not only with the reactive power variable at the same bus with constant power factor). For example, *P6*, *P9*, *P13* and *P14* are non-Gaussian variables that are correlated with active power injections at other buses. The same applies for *Q6*, *Q9*, *Q13* and *Q14*.

Figures 4.6 and 4.7 present the PDFs of active and reactive power flow from *Bus 9* to *Bus 14*. In the case of the active power flow, the difference between PDFs is negligible. On the other hand, the PDF of reactive power flow obtained from the GCCM has some difference with respect to the Monte Carlo simulation. In fact, Figure 4.7 corresponds to the largest difference between PDFs obtained from the two methods.

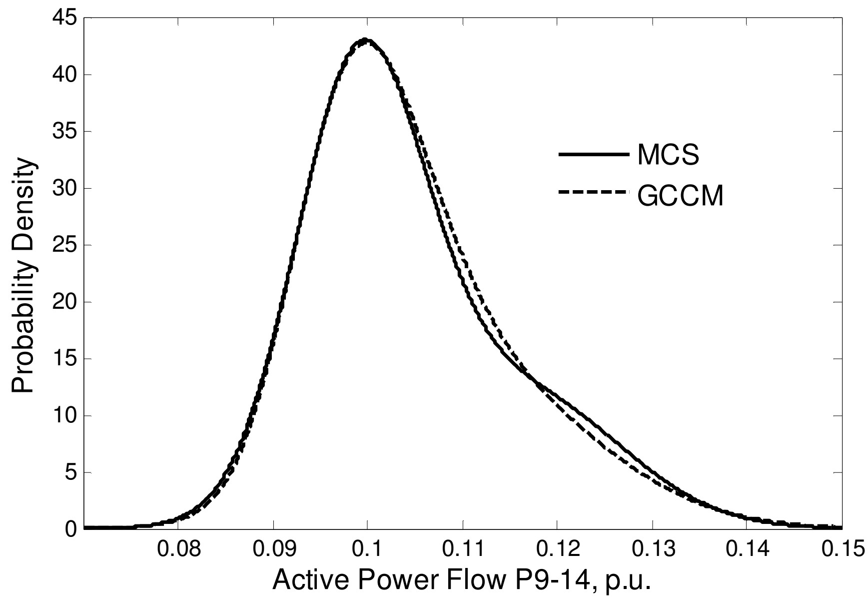

Figure 4.6: PDF of active power flow from Bus 9 to Bus 14 (case 2).

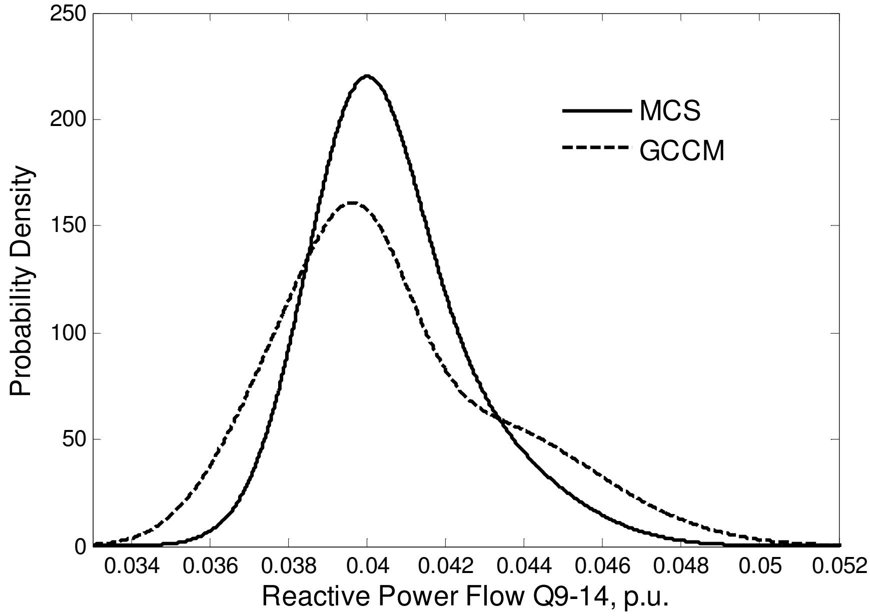

Figure 4.7: PDF of reactive power flow from Bus 9 to Bus 14 (case 2).

Similarly, Figures 4.8 and 4.9 present the PDFs of active and reactive power flow from *Bus 13* to *Bus 14*. Here, the PDF of active power flow obtained from the GCCM is less accurate than the PDF of the reactive power flow at the same transmission line. These errors are caused by assuming a fixed correlation coefficient between variables for all the WLS runs.

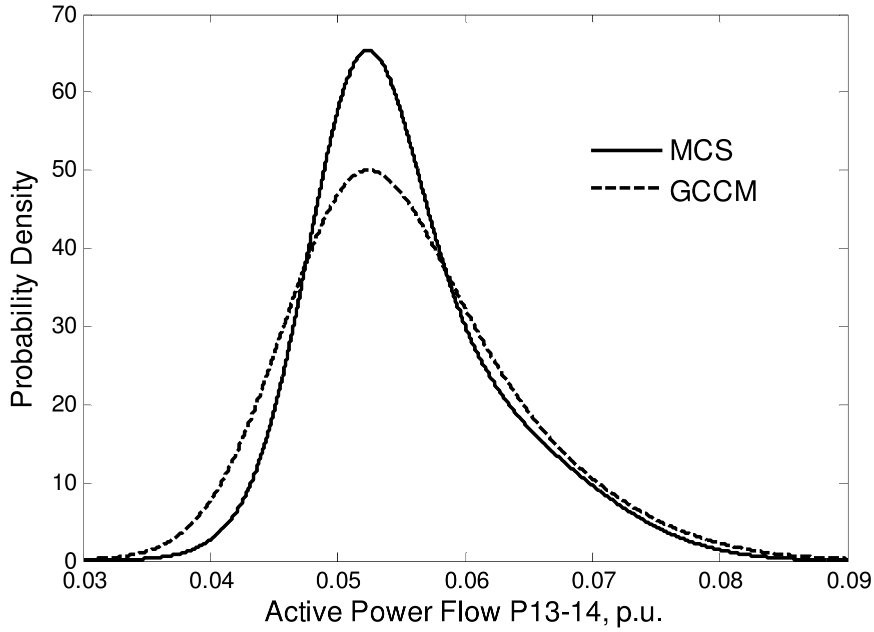

Figure 4.8: PDF of active power flow from Bus 13 to Bus 14 (case 2).

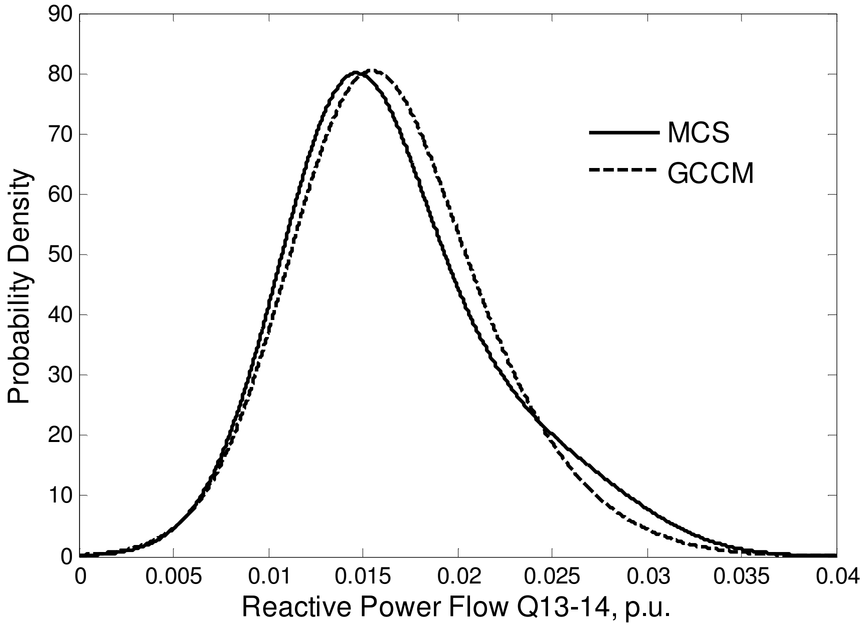

Figure 4.9: PDF of reactive power flow from Bus 13 to Bus 14 (case 2).

Figure 4.10 presents the PDF of bus voltage at *Bus 13*. Here, the difference between PDFs is slightly larger than in *Case 1*, see Figure 4.5.

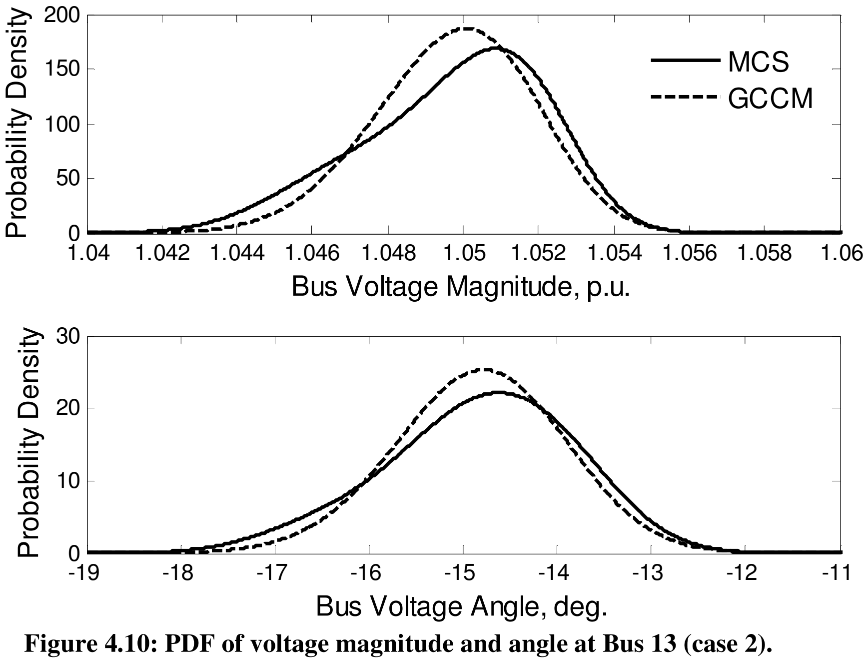

Figure 4.10: PDF of voltage magnitude and angle at Bus 13 (case 2).

Table 4.3 summarises the percentage errors for *Case 2*. The average percentage errors of the mean values are still small, as in *Case 1*. However, the average percentage error of the standard deviations has increased to 9%.

Table 4.3: Average value of percentage errors Case 2.

	θ	V	P_i	Q_i	P_t	Q_t
μ	0.02	0.00	0.01	0.21	0.03	0.38
σ	9.32	6.17	0.41	2.41	8.64	9.26

The increase in approximation errors is explained in Section 4.3.

4.1.2 57-bus IEEE Test System Simulation

The network configuration and line parameters of the 57-bus test system were obtained from [64] and they are presented in Appendix G.2. All the loads are assumed to have a constant power factor and the power injections at all buses are assumed to be Gaussian random variables with mean values presented in Appendix G.2. and $CV = 10\%$.

Three wind farms are installed in the network at *Buses 4*, *22* and *36*. Without loss of generality, the wind farms are modelled as PQ buses [66] and it is assumed that each wind farm is controlled such that the power factor is kept constant at 0.95 p.u. This power factor could be changed depending on the needs of the network [67].

The problem here consists of determining the stochastic flows close to the wind farms. Table 4.4 presents the GMM parameters of the non-Gaussian PDFs used to model the wind farm active power (P) outputs; all data is given in p.u. unless specified. Note that each of the GMMs has five components.

Table 4.4: GMM parameters of active power injections (*P*), in p.u. for 57-bus test system

	μ_1	μ_2	μ_3	μ_4	μ_5	σ_1	σ_2	σ_3	σ_4	σ_5	ω_1	ω_2	ω_3	ω_4	ω_5	CV
P4	0.25	0.35	0.45	0.70	0.95	0.08	0.13	0.12	0.10	0.05	0.3	0.2	0.2	0.2	0.1	53%
P22	0.10	0.13	0.18	0.30	0.46	0.02	0.05	0.05	0.06	0.03	0.2	0.2	0.2	0.2	0.2	60%
P36	0.05	0.08	0.14	0.26	0.34	0.01	0.03	0.05	0.06	0.02	0.2	0.2	0.2	0.2	0.2	67%

An approximation of typical PDFs of wind farms outputs (active powers) has been used in this work. These PDFs can be obtained from previous statistical studies, which take into account wind speed histograms at the wind farm location and the power curve of such wind turbines. However, such study is out of the scope of this work.

The large variability of wind power outputs is taken into account in the example and it is reflected in the large *CV* presented in Table 4.4. Smaller *CV* could be used instead, but it would depend on the level of variability of the wind farm power output at the period of interest (minutes, hours, etc).

One half of the power loads in the network has a correlation factor of $\rho = 0.8$ (Group 1). The other half has a correlation factor of $\rho = 0.8$ (Group 2) and the correlation coefficient between Group 1 and Group 2 is $\rho = 0.4$. The correlation factor between wind farms power outputs is $\rho = 0.8$, but they are assumed to be completely uncorrelated to the power demand.

In order to reduce the number of WLS runs, each of the three GMMs, presented in Table 4.4, were reduced from five to four and three components by using the Williams method (described in Section 3.2). The number of Monte Carlo trials is $N_s = 10000$ (which produced minimum variation of MCS results) and the number of WLS runs in the GCCM is $N_r = 125$, 64 or 27, depending on the number of combinations after the Gaussian mixture reductions.

Figures 4.11 and 4.12 present the estimated PDFs of power flows *P3-4* and *Q3-4*. The PDFs obtained from the GCCM provide a good approximation of the PDF obtained from the Monte Carlo simulation. As it is seen in the plots, the reduction of Gaussian components had little impact on the final approximation of the power flows in this transmission corridor.

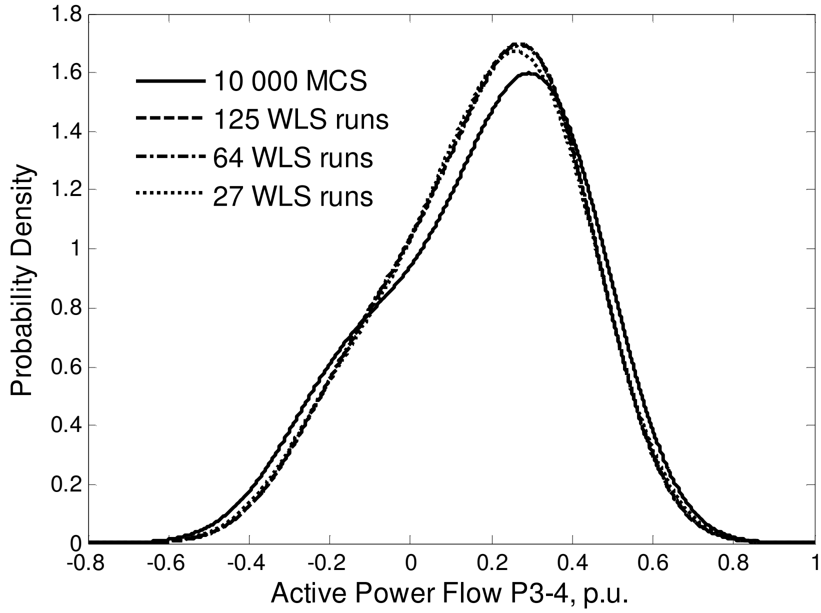

Figure 4.11: PDF of P3-4 with reduced Gaussian components.

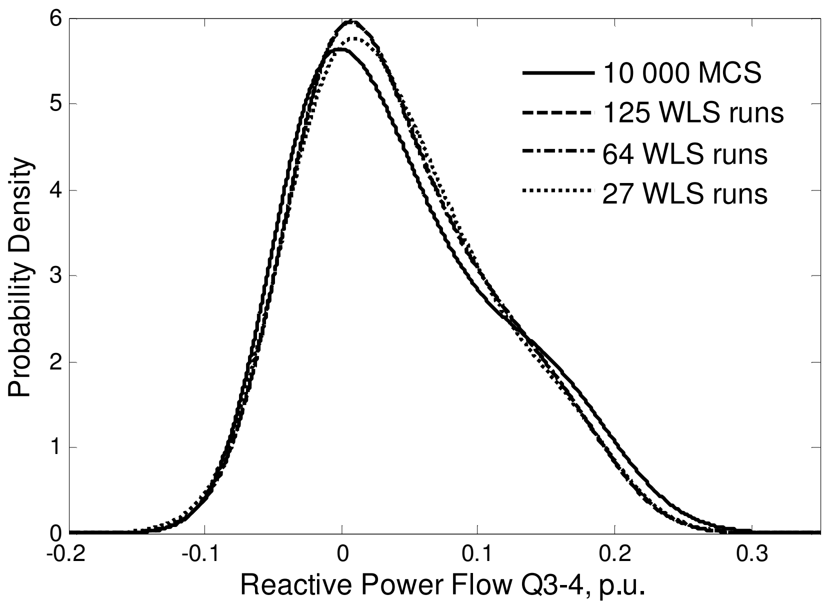

Figure 4.12: PDF of Q3-4 with reduced Gaussian components.

The assumption of a fixed correlation coefficient for all the WLS runs had higher impact on the approximation of some power flows at the proximities of *Bus 4*, as presented in Figures 4.13 and 4.14.

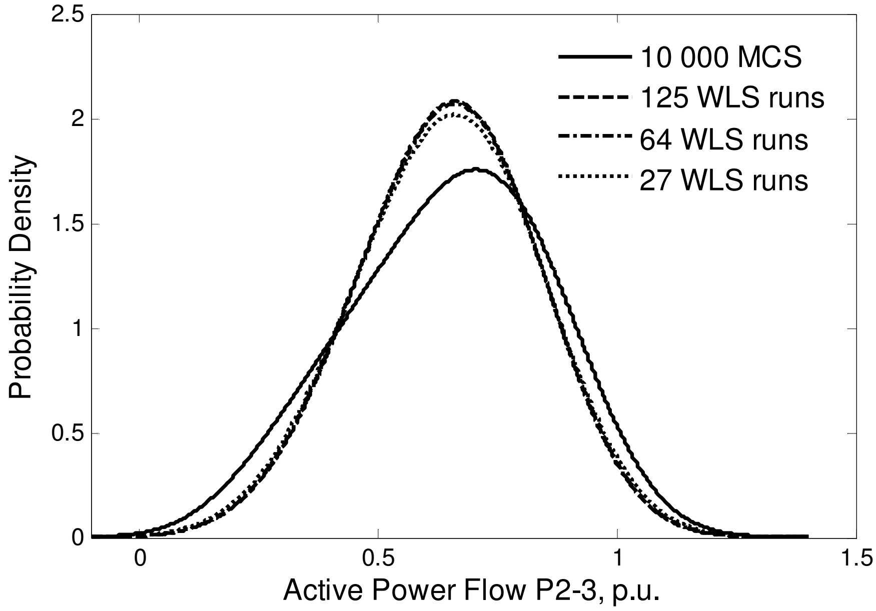

Figure 4.13: PDF of P2-3 with reduced Gaussian components.

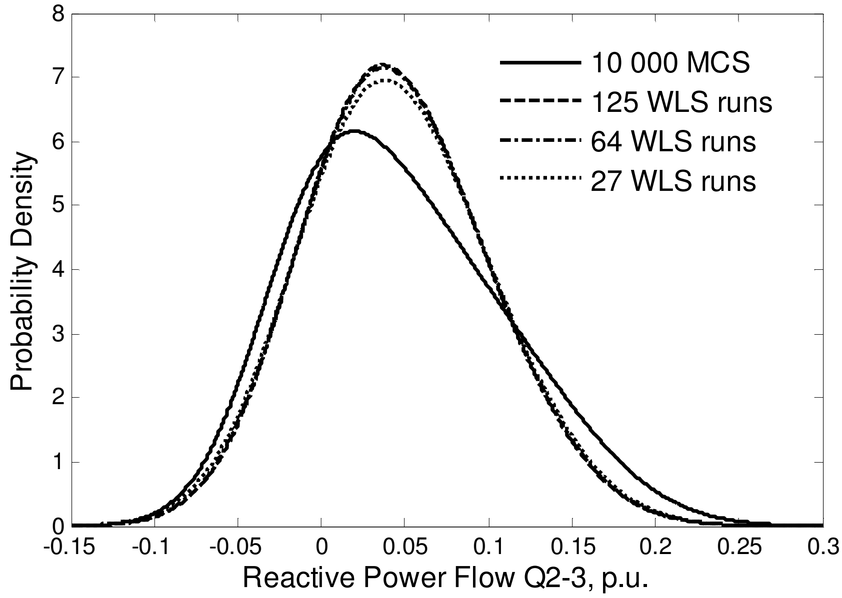

Figure 4.14: PDF of Q2-3 with reduced Gaussian components.

Figures 4.15 and 4.16 present the PDFs of active and reactive power flows from *Bus 22* to *Bus 38*. The approximation of the PDFs with 125 and 64 WLS runs is very similar to the PDF from the Monte Carlo simulation. When the number of WLS is reduced to $N_r = 27$, some accuracy is lost but the shape of the distribution remains similar.

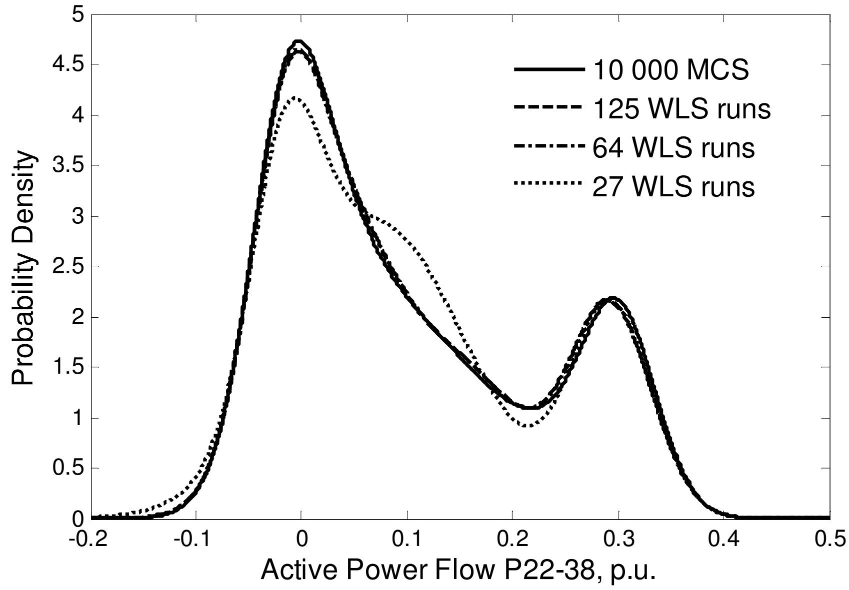

Figure 4.15: PDF of P22-38 with reduced Gaussian components.

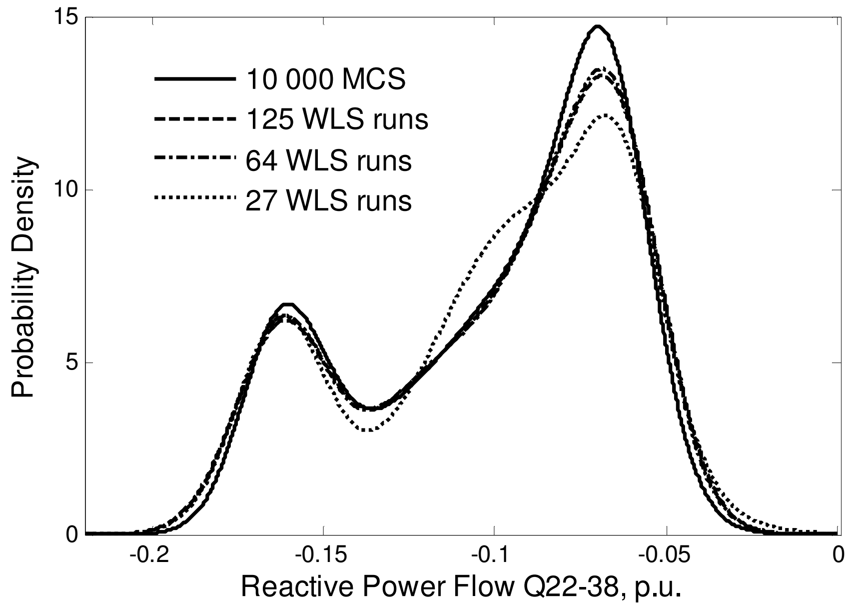

Figure 4.16: PDF of Q22-38 with reduced Gaussian components.

Figures 4.17 and 4.18 present the PDFs of the power flows with the largest difference between the Monte Carlo simulations and the Gaussian component combination method, at the surroundings of *Bus 22*. For fewer WLS runs, the resulting PDF better approximates the Monte Carlo PDF. Similar was found in Figures 4.13 and 4.14.

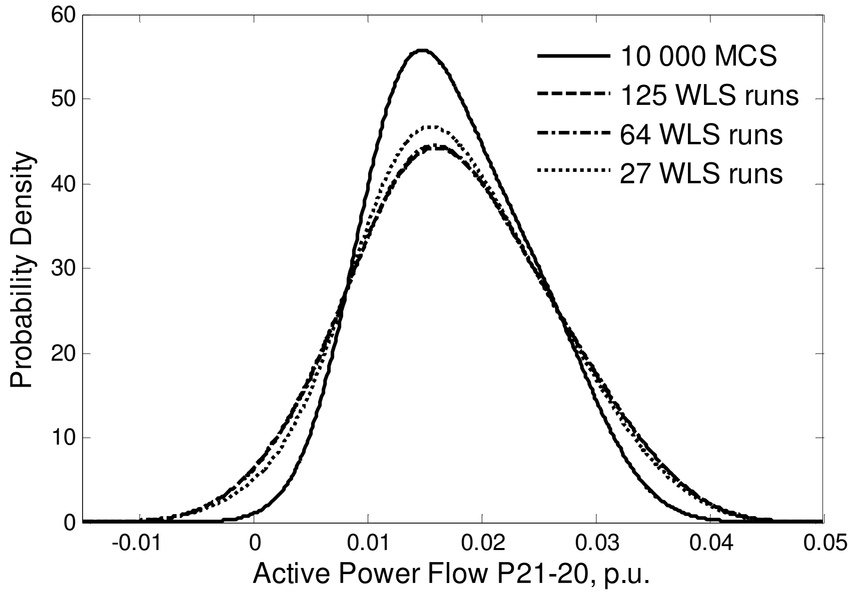

Figure 4.17: PDF of P21-20 with reduced Gaussian components.

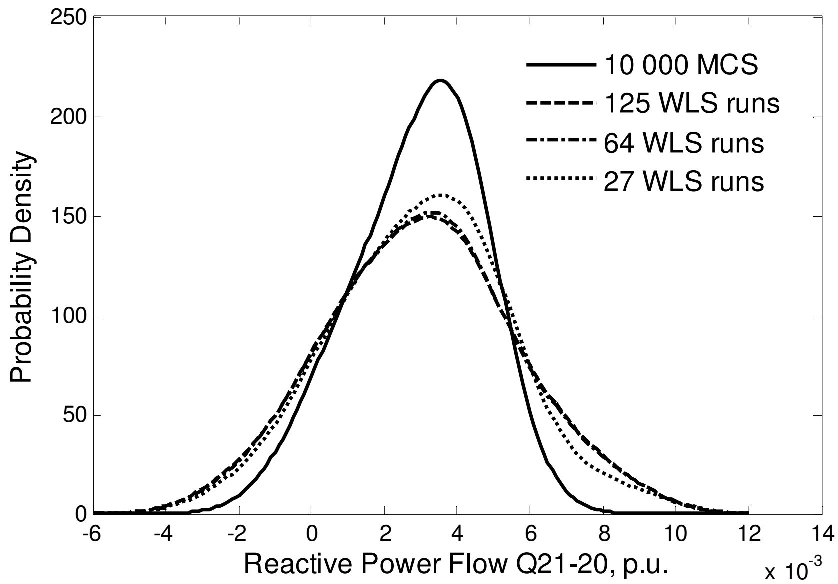

Figure 4.18: PDF of Q21-20 with reduced Gaussian components.

Although some accuracy is lost when using fewer Gaussian components (see Figures 4.15 and 4.16), the errors introduced by assuming a fixed correlation coefficient for all the WLS runs have less effect on flows in or out of *Buses 4* and *22*. Similarly, Figures 4.19 and 4.20 present the PDFs of power flows from *Bus 36* to *Bus 37*. The flow direction may change depending on the wind generation at *Bus 36*. The reduction of components of the original GMM has higher impact on the accuracy of the PDFs.

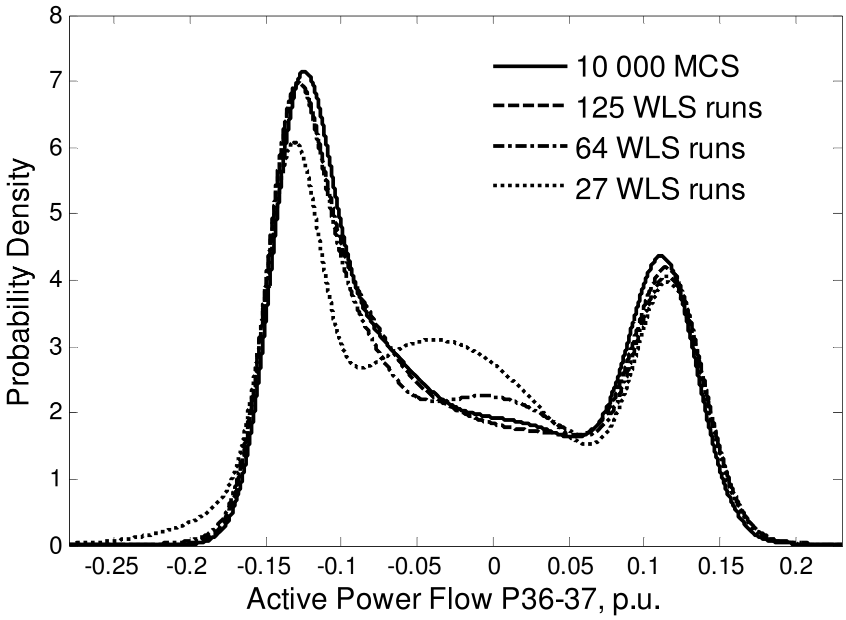

Figure 4.19: PDF of P36-37 with reduced Gaussian components.

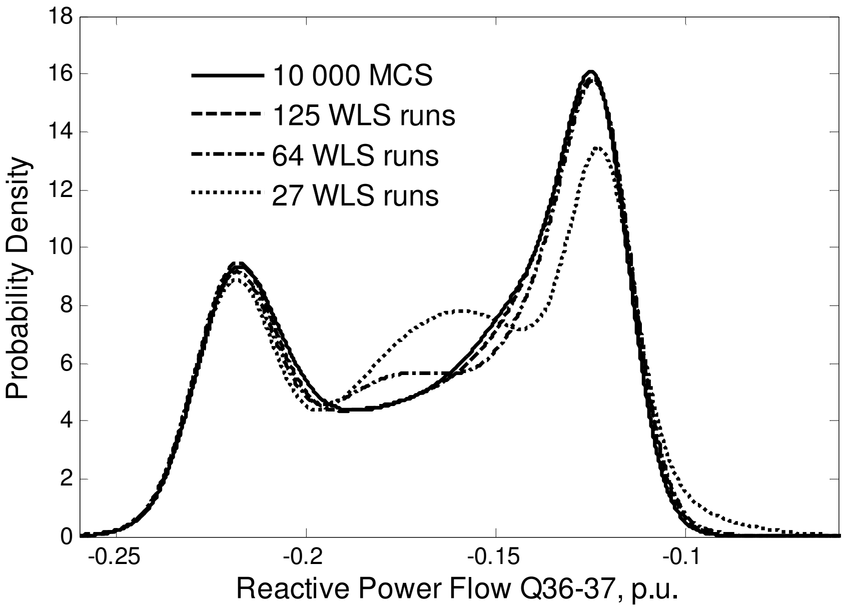

Figure 4.20: PDF of Q36-37 with reduced Gaussian components.

The less accurate PDFs of power flows, close to *Bus 36*, are presented in Figures 4.21 and 4.22. In this case, only the mean value is very similar to the mean value obtained from the Monte Carlo simulation.

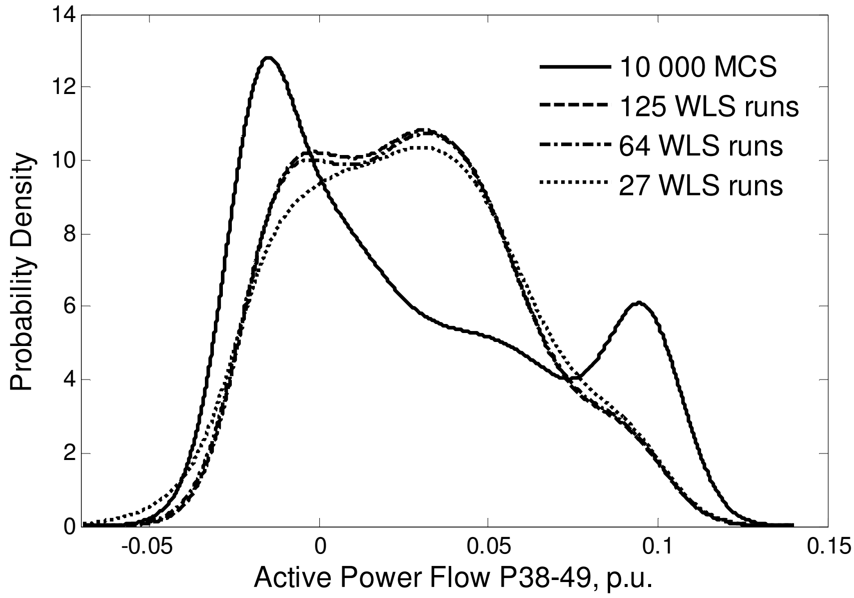

Figure 4.21: PDF of P38-49 with reduced Gaussian components.

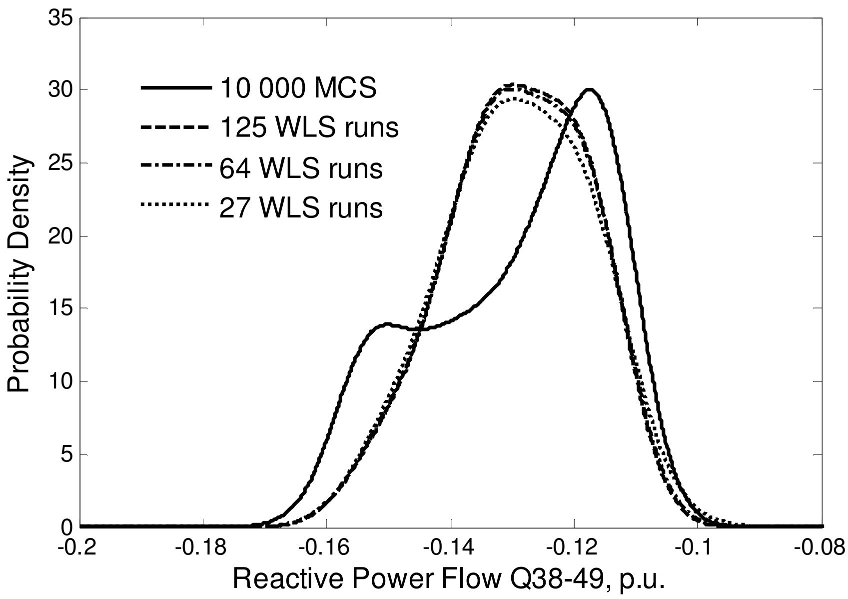

Figure 4.22: PDF of Q38-49 with reduced Gaussian components.

Figures 4.23 and 4.24 present the PDFs of voltages at *Buses 22* and *36*. It is interesting to note that the PDFs of voltage magnitudes are almost Gaussian distributed and the resulting PDFs are very similar to the MCS. However, the resulting PDFs of bus angles are affected by the assumptions made for each WLS run.

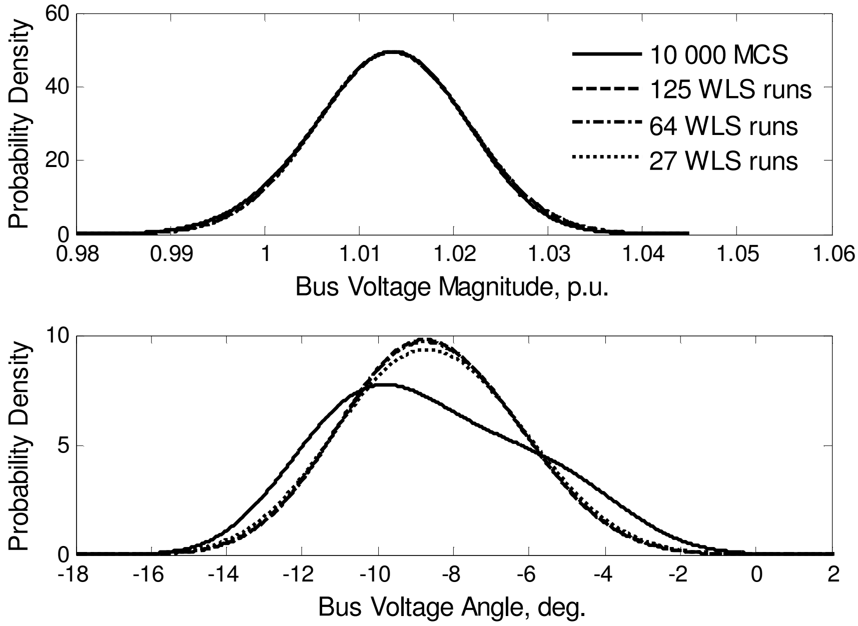

Figure 4.23: PDF of voltage magnitude and angle at Bus 22 with reduced Gaussian components.

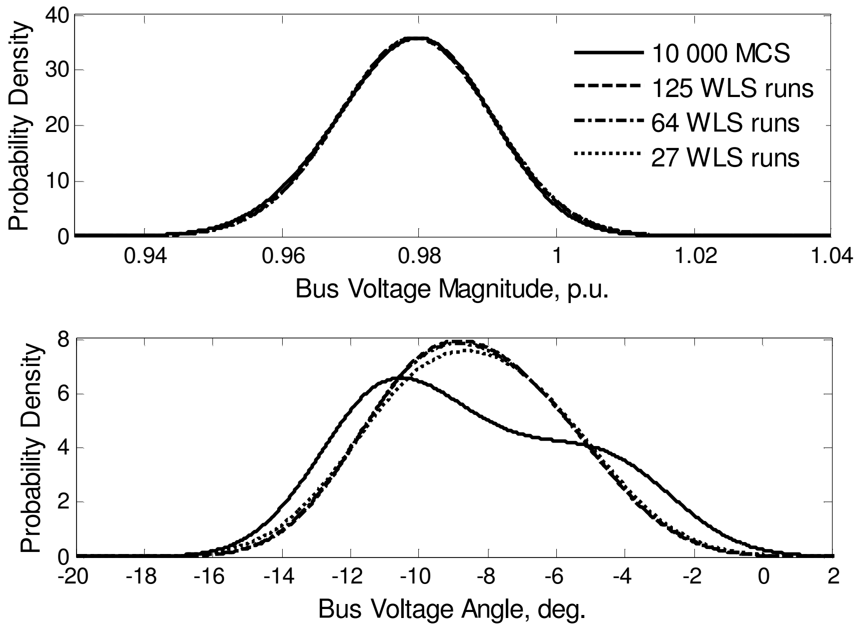

Figure 4.24: PDF of voltage magnitude and angle at Bus 36 with reduced Gaussian components.

Table 4.5 presents the average value of the percentage errors of mean (μ) and standard deviations (σ) obtained from the GCCM with respect to the MCS. Here, the sub-indices i and t stand for injected and transmitted powers, respectively.

The percentage errors of means (μ) are low for all the analysed cases (the maximum value is approximately 1.85% for Q_i with $N_r = 27$). The large percentage error of standard deviations in bus angles is due to the comparison of two small numbers. In addition, the overall standard deviation percentage errors are reduced for less WLS runs (N_r). It is concluded that fewer WLS runs reduces the propagation of errors due to the assumption of a fixed correlation coefficient for each Gaussian combination (WLS run).

Table 4.5: Average value of percentage errors

N_r	Par.	θ	V	P_i	Q_i	P_t	Q_t
125	μ	*0.3065*	*0.0028*	*0.0093*	*1.6976*	*0.1737*	*1.4068*
	σ	14.2751	0.8274	0.2819	0.6137	9.2176	8.1245
64	μ	*0.8077*	*0.0030*	*0.0095*	*1.7234*	*0.1861*	*1.4765*
	σ	13.7651	0.3164	0.2735	0.602	8.9065	7.8807
27	μ	*0.3429*	*0.0036*	*0.0097*	*1.8455*	*0.2123*	*1.6408*
	σ	11.6262	0.7303	0.2385	0.5565	7.5932	6.8521

In terms of computational demands, the proposed GCCM requires approximately 3% (with $N_r = 144$) and 1.25% (with $N_r = 125$) of the time required by MCS for the 14-bus and 57-bus test systems, respectively.

The test demonstrated that better approximation of the input variables (requiring more Gaussian combinations) leads to propagation of errors in the surrounding of these variables. A large number of Gaussian components will inevitably end up with a large N_r, but further reduction of the Gaussian components will destroy the original distribution of the input variables; a balance is therefore required.

4.2 Radial Networks

Probabilistic load flow studies are required in radial distribution networks due to the low availability of real-time measurements. The lack of sufficient real-time measurements reduces the capacity to monitor the actual operating conditions of the network but, more importantly, to detect the possibility of reversed flows, over flows, and voltage levels that are outside limits, due to the installation of distributed generation.

In this Section, the GCCM is tested and compared with MCS for probabilistic load flow studies in radial distribution networks. Similar to the previous Sections, some of the input variables are assumed to be correlated variables modelled by GMMs.

4.2.1 69-bus IEEE Test System Simulations

The network parameters and topology of the system were taken from [68] and they are presented in Appendix G.3. All the loads are assumed to have a constant power factor calculated from the active (*P*) and reactive (*Q*) power demands in Appendix G.3.

The study starts from the assumption that the network operator has run statistical studies to determine the probability distribution of the power injections at the period of interest. For those power demands (or generation output) whose marginal distributions are non-Gaussian, the EM algorithm should be used to determine the respective GMMs.

The power demands at all buses, except for three of them, are assumed to be Gaussian random variables with mean values listed in Appendix G.3 and Coefficient of Variation (*CV*) equal to 20%. The active power demands in *Buses 11*, *21,* and *68* are modelled by non-Gaussian PDFs represented by GMMs. In addition, non-monitored wind generation is installed at *Buses 49* and *52* and they have been modelled as PQ buses with constant leading power factor of 0.95.

Table 4.6 presents the parameters of the GMMs used to model the wind active power output and the three non-Gaussian active power demands. All data is given in p.u. (1 MVA base).

Table 4.6: Original parameters of GMM in radial network

	μ_1	μ_2	μ_3	μ_4	σ_1	σ_2	σ_3	σ_4	ω_1	ω_2	ω_3	ω_4
P11	-0.142	-0.120	–	–	0.006	0.010	–	–	0.5	0.5	–	–
P21	-0.065	-0.077	-0.093	-0.108	0.005	0.006	0.003	0.009	0.22	0.50	0.13	0.15
P49	0.070	0.110	0.180	–	0.020	0.030	0.040	–	0.30	0.40	0.30	–
P52	0.036	0.060	0.108	0.168	0.006	0.016	0.040	0.012	0.20	0.20	0.40	0.20
P68	-0.016	-0.047	-0.028	–	0.005	0.018	0.009	–	0.45	0.11	0.44	–

Due to the assumption of a constant power factor, the reactive powers at all buses are completely correlated with the active power injection at the same bus. The correlation coefficient between P and Q is included in (3.50) and it is kept constant for all the combinations of Gaussian components. In addition, as the power factor at all buses is assumed to be constant, the mean μ_Q and standard deviation σ_Q of the Gaussian component of reactive power demand are obtained from (4.1) and (4.2).

Similar to the meshed networks, the correlation coefficient between a pair of input variables should be taken from previous statistical studies. The correlations between input variables are defined as follows:

- Loads connected between *Bus 6* and *Bus 27* have a correlation coefficient of $\rho = 0.9$ (Group 1).
- Loads connected between *Bus 28* and *Bus 41* have a correlation coefficient of $\rho = 0.8$ (Group 2)
- Loads connected between *Bus 42* and *Bus 69* have a correlation coefficient of $\rho = 0.8$ (Group 3).
- The active power generation at *Buses 49* and *52* have a correlation coefficient of $\rho = 0.9$ but they are assumed not correlated to the active power demands.
- The correlation coefficient between Groups 1, 2 and 3 is $\rho = 0.4$.

4.2.1.1 Case 1: Probabilistic Load Flows

This study focuses on the effect of including correlation between variables (demand or generation) in radial distribution networks. The network topology used in the load flow study should be the one that best represent the typical network configuration of the season. During and after network reconfigurations, the network topology must be updated.

The impact of different network configurations was not addressed in this study. However, it is also possible to consider the probability of different network configurations, see the Discussion in Section 4.3.

The number of WLS runs needed to obtain the PLF solutions is calculated from (3.49), from which N_r is found to be 288 runs. The PDFs obtained from the proposed method are compared to 10 000 Monte Carlo power flows calculations using the Backward/Forward sweep method proposed in [69] and explained in Appendix D. Each power flow calculation uses a set of samples of power demand (or generation output) from the marginal distributions defined above. The correlation between input variables was included in the MCS using the methodology explained in Chapter 3.

In order to reduce the number of WLS runs in the Gaussian combination method, the GMMs representing the power injections *P68*, *P49,* and *P21* have been reduced by one component. This results in only 96 WLS runs. The selection of the reduced Gaussian mixtures and the performance of the optimised reduction method are extended in sub-Section 4.2.1.3.

Figure 4.25 presents the PDFs of active and reactive powers flowing through branch *51-52*. The PDFs show that for high amounts of generated power in *Bus 52*, the active power flow *51-52* may change direction.

The PDFs obtained from the GCCM are very similar to the MCS solution. In addition, the reduction of WLS runs had minimum impact on the estimated powers, as shown in Figure 4.25.

The PDFs of the voltage magnitude and voltage angle of *Bus 52* are presented in Figure 4.26. The large variability of the voltage magnitude is caused by the large variations of generated power in *Bus 52*. Similar to the power flow calculations, the approximation of the WLS runs is very similar to the MCS.

Figure 4.27 presents the power flows through branch *20-21*. In this case, there is a larger difference between the PDFs obtained before and after the GMM reductions. The difference is easier to appreciate because the GMM representing the power demand *P21* was reduced and the probability density of the power flows is directly related to the power injection at Bus *21*.

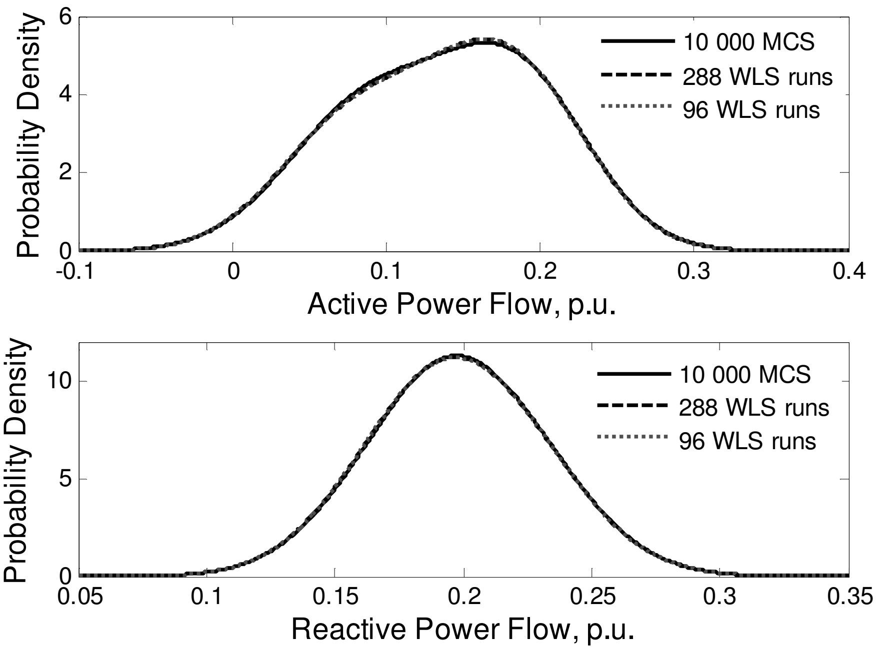

Figure 4.25: Comparison of estimated PDFs of active and reactive power flows from Bus 51 to Bus 52.

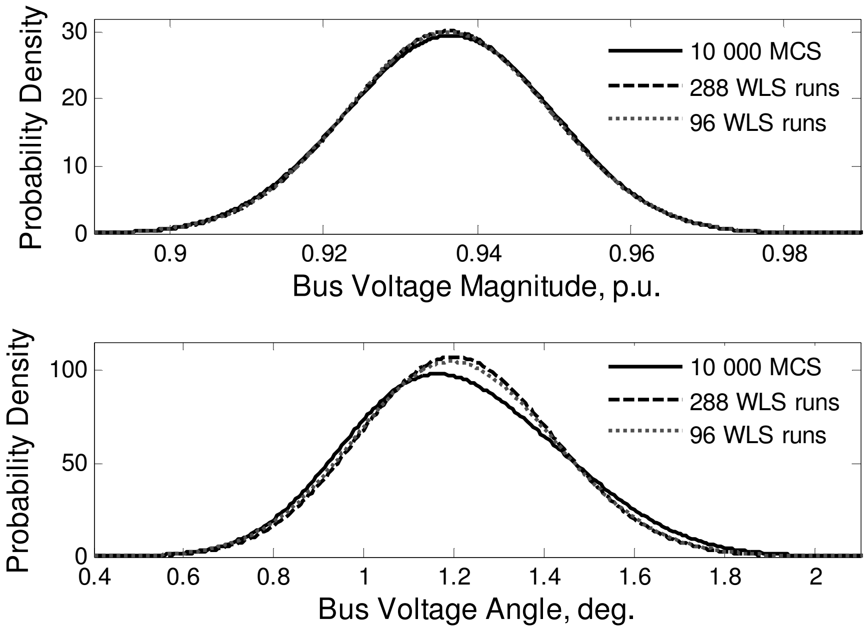

Figure 4.26: Comparison of estimated PDF of voltage (magnitude and angle) at Bus 52.

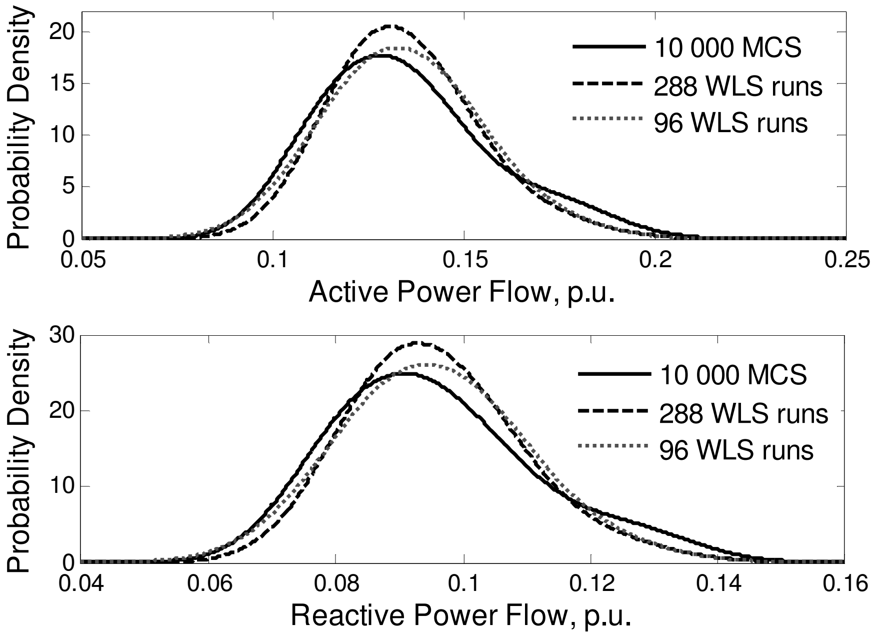

Figure 4.27: Comparison of estimated PDF of active and reactive power flows from Bus 20 to Bus 21.

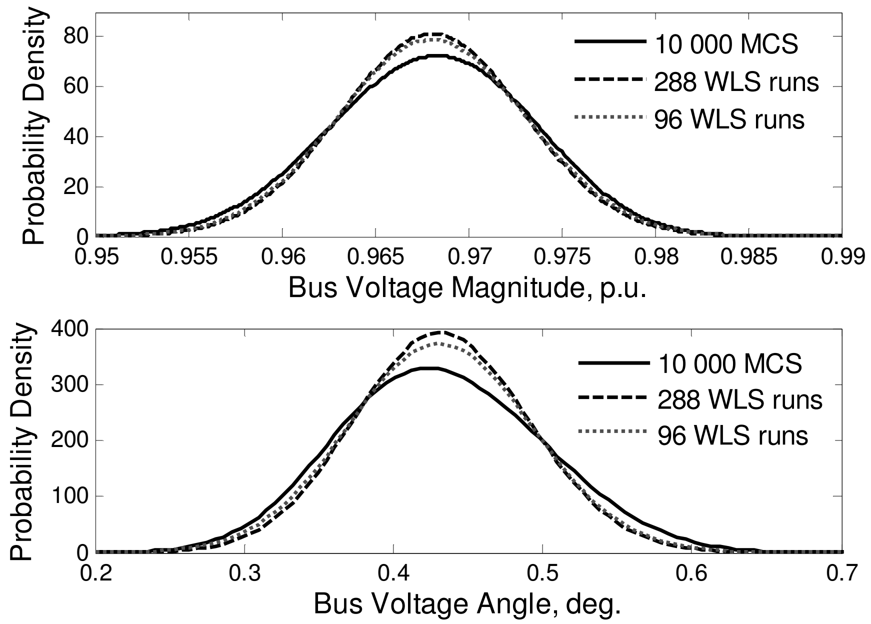

Figure 4.28: Comparison of estimated PDF of voltage (magnitude and angle) at Bus 21.

The PDFs of voltage magnitude and voltage angle of *Bus 21* is presented in Figure 4.28. Similar to the power flows, the approximations of the PDFs are acceptable and the upper and lower limits of voltages and power flows obtained from the WLS runs are in agreement with those obtained from the MCS. The few errors of approximation are introduced by the assumption that the correlation between Gaussian components that belong to two particular Gaussian mixtures is the same as the correlation between those Gaussian mixtures.

An alternative to the assumption above is not to include the correlation in the formulation i.e. the covariance matrix **R** becomes diagonal for all the WLS runs. Figure 4.29 shows the effect in voltage magnitude of (a) *Bus 27* and (b) *Bus 56* when correlation between variables is neglected. As it is shown in the plot, the resulting PDFs obtained from the formulation without (w/o) considering correlation have smaller deviation with respect to their mean value. Consequently, neglecting the correlation between input variables may lead to wrong estimated PDFs with different limits of voltages.

In terms of time demands, the GCCM with $N_r = 288$ WLS runs took only 4.7% of the total time required by the MCS. In addition, the elimination of three components from the original GMMs resulted in a 66% reduction of the time demand of the PLF.

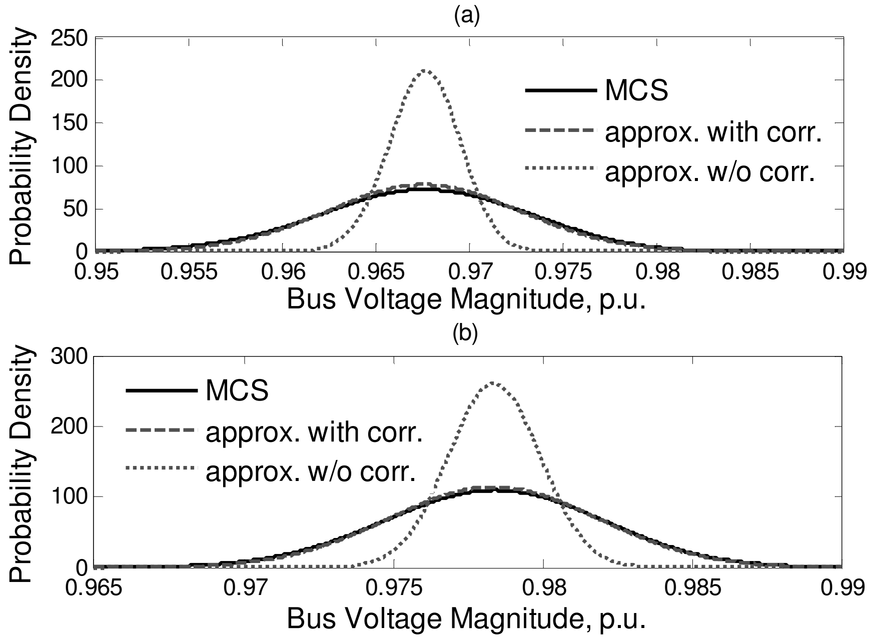

Figure 4.29: Influence of correlation in estimated voltages on (a) Bus 27 and (b) Bus 56.

4.2.1.2 Case 2: State Estimation

The above methodology is extended to the problem of State Estimation (SE). As there are few real-time measurements available in the distribution network, it is necessary to include pseudo-measurements to make the system observable. The PDFs of power demand and power generation output of non-monitored buses become the pseudo-measurements that can be represented by random variables modelled by GMMs. Therefore, the same methodology is used as in the probabilistic load flows but including the real-time and virtual measurements.

The inclusion of the real-time measurements does not increase the number of the WLS runs as they are assumed to be Gaussian distributed. Unlike the probabilistic load flow problem presented before, each WLS run is an over-determined problem due to the presence of real-time measurements and probabilistic distributions of power injections.

The inclusion of real-time (*rt*) measurements is now studied in this Section. Nine *rt* measurements are included in the SE: two power flow measurements in branches *0-1* and *9-42*, four current measurements in branches *9-10*, *2-28*, *4-36* and *8-40,* and three voltage magnitude measurements in Buses *0*, *4* and *9*. In order to avoid convergence problems, the current measurements are replaced by their squared value [70].

The PDFs of power demand and power generation are used as pseudo-measurements to make the system observable and to provide detailed information of the likely power demand/generation at each bus. The same correlation coefficients used in the PLF are used in the SE. In addition, the *rt* noisy measurements were taken from a deterministic load flow, presented in Appendix G.3, using inputs of power injections within the maximum and minimum limits of the pseudo-measurements.

Figure 4.30 presents the estimation of the active power flows through branches *20-21* and *51-52* with and without (w/o) correlation included. The three curves were obtained using $N_r = 98$ WLS runs.

The solid line corresponds to the solution of the PLF and it was included for comparison purposes only. The inclusion of the *rt* measurements makes it possible to obtain a better estimation of the most likely active power flowing through line *20-21*. In the case of branch

51-52, the larger uncertainty is caused by the large variability of the generated power in *Bus 52*.

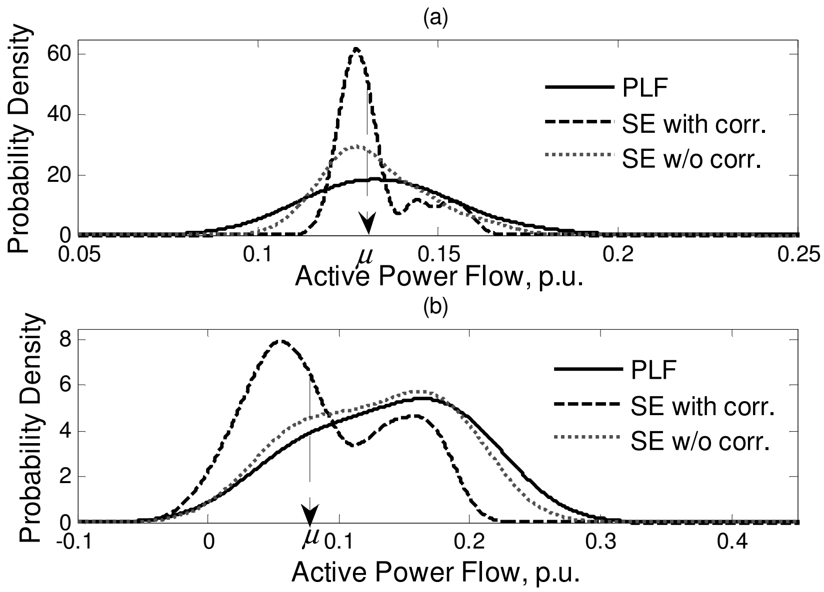

Figure 4.30: Estimated active power flows in (a) branch 20-21 and (b) branch 51-52.

Similarly, Figure 4.31 presents the estimated active powers flowing through (a) branch *10-11* (close to *rt* measurement) and (b) branch *67-68* (far from *rt* measurements).

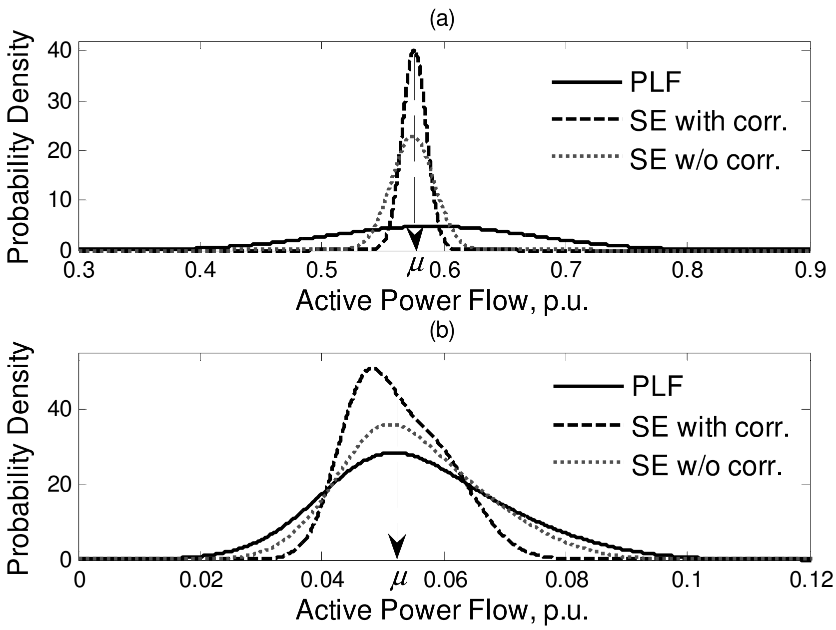

Figure 4.31: Estimated active power flows in (a) branch 10-11 and (b) branch 67-68.

The power flow through line *10-11* is much easier to identify with respect to the PLF study. On the contrary, the estimated power flow through line *67-68* has little impact when the *rt* measurements at the sending end of the feeders are included.

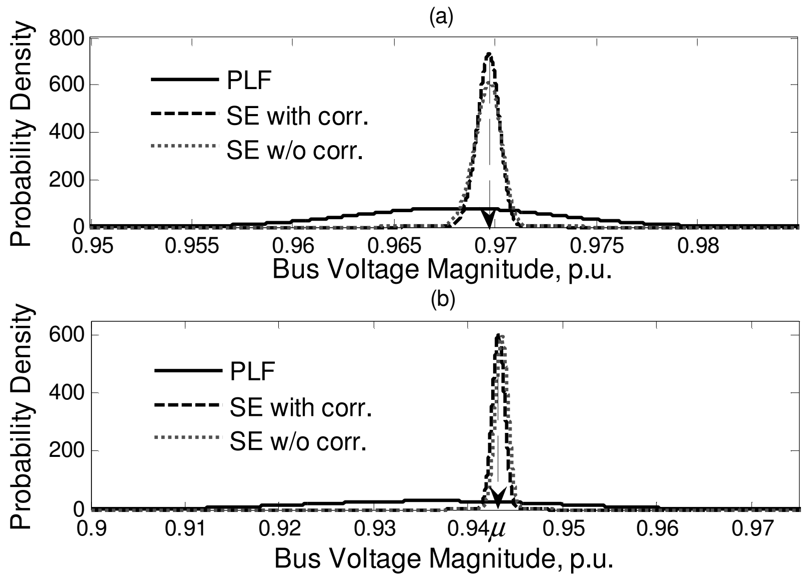

Figure 4.32: Estimated Voltage Magnitude at (a) Bus 21 and (b) Bus 52.

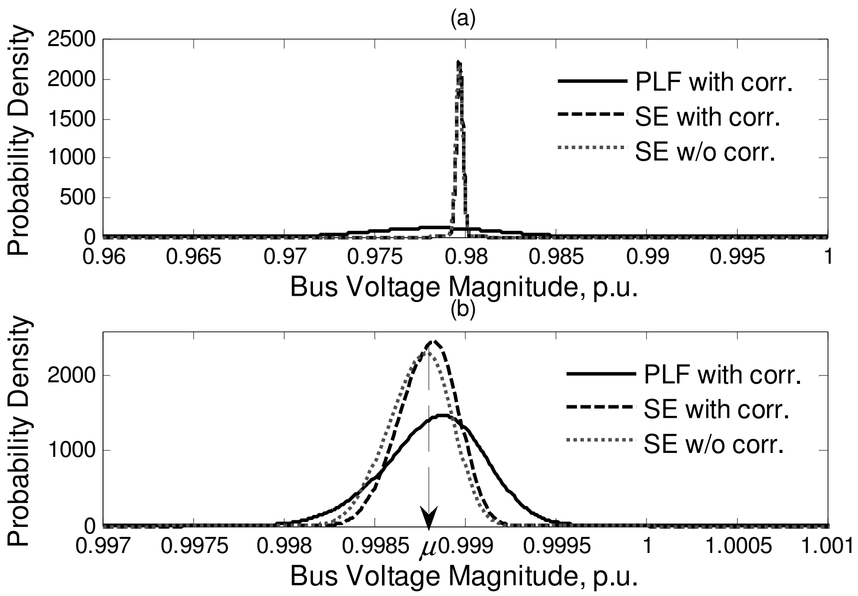

Figure 4.33: Estimated Voltage Magnitude at (a) Bus 11 and (b) Bus 68.

Figures 4.32 and 4.33 present the estimated voltage magnitude at *Buses 21* and *52, 11,* and *68,* respectively. The impact of the inclusion of *rt* measurements is evident in the estimated voltages, particularly for those buses close to the sending end of the feeders.

From these results, it is found that when a GMM is used to model power injections located at the sending end of a feeder, the GMM will have less effect on the estimated flows and voltages around it, particularly if this power injection is relatively small compared to the sum of the power injections along the feeder. On the other hand, the GMM of power injection at the very far end of a feeder will have a higher effect as presented in Figure 4.31(b).

The final value used to estimate the most likely value of voltages, power flows, and power injections is the mean value μ obtained from (3.4), as presented in Figures 4.30 to 4.33. For example, in Figure 4.30(a), the mean value of *P20-21* is μ = 0.1326 p.u. and the actual value is 0.1349 p.u. with only a 1.70% estimation error. In Figure 4.30(b) the mean value of *P51-52* is μ = 0.0874 but the actual value is 0.0604 with a 44.7% estimation error. This error is caused by the high uncertainty of the generated power in Bus *52*. Likewise, the mean value of *P10-11* is μ = 0.5760 p.u. (error is 0.42%) whereas the mean value of *P67-68* is μ = 0.0525 p.u. (error is 12.93%).

Table 4.7 presents the average of the estimation errors of the SE for bus voltages (V and θ), power injections (P_i and Q_j), and transferred power flows (P_t and Q_t).

Table 4.7: Average of estimation errors for radial network

variable	V	θ	P_i	Q_i	P_t	Q_t
ε %	0.04	2.79	10.00	10.79	7.10	7.28

Although the test only considered balanced conditions, the methodology can be extended to three phase unbalanced conditions given the PDFs of bus power injection for each phase and their correlation coefficient.

4.2.1.3 Selection of GMM for Reduction

As it was explained in sub-Section 4.2.1.1, the reduction of the number of WLS runs N_r was achieved by reducing one component of the Gaussian mixtures that model *P68*, *P49,* and *P21*.

The selection of the GMM to be reduced depends on the importance and desired accuracy of each GMM. However, if there is no particular priority of importance among the mixtures, it is critical to select the GMM that, when reduced to *M* components, better approximates the corresponding Gaussian mixture with *M+1* components. This approximation is quantified by the normalised ISD defined in (3.29).

Figure 4.34 presents the J_s^N after one component is reduced for each of the GMMs. For all the GMMs, the optimised approach finds a set of reduced parameters that better approximates the original mixture compared to the pair-merging method; see Figures 4.34 (a) and 4.34 (b).

In the first reduction attempt, the GMM representing *P68* is less affected after the elimination of one component; see Figure 4.34(b). In the second reduction attempt, when *P68* is already reduced, the GMM representing *P49* is selected and *P21* is finally selected in the third reduction attempt. The proposed selection ensures that the PLF and SE with fewer WLS runs have similar results when compared to the formulation with the original combination of Gaussian components.

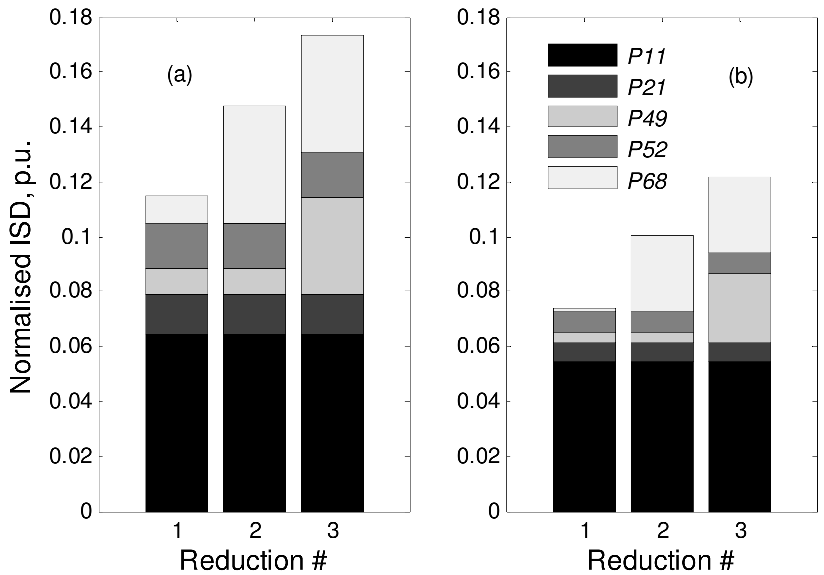

Figure 4.34: J_s^N for reduced Gaussian mixtures using (a) the pair merging method and (b) the optimised approach.

Figure 4.35 presents the reduction of the GMM representing the active power demand at *Bus 68*. The resulting GMM with two components is very similar to the original (solid line) mixture. The solution obtained from the pair-merging method was used as the initial guess of the optimised approach.

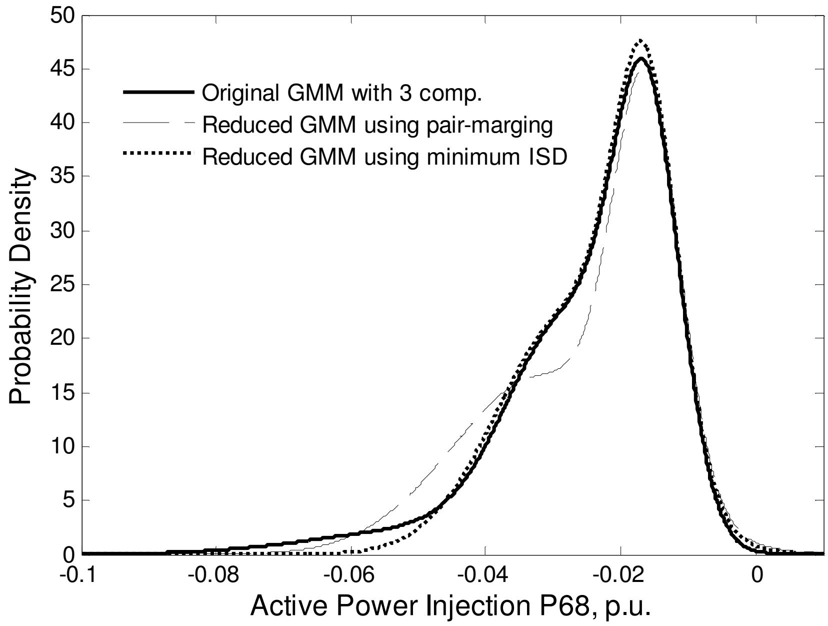

Figure 4.35: Reduced Gaussian mixture to represent the power injection at Bus 68.

4.3 Discussion

The GCCM is an efficient approximation of MCS to estimate power flows and bus voltages in the presence of non-Gaussian correlated input variables. The methodology assumes that the correlation coefficient between Gaussian components that belong to two particular Gaussian mixtures is the same as the correlation between those Gaussian mixtures. The assumption is truly valid for the input variables P and Q at buses with constant power factor, in which $\rho = 1$, as it was demonstrated in *Case 1* for the 14-bus test system.

In any other case, the assumption is just an approximation and it introduces some errors in the calculated PDFs of bus voltages and power flows at the proximities of the non-Gaussian distributed power injections.

These errors become more notable when the correlated non-Gaussian input variables have large *CV* and when they are modelled by many Gaussian components. For this reason, the estimated power flows in the proximities of these input variables are more accurate when using fewer Gaussian components to model the correlated input variables, as shown in Figures 4.13-4.14 and 4.17-4.18.

It was found that the methodology can be implemented in both meshed and radial networks. The approximation provides more realistic results when compared to not including any correlation between variables.

In the case of radial distribution systems, the problem becomes an over-determined state estimation calculation when real-time measurements are included in the WLS formulation.

From the simulated cases, it is concluded that power injections, modelled as GMMs, have greater effect on the estimated flows and voltages around it when they are far from the real-time measurements or when these power injections are relatively large compared to the sum of the power injections along the feeder.

The methodology can also be extended to consider the uncertainty of the network topology. The line parameters of the branch whose connection status is uncertain should be included in the state vector. These parameters should be modelled as discrete variables with two possible values: the actual parameters (branch connected) or zero (branch disconnected).

Finally, as the method is based on multiple WLS runs, it only considers the equivalent (aggregated) power injections (active and reactive) for each bus, this being a limitation to consider more than one wind farm at the same bus. Under these circumstances, an aggregated wind farm has to be used instead.

4.4 Summary

The uncertainty of power demand and generation is studied by means of probabilistic load flows. These studies take into account the variability of the input variables to determine the most likely power flows and voltages given the marginal distribution and correlation coefficient between input variables for a certain period. This Chapter explored the use of multiple WLS runs to process non-Gaussian correlated input variables in probabilistic studies of meshed and radial networks.

In the proposed Gaussian Component Combination Method (GCCM), the assumption used to incorporate correlated variables introduces some errors in the resulting PDFs of power flows in the surroundings of the non-Gaussian correlated variables. It was found that the approximation errors increase for non-Gaussian input variables with large variability (above 10%-15%). However, it is concluded that the approximation is still acceptable as the resulting PDFs maintained the marginal distribution of the PDFs obtained from the Monte Carlo simulations.

The next Chapters of this Thesis are focused on the estimation of the system condition (voltages and power flows) using real-time measurements only. Unlike the studies in Chapters 3 and 4, the errors of the input variables (measurements) are Gaussian distributed with low level of variability (0.1%-2%).

Chapter 5 Synchronised Measurements in State Estimation

Occurrence of large disturbance events in power systems has encouraged the idea of using Wide Area Monitoring (WAM) system based on Phasor Measurement Units (PMU) to identify the sequence of events leading to blackout but also to prevent them by having a better knowledge of the system in real-time.

A PMU is able to measure phasors of voltage and currents, commonly called synchrophasors, which are estimated at a known instant (time tag). In order to obtain simultaneous phasor measurements across the system, these phasors have to be synchronised at the same time tag. This is achieved by using a sampling clock input, controlled by a Global Positioning System (GPS), in each PMU [19].

The building blocks of a WAM system consist of the PMUs, the communication links, the Phasor Data Concentrators (PDC) and the data server. Figure 5.1 presents a typical architecture of WAM systems. The communication links are represented by a Wide Area Network (WAN) cloud.

The PDC collects and stores the information gathered by groups of PMUs. The PDCs are connected to either a higher level PDC, also called Super PDC, or to the data servers which manage and prepare all the information to be used in the control centre.

Among the first applications of synchrophasors are enhanced visualisation of the power system, post disturbance analysis and model validations [20]. For example, post disturbance analysis based on synchrophasors have been reported in [71, 72]. Additionally, power angle monitoring, power oscillation monitoring, and other on-line application for angular, frequency and voltage stability applications will be deployed in the next years.

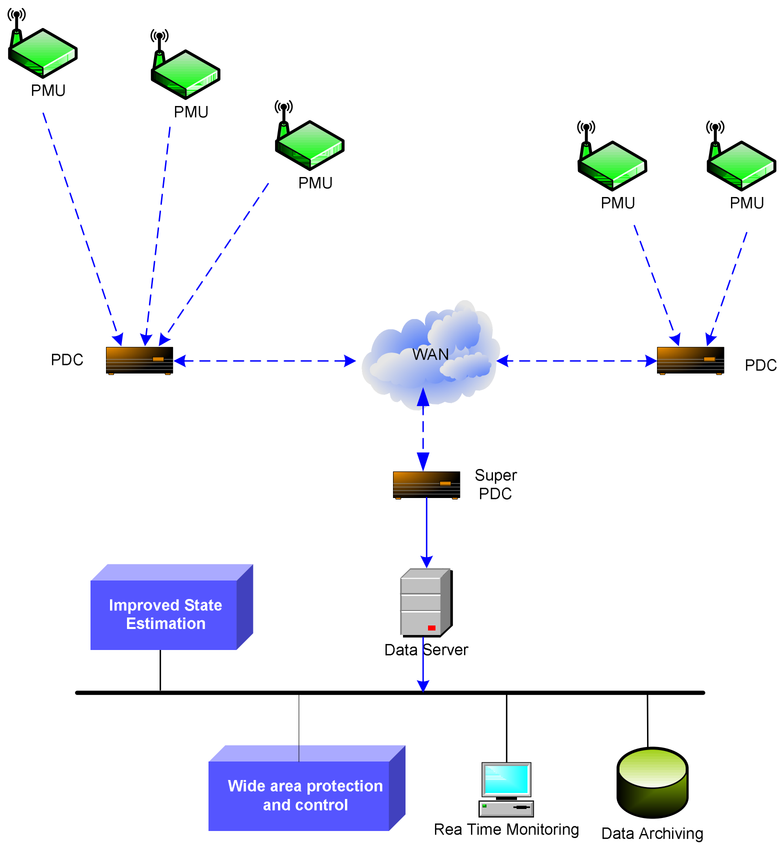

Figure 5.1: Typical Architecture of a Wide Area Monitoring system

This chapter is focused on the study of alternatives for including PMU measurements in existing state estimators. Section 5.1 present the concept of hybrid state estimation and it presents three different formulations for hybrid state estimators. Section 5.2 introduces the problem of uncertainty propagation in some hybrid state estimators and it presents two approaches for calculating these propagations. Finally, Section 5.3 and 5.4 present the study cases and the summary of the Chapter, respectively.

5.1 Hybrid State Estimators

There are two possibilities for including PMU measurements in existing state estimators as presented in Figure 5.2.

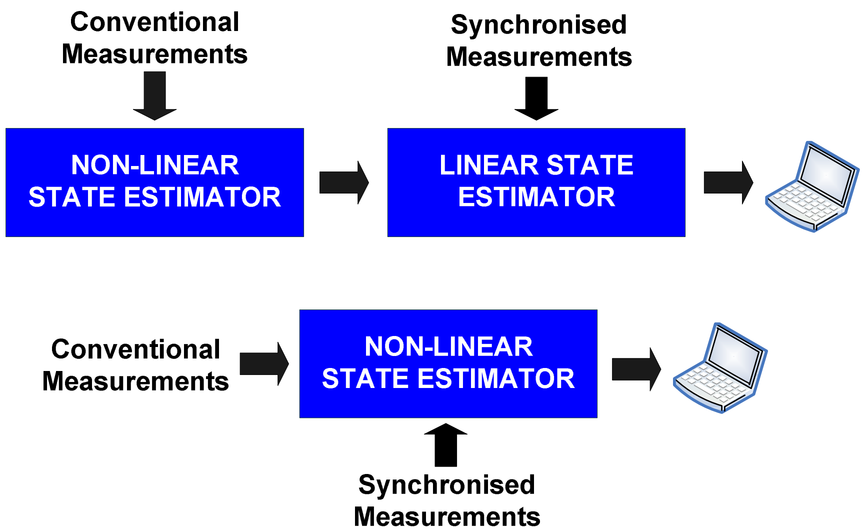

Figure 5.2: Two alternatives for including synchronised measurements in SE

The first option consists of a two-step hybrid state estimator in which the conventional measurements are firstly processed in the classical non-linear WLS method. The only condition is that the conventional measurements must be enough to make the system observable. The estimated state vector and the synchronised measurements are later used to correct the non-linear state estimation result in a single iteration, as presented in Figure 5.2. This is the hybrid estimator proposed in [26]. The main benefit is that there is no need to change the algorithm of existing estimator. However, a transformation of states from polar to rectangular coordinates is needed before using the linear estimator.

The other approach is to combine both sets of measurements and include them in a single step as presented in Figure 5.2. One of the major challenges in hybrid estimators is how to integrate PMU measurements of currents in the estimation problem.

Reference [73] proposed the use of polar form of currents in the state estimation. The relation between the currents and the system states is represented by:

$$I_{ij} = \sqrt{I_{ijR}^2 + I_{ijI}^2} \tag{5.1}$$

$$\theta_{ij} = \tan^{-1}\left(I_{ijI} / I_{ijR}\right) \tag{5.2}$$

with I_{ijR} and I_{ijI} expressed by:

$$I_{ijR} = g_{ij}(V_i \cos\theta_i - V_j \cos\theta_j) - b_{ij}(V_i \sin\theta_i - V_j \sin\theta_j) - b_{si}V_i \sin\theta_i + g_{si}V_i \cos\theta_i \quad (5.3)$$
$$I_{ijI} = g_{ij}(V_i \sin\theta_i - V_j \sin\theta_j) + b_{ij}(V_i \cos\theta_i - V_j \cos\theta_j) + b_{si}V_i \cos\theta_i + g_{si}V_i \sin\theta_i \quad (5.4)$$

The main benefit of this formulation is that the synchrophasors of currents are used directly in the estimator, i.e. they are not transformed. As drawback, the authors reported convergence problems in this formulation.

It is possible to take a simple 2-bus system and demonstrate that, using the polar form of currents as presented in (5.1)-(5.2), the corresponding Jacobian elements of these measurements become undefined for lightly loaded lines and $b_{si} = 0$ [18]. Moreover, even without those conditions, the corresponding Jacobian elements can abruptly change in sign and magnitude for consecutive iterations.

Let us consider a transmission line modelled by the following parameters: *R*=0.01; *X*=0.1; *B*=0.20, all in per unit. The variations of the Jacobian elements corresponding to the current angle derivatives are plotted in Figures 5.3 and 5.4:

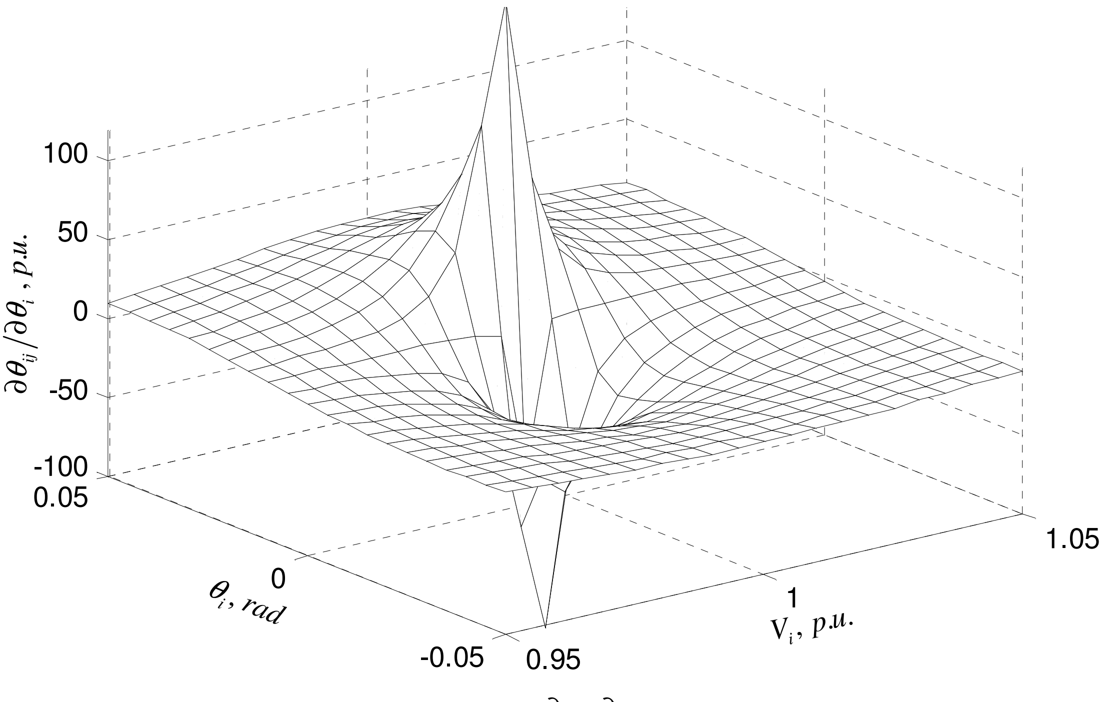

Figure 5.3: Variation of Jacobian element $\partial\theta_{ij}/\partial\theta_i$ with respect to small changes of θ_i and V_i

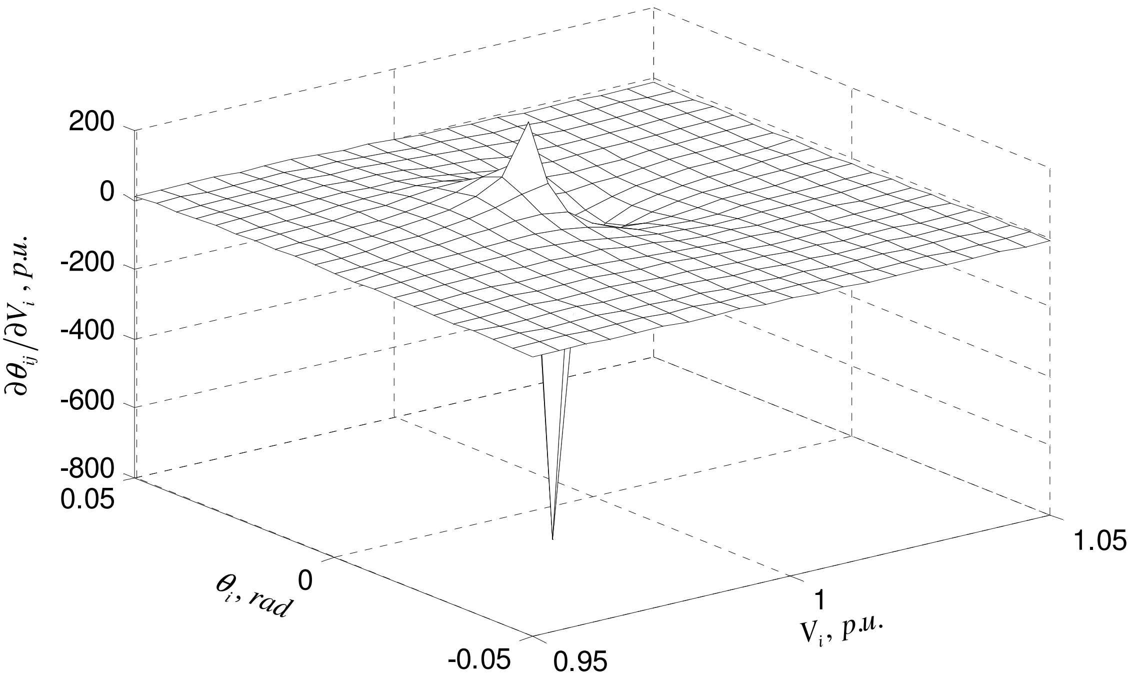

Figure 5.4: Variation of Jacobian element $\partial\ \theta_{ij}/\partial\ V_i$ with respect to small changes of θ_i and V_i

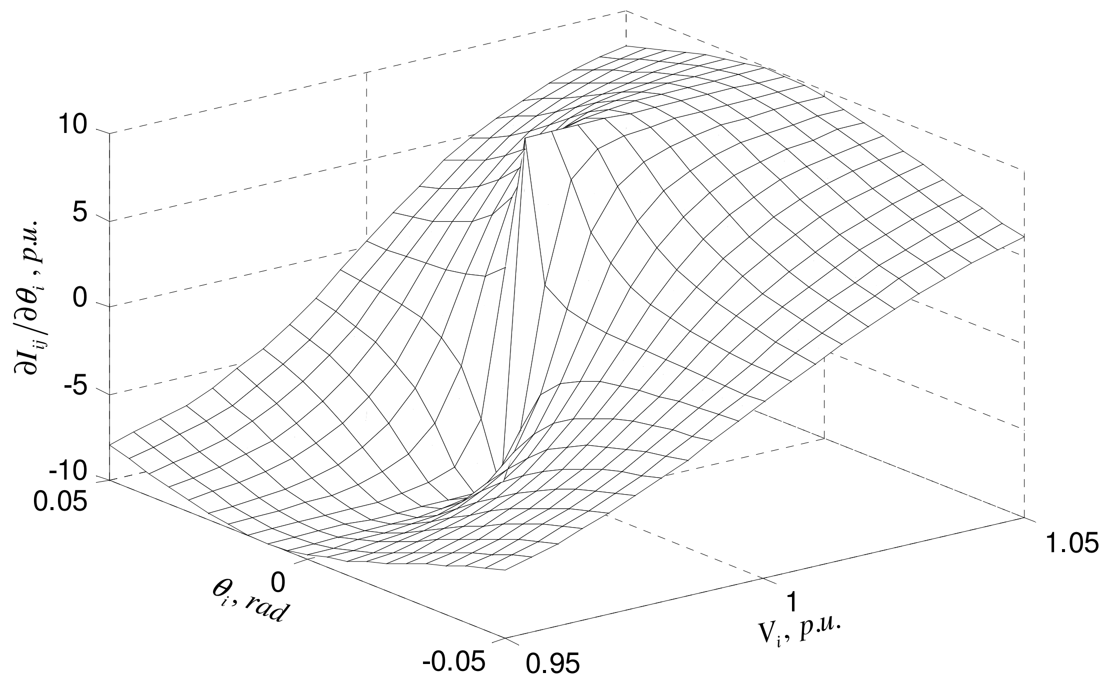

Figure 5.5: Variation of Jacobian element $\partial\ I_{ij}/\partial\ \theta_i$ with respect to small changes of θ_i and V_i

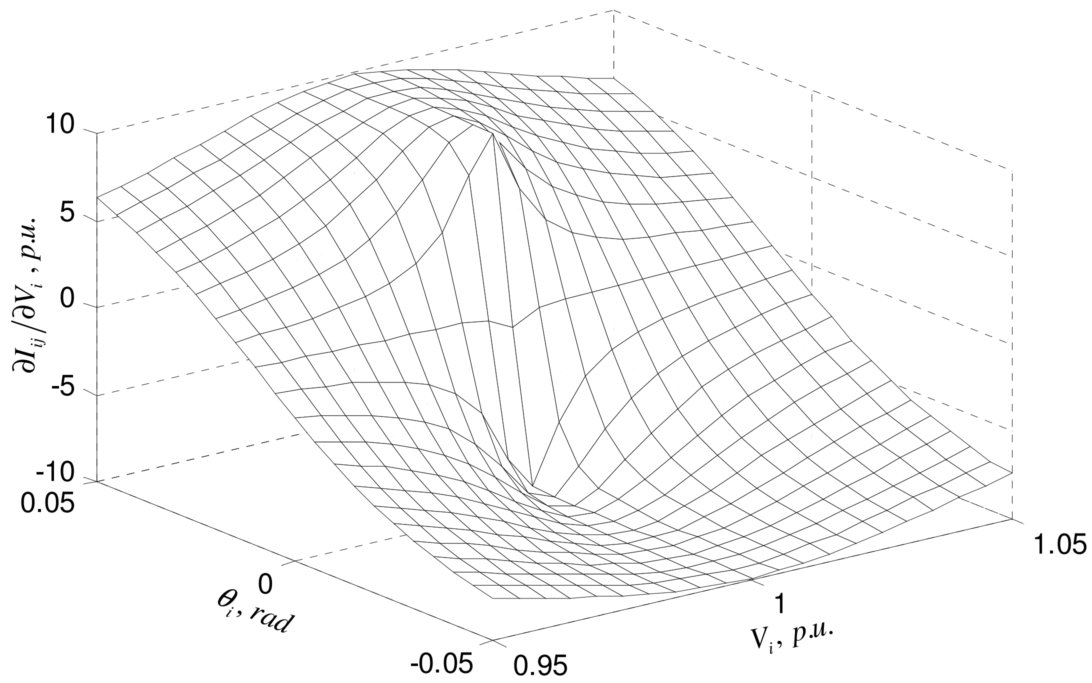

Figure 5.6: Variation of Jacobian element ∂ I_{ij}/ ∂ V_i with respect to small changes of θ_i and V_i

Similar results are obtained for derivatives of current magnitudes as presented in Figures 5.5 and 5.6. However, these variations of derivatives are less pronounced.

For a fixed voltage level in bus k, i.e. $V_k = 1$ and $\theta_k = 0$, the Jacobian elements, corresponding to polar form currents, can abruptly change for small variations of V_i and θ_i: These significant variations of the Jacobian elements cause an oscillatory behaviour in the estimation process because the PMU measurements are heavily weighted as compared to conventional measurements.

On the contrary, smooth variations (planes) are found when plotting partial derivatives of rectangular form of branch currents as presented in Figures 5.7 - 5.10.

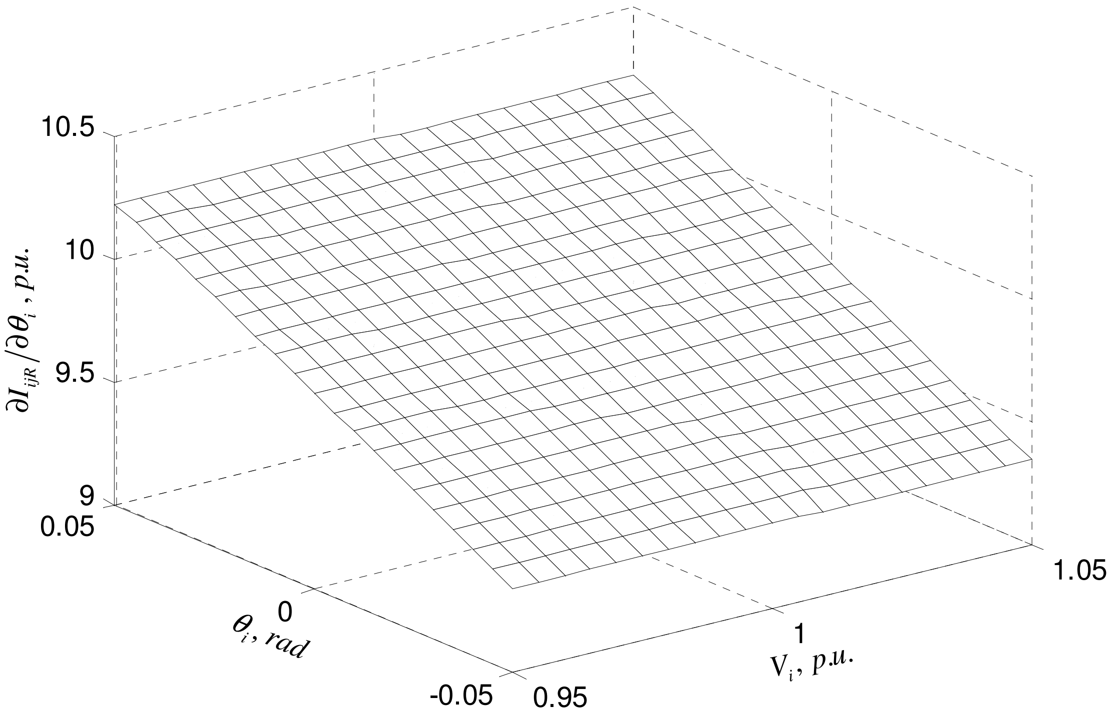

Figure 5.7: Variation of Jacobian element $\partial I_{ijR}/\partial \theta_i$ with respect to small changes of θ_i and V_i

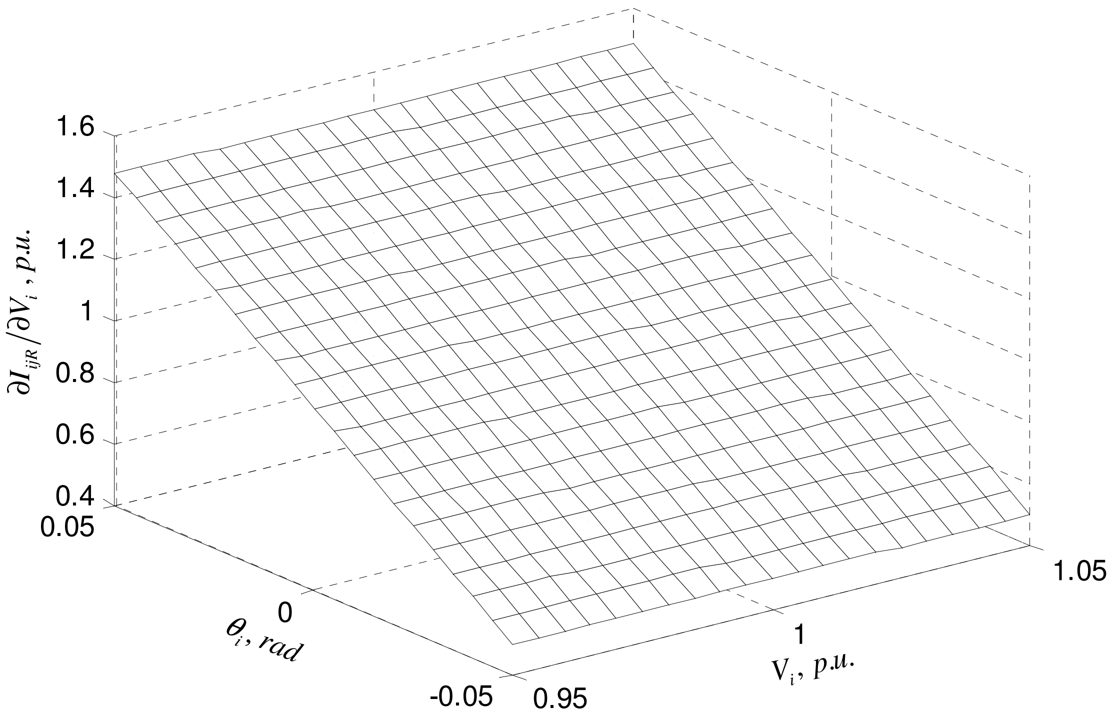

Figure 5.8: Variation of Jacobian element $\partial I_{ijR}/\partial V_i$ with respect to small changes of θ_i and V_i

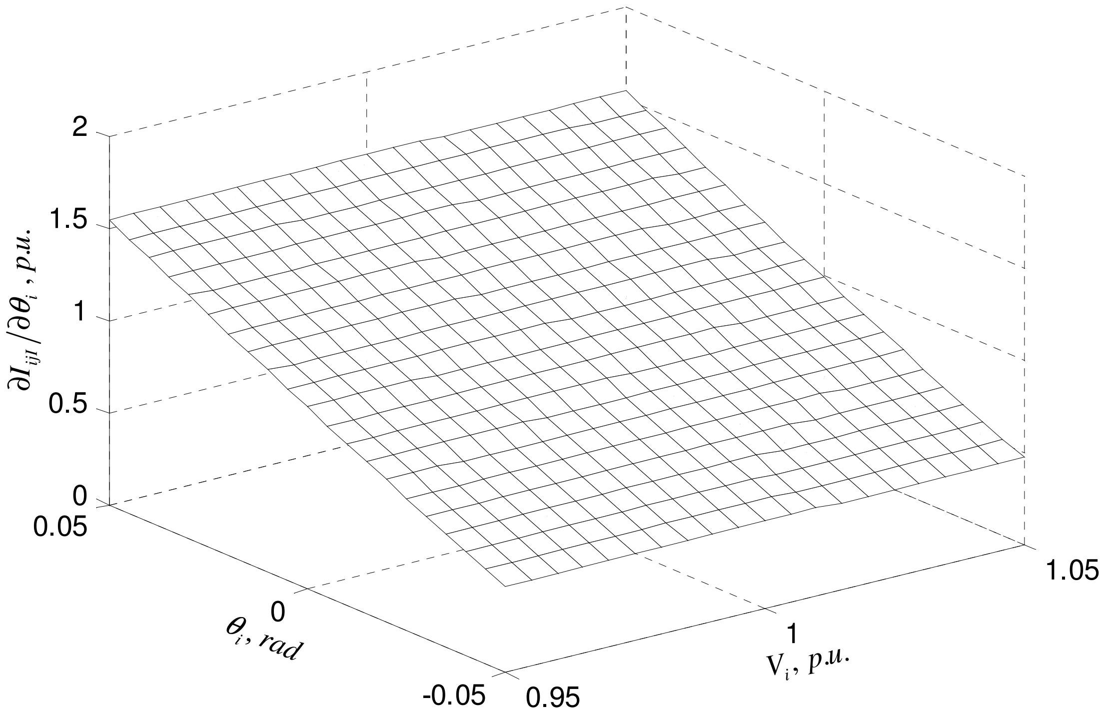

Figure 5.9: Variation of Jacobian element $\partial I_{ijl}/\partial \theta_i$ with respect to small changes of θ_i and V_i

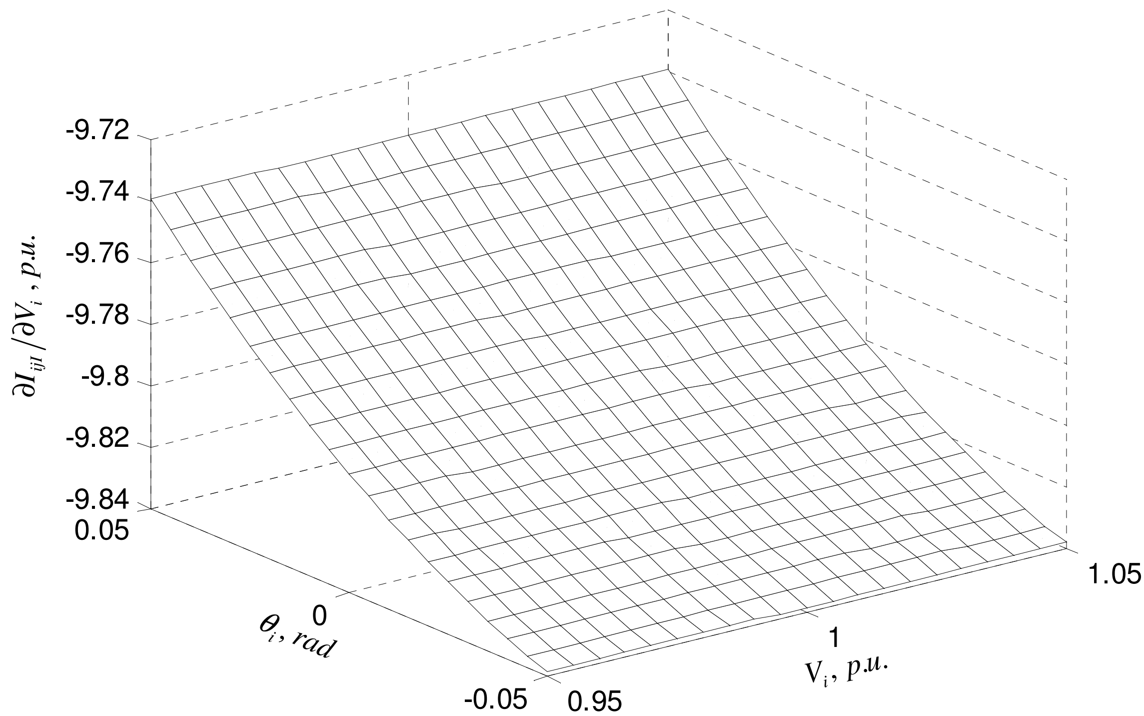

Figure 5.10: Variation of Jacobian element $\partial I_{ijl}/\partial V_i$ with respect to small changes of θ_i and V_i

Generally, no convergence problems are encountered when the currents are expressed in terms of rectangular components. This formulation is explained in Section 5.1.1.

5.1.1 Rectangular Currents Formulation

Reference [27] uses the transformation of polar to rectangular form of currents to take advantage of their better convergence properties, as follows:

$$I_{ij}\angle\theta_{ij} = I_{ijR} + jI_{ijI} \tag{5.5}$$

However, it is necessary to estimate the propagation of the measurement uncertainties during the transformation [27, 74, 75]. Thus, the assignment of variances (square of the standard deviations) of the new measurements must be obtained from uncertainty propagation methods, as extended in Section 5.2.

Table 5.1 presents the new Jacobian elements to be included in the **H** matrix of the WLS formulation. These elements correspond to the rectangular form of currents measurements obtained from the partial derivatives of (5.3) and (5.4) with respect to the voltage magnitude and angle of the sending bus *i* and the receiving bus *j*.

Table 5.1: Elements of H corresponding to rectangular current measurements

$\frac{\partial I_{ijR}}{\partial \theta_i} = -V_i\left((g_{ij}+g_{si})\sin\theta_i + (b_{ij}+b_{si})\cos\theta_i\right)$	$\frac{\partial I_{ijI}}{\partial \theta_i} = V_i\left((g_{ij}+g_{si})\cos\theta_i - (b_{ij}+b_{si})\sin\theta_i\right)$
$\frac{\partial I_{ijR}}{\partial \theta_j} = V_j\left(g_{ij}\sin\theta_j + b_{ij}\cos\theta_j\right)$	$\frac{\partial I_{ijI}}{\partial \theta_j} = V_j\left(-g_{ij}\cos\theta_j + b_{ij}\sin\theta_j\right)$
$\frac{\partial I_{ijR}}{\partial V_i} = (g_{ij}+g_{si})\cos\theta_i - (b_{ij}+b_{si})\sin\theta_i$	$\frac{\partial I_{ijR}}{\partial V_j} = -g_{ij}\cos\theta_j + b_{ij}\sin\theta_j$
$\frac{\partial I_{ijI}}{\partial V_i} = (g_{ij}+g_{si})\sin\theta_i + (b_{ij}+b_{si})\cos\theta_i$	$\frac{\partial I_{ijI}}{\partial V_j} = -g_{ij}\sin\theta_j - b_{ij}\cos\theta_j$

5.1.2 Pseudo- Voltage Measurement Formulation

This method combines the measured bus voltage and currents flowing out of the PMU bus to approximate the voltage phasors in adjacent buses, as suggested in [76]-[77]. These calculated voltages replace the use of current measurements (polar or rectangular) in the state estimator. Due to the transformation of measurements, this formulation also requires an approximation of uncertainty propagation, as it will be presented in Section 5.2.

5.1.2.1 Non-PMU Bus Voltage Calculation

With reference to the pi-model presented in Figure 2.3, the voltage phasor at any bus *k* adjacent to a PMU bus *i*, can be expressed as:

$$\bar{V}_k = \frac{\bar{V}_i(g_{si} + jb_{si} + g_{ik} + jb_{ik}) - \bar{I}_{ik}}{g_{ik} + jb_{ik}} \tag{5.6}$$

Here $\bar{V}_i = V_i\angle\theta_i$ is the measured voltage phasor at bus *i* and $\bar{V}_k = V_k\angle\theta_k$ is the unknown voltage phasors at bus *k* and $\bar{I}_{ik} = I_{ik}\angle\theta_{ik}$ is the current phasor measured by the PMU at bus *i*. The term (g_{si}+jb_{si}) is the shunt admittance connected at bus *i* and (g_{ik}+jb_{ik}) is the series admittance of the transmission line connecting bus *i* and *k*. If the parameters *a*, *b* and *c* are defined as:

$$a = g_{ik}(g_{si} + g_{ik}) + b_{ik}(b_{si} + b_{ik}) \tag{5.7}$$
$$b = g_{ik}(b_{si} + b_{ik}) - b_{ik}(g_{si} + g_{ik}) \tag{5.8}$$
$$c = g_{ik}^2 + b_{ik}^2 \tag{5.9}$$

the bus voltage at bus *k* can be calculated in rectangular form as:

$$\bar{V}_k = V_{kR} + jV_{kI} \tag{5.10}$$

Where V_{kR} and V_{kI} are:

$$V_{kR} = (aV_i\cos\theta_i - bV_i\sin\theta_i - g_{ik}I_{ik}\cos\theta_{ik} - b_{ik}I_{ik}\sin\theta_{ik})/c \tag{5.11}$$
$$V_{kI} = (bV_i\cos\theta_i + aV_i\sin\theta_i + b_{ik}I_{ik}\cos\theta_{ik} - g_{ik}I_{ik}\sin\theta_{ik})/c \tag{5.12}$$

And the magnitude and angle of the bus voltage at bus *k* is,

$$V_k = \sqrt{V_{kR}^2 + V_{kI}^2} \tag{5.13}$$

$$\theta_k = \tan^{-1}\left(V_{kI}/V_{kR}\right) \tag{5.14}$$

The voltages obtained from (5.13)-(5.14) are used as pseudo-measurements in the vector of measurements **z**. These new pseudo-measurements are linearly related with the set of states **x**, as follows:

$$\mathbf{z} = \begin{bmatrix} \mathbf{z}_{conv} \\ \boldsymbol{\theta}_{pmu} \\ \mathbf{V}_{pmu} \\ \boldsymbol{\theta}_{pse} \\ \mathbf{V}_{pse} \end{bmatrix} \rightarrow \mathbf{h}(\mathbf{x}) = \begin{bmatrix} \mathbf{h}(\boldsymbol{\theta}, \mathbf{V}) \\ \boldsymbol{\theta} \\ \mathbf{V} \\ \boldsymbol{\theta} \\ \mathbf{V} \end{bmatrix} \tag{5.15}$$

Here, $\mathbf{z}_{conv}$ is the set of conventional measurements; $\boldsymbol{\theta}_{pmu}$ and $\mathbf{V}_{pmu}$ are the sets of bus voltage angles and magnitudes originally measured by the PMUs; $\boldsymbol{\theta}_{pse}$ and $\mathbf{V}_{pse}$ are the calculated pseudo-measurement sets of bus voltage angles and magnitudes respectively and $\boldsymbol{\theta}$ and $\mathbf{V}$ define the state vector **x**.

It is easy to extract from (5.15) that this estimator can be also decomposed into: a non-linear state estimator with only conventional measurements and a post-processor linear estimator, similar to the two step estimator presented in [26].

5.1.3 Constrained Formulation

This sub-Section presents an alternative formulation to include PMU measurements in state estimation. The aim of the proposed methodology is to avoid the transformation of measurements and consequently to avoid the propagation of uncertainty. In order to relate the current phasor measurements with bus voltages, a set of constraints is included, ensuring the observability of non-PMU buses adjacent to PMU buses.

This formulation starts with the introduction of a new set of states. The new vector is composed of all the bus voltages, as defined in Chapter 2, and an auxiliary state vector composed of the polar form of the branch currents measured by the PMUs:

$$\mathbf{x}^{new} = \left[\mathbf{x}^T, \mathbf{x}^{auxT}\right]^T \tag{5.16}$$

In the above equation,

$$\mathbf{x}^{aux} = [\theta_{ik}, I_{ik}]^T, \quad \forall \ i \in N_{PMU}, \ k \in N^i_{ADJ} \tag{5.17}$$

where N_{PMU} is the subset of PMU buses and N^i_{ADJ} is the subset of adjacent buses to the i-th PMU bus. This auxiliary state vector is introduced in order to apply direct measurements of currents in polar form. Also, these auxiliary states can be used to relate bus voltages from PMU buses and their adjacent buses, as it will be explained later.

The set of measurements $\mathbf{z}$ is made of injected and transferred active and reactive powers, bus voltage magnitudes and voltage and current phasors in polar form (angle and magnitude), measured by the PMUs:

$$\mathbf{z} = \begin{bmatrix} \mathbf{z}_{conv} \\ \boldsymbol{\theta}_{pmu} \\ \mathbf{V}_{pmu} \\ \boldsymbol{\theta}_I^{pmu} \\ \mathbf{I}_{pmu} \end{bmatrix} \rightarrow \mathbf{h}(\mathbf{x}^{new}) = \begin{bmatrix} \mathbf{h}(\boldsymbol{\theta}, \mathbf{V}) \\ \boldsymbol{\theta} \\ \mathbf{V} \\ \boldsymbol{\theta}_I \\ \mathbf{I} \end{bmatrix} \tag{5.18}$$

Here, $\boldsymbol{\theta}_I^{pmu}$ and $\mathbf{I}_{pmu}$ are the set of branch current angles and magnitudes respectively, measured by the PMUs. Since $\boldsymbol{\theta}_I$ and $\mathbf{I}$ are the introduced auxiliary state variables defined in (5.17), there is a linear relation between the states and the PMU measurements.

As the PMU currents are included as state variables, the voltage at any bus k adjacent to a PMU bus can be expressed in terms of state variables and line parameters. The voltage angle and magnitude for a bus k adjacent to a PMU at bus i, can now be expressed as:

$$V_k^i = f_V(V_i, \theta_i, I_{ik}, \theta_{ik}) \tag{5.19}$$

$$\theta_k^i = f_\theta(V_i, \theta_i, I_{ik}, \theta_{ik}) \tag{5.20}$$

As depicted in Figure 5.11, a bus k can be seen from more than one PMU, at buses j and i, but it depends on the network topology and location of the PMUs.

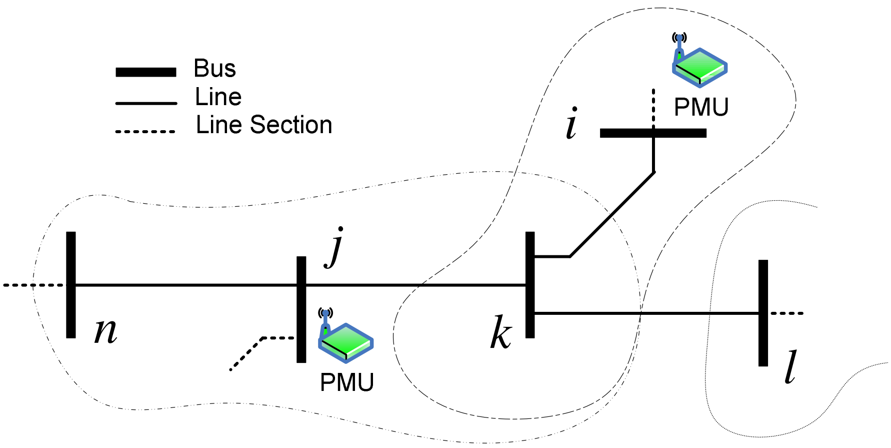

Figure 5.11: Location of PMUs in a section of a power network.

The following constraints are used to relate the PMU buses and their respective adjacent buses:

$$V_k - V_k^i = 0 \tag{5.21}$$

$$\theta_k - \theta_k^i = 0 \tag{5.22}$$

where V_k and θ_k are the state variables corresponding to bus k. These equations are grouped in a new vector **c**, and the minimisation problem in (2.12) is subject to the following equality constraint:

$$\mathbf{c}(\mathbf{x}^{new}) = \mathbf{0} \tag{5.23}$$

Table 5.2 presents the partial derivatives of (5.19)-(5.20) with respect to the new set of state variables. These partial derivatives are included in **C** matrix that corresponds to the partial derivatives of the equality constraints.

Table 5.2: Elements of C corresponding to equality constraints of voltages

$\frac{\partial V_k}{\partial \theta_i} = [V_{kI}(-\frac{b}{c}V_i \sin\theta_i + \frac{a}{c}V_i\cos\theta_i) + V_{kR}(-\frac{a}{c}V_i\sin\theta_i - \frac{b}{c}V_i\cos\theta_i)] / \sqrt{V_{kR}^2 + V_{kI}^2}$	$\frac{\partial \theta_k}{\partial \theta_i} = [V_{kR}(-\frac{b}{c}V_i \sin\theta_i + \frac{a}{c}V_i\cos\theta_i) - V_{kI}(-\frac{a}{c}V_i\sin\theta_i - \frac{b}{c}V_i\cos\theta_i)] / \left(V_{kR}^2 + V_{kI}^2\right)$
$\frac{\partial V_k}{\partial \theta_{ik}} = [V_{kI}(-\frac{I_{ik}}{c}b_{ik}\sin\theta_{ik} - \frac{I_{ik}}{c}g_{ik}\cos\theta_{ik}) + V_{kR}(\frac{I_{ik}}{c}g_{ik}\sin\theta_{ik} - \frac{I_{ik}}{c}b_{ik}\cos\theta_{ik})] / \sqrt{V_{kR}^2 + V_{kI}^2}$	$\frac{\partial \theta_k}{\partial \theta_{ik}} = [V_{kR}(-\frac{I_{ik}}{c}b_{ik}\sin\theta_{ik} - \frac{I_{ik}}{c}g_{ik}\cos\theta_{ik}) - V_{kI}(\frac{I_{ik}}{c}g_{ik}\sin\theta_{ik} - \frac{I_{ik}}{c}b_{ik}\cos\theta_{ik})] / \left(V_{kR}^2 + V_{kI}^2\right)$
$\frac{\partial V_k}{\partial V_i} = [V_{kI}(\frac{b}{c}\cos\theta_i + \frac{a}{c}\sin\theta_i) + V_{kR}(\frac{a}{c}\cos\theta_i - \frac{b}{c}\sin\theta_i)] / \sqrt{V_{kR}^2 + V_{kI}^2}$	$\frac{\partial \theta_k}{\partial V_i} = [V_{kR}(\frac{b}{c}\cos\theta_i + \frac{a}{c}\sin\theta_i) - V_{kI}(\frac{a}{c}\cos\theta_i - \frac{b}{c}\sin\theta_i)] / \left(V_{kR}^2 + V_{kI}^2\right)$
$\frac{\partial V_k}{\partial I_{ik}} = [V_{kI}(\frac{b_{ik}}{c}\cos\theta_{ik} - \frac{g_{ik}}{c}\sin\theta_{ik}) + V_{kR}(-\frac{g_{ik}}{c}\cos\theta_{ik} - \frac{b_{ik}}{c}\sin\theta_{ik})] / \sqrt{V_{kR}^2 + V_{kI}^2}$	$\frac{\partial \theta_k}{\partial I_{ik}} = [V_{kR}(\frac{b_{ik}}{c}\cos\theta_{ik} - \frac{g_{ik}}{c}\sin\theta_{ik}) - V_{kI}(-\frac{g_{ik}}{c}\cos\theta_{ik} - \frac{b_{ik}}{c}\sin\theta_{ik})] / \left(V_{kR}^2 + V_{kI}^2\right)$

Under the proposed formulation, Kirchoff's current Law is perfectly maintained while currents are free to vary as states in order to find the optimal estimation. Additionally, all measurements are used directly without any transformation in the estimation process.

The initial state vector guess is set to flat start for voltages (or the solution from the previous estimation) and the initial state of currents may be initialized with the actual measurement of the respective currents.

5.2 Uncertainty Propagation

The calculation of uncertainty propagation is an important task that has to be addressed when measurements are transformed or combined to create new set of measurements. Depending on the algorithm used, the inclusion of synchrophasors in the estimation problem may require transformation of power measurements into current measurements [78], conversion from polar to rectangular form [27] or combination with other measurements to create pseudo-measurements [77]. For all these cases, the calculation of the propagation of uncertainties is necessary in order to assign weights to the new measurements.

Let the initial set of measurement be defined as:

$$\mathbf{z} = [z_1, z_2, \dots, z_m]^T \tag{5.24}$$

where $\mathbf{z}$ is an $m \times 1$ vector of original measurements with mean vector $\bar{\mathbf{z}} = E[\mathbf{z}]$ and covariance matrix $\mathbf{P}_z$:

$$\mathbf{P}_z = E[(\mathbf{z} - \bar{\mathbf{z}})(\mathbf{z} - \bar{\mathbf{z}})^T] \tag{5.25}$$

The problem of uncertainty propagation is to find the $m_y \times 1$ mean vector $\bar{\mathbf{y}}$ and the $m_y \times m_y$ covariance matrix $\mathbf{P}_{y.}$ of $\mathbf{y}$ given:

$$\mathbf{y} = \mathbf{g}(\mathbf{z}) \tag{5.26}$$

where $\mathbf{y}$ is the $m_y \times 1$ vector of transformed measurements resulting from the non-linear function $\mathbf{g}(\mathbf{z})$.

5.2.1 Classical Uncertainty Propagation Method

The classical method approximates the calculation of the mean vector $\bar{\mathbf{y}}$ by neglecting the higher order terms of $\mathbf{g}(\mathbf{z})$ [79]:

$$\bar{\mathbf{y}} = E[\mathbf{g}(\mathbf{z})] \approx \mathbf{g}(\bar{\mathbf{z}}) \tag{5.27}$$

And the uncertainty of $\mathbf{y}$, represented by the covariance matrix $\mathbf{P}_y$, is also obtained from a linear approximation of $\mathbf{g}(\mathbf{z})$:

$$\mathbf{P}_y = \mathbf{G}_z \mathbf{P}_z \mathbf{G}_z^T \tag{5.28}$$

where,

$$\mathbf{G}_z = \frac{\partial \mathbf{g}(\mathbf{z})}{\partial \mathbf{z}} \tag{5.29}$$

Under these approximations, the mean vector and its covariance matrix $\mathbf{P}_y$ can result in errors if $\mathbf{g}(\mathbf{z})$ is highly non-linear and the uncertainty of $\mathbf{z}$ is large.

5.2.2 Unscented Transformation Method

This section presents a more accurate methodology to estimate the mean and covariance of transformed measurements, based on the *Unscented Transformation* (UT) approach. The idea of UT is to obtain a number of so called *sigma points*, deterministically chosen, which exactly capture the mean and covariance of the original distribution of $\mathbf{z}$. The sigma points are grouped in vectors and they approximate the distribution of $\mathbf{z}$ [79]. The sigma points are then propagated, one by one, in $\mathbf{g}(\mathbf{z})$ to estimate the mean vector $\bar{\mathbf{y}}$ and covariance matrix $\mathbf{P}_y$.

The main benefit of using UT over the classical method is that, for similar computational requirements, it provides higher accuracy as higher order terms of the non-linear function $\mathbf{g}(\mathbf{z})$ are considered. The *Unscented Transformation* approach can be described through the following three steps:

<u>Step 1</u>: Obtain a set of $2m$ vectors of sigma points that capture the mean and covariance of the original $m \times 1$ vector of original measurements $\mathbf{z}$:

$$\mathbf{Z}_i = \bar{\mathbf{z}} + \left(\sqrt{m\mathbf{P}_z}\right)_i,\ i=1,\ldots,m \tag{5.30}$$

$$\mathbf{Z}_{m+i} = \bar{\mathbf{z}} - \left(\sqrt{m\mathbf{P}_z}\right)_i,\ i=1,\ldots,m \tag{5.31}$$

where $\left(\sqrt{m\mathbf{P}_z}\right)_i$ is the i-th column of matrix $\sqrt{m\mathbf{P}_z}$.

<u>Step 2</u>: Propagate the sigma points through the non-linear functions $\mathbf{g}$:

$$\gamma_i = \mathbf{g}(\mathbf{Z}_i)\ ,\ i=1,\ldots,2m \tag{5.32}$$

<u>Step 3</u>: Calculate the mean and covariance for $\mathbf{y}$:

$$\bar{\mathbf{y}} = \frac{1}{2m}\sum_{i=1}^{2m}\gamma_i \tag{5.33}$$

$$\mathbf{P}_{\mathrm{y}} = \frac{1}{2m}\sum_{i=1}^{2m}\left[(\boldsymbol{\gamma}_i - \overline{\mathbf{y}})(\boldsymbol{\gamma}_i - \overline{\mathbf{y}})^{\mathrm{T}}\right] \tag{5.34}$$

The UT does not need to calculate a Jacobian matrix to cope with the non-linearity of **g**(**z**). Only $2m$ vectors of sigma points are needed to capture the distribution of **z** (for example, Gaussian) with subsequent evaluations in **g**(**z**) to calculate the new measurement uncertainties. As the sigma points are calculated deterministically, the UT requires less computational demands compared to Monte Carlo methods where thousands of evaluations are needed to capture the distribution of both **z** and **y** [80].

For example, let us consider a measurement set **z** in polar form, whose mean vector and covariance matrix are defined as follows:

$$\overline{\mathbf{z}} = \begin{bmatrix} \overline{r} \\ \overline{\theta} \end{bmatrix} = \begin{bmatrix} 1 \\ \pi/4 \end{bmatrix}, \quad \mathbf{P}_{\mathrm{z}} = \begin{bmatrix} \sigma_r^2 & 0 \\ 0 & \sigma_\theta^2 \end{bmatrix} = \begin{bmatrix} 0.050^2 & 0 \\ 0 & 0.035^2 \end{bmatrix}$$

It is desired to convert the measured data into rectangular form. The polar-to-rectangular non-linear transformation is,

$$\mathbf{g}(\mathbf{z}) = \begin{bmatrix} r\cos\theta & r\sin\theta \end{bmatrix}^T$$

Based on the UT approach, it is necessary to build the set of $2m$ sigma points, with $m = 2$:

$$\mathbf{Z} = \begin{bmatrix} 1.0707 & 1.0000 & 0.9293 & 1.0000 \\ 0.7854 & 0.8349 & 0.7854 & 0.7359 \end{bmatrix}$$

In order to obtain the propagated sigma points, each sigma point set $\mathbf{Z}_i$, (i-th column of **Z**) is evaluated in **g,** as presented in (5.32):

$$\boldsymbol{\gamma} = \begin{bmatrix} 0.7571 & 0.6713 & 0.6571 & 0.7412 \\ 0.7571 & 0.7412 & 0.6571 & 0.6713 \end{bmatrix}$$

Finally, the mean and covariance of the new sigma points are calculated using (5.33) and (5.34):

$$\overline{\mathbf{y}} = \begin{bmatrix} 0.7067 \\ 0.7067 \end{bmatrix}, \quad \mathbf{P}_y = 10^{-3} x \begin{bmatrix} 1.8622 & 0.6382 \\ 0.6382 & 1.8622 \end{bmatrix}$$

The UT approach approximates the true mean and covariance of **y** up to the third order [79]. In addition, the calculated covariance contains correct sign terms to the fourth and higher powers.

The mean and covariance of **y** obtained from the classical method based on linearization of **g**(**z**) is:

$$\bar{\mathbf{y}} = \begin{bmatrix} 0.7071 \\ 0.7071 \end{bmatrix}, \quad \mathbf{P}_y = 10^{-3} x \begin{bmatrix} 1.8625 & 0.6375 \\ 0.6375 & 1.8625 \end{bmatrix}$$

The classical method does not provide any extra information about higher order terms [79], consequently the UT mean vector and its covariance matrix should generally be more accurate than those obtained by the classical approach.

5.3 Study Cases

This section presents test results using the IEEE 14, 57 and 118 bus test systems. The network parameters and loading conditions are presented in [64]. The methodologies presented in sub-Sections 5.1.2 and 5.1.3 were compared to the rectangular PMU currents formulation presented in Section 5.1.1.

Table 5.3 lists the types of measurements used for the three test systems and the corresponding measurement uncertainties. The uncertainties in Table 5.3 are expressed in percentage of the actual measurement value and they are used to create the random noise in the measurements needed during the Monte Carlo simulations.

Table 5.3: Standard deviation of measurements

Conventional measurements			PMU measurements		
Voltage	Injected power	Power flows	Voltage	Current	Phase angle
0.2%	2%	2%	0.02%	0.03%	0.01°

5.3.1 SE Performance Index

The first performance index used in this work for comparison purposes is the variance of the estimated states:

$$\sigma_{\Sigma}^2 = \sum_{i=1}^{2N} (\hat{x}_i - x_i^t)^2 \tag{5.35}$$

where, $\hat{x}$ and x^t are the estimated and true state values respectively and N is the number of buses in the system. The second performance index relies on measurement errors and it is given by,

$$\xi(\hat{x}) = \sum_{i=1}^{m} \left(\hat{z}_i - z_i^t \right)^2 \Big/ \sum_{i=1}^{m} \left(z_i - z_i^t \right)^2 \tag{5.36}$$

where $\hat{z}$, z^t and z are the estimated, true, and available measurements, respectively. The result of the objective function is not used as a performance index since it does not quantify the accuracy of estimators. Nevertheless, it may be useful for detecting bad data by using a chi-square distribution test, if necessary.

In order to obtain a more reliable comparison from the estimator testing, 100 Monte Carlo simulations have been carried out. For each Monte Carlo simulation, the sample of a measurement is randomly taken from the distribution of the measurement around the mean (measured) value.

5.3.2 Placement of PMUs and Conventional Measurements

The conventional measurements were deterministically located in the system to create the set of existing measurements in the system:

- The 14-bus test system has flow measurements in 50% of its lines and power injection measurements at 57% of its buses.
- The 57-bus test system is assumed to have power flow measurements in 56% of its lines and power injection measurements at 35% of its buses.
- The 118-bus system has power flow measurements in 40% of its lines and power injection measurements at 42% of its buses.

Subsections 5.3.2.1 and 5.3.2.2 present the algorithms used in this work to locate the PMUs in the three test systems. Note that these subsections are included to justify the location of the PMUs only and these algorithms are not a contribution of this Thesis.

5.3.2.1 Measurement Redundancy Improvement

A valid criterion for including PMUs in the system is the improvement of local/global redundancy levels and elimination of *critical* measurements (redundancy level equal to zero).

The adequate performance of Bad Data Detectors (BDD), such as the normalized residual approach, depends on the availability of redundant measurements. It is important to eliminate *critical* measurements as they could never be detected as erroneous data, thus adversely affecting the performance of state estimators.

An optimal placement of PMUs in the system can eliminate *critical* measurements and can improve redundancy levels of *basic measurements* (set of measurements which are sufficient to make the system fully observable).

After observability analysis for the 14-bus IEEE test system, it was concluded that the number and location of the existing conventional measurements is enough to make the system fully observable.

Redundancy analysis indicated that there are measurements with redundancy levels equal to one and possible loss of a single measurement would result in various critical measurements, affecting Bad Data Detection (BDD) [38]. The optimal location of PMUs to improve local redundancy was determined using the method proposed in [39]. The objective function is:

$$\begin{gathered}\text{Minimise } \sum_{i=1}^{p} q_i \alpha_i \\ \text{Subject to } \mathbf{w} + \mathbf{F} \cdot \boldsymbol{\alpha} \geq \mathbf{b}\end{gathered} \tag{5.37}$$

where:

p	number of candidate PMUs.
q	vector of costs for installing candidate PMUs.
α	binary vector corresponding to candidates PMUs.

If a PMU is placed, α_i will be 1, otherwise 0. Additionally, **w** is a vector indicating the existing redundancy of the basic measurements and **F** is a matrix relating candidate PMUs and critical measurements (or any other basic measurement with low redundancy level). Moreover, vector **b** indicates the level of redundancy desired for each basic measurement. For **b=1**, it ensures that no critical measurements are present. Higher levels of local redundancy are obtained by increasing elements of **b**.

The same methodology was used for the 118 bus IEEE test system since local redundancy was also desired to be improved for BDD.

5.3.2.2 Enhancement of Network Observability

Power systems under low measurement availability and/or loss of communication links may lead to the loss of system observability, making the estimation problem unsolvable. In such cases, pseudo-measurements have to be included to recover observability, resulting in reduced estimation accuracy. An alternative procedure is to include a minimum number of PMUs to recover system observability if observable islands are identified.

Once observable islands are known, it is possible to formulate the optimisation problem which finds the minimum number of PMUs to recover system observability:

$$\begin{gathered} \text{Minimise } \sum_{i=1}^{p} q_i \alpha_i \\ \text{Subject to } \mathbf{F}_2 \cdot \boldsymbol{\alpha} \geq \mathbf{b}_2 \end{gathered} \tag{5.38}$$

The incidence matrix $\mathbf{F}_2$ relates candidate PMUs with the observable islands: $\mathbf{F}_2(k,i)$ is one if the *i*-th PMU is located inside or at boundary of island *k*, or zero otherwise.

In order to recover system observability, it is necessary that all islands are observed by at least one PMU. Based on this fact, vector $\mathbf{b}_2$ must be a unitary vector. Each element of $\mathbf{b}_2$ will correspond to each observable island previously identified. If PMU reliability is a concern, one could increase the values of $\mathbf{b}_2$ to guarantee system observability even under the outage of some PMUs.

In the 57 bus system, it was found that the system frequently splits into five observable islands due to failures of communication links. In order to avoid islanding, PMUs were optimally located over the system by using $\mathbf{b}_2 = \mathbf{2}$ in (5.38). This not only recovers system observability but ensures that the loss of any single PMU will not lead to unobservable conditions.

An equality constraint was included in (5.37) and (5.38) for all test cases to ensure that one PMU is located at the slack bus. This permits that all synchronised measurements can be referred to a common angle reference equal to zero, in the slack bus. The PMU placement sets for the three test systems are given in Table 5.4.

Table 5.4: Optimal location of PMUs

Test System	Buses with PMU
14 buses	1 and 4
57 buses	1, 9, 18, 19, 30, 31 and 55
118 buses	24, 40, 59, 69, 75, 80, 100, 103, 113 and 114

Figures 5.12-5.14 present the location of the conventional and synchronised measurements for the three test systems. Due to space limitations, Figure 5.14 does not include the synchronous condensers, see Appendix G.4 for details about these elements. Null power injection measurements were included as equality constraints.

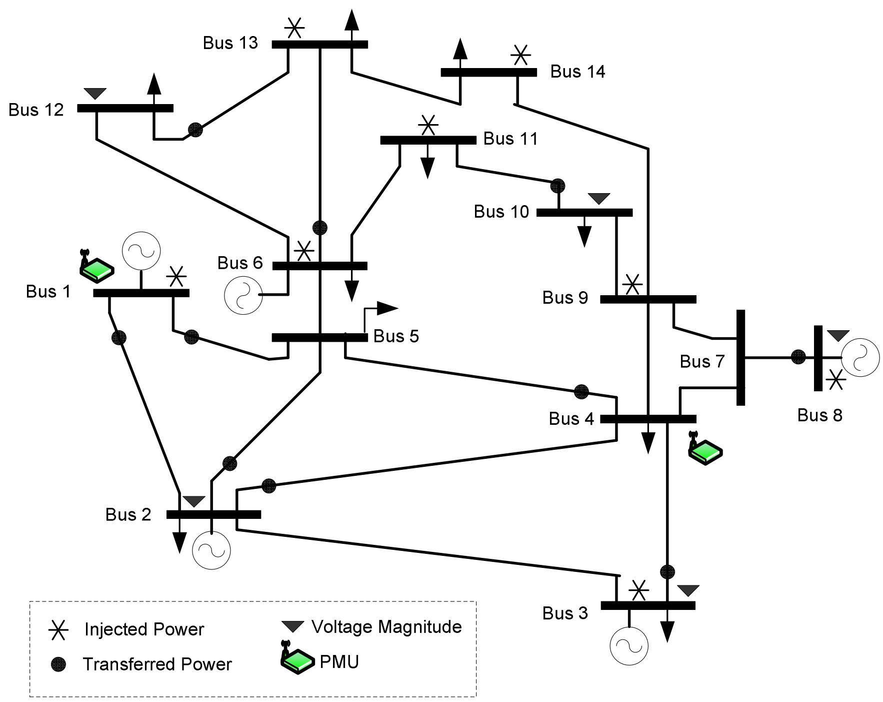

Figure 5.12: Measurement allocation in 14-bus test system

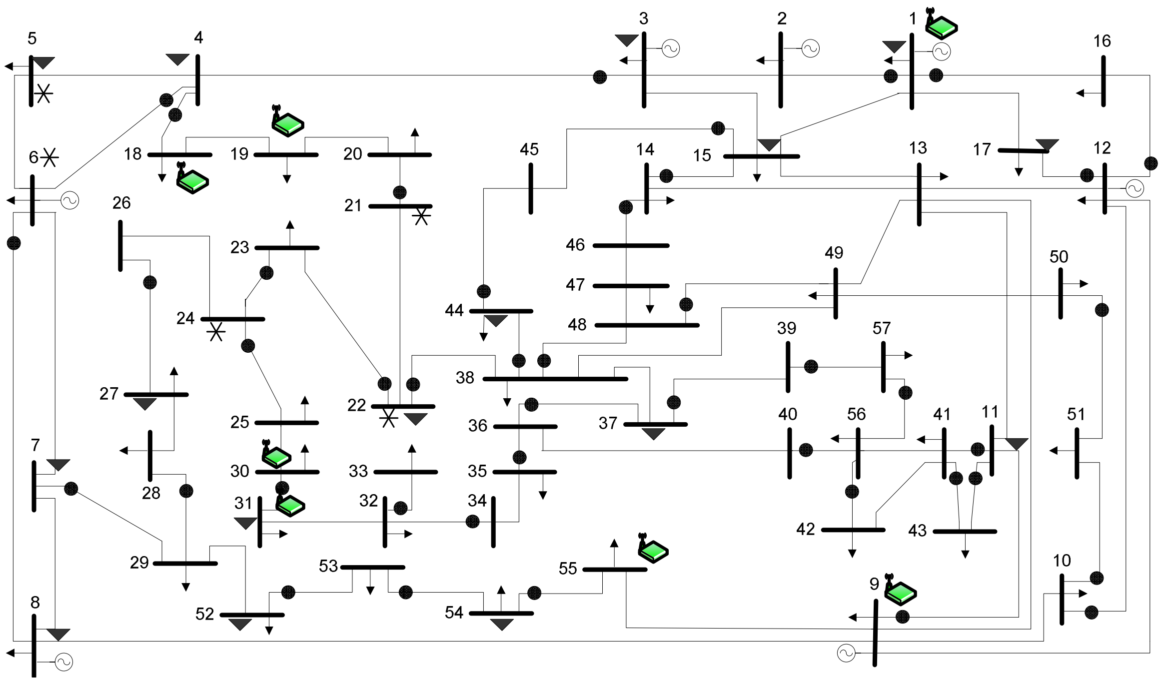

Figure 5.13: Measurement allocation in 57-bus test system

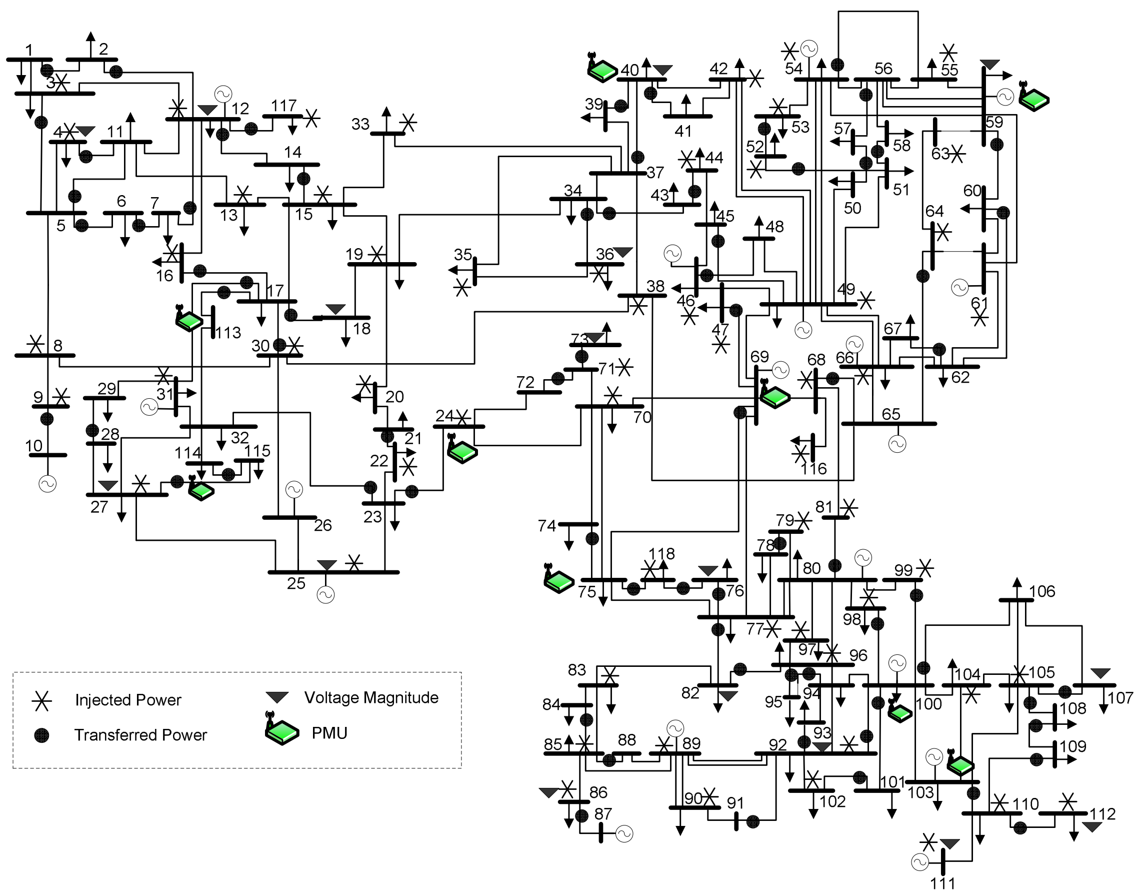

Figure 5.14: Measurement allocation in 118-bus test system

5.3.3 Assessment of Estimators

Three different methods for each test system have been used to assess the performance of the proposed estimator:

Method 1: Currents measured in polar form were transformed into rectangular form as proposed in [27] and presented in sub-Section 5.1.1. The transformation of measurements and uncertainties was carried out using the UT. In addition, constrained estimation was used for null power injections only.

Method 2: The state estimator was based on the *Pseudo-Voltage Measurement Approach*, as explained in sub-Section 5.1.2. Both, conventional and synchrophasor measurements were used to estimate the system state. Bus voltage measurements of adjacent buses to PMU buses are created according to (5.13)-(5.14). Therefore, if the IEEE 14 bus test system is taken as an example, besides voltage measurements at *Buses 1* and *4*, one obtains voltage measurements of *Buses 2, 3, 5, 7* and *9*. The uncertainties of these new measurements are obtained using the UT approach. Again, constrained estimation was used for null power injections only.

Method 3: The estimator is based on the constrained formulation presented in Section 5.1.3. The state vector was extended to include the polar form of PMU currents. For the IEEE 14 bus test system, there are 16 constraints that have to be met: 2 for null power equations at *Bus 7*, and 14 constraints for adjacent buses to PMU buses (*Buses 2* and *5* are observed twice by PMUs).

Figures 5.15 and 5.16 present the estimation errors obtained from the three methods using the 14-bus test system. The convergence criterion used in all estimation procedures was 10^{-6} p.u. The results were collected from 100 Monte Carlo simulations.

From Figures 5.15 and 5.16, it can be concluded that there is a clear advantage when using *Method 3* in comparison to *Method 2*. This is because PMU currents are used to relate states of both adjacent and PMU buses in the constrained formulation. On the other hand, *Method 2* loses some information, about the states of PMU buses provided by PMU currents, because the pseudo-measurements of voltage are modelled in terms of voltages of adjacent buses only. The constraints for *Method 3* are all fulfilled with a maximum error of 10^{-12} p.u. Figures 5.15 and 5.16 also demonstrate that the constrained formulation is comparable in accuracy to *Method 1* but there is no need to transform the PMU measurements.

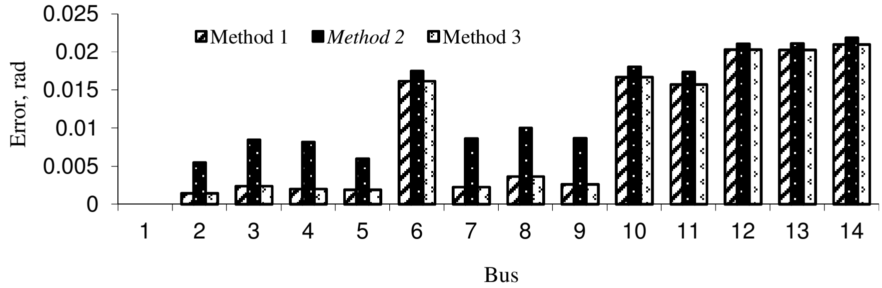

Figure 5.15: Voltage angle estimation errors for the IEEE 14 bus test system.

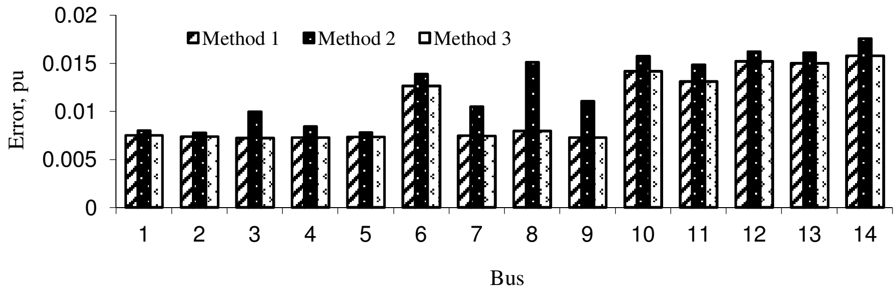

Figure 5.16: Voltage magnitude estimation errors for the IEEE 14 bus test system.

Table 5.5 presents a comparison of estimation accuracy based on performance indices for the 14, 57 and 118 bus test systems. The term S/C is the ratio of synchronised to conventional measurements in the system.

The estimations were significantly more accurate once synchronised measurements were included, as presented in Table 5.5. This validates that the presence of few PMU measurements substantially improves the accuracy of the estimations. For the 57 bus system, a classical state estimation cannot be solved because the system is not fully observable with only conventional measurements. In fact, this was the reason why PMUs were optimally installed in the network.

As expected for the 14 bus test system, the state variance and the measurement error index ξ are smaller in *Methods 1* and *3* than in *Method 2*. However, the objective function *J* is smaller in *Method 2*, which confirms that this index is not a measure of the accuracy of estimators, but it is still very useful for bad data detection based on statistical procedures.

In the case of the 57 bus test system, the number of constraints for *Method 3* is 72; from which, 30 constraints correspond to null power injections and the remaining 42 are constraints for adjacent buses to PMU buses.

In the case of the 118 bus test system, the number of constraints is 114. Here, 16 constraints correspond to null power injections and the other 98 constraints are used for adjacent buses to PMUs. It is again concluded that constrained and rectangular current formulations deliver more accurate estimations than the pseudo-voltage formulation.

Table 5.5: Estimation results for 100 Monte Carlo simulations

System		σ_{Σ}^{2}	ξ	J
14 buses S/C = 18/43	Method 1	5.8122×10^{-7}	0.0200	14.0015
	Method 2	7.4374×10^{-7}	*0.0320*	*13.3023*
	Method 3	5.8123×10^{-7}	0.0200	14.0186
S/C=0/43	*Classical*	1.3400×10^{-5}	*0.3587*	*6.2681*
57 buses S/C=56/146	Method 1	3.9829×10^{-6}	0.2287	49.5373
	Method 2	4.5251×10^{-6}	*0.2601*	*46.3422*
	Method 3	3.9825×10^{-6}	0.2288	49.6799
S/C=0/146	*Classical*	--	--	--
118 buses S/C=118/265	Method 1	5.2060×10^{-5}	0.4274	75.9057
	Method 2	5.5653×10^{-5}	*0.4493*	*66.1592*
	Method 3	5.2064×10^{-5}	0.4273	74.7258
S/C=0/265	*Classical*	6.1124×10^{-4}	*0.7334*	*15.0869*

Table 5.6 presents a comparison of computational speed and required iterations for all three hybrid estimators. The simulations were carried out using an Intel Core (TM) 2 6400 @ 2.13-

GHz CPU with 2.97 GB of RAM

Table 5.6: Time demands of hybrid estimators

Average	Method 1	Method 2	Method 3
Time [s]	0.7965	0.652	0.9666
Iterations	4.98	4.5	4.65

It is found that, on average, the constrained formulation (Method 3) requires slightly larger computing times than the other two methods. However, on average, the constrained formulation requires less iterations than the rectangular formulation approach. Table 5.6 does not consider the time required to transform PMU measurements and calculate the covariance matrix needed in *Methods 1* and *2*.

5.3.4 Estimation of Measurement Uncertainty

Let us consider the 14 bus test system. In *Method 2*, the currents measured from the PMU at *Bus 4* were transformed into pseudo-voltage measurements using the UT approach.

The calculated mean and covariance of the new pseudo-measurements were compared to the classical method using (5.27)-(5.28). Table 5.7 presents the estimated mean vector of the new pseudo-voltage measurements. Both methods deliver practically the same result since the variance of the original measurements is very small; this leads to insignificant errors caused by neglecting higher order terms of the true mean vector.

Table 5.7: Comparison of mean vector estimation

----	UT Method		Classical Method	
	$\|V\|$ [p.u.]	θ [rad]	$\|V\|$ [p.u.]	θ [rad]
Bus 2	1.0451318	-0.08690058	1.0451318	-0.08690058
Bus 3	1.00994583	-0.2220894	1.00994583	-0.2220894
Bus 5	1.01963618	-0.15303897	1.01963617	-0.15303897
Bus 7	1.06144752	-0.2331688	1.06144752	-0.2331688
Bus 9	1.05588427	-0.26074462	1.05588427	-0.26074462

In the same way, almost identical results were obtained when comparing the calculation of the new covariance matrix. For easier comparison, Table 5.8 presents the diagonal elements of the square root of the $\mathbf{P}_y$ matrix. The off-diagonal elements of $\mathbf{P}_y$ were found to be up to 50 times smaller than its diagonal elements. Their inclusion in the error covariance matrix $\mathbf{R}$ had a minimum effect over the estimation process.

Table 5.8: Comparison of standard deviation estimation

----	UT Method		Classical Method	
Uncertainty in p.u.	σ_θ x 10^4	σ_V x 10^4	σ_θ x 10^4	σ_V x 10^4
Bus 2	0.99232560	1.17570625	0.99232559	1.17570626
Bus 3	1.01721504	1.17441442	1.01721504	1.17441443
Bus 5	1.00702896	1.17533309	1.00702896	1.17533310
Bus 7	0.99255827	1.20305353	0.99255827	1.20305355
Bus 9	1.01286742	1.21486334	1.01286742	1.21486335

The expected errors due to neglecting the higher order terms of the non-linear function $\mathbf{g}(\mathbf{z})$ are negligible because the uncertainty of the original PMU measurement is very small. The higher the uncertainty of the original measurements the more inaccurate the calculated mean and covariance matrix of the new measurements will be when the linearised approach is used.

5.4 Summary

This Chapter studies three alternatives for including PMU measurements in power system state estimation, i.e. hybrid state estimation. As the direct use of PMU currents in polar form leads to convergence problems, this work presents different formulations for including (or replacing) these measurements. The first two formulations transform the PMU measurements into rectangular form or pseudo-voltage measurements and the third makes use of a constrained WLS formulation with no transformation of PMU measurements.

The proposed HCSE gives the possibility to implement the PMU currents in polar form. This avoids the transformation of measurements and the propagation of errors during the transformation. This is important because the errors are random variables, and the presence of large errors may affect the new transformed measurements. In addition, as the resulting (transformed) measurements are the combination of PMU voltages and currents, these measurements will be correlated.

The proposed methodology avoids this problem. To do so, it introduces a new set of constraints to estimate the bus voltages adjacent to PMU buses, and gives the possibility to correct and filter out small errors in PMU measurements. In other words, the resulting estimated line currents may be slightly different from the PMU current measurements.

The Unscented Transformation (UT) was also introduced to approximate the propagation of uncertainties in the hybrid state estimation formulations that required the transformation of PMU measurements.

The UT delivered almost identical results as the classical propagation method. It was found that the uncertainties of PMU measurements were so small that the errors caused by linearisation approximations in the classical method were negligible.

Chapter 6 is focused on the problem of estimating the state of large interconnected power networks. In order to cope with such a high dimensional problem, the PMU based state estimator is distributed into smaller independent local state estimators whose solutions must be in agreement with each other.

Chapter 6 Multi-Area State Estimation

Integrated state estimators are the most accurate option when estimating the state of a power system. They make use of all available measurements in the entire power network to estimate the system operating point. However, the size and complexity of large power networks suggests that a strategy of decentralising the estimation problem by distributing the computation into local area estimators may be beneficial [81]. This strategy is the main idea of *Multi Area State Estimators* (MASE). They provide reliable estimates for large-scale power systems with significantly reduced computational requirements when compared to the aforementioned integrated solutions.

Large scale incidents experienced in the last years has pointed out the need of more accurate real-time visibility of the system state beyond the area covered by the estimator of a country or region [82]. Additionally, it is important to obtain accurate estimates of the actual power transfers between areas as power transaction operations will rely on the information given by the state estimator.

MASE are classified according to their computing architecture [82]. One is based on a hierarchical scheme composed by a master processor (coordinator) that corrects the solution of the slave processors (local estimators) and the other architecture is based on a decentralised approach. In the decentralised option, the local estimators directly exchange information with those estimators in charge of neighbouring areas.

A good MASE (hierarchical or decentralised architecture) must fulfil the following basic requirements: a) high computational efficiency, b) accuracy should be similar to the integrated solution, c) highly robust to deal with topology changes, d) bad data processing for buses located close to boundary buses, and e) low data exchange between areas [82].

Some efforts have been made to obtain the same, or very similar, accuracy as the integrated solution. Reference [83] introduces an optimisation based method that reaches a wide-area sub-optimal solution by solving local area optimisation problems. This decentralised methodology was later extended in [84]. It is based on a Langrangian Relaxation technique that exchanges information between regions without using a central coordinator. Each area runs its own state estimator and waits for the most updated state estimation of the external boundary buses. The solution was found to be the same as the integrated one. The paper also proposed a bad data detection procedure within and between areas. In the case of measurement errors close to boundary buses, the algorithm requires to include measurements in boundary buses from other areas.

The *Diakoptic based* distributed estimator proposed in [30] is able to obtain the same accuracy as the integrated solution. In addition, the method proposed in [85] includes a set of virtual measurements to obtain consistent solutions in boundaries of different areas. However, the disadvantage of these methods is the data dependency among areas during the estimation process.

Reference [86] proposes a generalised state estimator including distribution and transmission networks made of three main levels of hierarchy. The lowest level is composed by local estimators at the substation level. Then an intermediate level is made of independent state estimators for each Transmission System Operator (TSO), and finally, the highest level that corresponds to a regional state estimator to fine-tune the solution provided by the TSOs affiliated with the interconnected system.

A hierarchical scheme is also presented in [75]. Here, a constraint formulation is used to deal with boundary measurements. The approach is found to have the same redundancy level and accuracy of a single centralised estimator.

At present, *two-level* estimators are the most common approach developed for MASE due to their simplicity and limited data exchange between areas [82]. In two-level MASE, the power system is separated into small observable subsystems, each one assigned with a slack (reference) bus to run a lower (local) level state estimation.

The state estimation solution of each subsystem is then collected by the central coordinator that unifies and coordinates the lower level solutions in order to obtain an overall estimate of the entire power system.

One challenge in two-level estimators, particularly during the coordination level, is how to deal with power injection measurements in boundary buses. If they are included, each area will have to provide some information about their internal topology to the coordination level [28]. This option might not be always feasible as utilities usually prefer to restrict their topology configuration information for privacy and/or security reasons. Additionally, considering power injection measurements in the coordination level makes it necessary to include the states of internal buses adjacent to boundary buses, which increase the size of the problem.

Another option would be not including the power injection measurements of boundary buses. However, this would result in a loss of information and lower redundancy at the coordination level.

The methodology proposed in this work avoids the use of power injection measurements of boundary buses in the coordination level. This reduces the data exchange between local and coordination estimators. Instead, a new set of transferred powers pseudo-measurements are included to maintain the redundancy level and accuracy of the coordination level. Moreover, wide area measurements obtained from PMUs are used in boundary buses and slack buses, improving the efficiency of both the lower (local) and the higher (coordination) estimation levels. The proposed PMU based MASE minimises the data exchange between local and coordination estimators.

The following sections explain in detail the set of measurements and vector of states for each local estimator and the information that is transmitted to the coordination level.

6.1 Local State Estimators

Each local area state estimator provides an estimate of the sub-system state based on the available measurements in each area. For any area *i*, the following three bus types are identified:

- Internal bus: any bus that is not adjacent (connected) to any external bus.
- Boundary bus: any bus adjacent to at least one external bus. The interconnection between a boundary bus and an external bus is referred to as a tie-line.
- External bus: any bus belonging to a different area that is connected to at least one boundary bus of area *i*, by a tie-line.

Let the set of measurements $\mathbf{z}_i$ in area *i* be defined as:

$$\mathbf{z}_i = \mathbf{h}(\mathbf{x}_i) + \mathbf{e}_i \tag{6.1}$$

where $\mathbf{h}(\mathbf{x}_i)$ is the set of non-linear equations relating the measurements with the state variables, $\mathbf{x}_i$ and $\mathbf{e}_i$ is the set of uncorrelated measurement errors with Gaussian distribution.

The state vector is defined as follows:

$$\mathbf{x}_i = [\mathbf{x}_i^{\text{int}}, \mathbf{x}_i^{\text{b}}, \mathbf{x}_i^{\text{ext}}]^T \tag{6.2}$$

where:

$\mathbf{x}_i^{\text{int}}$ is the set of bus voltages corresponding to the internal buses of area *i*.

$\mathbf{x}_i^{\text{b}}$ is the set of bus voltages corresponding to the boundary buses of area *i*.

$\mathbf{x}_i^{\text{ext}}$ is the set of bus voltages corresponding to the external buses of area *i*.

The best estimation of the system states in area *i* is obtained through the constrained WLS formulation introduced in Chapter 2.

Each local estimator must have enough measurements to make the system fully observable with redundant measurements to detect and eliminate bad data. Each area has its own reference; hence, there are *S* different slack buses in the interconnected power network, one for each area.

Based on the principle that each local estimator is independent of any other estimator (and vice versa), all synchrophasor measurements in area *i* will be referred to its local reference in the lower level estimation.

Figure 6.1 shows how the PMU measurements are referred to its own slack bus during the lower level estimation. Without loss of generality, it can be assumed that a PMU is located at the local slack bus. In fact, installing a PMU in each slack bus will improve the coordination level estimation, as will be explained later.

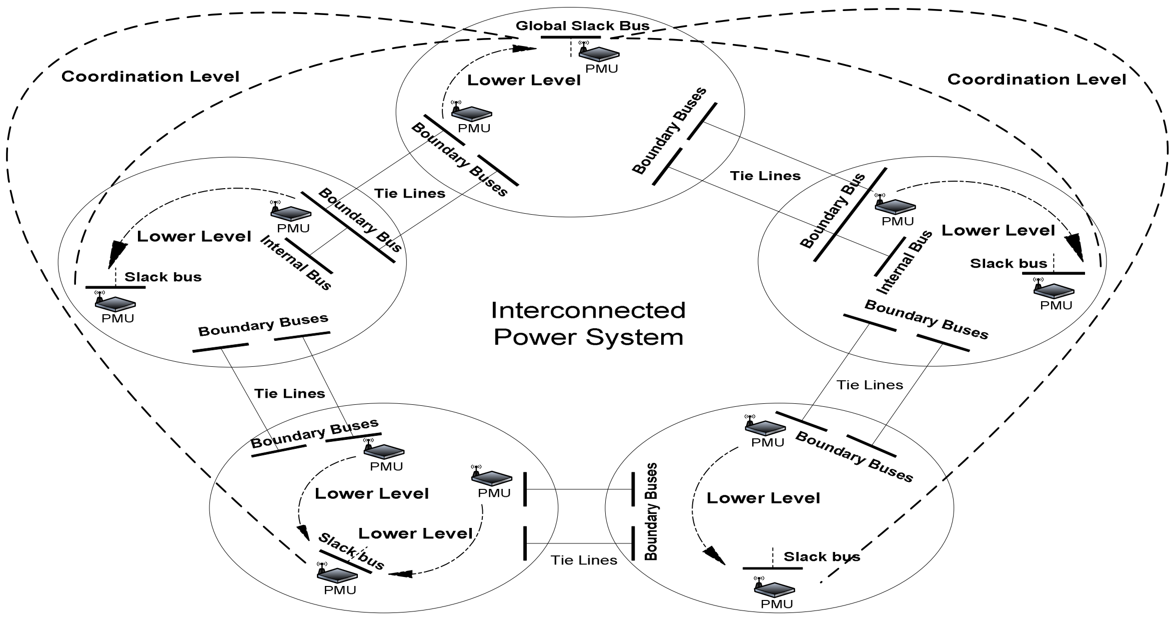

Figure 6.1: Multi-Area power system with PMU measurements for state estimation (local level and coordination level)

6.2 Coordination Level

The higher (coordination) level estimator uses the estimated states corresponding to boundary buses, obtained from local estimators, and those measurements at the boundaries of each area to create the set of measurements $\mathbf{z}_c$:

$$\mathbf{z}_c = \mathbf{h}(\mathbf{x}_c) + \mathbf{e}_c \tag{6.3}$$

The WLS method is also used to estimate the new set of states $\mathbf{x}_c$ at the coordination level. This vector is defined as:

$$\mathbf{x}_c = [\mathbf{x}_i^b, \theta_i^{sk}]^T \; \forall \; i = 1, 2, ..., S \tag{6.4}$$

where:

$\mathbf{x}_i^b$ is the set of boundary bus voltages in area i. In the coordination level all bus voltage angles are referred to the global slack bus.

θ_i^{sk} is the slack bus angle for area i referred to the global slack bus.

The set of measurements $\mathbf{z}_c$ in (6.3) is defined in sub-sections 6.2.1-6.2.3:

6.2.1 Synchronised Measurements

By including PMU measurements in MASE, the accuracy of the overall estimation (lower level and coordination level) is improved. Firstly, the PMUs improve measurement redundancy levels and the estimation accuracy of local estimators. Secondly, if PMUs are located at the boundaries of the subsystems, they will also improve the accuracy of the coordination level [28]. In addition, when PMUs are located at the slack bus of each subsystem, the angle difference between slack buses will be determined directly.

The synchronised measurements used in the Coordination Level can be separated in the following measurement vector:

$$\mathbf{z}_c^{sync} = \left[\boldsymbol{\theta}_i^b, \mathbf{V}_i^b, \mathbf{I}_{iR}^{ij}, \mathbf{I}_{iI}^{ij}, \boldsymbol{\theta}_i^{sk}\right]^T \; \forall \; i = 1, 2, ..., S. \tag{6.5}$$

where:

$\boldsymbol{\theta}_i^b$ is the set of boundary bus voltage angle measurements in area i referred to the local reference in area i.

$\mathbf{V}_i^b$ is the set of boundary bus voltage magnitudes in area i.

$\mathbf{I}_{iR}^{ij}$ and $\mathbf{I}_{iI}^{ij}$ are the real and imaginary part of measured currents from area i to area j. These phasor measurements are also referred to the local reference in area i.

$\boldsymbol{\theta}_i^{sk}$ is the slack bus's angle measurement in area i referred to the global reference.

The PMU measurements in boundary buses use the same reference (local slack bus), whilst the angle measurements of slack buses will be referred to the global reference (global slack bus), as presented in Figure 6.1.

Based on this, the voltage angle measurement θ_i^k in the boundary bus k of area i is represented in $\mathbf{h}(\mathbf{x}_c)$ as follows:

$$\theta_i^k \rightarrow h(\mathbf{x}_c) = \theta^k - \theta_i^{sk} \tag{6.6}$$

The real and imaginary components of the current measurement from bus i (in area i) to bus j (in area j) is represented as:

$$\begin{aligned} I_{iR}^{ij} &= (g_{ij} + g_{si})V^i \cos(\theta^i - \theta_i^{sk}) - (b_{ij} + b_{si})V^i \sin(\theta^i - \theta_i^{sk}) \\ &+ V^j (b_{ij} \sin(\theta^j - \theta_{\mathrm{i}}^{sk}) - g_{ij} \cos(\theta^j - \theta_i^{sk})) \end{aligned} \tag{6.7}$$

$$\begin{aligned} I_{iI}^{ij} &= (g_{ij} + g_{si})V^i \sin(\theta^i - \theta_i^{sk}) + (b_{ij} + b_{si})V^i \cos(\theta^i - \theta_i^{sk}) \\ &- V^j (g_{ij} \sin(\theta^j - \theta_i^{sk}) + b_{ij} \cos(\theta^j - \theta_i^{sk})) \end{aligned} \tag{6.8}$$

where $(g_{si}+jb_{si})$ is the shunt admittance connected at bus i, and $(g_{ij}+jb_{ij})$ is the series admittance of the tie-line connecting area i and j.

It is important to note that the slack bus angle of the area where the PMU is located must be included in the model because the PMU measurements are still referred to their local reference. However, the slack bus angle of area i is already referred to the global reference and therefore does not need any correction of reference.

6.2.2 Conventional Measurements

All transferred power measurements in tie-lines will be used by the coordination level. However, power injection measurements in boundary buses will not be used as it would be necessary to share information about internal topology of the areas. In addition, the size and complexity of the coordination level would increase.

Each area will provide minimum information about its internal topology configuration. Thus, whenever an injected power measurement is found (at a boundary bus), it will be replaced by the estimated transferred power, in the relevant tie-line, obtained by the local estimator.

As the injected power measurements of boundary buses are used in the lower level estimation, it is reasonable to believe that the estimated states related to these measurements are sufficiently accurate, see the simulated study case in Section 6.3. Thus, the estimated tie-line flows can be used as an effective way to maintain redundancy in the coordination level.

6.2.3 Pseudo-Measurements

The estimated bus voltages of all boundary buses $\hat{\mathbf{x}}^b$ will be used as pseudo-measurements in $\mathbf{z}_c$. The inverse of the *Gain Matrix* (covariance matrix of the estimated states) of the local estimators will be used to weight the pseudo-measurements at the coordination level:

$$\mathbf{P}_s = diag(\mathbf{H}^T \mathbf{R}_i^{-1} \mathbf{H})^{-1} \tag{6.9}$$

In addition, the covariance matrix of the new pseudo-measurements (corresponding to estimated transferred powers) can be approximated as:

$$\mathbf{P}_{sm} = \mathbf{H}_{sm} \mathbf{P}_s \mathbf{H}_{sm}^T \tag{6.10}$$

where $\mathbf{H}_{sm}$ contains the partial derivatives of the transferred powers in tie-lines with respect to the states corresponding to boundary buses. Thus, the vector of measurements $\mathbf{z}_c$ in the coordination level consists of:

$$\mathbf{z}_c = [\mathbf{z}_i^b, \mathbf{z}_i^p, \hat{\mathbf{x}}_i^b]^T \quad \forall\, i = 1, 2, ..., S \tag{6.11}$$

where:

$\mathbf{z}_i^b$ is the set of conventional and synchronised measurements in the boundary buses for area *i*

$\mathbf{z}_i^p$ is the set of estimated transferred powers whenever a boundary power injection measurement is found in area *i*.

$\hat{\mathbf{x}}_i^b$ is the set of estimated bus voltages in the boundary buses of area *i*.

Figure 6.2 shows the lower and higher level schemes for a power system with *S* areas. Each independent local estimator calculates the set of bus voltages $\mathbf{x}_i$ (internal, boundary, and external buses connecting area *i*).

The coordination level does not use any information regarding the internal topology of the areas.

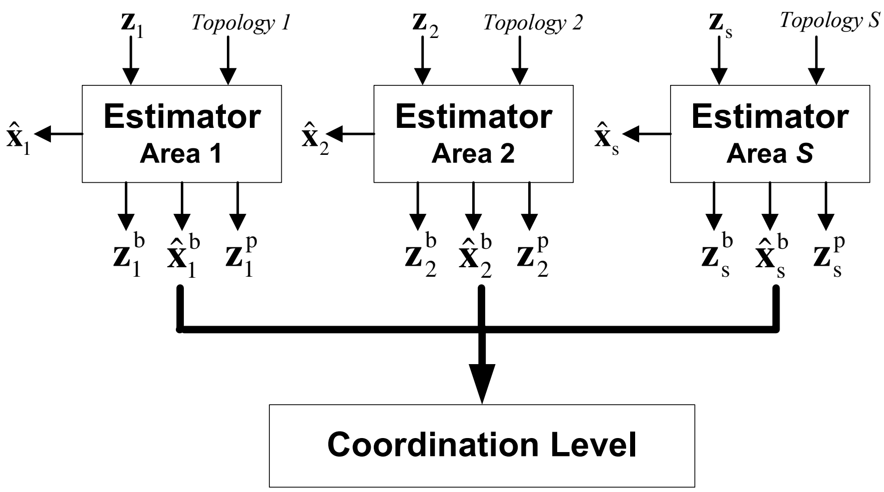

Figure 6.2: Data collection from local area estimators to the Coordination Level

With this information the coordinator estimates the states at the boundary buses, the power flows between subsystems (tie-line power flows) and the phase shift between the slack buses. The coordinator will deliver this information to the local estimators, which must then update their solution and correct any wrong local estimation if any bad data was identified at the coordination level.

6.3 Study Case

The proposed multi area state estimator with minimum data exchange has been tested by using the IEEE 300 bus system. The 300 bus system was arbitrarily split into seven (S = 7) different areas, as described in Table 6.1.

Table 6.1: 300 bus system divided into seven areas

Area	Buses	Branches	Boundaries	To Areas
1	101	129	16	2, 3, 4, 5, 7
2	45	56	10	1, 5
3	42	57	5	1, 4
4	45	62	4	1, 3
5	40	53	8	1, 2, 6
6	35	41	3	5
7	36	38	1	1

A power flow solution of the 300 bus system was used to obtain the real solution of the system condition. Tables 10.9 and 10.10 (in Appendix G.5) provide details of branch connections and power flow solution of the 300-bus test system. Figure 6.3 presents the connection of each area and the set of measurements located at boundary buses and tie-lines.

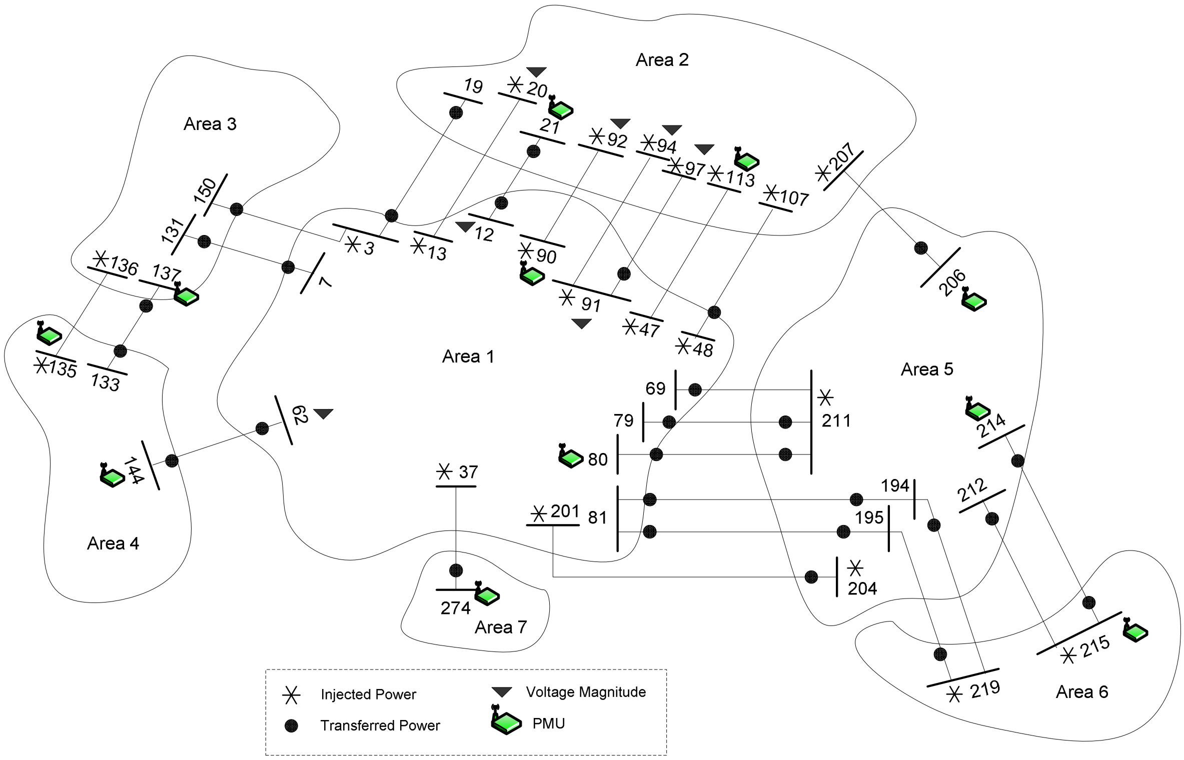

Figure 6.3: Boundary buses of Multi-Area System

6.3.1 Lower Level

The constrained WLS methodology was used to estimate the states of each area and the equality constraints were included to deal with any null power injection. The set of noisy measurements, obtained from the power flow solution, consists of conventional and synchronised measurements with the corresponding standard deviation shown in Table 6.2.

Table 6.2: Standard deviation of measurement in 300 bus test system

Conventional			Synchronised		
Voltage Mag.	Injected Power	Power Flows	Voltage Mag.	Current Mag.	Phase Angle
0.2%	2%	2%	0.02%	0.03%	0.01°

The set of measurements for each area is enough to make the system fully observable and there are no critical measurements so that bad data detection and identification is possible. In order to assess the effect of including PMU measurements in the MASE, the study separates the estimation results with and without including PMU measurements.

Table 6.3 and Table 6.4 present the solution of the WLS minimisation for each local estimator. A Chi-Square Distribution test was used to detect the presence of bad data in the set of measurements.

The last columns of Tables 6.3 and 6.4 indicate the threshold of the Chi-Square Distribution test for *m-n* degrees of freedom and confidence level of 95%. Here, *m* is the number of real and virtual measurements and *n* the number of states.

Table 6.3: Chi-Square test for BDD without PMUs

Area	*m-n*	$J(\hat{\mathbf{x}})$	$\mathbf{y}^t$
1	404	449.1295	451.8646
2	169	154.4236	200.3339
3	183	197.9825	215.5633
4	230	232.9748	266.3781
5	155	158.9062	185.0523
6	141	127.0613	169.7113
7	136	121.4063	164.2162

Table 6.4: Chi-Square test for BDD including PMUs

Area	*m-n*	$J(\hat{\mathbf{x}})$	$\mathbf{y}^t$
1	421	462.8011	469.8388
2	200	183.3602	233.9943
3	222	236.3207	257.7585
4	277	276.5873	316.8185
5	194	193.8542	227.4964
6	152	135.3046	181.7702
7	163	151.1606	193.7914

Based on the tables, it is concluded that each estimator is free of gross bad data. Otherwise, it would be necessary to identify and eliminate the gross error in the set of measurements.

Table 6.5 presents the estimation error of power flows in tie-lines that were obtained from the local estimators. The estimation errors lower than 1% in active (P_t) and reactive (Q_t) power flows were not presented.

Table 6.5: Percentage error of estimated active and reactive power flows

Buses		No PMU		PMU	
From	*To*	error P_t [%]	error Q_t [%]	error P_t [%]	error Q_t [%]
37	***274***	**0.54**	**193.55**	**0.06**	**143.79**
3	*19*	3.82	3.96	3.82	3.96
3	***150***	**22.49**	**1.07**	**22.00**	**1.10**
7	*131*	3.75	0.11	3.75	0.09
12	*21*	1.65	2.25	1.66	2.25
13	*20*	2.93	1.67	2.91	1.66
48	*107*	2.39	1.89	2.40	1.90
62	*144*	1.15	0.49	1.12	0.48
81	*195*	0.55	1.84	0.26	1.84
90	*92*	1.75	0.40	0.01	0.04
91	*94*	4.76	5.78	4.88	5.75
201	***204***	**16.56**	**9.67**	**16.68**	**6.59**
20	***13***	**29.43**	**7.85**	**19.37**	**8.29**
113	*47*	3.13	0.80	0.05	0.05
107	***48***	**71.13**	**0.06**	**60.59**	**0.10**
92	*90*	1.69	8.26	1.36	7.78
94	*91*	4.81	0.13	2.55	0.02
207	*206*	2.70	6.00	2.70	6.15
135	*136*	2.44	6.37	0.02	0.06
150	*3*	0.76	1.47	0.73	1.77
131	*7*	0.78	2.07	0.80	1.86
136	*135*	0.12	5.35	0.05	4.34
211	*69*	9.63	2.70	8.39	4.39
211	*80*	2.09	2.03	2.09	2.03
194	*81*	1.62	0.42	1.63	0.48
195	*81*	0.89	4.46	0.89	4.42
219	*194*	1.95	2.28	2.11	4.71
215	*212*	3.24	0.89	0.05	0.08
274	*37*	0.19	2.46	0.02	0.48

The largest estimation errors are highlighted in Table 6.5. These errors may produce estimation errors when the estimated power flows are used as pseudo-measurements in the coordination level. In the case of the reactive power transferred from *Bus 37* to *Bus 274*, the estimation error (in percentage) is very large because the actual value of *Q37-274* is close to zero.

From Table 6.5, it can be observed that the PMU measurements had little impact on the estimated power flow errors. This is because the corresponding branches are far from local PMU buses. Note that PMUs located at external boundary buses were not taken into consideration in the local area estimators because they are not local measurements.

The estimated power flows that were highly influenced by the PMUs were not listed in Table 6.5 because the estimated errors were below 1%. However, most of the estimated power flows presented in Table 6.5 had lower errors compared to the case where only conventional measurements were available.

6.3.2 Higher (Coordination) Level

The solution of local area estimators and measurements in boundary buses are used as input data in the coordination level. The following methods have been tested for comparison purposes:

Method 1: The coordination level includes internal buses adjacent to boundary buses so that the power injection measurements in the boundary buses can be used. The set of states are the bus voltage of the slack buses, boundary buses, and internal buses adjacent to them. Therefore, it is necessary to know the internal connections of boundary buses of each subsystem. In addition, equality constraints have been included for those boundary buses with null power injections.

Method 2: This is the coordination level proposed in this work. The set of states are the bus voltages of slack buses and boundary buses only. The power injections' measurements or null power injection measurements in boundary buses are not used in the coordination level. These measurements are replaced by the estimated transferred powers flowing in or out boundary buses.

Table 6.6 gives a good overview of the size of the coordination level estimation according to the methods cited above. The set of measurements includes conventional and synchronised measurements. It is clear that including power injection measurements in the coordination level will significantly increase the size and complexity of the problem as internal buses adjacent to boundary buses have to be considered.

Table 6.6: Size of coordination level

	Method 1	Method 2
Buses	115	48
Branches	113	25
m-n	185	201

Now it is necessary to check the accuracy of the simplified coordination level proposed in Method 2. The overall estimation performance is presented in Table 6.7 based on the performance index calculated by:

$$\sigma_{\Sigma}^{2} = \sum_{i=1} (\hat{x}_c^i - x_c^i)^2 \tag{6.12}$$

where $\hat{x}_c^i$ is the estimated state and x_c^i is the true state obtained from the power flow calculation. Since the number of states in Method 1 is larger than Method 2, the state variables considered in (6.12) are those corresponding to boundary buses only.

Table 6.7: Assessment of coordination level

	Method 1	Method 2
---	σ_{Σ}^{2}	σ_{Σ}^{2}
No PMUs	$5.38\text{x}10^{-5}$	$6.24\text{x}10^{-5}$
With PMUs	$1.80\text{x}10^{-6}$	$3.70\text{x}10^{-6}$

The results from Table 6.7 confirm that including PMUs in only a few boundary buses and all the slack buses improves the accuracy of the coordination level. Moreover, the performance index shows that excluding the power injection measurements in $\mathbf{z}_c$ has only a small impact on the accuracy of the coordination level.

The same effect was found when PMU measurements were not considered. Therefore, the price paid for excluding internal buses adjacent to boundary buses is relatively low when considering the benefits of simplicity, higher speed, and reduced problem size in the coordination level.

The following results present a detailed study of the estimation errors for each bus in the coordination level. Figures 6.4 and 6.5 show the absolute estimation errors of the coordination level for all boundary buses without including PMU measurements.

The figures show that the inclusion of the pseudo-measurements of transferred powers gives a good approximation of the power injection measurements. It is important to remember that Method 2 does not require information about the internal connection of boundary buses and the final estimation is still similar to that of Method 1.

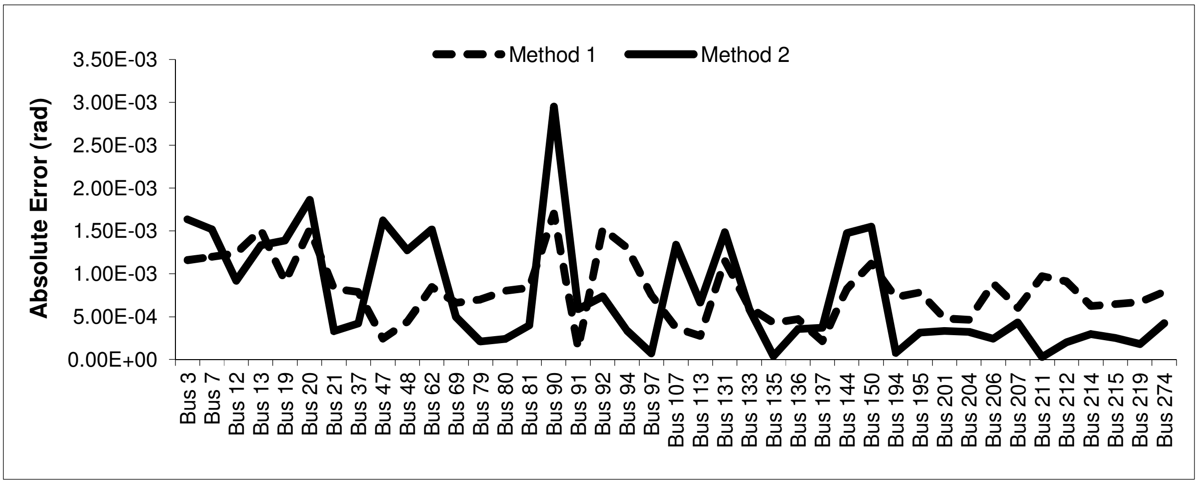

Figure 6.4: Absolute angle error for boundary buses without PMU measurements

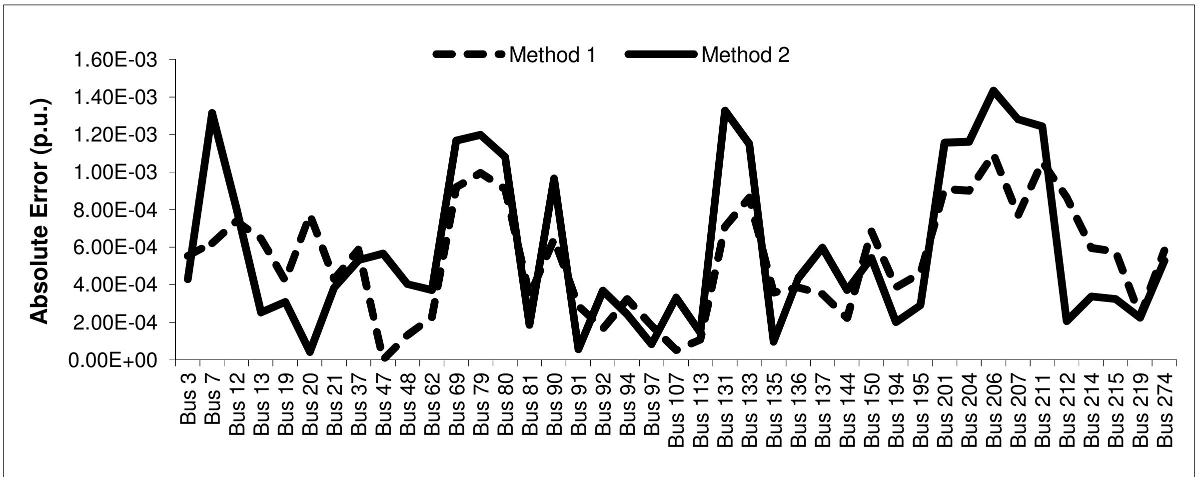

Figure 6.5: Absolute voltage magnitude error for boundary buses without PMU measurements

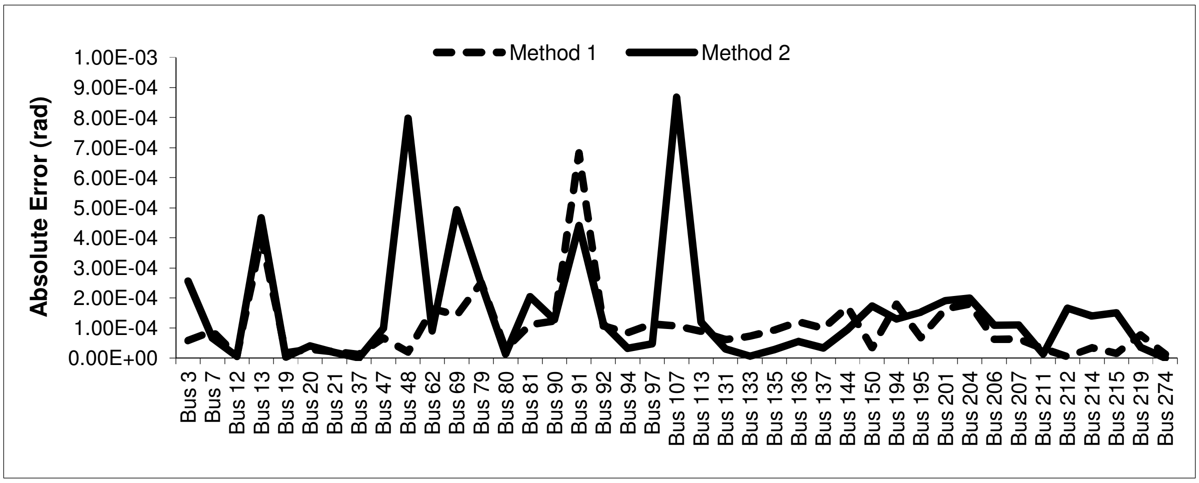

Figure 6.6: Absolute angle error for boundary buses including PMU measurements

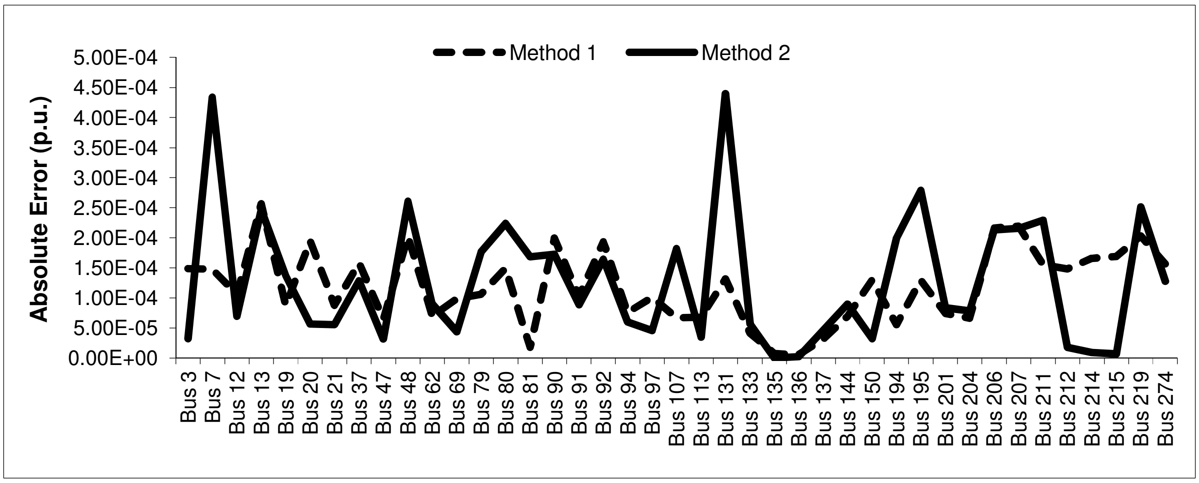

Figure 6.7: Absolute voltage magnitude error for boundary buses including PMU measurements

Figures 6.6 and 6.7 present the estimation error of voltages at boundary buses when the PMU measurements are included. The inclusion of these measurements reduced the estimation errors at all buses as compared to Figures 6.4 and 6.5.

When including the PMU measurements, it is noticed that the angle estimation error at *Buses 48* and *107* and the voltage magnitude estimation error at *Buses 7* and *131* are slightly larger when using *Method 2*. By looking at the pseudo-measurements of power flows listed in Table 6.5, it is found that the large estimation error of *P107-48* was propagated to the Coordination level and the real-time measurement in branch *48-107* made it no possible to fully correct this error, see Figure 6.3. Still, the error was not enough to be detected by the higher level estimator and the other errors included by the pseudo-measurements were filtered out in the Coordination level.

In the case of the voltage magnitude error in *Buses 7* and *131*, both null power injection buses, the difference of results is expected because the pseudo-measurements of power flows can never be as accurate as the fictitious null power injection measurement of *Buses 7* and *131*. Still, the advantage of *Method 2* is the reduced data exchange from local area estimators to the coordination estimator.

6.4 Summary

This chapter presented how the state estimator of large interconnected power systems can be decentralised into smaller local area state estimators to reduce the computational burden and complexity of processing large sets of measurements.

A valid assumption for using multi-area state estimation is the fact that errors in measurements from one area have little effect on the estimated bus voltages far from that location. Similarly, bad data is detected and corrected using available measurements close to the erroneous ones. It implies that splitting the state estimation into smaller sub-problems produces the minimum effect on internal buses but a correction of estimated states in boundary buses is necessary.

The efforts and contribution of this work were concentrated on reducing the size of the coordination level by not including power injection measurements of boundary buses so that no single internal bus is included in the formulation.

As PMU in boundary buses have independent channels to measure the phasor of currents in tie-lines, their presence does not make any change to the proposed coordination level but it does make a difference in terms of accuracy of estimated voltages in boundary buses and slack buses.

The results demonstrated that not including power injection measurements in the coordination level reduced the size of the problem. This reduction had little effect on the estimated boundary bus voltages as long as the redundancy level is maintained with pseudo-measurements of power flows and other available real measurements in boundary buses.

In addition, the best results were obtained when the estimated power flows from local area estimators were accurate. To achieve this, it is necessary to have reliable and accurate measurements in or close to boundary buses and maintain a good level of redundancy to detect and reject bad data.

Chapter 7 Dynamic State Estimation

Power system state estimators have been classically performed by a static approach, based on the Weighted Least Square (WLS) method, in which a single set of measurements is used to estimate the state of the system. Due to its simplicity and fast convergence properties, the WLS method has been widely used in control centres around the world. However, even when the accuracy of the static estimation is within acceptable limits under fully observable conditions, it cannot predict the future operating point of the system [87].

This limitation of the static estimator can be circumvented by Dynamic State Estimators (DSE). They provide not only an estimate of the current state from given measurements at time k, but also a prediction of the state vector at $k+1$, when the new set of measurements have not been processed. According to [87], no other estimator can produce better state estimations if the actual power system and the dynamic model incorporated into the dynamic estimator are in agreement.

Although the DSE was firstly explored at similar times as the static one, the DSE did not develop as the static ones. This is explained by the limited computing facilities in control centres to deal with the high dimensionality of the problem and the need to develop a dynamic model able to represent the system behaviour (transition of states) in an effective and simple way [88].

Nowadays, advances in Information and Communication Technologies are drivers for the development of new dynamic estimators. The availability of more accurate measurements with higher sampling frequencies (such as synchrophasors) can provide fast and accurate estimations for each time sample and can help to better model the transition of states. These estimators extract information from multiple scans and make use of dynamic models [89].

Among the benefits of the deployment of DSE are the prediction capacities for normal or emergency conditions, convergence even in presence of some observable islands and the ability to identify topology errors and gross bad data [87].

For example, reference [90] presents a voltage security monitoring scheme based on a dynamic state estimator that uses one-step-ahead forecast (from the prediction step of the DSE) to detect proximity of a voltage collapse in order to take corrective actions before the system becomes unstable.

The detection of sudden changes is also an advantage of DSE. This detection is based on the difference between the predicted and the update steps. Additionally, the work recently presented in [89, 91] take advantage of the prediction step in DSE to estimate the system state and any uncertain line parameters by means of synchronised measurements.

The development of a new and efficient hybrid dynamic estimator is explored to improve the filtering capacities of state estimators in power systems. For this purpose, a new state estimator based on the Unscented Kalman Filtering (UKF) technique is proposed and tested in this Chapter.

The first part of this Chapter consists of a brief introduction to the dynamic estimation problem. Later, a detailed explanation of Kalman filters is presented in Sections 7.2 and 7.3. A comparison study between the UKF and the Extended Kalman Filter (EKF), demonstrated on two representative test power systems is presented in Section 7.4. Finally, Sections 7.5 and 7.6 present the discussion and summary of the Chapter.

7.1 Dynamic State Estimators

In the early 1970s, a new state estimator able to track the system operating conditions, using consecutive and uncorrelated sets of measurements varying in time, was introduced [92]. It was based on the assumption that the network behaves in a quasi steady state manner determined by slow dynamic changes of the load. The modelling of the system dynamics and understanding of its mechanisms were critical for further development of DSE methods.

Figure 7.1 presents the structure of the DSE. It consists of two main blocks. The first one is the dynamic model, which represents a transition of the states $\mathbf{x}$, given the state estimation at *k-1* and the input vector $\mathbf{u}$ at *k-1*. This transition of states is also known as the prediction step because it predicts the set of states $\bar{\mathbf{x}}$ before the new set of measurements $\mathbf{z}$ are processed.

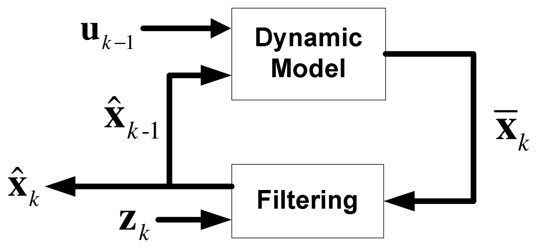

Figure 7.1: Structure of DSE

The second block consists of the filtering step that filters out bad data and updates the (predicted) set of states with the new set of measurements. Sub-sections 7.1.1 and 7.1.2 explains both the dynamic representation and the filtering problem in DSE of power systems.

7.1.1 Dynamic Model of the Power System

Different models for representing the slow system dynamics have been reported in the past [93-96]. Some of these models start from the assumption that the quasi steady state behaviour of the system, monitored in time steps of a few minutes, can be represented by a linear discrete-time transition (prediction) of states:

$$\mathbf{x}_{k+1} = \mathbf{F}_k \mathbf{x}_k + \mathbf{g}_k + \mathbf{q}_k \tag{7.1}$$

Here, $\mathbf{x}_k$ is the state vector consisting of magnitudes and angles of nodal voltages. Matrix $\mathbf{F}_k$ and vector $\mathbf{g}_k$ describe the transition process of the states and $\mathbf{q}_k$ is the white Gaussian noise vector of the prediction model at time *k*. The values of $\mathbf{F}$ and $\mathbf{g}$ can be obtained by online or offline methods.

A common and widely accepted approach for calculating $\mathbf{F}$ and $\mathbf{g}$ is the online parameter identification technique (the *Holt's* Method) introduced in [94]. Reference [96] proposed a method to calculate **F** and **g** based on a realistic state transition using the network equations. The transition for each state takes into account the effect of neighbour state variations.

Other techniques introduce load prediction to represent the transition of states more realistically [88, 97, 98]. The reason for doing this is that loads and generators are key factors determining the system dynamics. Moreover, changes of loads are more independent of one another and the pattern they follow is easier to predict. Once loads are predicted at all buses, a load flow calculation can provide the predicted state at time k+1. For all the methods cited above, a linear dynamic model for the state transition was considered to be sufficient for quasi stationary system behaviour [97].

7.1.2 Filtering Problem

The filtering process consists of comparing the set of real-time measurements **z** with the model equations **h**(**x**), as follows:

$$\mathbf{z}_{k+1} = \mathbf{h}(\mathbf{x}_{k+1}) + \mathbf{e}_{k+1} \tag{7.2}$$

where $\mathbf{z}_{k+1}$ is the measurement vector, $\mathbf{h}(\mathbf{x}_{k+1})$ is the nonlinear equations modelling the corresponding $\mathbf{z}_{k+1}$ as a function of state variables and network parameters and $\mathbf{e}_{k+1}$ is the Gaussian white noise of measurements at $k+1$.

The predicted state vector is corrected for each time instant k and any bad data in the set of measurements is filtered out. The state prediction (dynamic model) and the state correction (filtering) are processed using extensions of the Kalman Filter.

7.2 Kalman Filters

The Kalman Filter is a linear dynamic state estimator that propagates the mean and covariance of the state through time [79]. The mean of the state is the Kalman filter estimate of the state and the covariance of the state is the covariance of the Kalman Filter state estimate. Each time a set of measurement is received, the mean and covariance of the state is updated.

Suppose the linear system:

$$\mathbf{x}_k = \mathbf{F}\mathbf{x}_{k-1} + \mathbf{B}\mathbf{u}_{k-1} + \mathbf{q}_{k-1} \tag{7.3}$$

$$\mathbf{z}_k = \mathbf{H}\mathbf{x}_k + \mathbf{e}_k \tag{7.4}$$

where $\mathbf{q}_{k-1}$ and $\mathbf{e}_k$ are the system and measurement errors, with covariance matrix $\mathbf{Q}_{k-1}$ and $\mathbf{R}_{zk}$, respectively. Matrix $\mathbf{F}$ and $\mathbf{B}$ relate the previous state and the system input $\mathbf{u}_{k-1}$ with the actual state vector $\mathbf{x}_k$ whereas $\mathbf{H}$ relate the set of measurements $\mathbf{z}_k$ with the set of states. The problem consists of estimating the state vector given the state prediction (7.3) and the state update (7.4) at time k. This problem is reduced to having two types of measurements:

- The well known set of real-time measurements $\mathbf{z}_k$, defined in (7.4), with error covariance matrix $\mathbf{R}_{zk}$
- The pseudo-measurements consisting of the predicted states $\overline{\mathbf{x}}_k$, obtained from (7.3), with error covariance matrix $\mathbf{P}_{\overline{x}k}$.

Based on this, the new set of measurements $\tilde{\mathbf{z}}$ at time k is built up by:

$$\tilde{\mathbf{z}}_k = \begin{bmatrix} \mathbf{z}_k \\ \overline{\mathbf{x}}_k \end{bmatrix} = \begin{bmatrix} \mathbf{z}_k \\ \mathbf{F}\hat{\mathbf{x}}_{k-1} + \mathbf{B}\mathbf{u}_{k-1} \end{bmatrix}. \tag{7.5}$$

In order to estimate the value of $\mathbf{x}$ at time k, it is necessary to minimise the augmented objective function:

$$J(\mathbf{x}_k) = \frac{1}{2}\left[\mathbf{z}_k - \mathbf{H}_k\mathbf{x}_k\right]^T \mathbf{R}_{zk}^{-1}\left[\mathbf{z}_k - \mathbf{H}_k\mathbf{x}_k\right] + \frac{1}{2}\left[\overline{\mathbf{x}}_k - \mathbf{x}_k\right]^T \mathbf{P}_{\overline{x}k}^{-1}\left[\overline{\mathbf{x}}_k - \mathbf{x}_k\right]. \tag{7.6}$$

Note that this objective function has the same structure as a linear WLS problem. Hence, the WLS solution of (7.6) is:

$$\hat{\mathbf{x}}_k = [\tilde{\mathbf{H}}_k^T \mathbf{R}_{\tilde{z}k}^{-1} \tilde{\mathbf{H}}_k]^{-1} \tilde{\mathbf{H}}_k^T \mathbf{R}_{\tilde{z}k}^{-1} \tilde{\mathbf{z}}_k, \tag{7.7}$$

where $\tilde{\mathbf{H}}_k$ is the Jacobian matrix of the augmented set of measurements $\tilde{\mathbf{z}}_k$ and $\mathbf{R}_{\tilde{z}k}$ is the augmented covariance matrix. Equation (7.7) can be expressed as, see Appendix E:

$$\hat{\mathbf{x}}_k = \overline{\mathbf{x}}_k + \mathbf{K}_k\left(\mathbf{z}_k - \mathbf{H}_k\overline{\mathbf{x}}_k\right) \tag{7.8}$$

where matrix $\mathbf{K}_k$ is the Gain matrix defined by:

$$\mathbf{K}_k = \mathbf{P}_{\overline{x}k}\mathbf{H}_k^T\left(\mathbf{R}_{zk} + \mathbf{H}_k\mathbf{P}_{\overline{x}k}\mathbf{H}_k^T\right)^{-1}. \tag{7.9}$$

Finally, the covariance matrix of the updated state estimate is

$$\mathbf{P}_{\hat{x}k} = (\mathbf{I} - \mathbf{K}_k \mathbf{H}_k)\mathbf{P}_{\bar{x}k} \tag{7.10}$$

The advantage of the Kalman filter is that it is a recursive method and it can be used for online applications. It only uses the incoming set of measurements at instant k but keeps the information of the previous measurements by using the previous state estimate (at *k-1*). Unfortunately, most of the power system processes are non-linear and the Classical Kalman filter could be used in few real problems. In order to cope with more complex non-linear systems, such as the power systems, extensions of the Kalman filter have been developed and they are presented in the following Sections.

7.2.1 The Extended Kalman filter

Consider the case where the state prediction and state update are defined by non-linear equations:

$$\mathbf{x}_k = \mathbf{f}(\mathbf{x}_{k-1}, \mathbf{u}_{k-1}, \mathbf{q}_{k-1}) \tag{7.11}$$

$$\mathbf{z}_k = \mathbf{h}(\mathbf{x}_k, \mathbf{e}_k) \tag{7.12}$$

Functions **f** and **h** are non-linear equations representing the system and measurements models in terms of the state variables **x** and the input variables $\mathbf{u}_{k-1}$. In addition, $\mathbf{z}_k$ is the measurement vector whereas $\mathbf{q}_{k-1}$ and $\mathbf{e}_k$ are the system and measurement Gaussian noises with zero mean and uncorrelated covariance matrices $\mathbf{Q}_{k-1}$ and $\mathbf{R}_k$, respectively.

As the equations are non-linear, the Extended Kalman Filter (EKF) performs a linearisation of (7.11) and (7.12) around the previous and predicted state vectors, respectively. This is achieved by calculating the partial derivatives of **f** and **h** with respect to **x**, as follows:

$$\mathbf{F}_k = \frac{\partial \mathbf{f}(\hat{\mathbf{x}}_{k-1}, \mathbf{u}_{k-1}, \mathbf{0})}{\partial \mathbf{x}}, \tag{7.13}$$

$$\mathbf{H}_k = \frac{\partial \mathbf{h}(\bar{\mathbf{x}}_k, \mathbf{0})}{\partial \mathbf{x}}. \tag{7.14}$$

Once the equations are linearised, the EKF is executed similarly to the linear Kalman Filter. The predicted mean and covariance are approximated by:

$$\bar{\mathbf{x}}_k = \mathbf{f}(\hat{\mathbf{x}}_{k-1}, \mathbf{u}_{k-1}, \mathbf{0}), \tag{7.15}$$

$$\mathbf{P}_{\bar{x}k} = \mathbf{F}_k \mathbf{P}_{\hat{x}k-1} \mathbf{F}_k^T + \mathbf{Q}_{k-1}. \tag{7.16}$$

and the Gain matrix is approximated by:

$$\mathbf{K}_k = \mathbf{P}_{\bar{x}k}\mathbf{H}_k^T\left(\mathbf{H}_k\mathbf{P}_{\bar{x}k}\mathbf{H}_k^T + \mathbf{R}_k\right)^{-1}. \tag{7.17}$$

Based on this, the predicted state vector is updated with the new set of measurements at time *k*:

$$\hat{\mathbf{x}}_k = \bar{\mathbf{x}}_k + \mathbf{K}_k\left(\mathbf{z}_k - \mathbf{h}(\bar{\mathbf{x}}_k)\right), \tag{7.18}$$

$$\mathbf{P}_{\hat{x}k} = (\mathbf{I} - \mathbf{K}_k\mathbf{H}_k)\mathbf{P}_{\bar{x}k}. \tag{7.19}$$

The linear approximations of (7.11) and (7.12) lead to reduced accuracy of results because non-linear terms are neglected. To overcome this drawback, iterative Kalman filter methods have been proposed [98, 99]. However, the iteration procedure may become time consuming with significantly higher CPU requirements. This could be a particular obstacle in DSE, if the data refreshing rate is larger than in the classical steady state estimation.

A novel technique called the Unscented Kalman filter, based on the Unscented Transformation (UT) theory introduced in Chapter 5, presented an opportunity to cope with nonlinearities in dynamic state estimation. In this approach, the non-linear equations are not linearised as with the EKF. Instead, a statistical distribution of the state is propagated through the non-linear equations, providing better estimates of the actual state and the posterior covariance matrix.

7.2.2 The Unscented Kalman Filter

The Unscented Kalman Filter (UKF) is an efficient discrete-time recursive filter able to solve estimation problems in the following form:

$$\mathbf{x}_k = \mathbf{f}(\mathbf{x}_{k-1}, \mathbf{u}_{k-1}) + \mathbf{q}_{k-1} \tag{7.20}$$

$$\mathbf{z}_k = \mathbf{h}(\mathbf{x}_k) + \mathbf{e}_k. \tag{7.21}$$

Similar to the EKF formulation, $\mathbf{f}$ and $\mathbf{h}$ are both non-linear equations: $\mathbf{x}$ is the state vector, $\mathbf{u}_{k-1}$ is the set of input variables and $\mathbf{z}_k$ is the measurement vector. Vectors $\mathbf{q}_{k-1}$ and $\mathbf{e}_k$ are the system and measurement Gaussian noises with zero mean and uncorrelated covariance matrices $\mathbf{Q}_{k-1}$ and $\mathbf{R}_k$, respectively.

The main advantage of the UKF over the EKF is the fact that equations (7.20) and (7.21) are not linearised. This avoids the loss of higher order information and consequently improves the properties of the estimator [79]. Furthermore, as no Jacobian or Hessian matrices are needed, this offers computational advantages over the EKF. Instead, as described in Chapter 5, only multiple evaluations of a limited number of the sigma points in (7.20) and (7.21) are needed. In other words, for similar computational requirements, the UKF provides higher accuracy than the EKF as higher order terms of the non-linear model equations are considered.

The UKF consists of the following three major steps:

- Step 1: Sigma Points Calculation
- Step 2: Kalman filter State Prediction
- Step 3: Kalman filter State Correction

All three above mentioned steps are described below.

7.2.2.1 Sigma Points Calculation

For an initial $n\times 1$ state vector $\hat{\mathbf{x}}_{k\text{-}1}$, and the corresponding $n\times n$ covariance matrix $\mathbf{P}_{\hat{x}k\text{-}1}$, a set of $2n+1$ vectors is obtained, called *sigma points*. These sigma points are chosen deterministically and they capture the mean and covariance of the original distribution of $\hat{\mathbf{x}}_{k\text{-}1}$ exactly:

$$\hat{\mathbf{X}}_{k\text{-}1}^{0} = \hat{\mathbf{x}}_{k\text{-}1}, \tag{7.22}$$

$$\hat{\mathbf{X}}_{k\text{-}1}^{i} = \hat{\mathbf{x}}_{k-1} + \left(\sqrt{(n+\lambda)\mathbf{P}_{\hat{x}k\text{-}1}}\right)_i, \quad i = 1,...,n. \tag{7.23}$$

$$\hat{\mathbf{X}}_{k\text{-}1}^{n+i} = \hat{\mathbf{x}}_{k\text{-}1} - \left(\sqrt{(n+\lambda)\mathbf{P}_{\hat{x}k\text{-}1}}\right)_i, \quad i = 1,...,n. \tag{7.24}$$

where $\left(\sqrt{(n+\lambda)\mathbf{P}_{\hat{x}k\text{-}1}}\right)_i$ is the i-th column of the matrix $\sqrt{(n+\lambda)\mathbf{P}_{\hat{x}k\text{-}1}}$ (using the positive definite (PD) square root of a matrix), and parameter λ is defined as $\lambda = \alpha^2(n+\kappa) - n$. The parameter κ can be used to reduce the higher order errors of the mean and the covariance approximations. This parameter can be $\kappa = 3 - n$ or zero [79].

The scaling parameter α can be chosen between 0.001 and 1.0 p.u. Note that the PD square root matrix of $\mathbf{P}_{\hat{x}k\text{-}1}$ can be obtained from the calculation $\mathbf{P}_{\hat{x}k\text{-}1} = \mathbf{A}\mathbf{A}^{\mathbf{T}}$, where $\mathbf{A}$ is the lower triangular matrix obtained from the Cholesky factorisation of $\mathbf{P}_{\hat{x}k\text{-}1}$.

For the purpose of the estimation initialisation (i.e. when $k = 0$), the initial state vector and the initial covariance matrix have to be defined in advance according to *a priori* knowledge of the system.

Equations (7.22)-(7.24) can be expressed in the equivalent compact form,

$$\hat{\mathbf{X}}_{k\text{-}1} = [\hat{\mathbf{x}}_{k\text{-}1} \quad \cdots \quad \hat{\mathbf{x}}_{k\text{-}1}] + \sqrt{n+\lambda}[\mathbf{0} \quad \sqrt{\mathbf{P}_{\hat{x}k\text{-}1}} \quad -\sqrt{\mathbf{P}_{\hat{x}k\text{-}1}}], \tag{7.25}$$

where $\hat{\mathbf{X}}_{k\text{-}1}$ is a $n\times$ $(2n+1)$ matrix containing the sigma points calculated from $\hat{\mathbf{x}}_{k\text{-}1}$ and $\mathbf{P}_{\hat{x}k\text{-}1}$.

7.2.2.2 Kalman Filter State Prediction

The sets of sigma points calculated in *Step 1* are evaluated, one by one, through the *prediction* function defined in (7.20):

$$\overline{\mathbf{X}}_k^i = \mathbf{f}(\hat{\mathbf{X}}_{k\text{-}1}^i, \mathbf{u}_{k-1}), \tag{7.26}$$

where $\hat{\mathbf{X}}_{k-1}^i$ is the i-th column of matrix $\hat{\mathbf{X}}_{k-1}$ and the resulting $\overline{\mathbf{X}}_k$ is a $n\times(2n+1)$ matrix containing the propagated sigma points. Next, compute the predicted state mean vector $\overline{\mathbf{x}}_k$ and the predicted covariance matrix $\mathbf{P}_{\overline{x}k}$ as follows [79]:

$$\overline{\mathbf{x}}_k = \sum_{i=0}^{2n} \mathrm{W}_i^m \overline{\mathbf{X}}_k^i, \tag{7.27}$$

$$\mathbf{P}_{\overline{x}k} = \sum_{i=0}^{2n} \mathrm{W}_i^c \left[(\overline{\mathbf{X}}_k^i - \overline{\mathbf{x}}_k)(\overline{\mathbf{X}}_k^i - \overline{\mathbf{x}}_k)^T \right] + \mathbf{Q}_{k-1}. \tag{7.28}$$

The weights in (7.27)-(7.28) can be calculated using the following equations [100]:

$$W_0^m = \frac{\lambda}{n+\lambda}, \qquad W_0^c = \frac{\lambda}{(n+\lambda)} + (1-\alpha^2+\beta), \tag{7.29}$$

$$W_i^m = \frac{1}{2(n+\lambda)}, \tag{7.30}$$

$$W_i^c = \frac{1}{2(n+\lambda)}. \tag{7.31}$$

The variable β takes a value of two, typical for Gaussian distribution.

7.2.2.3 Kalman Filter State Correction

The predicted state mean vector and the covariance matrix calculated in *Step* 2 are used to update the sigma points. In compact form, the sigma points are obtained as,

$$\mathbf{X}_k^- = [\overline{\mathbf{x}}_k \quad \cdots \quad \overline{\mathbf{x}}_k] + \sqrt{c}[\mathbf{0} \quad \sqrt{\mathbf{P}_{\overline{x}k}} \quad -\sqrt{\mathbf{P}_{\overline{x}k}}]. \tag{7.32}$$

These new points are evaluated, one by one; in the non-linear update function $\mathbf{h}$ defined in (7.21), as follows,

$$\mathbf{Z}_k^{i-} = \mathbf{h}(\mathbf{X}_k^{i-}). \tag{7.33}$$

As above, $\mathbf{Z}_k^{-i}$ correspond to the *i*-th column of matrix $\mathbf{Z}_k^-$. The mean of the propagated points is calculated as follows,

$$\boldsymbol{\mu}_k = \sum_{i=0}^{2n} \mathrm{W}_i^m \mathbf{Z}_k^{-i}. \tag{7.34}$$

The measurement covariance matrix and the cross-covariance of the state and measurement are subsequently obtained as,

$$\mathbf{S}_k = \sum_{i=0}^{2n} \mathrm{W}_i^c \left[(\mathbf{Z}_k^{-i} - \boldsymbol{\mu}_k)(\mathbf{Z}_k^{-i} - \boldsymbol{\mu}_k)^T \right] + \mathbf{R}_k \tag{7.35}$$

$$\mathbf{C}_k = \sum_{\mathrm{i}=0}^{2n} \mathrm{W}_i^c \left[(\mathbf{X}_k^{-i} - \mathbf{x}_k^-)(\mathbf{Z}_k^{-i} - \boldsymbol{\mu}_k)^T \right] \tag{7.36}$$

The filter gain $\mathbf{K}_k$, the state $\hat{\mathbf{x}}_k$, and the covariance matrix $\mathbf{P}_{\hat{x}k}$ are computed by,

$$\mathbf{K}_k = \mathbf{C}_k \mathbf{S}_k^{-1} \tag{7.37}$$

$$\hat{\mathbf{x}}_k = \overline{\mathbf{x}}_k + \mathbf{K}_k [\mathbf{z}_k - \boldsymbol{\mu}_k] \tag{7.38}$$

$$\mathbf{P}_{\hat{x}k} = \mathbf{P}_{\overline{x}k} - \mathbf{K}_k \mathbf{S}_k \mathbf{K}_k^T \tag{7.39}$$

In general terms, for nonlinear systems, the UKF is easier to implement than the EKF because there is no need to calculate any derivative or Jacobian matrix. Additionally, the UKF results in approximations that are accurate to the third order for the Gaussian distribution, for any nonlinearity, and at least to the second order for non-Gaussian distributions, providing more accurate estimation compared to the EKF which linearises the system equations [101, 102].

To date, the UKF has been explored in few power system applications. The work presented in [103-105] provide good examples of the estimation capacity of the UKF in the non-linear problem of synchronous machine parameter estimation. In addition, the work presented in [106, 107] demonstrate how the UKF can be also used to filter noisy measurements to estimate frequency and amplitude of power system signals.

Unlike the applications mentioned above, the problem of power system state estimation is much larger. Based on this, it is desired to explore the benefits of the UKF in this very different but not less challenging problem.

7.3 Power System State Estimation using the UKF

The UKF is very useful for estimating the unknown state variables, or parameters, of non-linear systems. This gives us the opportunity to apply more realistic and complex power system models without having difficulties caused by the linearisation process.

In this work, the non-linear equations correspond to the mathematical models of transferred and injected active and reactive powers, which are functions of nodal voltages and line parameters. However, a linear model is used to represent the smooth dynamics of the system determined by the slow load variations.

The DSE presented in this work only considers the aforementioned slow load variations. The other faster system dynamics, created by large disturbances in interconnected networks, has not been addressed in this Thesis. Nevertheless, the application of the UKF to estimate power system states and parameters of synchronous machines during transient conditions can be found in [104, 108] as part of the results achieved during this PhD project.

7.3.1 Dynamic Model of the System

Given a state vector $\mathbf{x}$ composed of the set of voltage magnitudes and angles, the dynamics of the system (prediction for $\mathbf{x}_{k+1}$) can be modelled as a discrete time formulation, as detailed in (7.1) and (7.2):

$$\mathbf{x}_{k+1} = \mathbf{F}_k \mathbf{x}_k + \mathbf{g}_k + \mathbf{q}_k \tag{7.40}$$

$$\mathbf{z}_{k+1} = \mathbf{h}(\mathbf{x}_{k+1}) + \mathbf{e}_{k+1} \tag{7.41}$$

where matrix $\mathbf{F}$ and vector $\mathbf{g}$ are updated online using the *Holt's Linear Exponential Smoothing* technique [94]:

$$\mathbf{F}_k = \alpha_k (1+\beta_k) \cdot \mathbf{I} \tag{7.42}$$

$$\mathbf{g}_k = (1+\beta_k)(1-\alpha_k)\overline{\mathbf{x}}_k - \beta_k \mathbf{a}_{k-1} + (1-\beta_k)\mathbf{b}_{k-1} \tag{7.43}$$

where $\mathbf{I}$ is the identity matrix, and both α_k and β_k are parameters lying in the range from 0 to 1, $\overline{\mathbf{x}}_k$ is the predicted state vector at time k, and vectors $\mathbf{a}$ and $\mathbf{b}$ at time k, are obtained as:

$$\mathbf{a}_k = \alpha_k \hat{\mathbf{x}}_k + (1-\alpha_k)\overline{\mathbf{x}}_k \tag{7.44}$$

$$\mathbf{b}_k = \beta_k(\mathbf{a}_k - \mathbf{a}_{k\text{-}1}) + (1-\beta_k)\mathbf{b}_{k\text{-}1} \tag{7.45}$$

Note that α_k and β_k must not be confused with parameters α and β used in the UKF approach. The application of this method provides good predictions even when each state variable is assumed to be independent (*uncorrelated*) of all others.

Vector $\mathbf{z}_{k+1}$ in (7.41) consists of power system measurements, including injected and transferred active and reactive powers, voltage magnitudes, or wide area synchrophasors obtained from Phasor Measurement Units (PMU).

The synchrophasors of bus voltages are linearly related to the state variables whereas the synchrophasors of branch currents, in rectangular or polar form, are represented as non-linear functions in terms of the state variables, as discussed in Chapter 5.

The conventional and synchronised measurements can be simultaneously used in the proposed formulation i.e. a hybrid dynamic estimator. In fact, the inclusion of synchrophasors does not make any change in the formulation.

7.3.2 State Prediction and Correction

The UKF algorithm used to estimate the state of a power system with N buses starts with an assumption of the initial state vector $\hat{\mathbf{x}}_0$ and the corresponding covariance matrix $\mathbf{P}_{\hat{x}0}$. Since the reference bus angle is known and it is invariant in time, the state vector has a dimension $n = 2N\text{-}1$ equal to the number of the unknown state variables.

According to (7.25), the set of $2n+1$ sigma points are calculated, obtaining $\hat{\mathbf{X}}_0$. These sets of sigma points (each column of $\hat{\mathbf{X}}_0$) are evaluated, one by one, in the prediction equation (7.26), creating by this a matrix containing the propagated sigma points at $k = 1$:

$$\overline{\mathbf{X}}_1^i = \mathbf{F}_0\hat{\mathbf{X}}_0^i + \mathbf{g}_0 \tag{7.46}$$

where $\overline{\mathbf{X}}_1^i$ and $\hat{\mathbf{X}}_0^i$ are the i-th columns of matrices $\overline{\mathbf{X}}_1$ and $\hat{\mathbf{X}}_0$ respectively. $\mathbf{F}_0$ and $\mathbf{g}_0$ are initialised from (7.42) and (7.43).

Then, the predicted state vector and the predicted covariance matrix at time $k = 1$ are obtained using (7.27) and (7.28). A new set of sigma points is built, according to (7.32), which capture the distribution of the predicted state vector. These sigma points are grouped in matrix $\mathbf{X}_1^-$ and they are propagated through the measurement update equations (7.33):

$$\mathbf{Z}_1^{-i} = \mathbf{h}(\mathbf{X}_1^{-i}) \tag{7.47}$$

As above, $\mathbf{Z}_1^{-i}$ and $\mathbf{X}_1^{-i}$ correspond to the *i*-th column of $\mathbf{Z}_1^-$ and $\mathbf{X}_1^-$, respectively.

The mean and measurement covariance matrices are obtained using (7.34)-(7.36), whilst the filter gain, the states, and the covariance matrix are calculated using (7.37)-(7.39). The procedure above is repeated for every time instant *k*.

From the above mathematical description of the Unscented Kalman Filter, it is obvious that it does not require the computation of the Jacobian matrix, making the method easier to implement with similar computational requirements.

7.3.3 Detection of Anomalies

The presence of gross bad data in measurements and sudden changes of states caused by topology errors or sudden disconnection of generators/loads are considered as anomalies. These anomalies degrade the accuracy of the DSE if they are not detected during the estimation process, independently of the filtering technique applied.

The advantage of having a predicted state vector for time *k* is that it helps to identify the presence of these anomalies through the normalised innovation vector $\boldsymbol{\tau}_k$. For the *i*-th measurement, the normalised innovation process in the UKF is:

$$\tau_{k,i} = v_{k,i} / \rho_{k,i}\,,\ \text{i}=1,2,\ldots,m \tag{7.48}$$

where,

$$v_{k,i} = z_{k,i} - \mu_{k,i} \tag{7.49}$$

$$\rho_{k,i}^2 = \sum_{j=0}^{2n} W_j^c (\mathbf{Z}_{k,i}^{-j} - \mu_{k,i})^2 + r_{k,i}^2 \tag{7.50}$$

in which $\mathbf{Z}_{k,i}^{-j}$ is the *(i,j)* element of $\mathbf{Z}_k^-$ and $r_{k,i}^2$ is the *i*-th diagonal element of $\mathbf{R}_k$. Additionally, a random variable Λ_k whose samples are the normalised innovation process will exhibit a normal distribution with zero mean and unit variance [93, 99] .

Normally, in the presence of gross bad data the corresponding normalised innovation element $\tau_{k,i}$ will exhibit a large magnitude compared to other elements of vector $\boldsymbol{\tau}_k$. Additionally, the distribution of Λ_k will be distorted, with respect to the symmetrical distribution seen during normal conditions. This facilitates the identification of bad data that can be rejected from the set of measurements [97].

In the case of a sudden state change, the set of measurements located close to the disturbance will exhibit a large magnitude in the corresponding $\tau_{k,i.}$ Here, Λ_k still presents a symmetrical distribution with different mean and variance.

An option to reduce the effect of sudden state change is to minimise the impact of the prediction step by increasing the value of $\mathbf{Q}_k$. This is equivalent to concentrating the estimation on the filtering step that is going to update the vector of states to the new state condition. In the case of topology errors, the corrections are made by running a topology estimation or line parameter estimation [93].

Discrimination between bad data and sudden state change anomalies is necessary to determine the action that minimises the effect of the anomaly, once detected. The method adopted in this work is based on the skewness ψ_k of the distribution of Λ_k, which is a measure of the level of asymmetry in the distribution.

As stated before, in the presence of bad data the distribution of Λ_k loses the symmetry of the normal distribution, but for any other anomaly the distribution remains symmetrical. Based on this, the occurrence of bad data can be identified by the skewness test [93]:

$$\begin{cases} \text{Bad data} & if \quad |\psi_{\mathrm{k}}| \geq \psi_{\max} \\ \text{Any other anomaly} & if \quad |\psi_{\mathrm{k}}| < \psi_{\max} \end{cases} \tag{7.51}$$

The value of ψ_k is calculated as follows:

$$\psi_k = M_{3,k} / \sigma_k^3 \tag{7.52}$$

where M_3 is the third central moment and σ the standard deviation of the distribution, as follows:

$$M_{3,k} = E\{\Lambda_k^3\} - 3\upsilon_k E\{\Lambda_k^2\} + 2\upsilon_k^3 \tag{7.53}$$

$$\sigma_k^2 = E\{\Lambda_k^2\} - \upsilon_k^2 \tag{7.54}$$

$$\upsilon_k = E\{\Lambda_k\} \tag{7.55}$$

The threshold value ψ_{max} depends on the system and can be identified using offline simulations.

7.4 Study Cases

The methodology presented in Section 7.3 is validated in the IEEE 14-bus and 57-bus test systems [64], see Appendices G.1 and G.2 for details. In both test systems, the UKF was compared with the EKF and the static state estimator to show the benefits of the dynamic estimators.

In order to simulate the slow dynamics of the test systems, the smooth load changes were obtained by running 50 load flow calculations under different loading conditions. The loads were varied following a linear trend of 10%, 20%, or 30% over the entire time interval with a random fluctuation of 3%.

In the simulated scenarios, the time interval between two scans of measurements is one to two minutes. This time can be reduced but it will depend on the frequency at which the readings from the remote units arrive at the control centre. In addition, given the advances in communication and information technology, in the near term these measurements will be available at shorter periods of time, which justifies the use of linear trends to model the transition of the states, as presented in this work.

In the simulations, the generator outputs were changed according to the assignment of the participation factors. This methodology avoids the overload of the swing bus and provides more realistic system operation.

In order to test the proposed power system dynamic state estimator, three different scenarios were considered:

1. *Normal operation condition in 14-bus test system:* All loads change according to the above specified linear trend. Noisy measurements were included but none of them corresponded to large bad data.
2. *Sudden load step change in 14-bus test system:* A portion of the load in Bus 2 was suddenly disconnected at time instant k = 30.
3. *Presence of bad data in 57-bus test system*: The active and reactive transferred power measurements in *branch 1-2* were corrupted by Gaussian random errors whose standard deviations were 15 times larger than those presented in Table 5.3. The errors were included at k = 25 and disappeared thereafter.

7.4.1 Performance Indices

The assessment of the UKF performance and its comparison with the EKF and the static estimator was carried out using the following performance indices [109, 110]:

1. *The estimation error is assessed using:*

$$\xi_k = \frac{1}{n}\sum_{i=1}^{n}\left|\mathbf{x}_k^i - \mathbf{x}_k^{i\,t}\right| \tag{7.56}$$

where $\mathbf{x}$ and $\mathbf{x}^t$ are respectively the filtered and the true (actual) state vectors.

2. *The Overall Performance Index (OPI) is obtained as:*

$$OPI_k = \frac{\sum\left|\hat{z}_k^i - z_k^{i\,t}\right|}{\sum\left|z_k^i - z_k^{i\,t}\right|} \tag{7.57}$$

In which $\hat{z}_k^i$ is the estimated measurement vector, z_k^i is the noisy (real) measurement vector, and $z_k^{i\,t}$ is the true vector of measurements.

7.4.2 Simulation Results

The results are now presented to demonstrate the benefits of using dynamic state estimators. The 14-bus test system is used to demonstrate the performance of the estimators in normal conditions and sudden changes whereas the 57-bus test system is used to assess the capabilities of the dynamic estimators to detect and identify bad data.

The measurement allocation of conventional and synchronised measurements is presented in Figures 5.12 and 5.13. Additionally, the set of measurements were corrupted with random additive Gaussian noise with zero mean and standard deviation presented in Table 5.3.

To initialise *Holt's technique*, the first two samples (at times $k = 0$ and $k = 1$) of voltage magnitudes and angles were taken from the last two state estimation solutions, see Appendix F.1. This means that the estimation process runs from time instant $k = 2$ up to $k = 50$ and uses $\alpha_k = 0.8$ and $\beta_k = 0.5$ in (7.42)-(7.43) during the entire time interval, as proposed in [94]. Additionally, as the states at $k = 0$ and $k = 1$ were assumed to be known and accurate, the diagonal elements of matrix $\mathbf{P}_0$ were set to 10^{-6}. Furthermore, the elements of the diagonal matrix $\mathbf{Q}_{k-1}$ were kept constant at 10^{-6} during the simulation [109].

7.4.2.1 Normal Operation Case in 14-bus Test System

Table 7.1 presents the performance indices of the static state estimator, the EKF, and the UKF for normal operating conditions with and without synchronised measurements. The inclusion of the prediction stage in dynamic estimators allows better filtering of measurement noise that results in more accurate estimations. This can be seen in the reduction of the performance indices when compared to the static estimator.

Table 7.1: Performance indices during normal conditions for 14-bus test system

Case	Index	Static	EKF	UKF
No PMU	$\xi \times 10^4$ [p.u]	9.5316	*5.7015*	5.698
	OPI [p.u]	0.6349	*0.4959*	0.4691
PMU	$\xi \times 10^4$ [p.u]	4.0865	*2.7394*	2.658
	OPI [p.u]	0.2464	*0.2188*	0.1948

Figure 7.2 presents the plots of the *OPI* for the 14-bus test system when only conventional measurements are used. Under normal operating conditions, the UKF has lower *OPI* than that of the EKF or the static estimator.

Figure 7.3 presents the *OPI* when conventional and synchronised measurements are used. The presence of more accurate measurements (synchrophasors) makes it possible to reduce the *OPI* for all three state estimators if compared to Figure 7.2.

Similarly as in Figure 7.2, the UKF obtains the most accurate estimations. This proves that the UKF has higher filtering capacities during slow dynamic changes than the corresponding EKF estimator as higher non-linear terms of the measurement equations are considered during the estimation process.

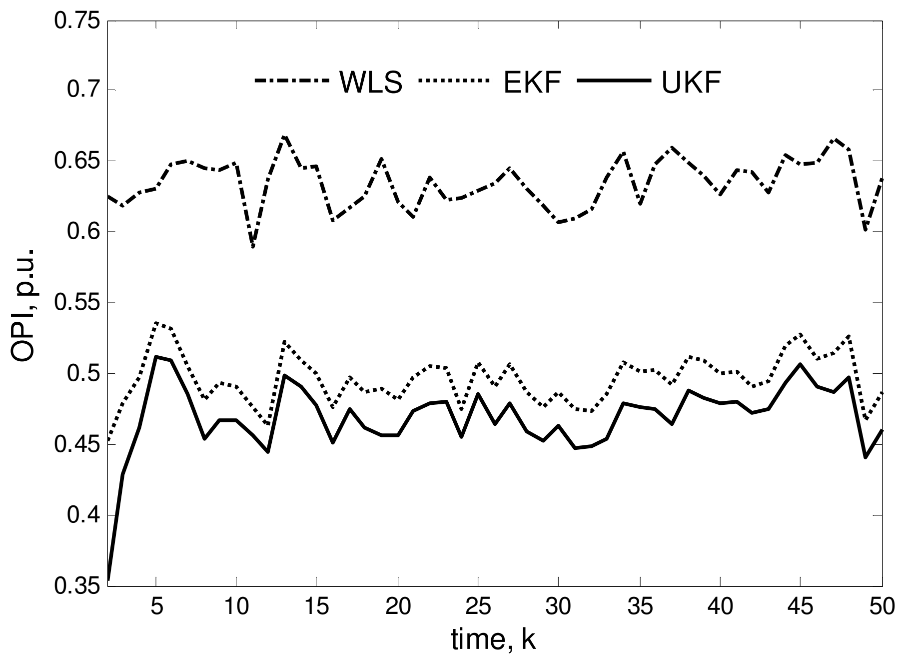

Figure 7.2: *OPI* for normal conditions in the 14-bus system with conventional measurements

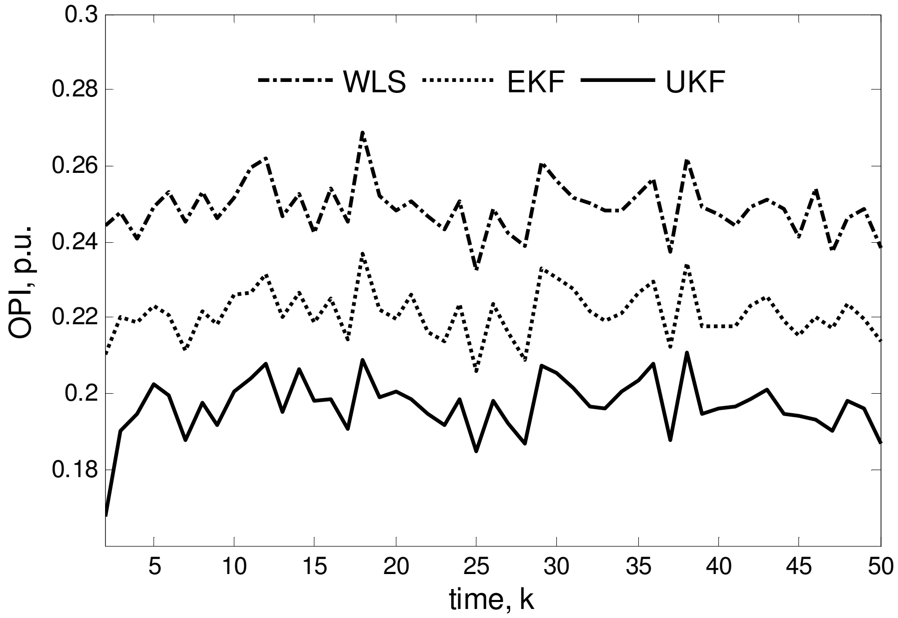

Figure 7.3: *OPI* for normal conditions in the 14-bus system with PMU measurements

7.4.2.2 Sudden Load Changes in 14-bus Test System

The second scenario considered in this test system was the outage of a certain percentage of the load in *Bus 2* at $k = 30$.

Figure 7.4 presents the *OPI* for the entire observation time interval. Here both the UKF and the EKF have low estimation performance when the sudden load change occurs. This is because the dynamic estimators take into consideration the previous state estimation (before the sudden change), which is very different to the actual state condition. Since the static WLS does not consider previous estimations, the actual estimation is not affected from the sudden load change.

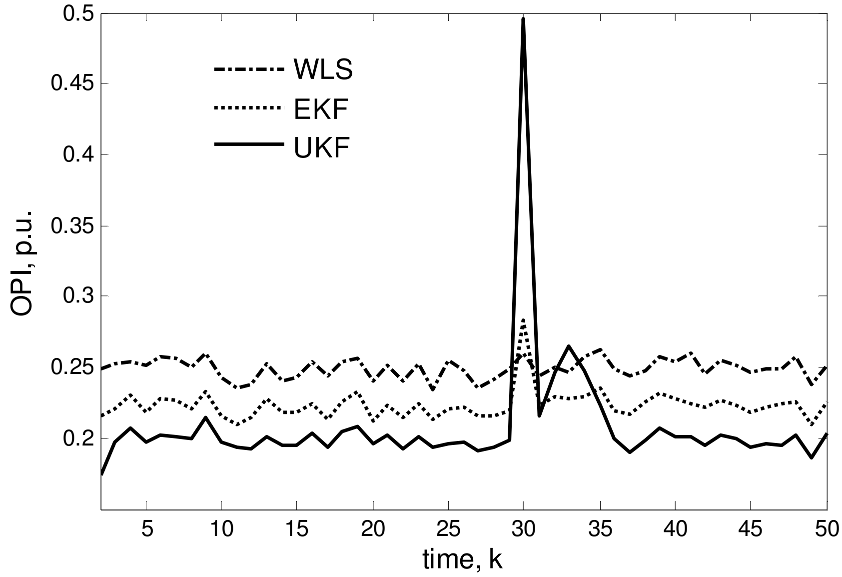

Figure 7.4: ***OPI*** **calculation for sudden load change in 14-bus system with PMU measurements**

From Figure 7.4, it is clear that the UKF is more sensitive than the EKF to abrupt changes of states. However, as soon as the estimator is able to track the new operating point, the UKF estimation is again better than the EKF estimation results.

Figure 7.5 presents the skewness of the distribution of Λ_k for all k instants. Even during the sudden state change at $k = 30$, the skewness is below a pre-defined threshold of 3.0 p.u. This is an indication that there is no presence of bad data and the dynamic estimators cannot detect any anomaly, unless the normalised innovation vector is assessed.

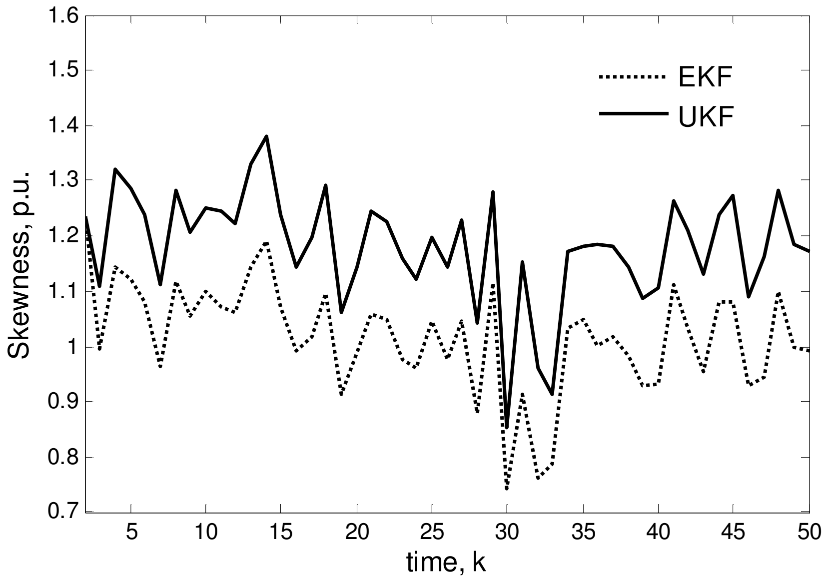

Figure 7.5: Skewness calculation for sudden load change in 14-bus system with PMU measurements

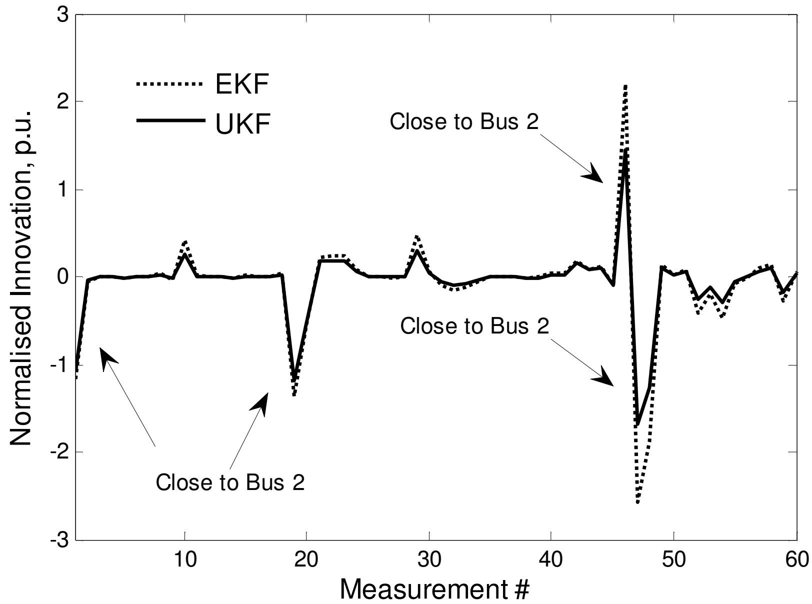

Figure 7.6: Normalised Innovation vector for sudden load change in 14-bus system with PMU measurements

Figure 7.6 shows the normalised innovation vector during the sudden load change (at $k = 30$). This study finds that there are at least four measurements whose normalised innovation processes are considerably larger than that of the other measurements. As these four measurements are all related to *Bus 2*, there is an indication that the operating condition in the surrounding of *Bus 2* is different with respect to the predicted operating condition. As a consequence, a sudden change of the state is detected around *Bus 2*.

There are different actions that can be taken once a sudden change of states is detected. The first option is to increase the covariance matrix $\mathbf{P}_{\hat{x}k\text{-}1}$ so that the estimator neglects the predicted state vector. The second option, and probably the most accurate alternative, would be to use the static estimator once the sudden change is detected. The dynamic estimator would be used again when the system model is able to track the new operating point. In cases where the prediction step is based on load prediction approaches, an approximation of the load/generation change should be incorporated.

7.4.2.3 Presence of Large Bad Data in 57-bus Test System

The 57-bus test system is now used to assess the performance of the dynamic estimators in presence of gross bad data. In this test system, the set of measurements is composed by the conventional and synchronised measurements.

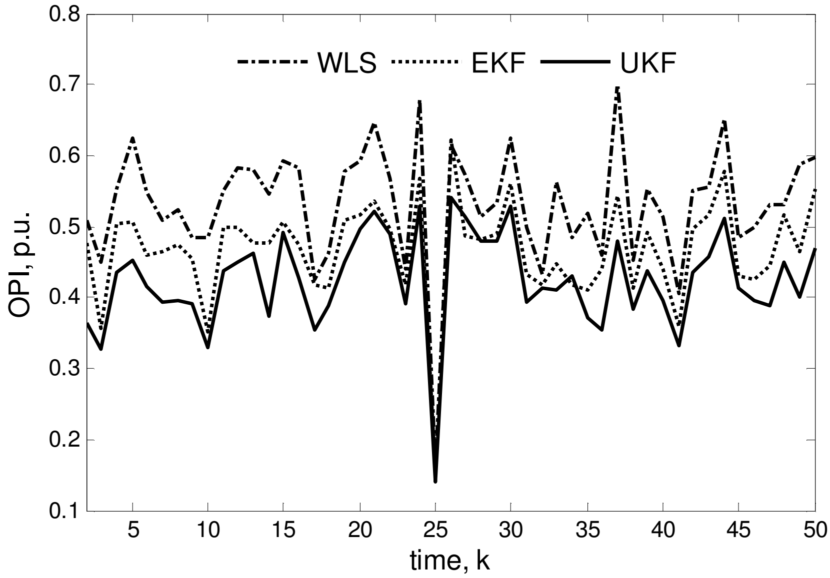

Figure 7.7: *OPI* during bad data at *k* = 25, in the 57-bus system with PMU measurements

Figure 7.7 presents the *OPI* for all *k* instants. From the plot, it is confirmed that the estimation results are affected when gross errors are undetected in the set of measurements. This suggests that the inclusion of a bad data processor would be very beneficial.

Figure 7.8 shows the *skewness* of the distribution of Λ_k calculated using both the UKF and the EKF. It can be seen that very similar results are obtained. At the time of the bad data occurrence ($k = 25$), the skewness reaches values beyond the maximum value $\psi_{max} = 3$ p.u., which is an indication of the presence of bad data.

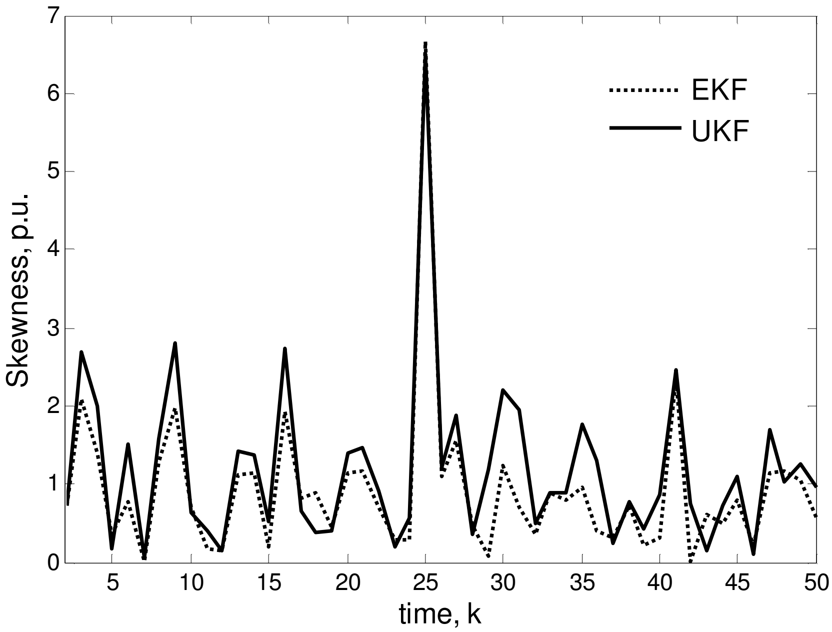

Figure 7.8: Bad data detection using the Skewness calculation in the 57-bus system with PMU measurements

The detection method presented in Figure 7.8 is the equivalent to the Chi-Square distribution test introduced in Chapter 2 for static state estimators. Figure 7.9 presents the Chi-Square distribution test for all the *k* instants. Similar to Figure 7.8, gross bad data is detected when $k = 25$.

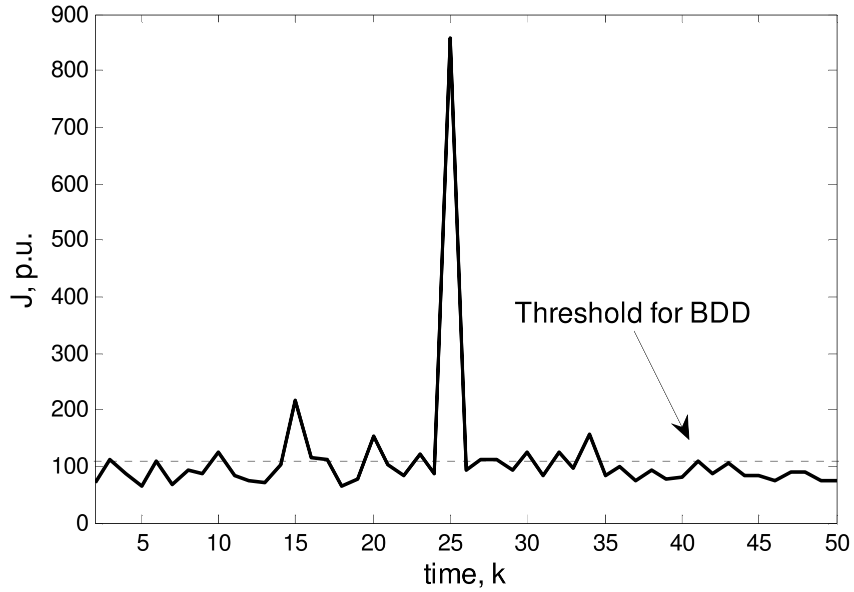

Figure 7.9: Bad data detection using the Chi-Square test in the 57-bus system with PMU measurements

Unlike the dynamic estimators, the static estimator wrongly detects the presence of bad data at $k = 15$. The availability of pseudo-measurements (predicted states) in dynamic estimators makes it possible to better determine the presence of bad data in the set of measurements.

The next step in any bad data processor is the identification of wrong measurements. After a number of multiple simulations, it was concluded that measurements whose normalised innovation process τ_i are larger than 1.5 *p.u.* must be rejected from the set of measurements. This threshold must be selected with caution. A low threshold may identify measurements which are correct as erroneous data whereas a high threshold may consider wrong measurements as good ones.

The threshold used in this work was able to identify all the bad data simulated in the test systems for different measurements and levels of redundancy. On the other hand, it was found that in few cases, the threshold of 1.5 p.u. erroneously identified good measurements as bad data, but they were not eliminated from the set of measurements because the *Skewness* test did not detect any anomaly in the set of measurements. Based on this, it is preferable to use a low threshold and check the *Skewness* test before considering the rejection of measurements.

Figure 7.10 presents the normalised innovation vector at $k = 25$. Here, the normalised vector indicates that the power transfer measurements *P12* and *Q12* have large errors and must be rejected.

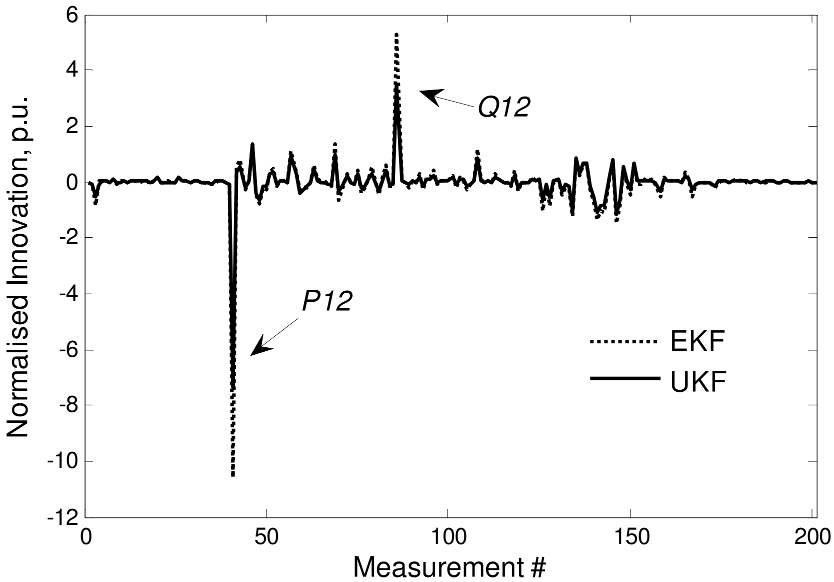

Figure 7.10: Bad data identification at k = 25 in 57-bus system with PMU measurements

Once *P12* is eliminated, a second calculation of the normalised innovation vector indicates that the reactive power *Q12* from *Bus 1* to *Bus 2* is also a wrong measurement and must be rejected. When these erroneous measurements are rejected, the UKF and EKF again deliver similar results as for normal operating conditions.

It is important to mention that measurement redundancy is necessary to ensure the filtering capacities of the dynamic estimator. Low redundancy levels may lead to insufficient information to identify bad data that could easily result in erroneous state estimations if the prediction step is inaccurate.

It is also interesting to compare the normalised innovation vector with the normalised residual vector at $k = 25$, see Chapter 2. Figure 7.11 shows that the normalised residual vector identifies the same pair of transferred power measurements but it also identifies two PMU measurements as erroneous, when they are actually correct.

The better performance of the normalised innovation vector is related to the higher measurement redundancy level of dynamic estimators that make use of the prediction step and it helps to better identify the erroneous measurements.

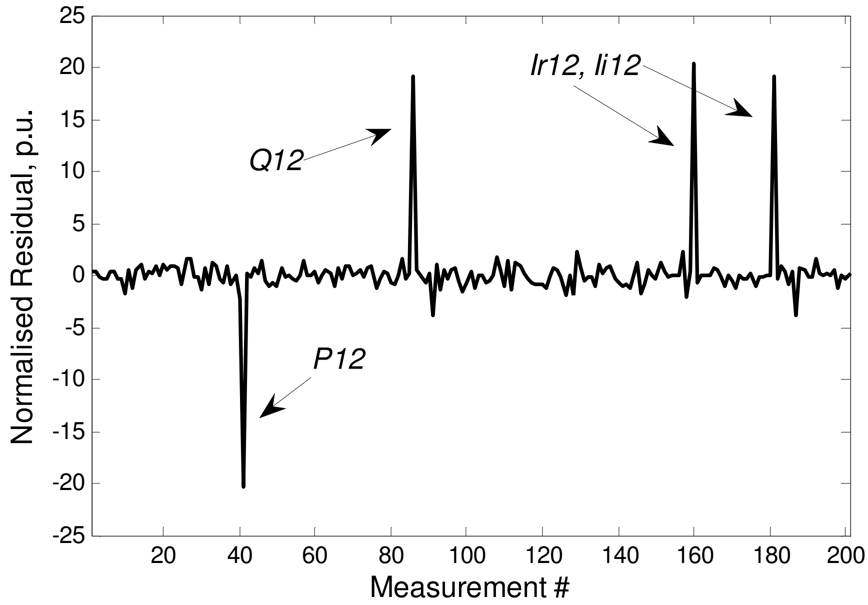

Figure 7.11: Bad data identification using normalised residual analysis at k = 25 in 57-bus system with PMU measurements

7.5 Discussion

The proposed DSE was based on a linear transition of states. However, given the properties of the UKF to deal with non-linear models, the above DSE can be used with a generalised non-linear transition of states. Further studies must concentrate on using more accurate models to represent the transition of the states, able to consider and correct for sudden changes of states.

With respect to this work, it was found that the Holt's parameters' values α_k and β_k can affect the accuracy of the prediction step if not selected adequately. The values adopted in this work delivered very good prediction results. Nevertheless, more appropriate values could be selected from off-line studies.

Different parameter values could be used in the UKF when creating the sigma points. The parameters α, β and κ in (7.23) and (7.24) affect the higher order approximation of the non-linear equations. However, changes of the recommended parameter values had low impact on the final accuracy of the UKF estimation. For instance, using $\kappa = 3- n$ or $\kappa = 0$ did not affect the estimation result for any scenario or power system.

It was also found that the UKF has similar computational requirements to the EKF. In fact, the major challenge of these dynamic estimators is how to simplify the calculation of covariance matrices for large scale power systems. For example, in order to improve the computational efficiency, the covariance matrix can be kept constant during few consecutive time instants for normal operating conditions. Additionally, since the $\mathbf{S}_k$ matrix is very sparse, one could calculate the gain matrix $\mathbf{K}_k$ using sparsity techniques. Alternatively, one can reduce the dimension of the problem using hierarchical estimators [87, 111].

The disadvantage of the proposed UKF based dynamic estimator is the inability to deal with equality constraints to represent null power injection measurements. More work is to be done on this matter to overcome this limitation.

7.6 Summary

The ability to process faster and more accurate measurements (such as synchrophasors) makes us re-think the feasibility of using Dynamic State Estimators (DSE) in modern power system control rooms.

The main advantage of DSE with respect to static estimators is the prediction step. The DSE not only estimates the actual system state but it predicts the future system state before the new set of measurements arrives at the control centre.

The work presented in this Chapter proposes the implementation of the UKF in power system state estimation.

It was found that the proposed UKF based DSE performs better than the EKF with very similar computational demands. In order to determine the effectiveness of the proposed DSE, two test systems were simulated under different operating conditions.

From the simulation tests, it was found that the DSE obtains better estimation results than the static one if the system model is accurate and represents the actual transition of the states. By using the prediction step, the DSE can detect the unexpected change of states, see the 14-bus test system, and it can detect and eliminate bad data, as presented for the 57-bus test system.

In terms of detection and elimination of bad data, the Skewness test and the normalised innovation vector were compared with the Chi-Square distribution test and the normalised residual method (in static estimators). Due to the availability of a prediction step in DSE (used as pseudo-measurements), the measurement redundancy of the system was higher than the static estimator that helped to detect and eliminate the truly erroneous measurements.

More work is to be done to take advantage of the UKF to deal with non-linear systems. That is, a more accurate model of the transition of states should be applied and compared with respect to the linear transition model used in this work. Additionally, the proposed method can be extended to consider larger networks in which hierarchical schemes may be required.

Chapter 8 Conclusions and Future Work

This PhD Thesis presented new algorithms to analyse the impact of uncertainty in power system operation and to enhance the state estimation practice of power systems supported by Phasor Measurement Units.

The following Sections summarise the main conclusions drawn from the results presented in this PhD Thesis and present some suggestions for future work that were not addressed in this piece of research due to time limitations.

8.1 Conclusions

This Thesis introduced and tested a new Probabilistic Load Flow (PLF) methodology based on multiple Weighted Least Square (WLS) runs. The main advantage of this approach is that it uses the actual Probability Density Functions (PDFs) of the input variables rather than only the first statistical moments.

A comparison of different methods to simplify Gaussian Mixture Models (GMMs) used to represent non-Gaussian power system variables was presented. The reduction methods helped to decrease the number of WLS runs of the proposed PLF while maintaining a good approximation of the original distributions.

It was found that the Integral Squared Difference (ISD) discrimination method always identified the pair of components that when merged produced the minimum difference between the original and the reduced Gaussian mixture. However, this method was found to be time consuming compared to the Kullback-Leibler (KL) upper bound or the Squared Distance (SD) algorithms.

The KL upper bound algorithm was found to be very efficient in terms of computational demands and accuracy. This can be the best choice if the number of Gaussian components to merge is high.

The fine tuning method obtains better reductions than any pair-merging method. However, the pair merging methods can be used as an initial guess to ensure the convergence of the optimal based method.

From the validation of the proposed PLF study in Chapter 4, it was found that few errors of approximation are introduced by the assumption that the correlation between Gaussian components that belong to two particular Gaussian mixtures is the same as the correlation between those Gaussian mixtures.

This assumption introduces some errors in the calculated PDFs of bus voltages and power flows at the proximities of the non-Gaussian distributed power injections. These errors become more evident when the correlated Gaussian mixtures have large Coefficient of Variation (*CV)* and when they are modelled by many Gaussian components. For this reason, the calculated PDFs of voltage and power flows are closer to the Monte Carlo Simulation (MCS) plots when fewer Gaussian components are used to model the correlated input variables.

It was found that the proposed PLF can be implemented in both meshed and radial networks. The approximation provides more realistic results when compared to not including any correlation between variables.

In the case of radial distribution systems, the problem becomes an over-determined state estimation calculation when real-time measurements are included in the WLS formulation. From the simulated cases, it is concluded that power injections, modelled as GMMs, have greater effect on the estimated flows and voltages around it when they are far from the real-time measurements or when these power injections are relatively large compared to the sum of the power injections along the feeder.

A study of different alternatives for including synchronised measurements in power system state estimation was presented in the Thesis. It was found that the WLS formulation has convergence problems when the current measurements are expressed in polar form. This is caused by abrupt changes in sign and magnitude of the corresponding Jacobian elements for consecutive iterations. The study shows that a constraint formulation can be used to include synchronised measurements in polar form. The level of accuracy is similar to that of rectangular form but the constraint formulation avoids the propagation of measurement uncertainty. On the contrary, it was found that the pseudo-voltage formulation reduces the accuracy of the hybrid state estimator.

The research work demonstrated how the state estimation problem of large interconnected power systems can be decentralised into smaller local area state estimators. This decentralisation is carried out to reduce the computational burden and complexity of processing large sets of measurements. The mismatch between boundary buses was corrected by using the coordination level's state estimation.

Multi-area state estimators are based on the assumption that errors in measurements from one area have little effect on the estimated bus voltages in other areas. The results demonstrated that not including power injection measurements in the coordination level reduced the size of the problem. This reduction had little effect on the estimated boundary bus voltages as long as the redundancy level is maintained with pseudo-measurements of power flows and other available real measurements in boundary buses.

The most accurate estimation results were obtained when the estimated power flows from local area estimators were accurate. To achieve this, it is necessary to have reliable and accurate measurements in or close to boundary buses and maintain a good level of redundancy to detect and reject bad data.

The study of including synchronised measurements in modern state estimators was also extended to the problem of Dynamic State Estimators (DSE). The main benefit of dynamic estimators is that they can process faster and more accurate measurements (such as PMU measurements) and it is possible to take advantage of the predictive nature of the DSE. By using the prediction step, the DSE can detect the unexpected change of states and the presence of bad data.

It was found that the Unscented Kalman Filter (UKF) performs better than the Extended Kalman Filter (EKF) with very similar computational demands. Although both filters are affected by sudden changes of states, the UKF was found to be more sensitive than the EKF.

The study also compared the dynamic and static state estimators in terms of detection and elimination of bad data. Due to the availability of a prediction step in DSE, the measurement redundancy was higher than in the static estimator and this helped to better detect and eliminate the truly erroneous measurements.

8.2 Future Work

This Thesis presented a new PLF for including non-Gaussian correlated input variables. The test results showed that assuming a constant correlation coefficient for all the WLS runs creates some approximation errors in the PDFs of power flows close to the non-Gaussian correlated input variables. These errors were more evident when the input variables were modelled by many Gaussian components and when the *CV* was large (> 50%). There is an opportunity to explore a different assumption to include correlation between the input variables in each WLS run.

The distribution system state estimator, as an extension of the PLF methodology, can be improved to consider stochastic topology changes. The line parameters of the branch whose connection status is uncertain should be included in the state vector. These parameters should be modelled as discrete variables with two possible values: the actual parameters (branch connected) or zero (branch disconnected). However, as the discrete probabilities are approximated as Gaussian delta functions (modelled as GMMs), this would result in more WLS runs.

A comparison of three hybrid state estimators was presented in Chapter 5. The comparison was based on accuracy for normal operating conditions. This comparison can be extended to account for the impact of parameter errors on hybrid state estimators. It is likely that some methods will be more affected and some others may be more adequate to detect these parameter errors.

Although optimal location of PMU was not addressed in this PhD Thesis (due to the large amount of available literature related to this topic), it is important to point out the need for the optimal placement of PMUs for Multi-Area State Estimation. The optimal location of PMUs should be assessed in terms of estimation accuracy, ability to improve redundancy levels, and observability of boundary and adjacent-to-boundary buses.

As it was presented in Chapter 7, the dynamic state estimator based on the UKF is largely affected during sudden changes of states. This is caused by the difference between the prediction step and the new set of measurements. Since the sudden change of states can be detected from the innovation vector, future work should be focused on algorithms to re-adjust the prediction step to make sure that the prediction step is in agreement with the new set of measurements.

More work is to be done to take advantage of the UKF to deal with non-linear systems. That is, a more accurate model of the transition of states should be applied and compared with respect to the linear transition model used in this work. Additionally, the proposed DSE can be extended to consider larger networks in which hierarchical schemes may be required.

8.3 Final Thesis Summary

The aim of this Thesis was to provide a step forward to estimate the operating conditions of electric power systems in the presence of uncertain input variables, and to improve the state estimation practice by exploring different formulations for including synchronised phasor measurements in static and dynamic state estimators.

Through the successful completion of the research carried out for this Thesis, it has been shown that accurate PLF studies can be carried out by the Gaussian Component Combination Method (GCCM) as an alternative to Monte Carlo simulations. The GCCM uses the exact

PDFs of the input variables and their correlation coefficient. This is an improvement on the current knowledge because most of the previous PLF methods only use the first statistical moments (e.g., Point Estimate method) and some others have neglected the effect of correlation between input variables.

The presented work also demonstrated that it is possible to use polar form of currents (from PMUs) in hybrid state estimation without any transformation of variables or measurements. In addition, the Thesis introduced a new algorithm for reducing the data exchange in multi-area state estimators. The advantage of this approach, with respect to previous formulations, is that it only used the boundary and the references buses in the coordination level. The reduction of the problem was found to be very effective because the accuracy of the estimation results were similar to the results without the proposed simplification.

Finally, this Thesis showed that the DSE can be as effectively as the Static State Estimator (SSE) that is currently used in control systems. This work is a good contribution to the current knowledge because it demonstrated that the proposed UKF based DSE performs better than the classical EKF based DSE, and it has the potential to be used in more complex non-linear models of the power system. The proposed DSE will encourage future researchers to explore the advantages of the UKF in state estimation and model validation of power systems during transient conditions.

References

[1] A. Gomez-Exposito, A.J. Conejo, and C. Canizares, *Electric Energy Systems: Analysis and Operation*. London: CRC Press, 2009.

[2] J. M. Morales, L. Baringo, A. J. Conejo, and R. Minguez, "Probabilistic power flow with correlated wind sources," *IET Generation, Transmission & Distribution*, vol. 4, no. 5, pp. 641-651, May 2010.

[3] B. Borkowska, "Probabilistic Load Flow," *IEEE Transactions on Power Apparatus and Systems*, vol. PAS-93, no. 3, pp. 752-755, May 1974.

[4] D. Villanueva, J. L. Pazos, and A. Feijoo, "Probabilistic Load Flow Including Wind Power Generation," *IEEE Transactions on Power Systems*, vol. 26, no. 3, pp. 1659 - 1667 Aug. 2011.

[5] R. N. Allan and M. R. G. Al-Shakarchi, "Probabilistic a.c. load flow," *Proceedings of the IEEE*, vol. 123, no. 6, pp. 531-536, Jun. 1976.

[6] A. M. L. d. Silva and V. L. Arienti, "Probabilistic load flow by a multilinear simulation algorithm," *IEE Proceedings: Generation, Transmission and Distribution*, vol. 137, no. 4, pp. 276-282, Jul. 1990.

[7] J. F. Dopazo, O. A. Klitin, and A. M. Sasson, "Stochastic load flows," *IEEE Transactions on Power Apparatus and Systems*, vol. 94, no. 2, pp. 299- 309, Mar. 1975.

[8] C. L. Su, "Probabilistic load-flow computation using point estimate method," *IEEE Transactions on Power Systems*, vol. 20, no. 4, pp. 1843-1851, Nov. 2005.

[9] J. M. Morales and J. Perez-Ruiz, "Point Estimate Schemes to Solve the Probabilistic Power Flow," *IEEE Transactions on Power Systems*, vol. 22, no. 4, pp. 1594-1601, Nov. 2007.

[10] J. Usaola, "Probabilistic load flow with wind production uncertainty using cumulants and Cornish-Fisher expansion," *International Journal of Electrical Power & Energy Systems*, vol. 31, no. 9, pp. 474-481. 2009.

[11] M. Matos and R. J. Bessa, "Setting the operating reserve using probabilistic wind power forecasts," *IEEE Transactions on Power Systems*, vol. 26, no. 2, pp. 594-603, May 2011.

[12] H. Bludszuweit, J. A. Dominguez-Navarro, and A. Llombart, "Statistical analysis of wind power forecast error," *IEEE Transactions on Power Systems*, vol. 23, no. 3, pp. 983-991, Aug. 2008.

[13] T. P. Chang, "Estimation of wind energy potential using different probability density functions," *Applied Energy*, vol. 88, no. 5, pp. 1848-1856, May 2011.

[14] A. K. Ghosh, D. L. Lubkeman, M. J. Downey, and R. H. Jones, "Distribution circuit state estimation using a probabilistic approach," *IEEE Transactions on Power Systems*, vol. 12, no. 1, pp. 45-51, Feb. 1997.

[15] S. W. Heunis and R. Herman, "A probabilistic model for residential consumer loads," *IEEE Transactions on Power Systems*, vol. 17, no. 3, pp. 621-625, Aug. 2002.

[16] R. Singh, B. C. Pal, and R. A. Jabr, "Statistical Representation of Distribution System Loads Using Gaussian Mixture Model," *IEEE Transactions on Power Systems*, vol. 25, no. 1, pp. 29-37, Feb. 2010.

[17] A. Wood and B. F. Wollenberg, *Power Generation Operation and Control*, 2nd ed, 1996.

[18] A. Abur and A. Gomez-Exposito, *Power System State Estimation: Theory and Implementation*. New York: Marcel Dekker, 2004.

[19] J. De La Ree, V. Centeno, J.S. Thorp, and A. G. Phadke, "Synchronized Phasor Measurement Applications in Power Systems," *IEEE Transactions on Smart Grid*, vol. 1, no. 1, pp. 20-27, Jun. 2010.

[20] V. Terzija, G. Valverde, C. Deyu, P. Regulski, V. Madani, J. Fitch, S. Skok, M.M. Begovic, and A. Phadke, "Wide-Area Monitoring, Protection, and Control of Future Electric Power Networks," *Proceedings of the IEEE*, vol. 99, no. 1, pp. 80-93, Jan. 2011.

[21] "IEEE Standard for Synchrophasors for Power Systems," IEEE Standard C.37.118-2005, 2005.

[22] K. E. Martin, "Synchrophasor Standards Development - IEEE C37.118 & IEC 61850," presented at 44th Hawaii International Conference on System Sciences Hawaii, 2011.

[23] A. G. Phadke, J.S. Thorp, and K. J. Karimi, "State Estimation with Phasor Measurements," *IEEE Transactions on Power Systems*, vol. 1, no. 1, pp. 233-241, Feb. 1986.

[24] J.S. Thorp, A.G. Phadke, and K. J. Karimi, "Real Time Voltage-Phasor Measurement For Static State Estimation," *IEEE Transactions on Power Apparatus and Systems,*, vol. PAS-104, no. 11, pp. 3098-3106, Nov. 1985.

[25] R. Zivanovic and C. Cairns, "Implementation of PMU technology in state estimation: an overview," presented at IEEE AFRICON 4th, 1996.

[26] Z. Ming, V.A. Centeno, J.S. Thorp, and A. G. Phadke, "An Alternative for Including Phasor Measurements in State Estimators," *IEEE Transactions on Power Systems*, vol. 21, no. 4, pp. 1930-1937, Nov. 2006.

[27] T. S. Bi, X. H. Qin, and Q. X. Yang, "A novel hybrid state estimator for including synchronized phasor measurements," *Electric Power Systems Research*, vol. 78, no. 8, pp. 1343-1352, Aug. 2008.

[28] L. Zhao and A. Abur, "Multi area state estimation using synchronized phasor measurements," *IEEE Transactions on Power Systems*, vol. 20, no. 2, pp. 611-617, May 2005.

[29] J. Weiqing, V. Vittal, and G. T. Heydt, "A Distributed State Estimator Utilizing Synchronized Phasor Measurements," *IEEE Transactions on Power Systems*, vol. 22, no. 2, pp. 563-571, May 2007.

[30] J. Weiqing, V. Vittal, and G. T. Heydt, "Diakoptic State Estimation Using Phasor Measurement Units," *IEEE Transactions on Power Systems*, vol. 23, no. 4, pp. 1580-1589, Nov. 2008.

[31] H. R. Sirisena and E. P. M. Brown, "Representation of non-Gaussian probability distributions in stochastic load-flow studies by the method of Gaussian sum approximations," *IEE Proceedings*, vol. 130, no. 4, pp. 50-59, Jul. 1983.

[32] A. Monticelli, "Electric power system state estimation," *Proceedings of the IEEE*, vol. 88, no. 2, pp. 262-282, Feb. 2000.

[33] R.R. Nucera and M. L. Gilles, "A blocked sparse matrix formulation for the solution of equality-constrained state estimation," *IEEE Transactions on Power Systems*, vol. 6, no. 1, pp. 214-224, Feb. 1991.

[34] F.F. Wu and A. Monticelli, "Network Observability: Theory," *IEEE Transactions on Power Apparatus and Systems*, vol. PAS-104, no. 5, pp. 1042-1048, May 1985.

[35] T.L. Baldwin, L. Mili, M.B. Boisen, and R. Adapa, "Power system observability with minimal phasor measurement placement," *IEEE Transactions on Power Systems*, vol. 8, no. 2, pp. 707-715, May 1993.

[36] G.R. Krumpholz, K.A. Clements, and P. W. Davis, "Power System Observability: A Practical Algorithm Using Network Topology," *IEEE Transactions on Power Apparatus and Systems*, vol. PAS-99, no. 4, pp. 1534-1542, Jul. 1980.

[37] J. B. A. London, Jr., L. F. C. Alberto, and N. G. Bretas, "Network observability: identification of the measurements redundancy level," presented at International Conference on Power System Technology. , 2000.

[38] N. G. Bretas and J. B. A. London, Jr., "Measurement placement design and reinforcement for state estimation purposes," presented at Power Tech Proceedings, Porto, 2001.

[39] C. Jian and A. Abur, "Placement of PMUs to Enable Bad Data Detection in State Estimation," *IEEE Transactions on Power Systems*, vol. 21, no. 4, pp. 1608-1615, Nov. 2006.

[40] A. Monticelli and F. F. Wu, "Network Observability: Identification of Observable Islands and Measurement Placement," *IEEE Transactions on Power Apparatus and Systems*, vol. PAS-104, no. 5, pp. 1035-1041, May 1985.

[41] B. Gou and A. Abur, "A direct numerical method for observability analysis," *IEEE Transactions on Power Systems*, vol. 15, no. 2, pp. 625-630, May 2000.

[42] G. Peters and J. H.Wilkinson, "The least-squares problem and pseudoinverses," *Computer Journal*, vol. 13, no. 4, pp. 309–316, Aug. 1970.

[43] G.N. Korres and G. C. Contaxis, "A reduced model for bad data processing in state estimation," *IEEE Transactions on Power Systems*, vol. 6, no. 2, pp. 550-557, May 1991.

[44] E. Handschin, F.C. Schweppe, J. Kohlas, and A. Fiechter, "Bad data analysis for power system state estimation," *IEEE Transactions on Power Apparatus and Systems*, vol. 94, no. 2, pp. 329-337, May 1975.

[45] A. Monticelli, *State Estimation in Electric Power Systems: A Generalized Approach*. Massachusetts: Kluwer Academic Publishers, 1999.

[46] A. Monticelli and A. Garcia, "Reliable Bad Data Processing for Real-Time State Estimation," *IEEE Transactions on Power Apparatus and Systems*, vol. PAS-102, no. 5, pp. 1126-1139, May 1983.

[47] K.A. Clements and P. W. Davis, "Multiple Bad Data Detectability and Identifiability: A Geometric Approach," *IEEE Transactions on Power Delivery*, vol. 1, no. 3, pp. 355-360, Jul. 1986.

[48] R. N. Allan, A. M. L. d. Silva, and R. C. Burchett, "Evaluation Methods and Accuracy in Probabilistic Load Flow Solutions," *IEEE Transactions on Power Apparatus and Systems*, vol. PAS-100, no. 5, pp. 2539-2546, May 1981.

[49] P. Zhang and S. T. Lee, "Probabilistic load flow computation using the method of combined cumulants and Gram-Charlier expansion," *IEEE Transactions on Power Systems*, vol. 19, no. 1, pp. 676-682, Feb. 2004.

[50] J. Usaola, "Probabilistic load flow with correlated wind power injections," *Electric Power Systems Research*, vol. 80, no. 5, pp. 528-536, May 2010.

[51] D. C. Montgomery and G. C. Runger, *Applied Statistics and Probability for Engineers*, 3rd ed. New York: John Wiley & Sons. Inc, 2002.

[52] D. J. Salmond, "Mixture Reduction Algorithms for Point and Extended Object Tracking in Clutter," *IEEE Transactions on Aerospace and Electronic Systems*, vol. 45, no. 2, pp. 667-686, Apr. 2009.

[53] "Matlab Statistical Toolbox User's Guide," in *http://www.mathworks.com*.

[54] J. L. Williams and P. S. Maybeck, "Cost-function-based Gaussian mixture reduction," presented at 6th International Conference on Information Fusion, 2003.

[55] A. Runnalls, "A Kullback-Leibler approach to Gaussian mixture reduction," *IEEE Transactions on Aerospace and Electronic Systems*, vol. 43, no. 3, pp. 989-999, Jul. 2007.

[56] D. J. Salmond, "Mixture reduction algorithms for target tracking in clutter," *Proceedings of SPIE,* vol. 1305, pp. 434-445. Jan. 1990.

[57] D. Schieferdecker and M. F. Huber, "Gaussian mixture reduction via clustering," presented at 12th International Conference on Information Fusion, 2009.

[58] U. D. Hanebeck, K. Briechle, and A. Rauh, "Progressive Payes: A New Framework for Nonlinear State Estimation," in *Proceedings of SPIE*, vol. 5099, pp. 256-267, Apr. 2003

[59] M. F. Huber and U. D. Hanebeck, "Progressive Gaussian mixture reduction," presented at 11th International Conference on Information Fusion, 2008.

[60] L. Kocis and W. J. Whiten, "Computational investigations of low-discrepancy sequences," *ACM Transactions on Mathematical. Software*, vol. 23, no. 2, pp. 266-294, Jun. 1997.

[61] P. Bratley and B. L. Fox, "Algorithm 659 Implementing Sobol's Quasirandom Sequence Generator," *ACM Transactions on Mathematical Software*, vol. 14, no. 1, pp. 88-100, Mar. 1988.

[62] C. T. d. Santos, A. Samaranayaka, and B. Manly, "On the use of correlated beta random variables with animal population modelling," *Ecological Modelling*, vol. 215, no. 4, pp. 293-300, Jul. 2008.

[63] P.-L. Liu and A. Der Kiureghian, "Multivariate distribution models with prescribed marginals and covariances," *Probabilistic Engineering Mechanics*, vol. 1, no. 2, pp. 105-112. 1986.

[64] R. Christie, "Power system test archive. [Online] http://www.ee.washington.edu/research/pstca ": The University of Washington, 1999.

[65] S. Chun-Lien, "Probabilistic load-flow computation using point estimate method," *IEEE Transactions on Power Systems*, vol. 20, no. 4, pp. 1843- 1851, Nov. 2005.

[66] A. E. Feijoo and J. Cidras, "Modeling of wind farms in the load flow analysis," *IEEE Transactions on Power Systems*, vol. 15, no. 1, pp. 110-115, Feb. 2000.

[67] P. Chen, P. Siano, B. Bak-Jensen, and Z. Chen, "Stochastic Optimization of Wind Turbine Power Factor Using Stochastic Model of Wind Power," *IEEE Transactions on Sustainable Energy*, vol. 1, no. 1, pp. 19-29, Apr. 2010.

[68] M. E. Baran and F. F. Wu, "Optimal capacitor placement on radial distribution systems," *IEEE Transactions on Power Delivery*, vol. 4, no. 1, pp. 725-734, Jan. 1989.

[69] D. Shirmohammadi, H. W. Hong, A. Semlyen, and G. X. Luo, "A compensation-based power flow method for weakly meshed distribution and transmission networks," *IEEE Transactions on Power Systems*, vol. 3, no. 2, pp. 753-762, May 1988.

[70] K. I. Geisler, "Ampere Magnitude Line Measurements for Power Systems State Estimation," *IEEE Transactions on Power Apparatus and Systems*, vol. PAS-103, no. 8, pp. 1962-1969, Aug. 1984.

[71] R.O. Burnett, M.M Butts, T.W. Cease, V. Centeno, G. Michel, R.J. Murphy, and A.G. Phadke, "Synchronized phasor measurements of a power system event," *IEEE Transactions on Power Systems*, vol. 9, no. 3, pp. 1643-1650, Aug. 1994.

[72] J. Rasmussen and P. Jorgensen, "Synchronized phasor measurements of a power system event in eastern Denmark," *IEEE Transactions on Power Systems*, vol. 21, no. 1, pp. 278- 284, Feb. 2006.

[73] S. Chakrabarti, E. Kyriakides, G. Ledwich, and A. Ghosh, "Inclusion of PMU current phasor measurements in a power system state estimator," *IET Generation, Transmission & Distribution*, vol. 4, no. 10, pp. 1104-1115, Oct. 2010.

[74] S. Chakrabarti and E. Kyriakides, "PMU Measurement Uncertainty Considerations in WLS State Estimation," *IEEE Transactions on Power Systems,*, vol. 24, no. 2, pp. 1062-1071, May 2009.

[75] G. N. Korres and N. M. Manousakis, "State estimation and bad data processing for systems including PMU and SCADA measurements," *Electric Power Systems Research*, vol. 81, no. 7, pp. 1514-1524, Jul. 2011.

[76] C. Bruno, C. Candia, L. Franchi, G. Giannuzzi, M. Pozzi, R. Zaottini, and M. Zaramella, "Possibility of enhancing classical weighted least squares State Estimation with linear PMU measurements," presented at IEEE PowerTech, Bucharest, 2009.

[77] S. Chakrabarti, E. Kyriakides, G. Valverde, and V. Terzija, "State estimation including synchronized measurements," presented at IEEE PowerTech, Bucharest, 2009.

[78] C. Yunzhi, H. Xiao, and G. Bei, "A new state estimation using synchronized phasor measurements," presented at IEEE International Symposium on Circuits and Systems 2008.

[79] D. Simon, *Optimal State Estimation: Kalman, H infinity, and Nonlinear Approaches*. New Jersey: John Wiley & Sons, Inc, 2006.

[80] S. Chakrabarti, E. Kyriakides, and M. Albu, "Uncertainty in Power System State Variables Obtained Through Synchronized Measurements," *IEEE Transactions on Instrumentation and Measurement*, vol. 58, no. 8, pp. 2452-2458, Aug. 2009.

[81] Th. Van Cutsem, J.L. Horward, and M. Ribbens-Pavella, "A Two-Level Static State Estimator for Electric Power Systems," *IEEE Transactions on Power Apparatus and Systems*, vol. PAS-100, no. 8, pp. 3722-3732, Aug. 1981.

[82] A. Gómez-Expósito, A. d. l. V. Jaén, C. Gómez-Quiles, P. Rousseaux, and T. V. Cutsem, "A taxonomy of multi-area state estimation methods," *Electric Power Systems Research*, vol. 81, no. 4, pp. 1060-1069, Apr. 2010.

[83] A.J. Conejo, S. de la Torre, and M. Canas, "An Optimization Approach to Multiarea State Estimation," *IEEE Transactions on Power Systems*, vol. 22, no. 1, pp. 213-221, Feb. 2007.

[84] E. Caro, A. J. Conejo, and R. Minguez, "Decentralized State Estimation and Bad Measurement Identification: An Efficient Lagrangian Relaxation Approach," *IEEE Transactions on Power Systems*, vol. 26, no. 4, pp. 2500-2508, Nov. 2011.

[85] R. Ebrahimian and R. Baldick, "State estimation distributed processing for power systems," *IEEE Transactions on Power Systems*, vol. 15, no. 4, pp. 1240-1246, Nov. 2000.

[86] A. Gomez-Exposito, A. Abur, A. d. l. V. Jaen, and C. Gomez-Quiles, "A Multilevel State Estimation Paradigm for Smart Grids," *Proceedings of the IEEE*, vol. 99, no. 6, pp. 952-976, Jun. 2011.

[87] P. Rousseaux, T. Van Cutsem, and T. E. Dy Liacco, "Whither dynamic state estimation?," *International Journal of Electrical Power & Energy Systems*, vol. 12, no. 2, pp. 104-116, Apr. 1990.

[88] P. Rousseaux, D. Mallieu, T. V. Cutsem, and M. Ribbens-Pavella, "Dynamic state prediction and hierarchical filtering for power system state estimation," *Automatica*, vol. 24, no. 5, pp. 595-618, Sept. 1988.

[89] B. Xiaomeng, X. R. Li, H. Chen, D. Gan, and J. Qiu, "Joint Estimation of State and Parameter With Synchrophasors—Part I: State Tracking," *IEEE Transactions on Power Systems*, vol. 26, no. 3, pp. 1196-1208, Aug. 2011.

[90] A. C. Z. d. Souza, J.C.S. de Souza, and A. M. L. d. Silva, "On-line voltage stability monitoring," *IEEE Transactions on Power Systems*, vol. 15, no. 4, pp. 1300-1305, Nov. 2000.

[91] B. Xiaomeng, X. R. Li, H. Chen, D. Gan, and J. Qiu, "Joint Estimation of State and Parameter With Synchrophasors—Part II: Parameter Tracking," *IEEE Transactions on Power Systems*, vol. 26, no. 3, pp. 1209-1220, Aug. 2011.

[92] A. S. Debs and R. E. Larson, "A Dynamic Estimator for Tracking the State of a Power System," *IEEE Transactions on Power Apparatus and Systems*, vol. PAS-89, no. 7, pp. 1670-1678, Sept. 1970.

[93] K. Nishiya, J. Hasegawa, and T. Koike, "Dynamic state estimation including anomaly detection and identification for power systems," *IEE Proceedings on Generation, Transmission and Distribution*, vol. 129, no. 5, pp. 192-198, Sept. 1982.

[94] A. M. Leite da Silva, M. B. Do Coutto Filho, and J. F. de Queiroz, "State forecasting in electric power systems," *IEE Proceedings on Generation, Transmission and Distribution*, vol. 130, no. 5, pp. 237-244, Sept. 1983.

[95] A. M. L. d. Silva, M. B. d. C. Filho, and J. M. C. Cantera, "An Efficient Dynamic State Estimation Algorithm including Bad Data Processing," *IEEE Transactions on Power Systems*, vol. 2, no. 4, pp. 1050-1058, Nov. 1987.

[96] G. Durgaprasad and S. S. Thakur, "Robust dynamic state estimation of power systems based on M-Estimation and realistic modeling of system dynamics," *IEEE Transactions on Power Systems*, vol. 13, no. 4, pp. 1331-1336, Nov. 1998.

[97] A. K. Sinha and J. K. Mondal, "Dynamic state estimator using ANN based bus load prediction," *IEEE Transactions on Power Systems*, vol. 14, no. 4, pp. 1219-1225, Nov. 1999.

[98] E. A. Blood, B. H. Krogh, and M. D. Ilic, "Electric power system static state estimation through Kalman filtering and load forecasting," presented at Power and Energy Society General Meeting - Conversion and Delivery of Electrical Energy in the 21st Century, 2008 IEEE, 2008.

[99] N. G. Bretas, "An iterative dynamic state estimation and bad data processing," *International Journal of Electrical Power & Energy Systems*, vol. 11, no. 1, pp. 70-74, Jan. 1989.

[100] S. Sarkka, "On Unscented Kalman Filtering for State Estimation of Continuous-Time Nonlinear Systems," *Automatic Control, IEEE Transactions on*, vol. 52, no. 9, pp. 1631-1641, Sept. 2007.

[101] S. Julier, J. Uhlmann, and H. F. Durrant-Whyte, "A new method for the nonlinear transformation of means and covariances in filters and estimators," *IEEE Transactions on Automatic Control*, vol. 45, no. 3, pp. 477-482, Mar. 2000.

[102] S. J. Julier and J. K. Uhlmann, "Unscented filtering and nonlinear estimation," *Proceedings of the IEEE*, vol. 92, no. 3, pp. 401-422, Mar. 2004.

[103] M. Huang, W. Li, and W. Yan, "Estimating parameters of synchronous generators using square-root unscented Kalman filter," *Electric Power Systems Research*, vol. 80, no. 9, pp. 1137-1144, Sept. 2010.

[104] G. Valverde, E. Kyriakides, G. T. Heydt, and V. Terzija, "Nonlinear Estimation of Synchronous Machine Parameters Using Operating Data," *IEEE Transactions on Energy Conversion*, vol. 26, no. 3, pp. 831-839, Sept. 2011.

[105] E. Ghahremani and I. Kamwa, "Online State Estimation of a Synchronous Generator Using Unscented Kalman Filter From Phasor Measurements Units," *IEEE Transactions on Energy Conversion*, vol. 26, no. 4, pp. 1099-1108, Dec. 2011.

[106] J. Zhang, A. Swain, N.-K. C. Nair, and J. J. Liu, "Estimation of power quality using an unscented Kalman filter," presented at IEEE TENCON, Region 10 Conference, 2007.

[107] H. Novanda, P. Regulski, F.M. Gonzalez-Longatt, and V. Terzija, "Unscented Kalman Filter for frequency and amplitude estimation," presented at IEEE PowerTech, Trondheim, Norway, 2011.

[108] G. Valverde, E. Kyriakides, and V. Terzija, "A non-linear approach for on-line parameter estimation of synchronous machines," presented at Power System Computational Conference (PSCC), Stockholm, 2011.

[109] S. Chun-Lien and L. Chan-Nan, "Interconnected network state estimation using randomly delayed measurements," *IEEE Transactions on Power Systems*, vol. 16, no. 4, pp. 870-878, Nov. 2001.

[110] S. Kuang-Rong and H. Shyh-Jier, "Application of a robust algorithm for dynamic state estimation of a power system," *IEEE Transactions on Power Systems*, vol. 17, no. 1, pp. 141-147, Feb. 2002.

[111] J. K. Mandal and A. K. Sinha, "Hierarchical dynamic state estimation incorporating measurement function non-linearities," *International Journal of Electrical Power & Energy Systems*, vol. 19, no. 1, pp. 57-67, Jan. 1997.

Appendices

10.1 Appendix A

10.1.1 A.1: Solution of WLS Formulation

Given the set of measurements $\mathbf{z}$ modelled as:

$$\mathbf{z} = \mathbf{h}(\mathbf{x}) + \mathbf{e} \tag{10.1}$$

where $\mathbf{h}(\mathbf{x})$ is the set of non-linear functions relating the set of measurements with the state variables $\mathbf{x}$, and $\mathbf{e}$ is the set of measurement errors with mean value $E[\mathbf{e}] = \mathbf{0}$ and covariance matrix $\mathbf{R} = E[\mathbf{e} \cdot \mathbf{e}^T] = diag\{\sigma_1^2, \sigma_2^2, \dots, \sigma_m^2\}$, the WLS estimate of the state vector $\mathbf{x}$ is defined as the value $\hat{\mathbf{x}}$ that minimizes the weighted sum of the squares of the measurement residual $\mathbf{r} = \mathbf{z} - \mathbf{h}(\mathbf{x})$. Hence, the objective is to minimize:

$$J(\mathbf{x}) = [\mathbf{z} - \mathbf{h}(\mathbf{x})]^T \mathbf{R}^{-1} [\mathbf{z} - \mathbf{h}(\mathbf{x})] \tag{10.2}$$

At the minimum, the first order optimality condition must be satisfied. This is,

$$\boldsymbol{g}(\hat{\mathbf{x}}) = \frac{\partial J(\hat{\mathbf{x}})}{\partial \mathbf{x}} = -\mathbf{H}^T(\hat{\mathbf{x}})\, \mathbf{R}^{-1}[\mathbf{z} - \mathbf{h}(\hat{\mathbf{x}})] = 0 \tag{10.3}$$

where $\mathbf{H}(\hat{\mathbf{x}}) = \partial \mathbf{h}(\hat{\mathbf{x}}) / \partial \mathbf{x}$.

By expanding $\boldsymbol{g}(\hat{\mathbf{x}})$ into its Taylor series around the initial guess $\mathbf{x}^k$, and neglecting the second and higher order terms:

$$\boldsymbol{g}(\hat{\mathbf{x}}) = g(\mathbf{x}^k) + \mathbf{G}(\mathbf{x}^k)(\hat{\mathbf{x}} - \mathbf{x}^k) + \cdots = 0 \tag{10.4}$$

One obtains an iterative solution known as the Gauss-Newton method:

$$\mathbf{x}^{k+1} = \mathbf{x}^k - [\mathbf{G}(\mathbf{x}^k)]^{-\mathbf{1}} \boldsymbol{g}(\mathbf{x}^k), \tag{10.5}$$

where $\hat{\mathbf{x}}$ has been replaced by $\mathbf{x}^{k+1}$ which is the solution at the (*k+1*)-th iteration. Additionally,

$$\mathbf{G}(\mathbf{x}^k) = \frac{\partial \boldsymbol{g}(\mathbf{x}^k)}{\partial \mathbf{x}} = \mathbf{H}^T(\mathbf{x}^k)\,\mathbf{R}^{-1}\mathbf{H}(\mathbf{x}^k) \tag{10.6}$$

$$\boldsymbol{g}(\mathbf{x}^k) = -\mathbf{H}^T(\mathbf{x}^k)\,\mathbf{R}^{-1}[\mathbf{z} - \mathbf{h}(\mathbf{x}^k)] \tag{10.7}$$

with $\mathbf{G}(\mathbf{x}^k)$ called the Gain matrix. Therefore, the solution for $\mathbf{x}^{k+1}$ is:

$$\mathbf{x}^{k+1} = \mathbf{x}^k + [\mathbf{G}(\mathbf{x}^k)]^{-\mathbf{1}}\mathbf{H}^T(\mathbf{x}^k)\,\mathbf{R}^{-1}[\mathbf{z} - \mathbf{h}(\mathbf{x}^k)] \tag{10.8}$$

However, the Gain matrix is typically not inverted, but decomposed into its triangular factors, and the following linear set of equations are solved using forward/backward substitutions at each iteration *k*:

$$\mathbf{G}(\mathbf{x}^k)\Delta\mathbf{x}^k = \mathbf{H}^T(\mathbf{x}^k)\,\mathbf{R}^{-1}[\mathbf{z} - \mathbf{h}(\mathbf{x}^k)] \tag{10.9}$$

with $\Delta\mathbf{x}^k = \mathbf{x}^{k+1} - \mathbf{x}^k$.

10.1.2 A.2: Solution of constraint WLS Formulation

Lagrange theory is now used to include the set of equality constraints $\mathbf{c}(\mathbf{x})$ in the WLS formulation. The new minimization problem becomes:

$$L(\mathbf{x}, \boldsymbol{\lambda}_c) = [\mathbf{z} - \mathbf{h}(\mathbf{x})]^T\mathbf{R}^{-1}[\mathbf{z} - \mathbf{h}(\mathbf{x})] - \boldsymbol{\lambda}_{\mathbf{c}}^T\mathbf{c}(\mathbf{x}), \tag{10.10}$$

where $\boldsymbol{\lambda}_c$ is the vector of Lagrange multipliers. In order to find the minimum of *L*, the first order optimality conditions are derived:

$$\frac{\partial L(\hat{\mathbf{x}}, \boldsymbol{\lambda}_c)}{\partial \mathbf{x}} = 0 \tag{10.11}$$

$$\frac{\partial L(\hat{\mathbf{x}}, \boldsymbol{\lambda}_c)}{\partial \boldsymbol{\lambda}_c} = 0 \tag{10.12}$$

From which, it is obtained:

$$\frac{\partial L(\hat{\mathbf{x}}, \boldsymbol{\lambda}_c)}{\partial \mathbf{x}} = -\mathbf{H}^T(\hat{\mathbf{x}})\,\mathbf{R}^{-1}\mathbf{r}(\hat{\mathbf{x}}) - \mathbf{C}^T(\hat{\mathbf{x}})\mathbf{c}(\hat{\mathbf{x}}) = \mathbf{0} \tag{10.13}$$

$$\frac{\partial L(\hat{\mathbf{x}}, \boldsymbol{\lambda}_{\mathrm{c}})}{\partial \boldsymbol{\lambda}_{\mathrm{c}}} = -\mathbf{c}(\hat{\mathbf{x}}) = \mathbf{0} \tag{10.14}$$

where $\mathbf{r}(\hat{\mathbf{x}}) = \mathbf{z} - \mathbf{h}(\hat{\mathbf{x}})$ is the measurement residual vector and $\mathbf{C}(\hat{\mathbf{x}}) = \partial \mathbf{c}(\hat{\mathbf{x}})/\partial \mathbf{x}$.

The Gauss Newton method is used again to solve the set of non-linear equations iteratively. The truncated Taylor series expansion of $\mathbf{r}(\hat{\mathbf{x}})$ and $\mathbf{c}(\hat{\mathbf{x}})$ around the initial guess $\mathbf{x}^k$ is:

$$\mathbf{r}(\hat{\mathbf{x}}) \approx \mathbf{r}(\mathbf{x}^k) - \mathbf{H}(\mathbf{x}^k)\Delta\mathbf{x}^k \tag{10.15}$$
$$\mathbf{c}(\hat{\mathbf{x}}) \approx \mathbf{c}(\mathbf{x}^k) - \mathbf{C}(\mathbf{x}^k)\Delta\mathbf{x}^k \tag{10.16}$$

From these linear approximations, (10.13) and (10.14) are rewritten as the iterative expression:

$$\begin{bmatrix} \mathbf{H}^T(\mathbf{x}^k)\, \mathbf{R}^{-1}\mathbf{H} & -\mathbf{C}^T(\mathbf{x}^k) \\ -\mathbf{C}(\mathbf{x}^k) & \mathbf{0} \end{bmatrix} \begin{bmatrix} \Delta\mathbf{x}^k \\ \boldsymbol{\lambda}_{\mathrm{c}}^{k+1} \end{bmatrix} = \begin{bmatrix} \mathbf{H}^T(\mathbf{x}^k)\, \mathbf{R}^{-1}[\mathbf{z} - \mathbf{h}(\mathbf{x}^k)] \\ \mathbf{c}(\mathbf{x}^k) \end{bmatrix} \tag{10.17}$$

where $\Delta\mathbf{x}^k = \mathbf{x}^{k+1} - \mathbf{x}^k$, and $\hat{\mathbf{x}}$ has been replaced by $\mathbf{x}^{k+1}$.

10.2 Appendix B

10.2.1 B.1: LU Decomposition

A $m \times n$ matrix $\tilde{\mathbf{A}}$ whose rank is n can be decomposed into $\tilde{\mathbf{A}} = \mathbf{LU}$ where $\mathbf{L}$ is a lower-triangular and $\mathbf{U}$ is upper triangular. The decomposition starts with the original $\tilde{\mathbf{A}}$ matrix:

$$\tilde{\mathbf{A}} = \begin{bmatrix} a_{11} & a_{12} & a_{13} & \cdots & a_{1n} \\ a_{21} & a_{22} & a_{23} & \cdots & \vdots \\ a_{31} & a_{32} & a_{33} & \cdots & \vdots \\ \vdots & \ddots & \vdots & \ddots & \vdots \\ a_{n1} & a_{n2} & a_{n3} & \cdots & a_{nn} \\ \vdots & \vdots & \vdots & \ddots & \vdots \\ a_{m1} & a_{m2} & a_{m3} & \cdots & a_{mn} \end{bmatrix}. \tag{10.18}$$

Here, n steps are needed to complete the decomposition. Before the $s = 3rd$ step, the matrix $\tilde{\mathbf{A}}_{s=2}$ is obtained:

$$\tilde{\mathbf{A}}_{s=2} = \begin{bmatrix} u_{11} & u_{12} & u_{13} & \cdots & u_{1n} \\ l_{21} & u_{22} & u_{23} & \cdots & \vdots \\ l_{31} & l_{32} & a_{33} & \cdots & \vdots \\ \vdots & \ddots & \vdots & \ddots & \vdots \\ l_{n1} & l_{n2} & a_{n3} & \cdots & a_{nn} \\ \vdots & \vdots & \vdots & \ddots & \vdots \\ l_{m1} & l_{m2} & a_{m3} & \cdots & a_{mn} \end{bmatrix}. \tag{10.19}$$

At the s-th step,

a) If a_{ss} is zero, find the first non-zero element a_{ps} ($p > s$) in the s-th column and exchange the s-th and p-th rows.
b) Compute $l_{is} = a_{is}/a_{ss}$ with $i > s$ and store it in position $\tilde{\mathbf{A}}\,(i,s)$.
c) For each element j in row s (for $j = s+1,\dots, n$), obtain a new a_{ij} given by a_{ij}-$l_{is}a_{sj}$ and overwrite it on the old a_{ij}. Make $u_{ij} = a_{ij}$.
d) Advance, $s = s+1$. If $s = n$ stop. Else, go back to a).

After the n steps, obtain the $\mathbf{U}$ and $\mathbf{L}$ factors from $\tilde{\mathbf{A}}$:

$$U=\begin{bmatrix} u_{11} & u_{12} & u_{13} & \cdots & u_{1n} \\ 0 & u_{22} & u_{23} & \cdots & u_{2n} \\ 0 & 0 & u_{33} & \cdots & u_{3n} \\ \vdots & \vdots & \vdots & \ddots & \vdots \\ 0 & 0 & 0 & \cdots & u_{nn} \end{bmatrix}, \quad L=\begin{bmatrix} 1 & 0 & 0 & \cdots & 0 \\ l_{21} & 1 & 0 & \cdots & \vdots \\ l_{31} & l_{32} & 1 & \cdots & 0 \\ \vdots & \ddots & \vdots & \ddots & \vdots \\ l_{n1} & l_{n2} & l_{n3} & \cdots & 1 \\ \vdots & \vdots & \vdots & \ddots & \vdots \\ l_{m1} & l_{m2} & l_{m3} & \cdots & l_{mn} \end{bmatrix}. \tag{10.20}$$

10.3 Appendix C

10.3.1 C.1: Solution of sub-vector $h_j(\cdot)$

The closed form solution of sub-vector $\mathbf{h}_j(\cdot)$ is as follows:

$$\mathbf{h}_j(\bar{\eta}) = \begin{bmatrix} \frac{2}{\tilde{\omega}_j} & 0 & 0 \\ \frac{-\tilde{\mu}_j}{\tilde{\sigma}_j^2} & \frac{1}{\tilde{\sigma}_j^2} & 0 \\ \frac{\tilde{\mu}_j^2 - \tilde{\sigma}_j^2}{\tilde{\sigma}_j^3} & \frac{-2\tilde{\mu}_j}{\tilde{\sigma}_j^3} & \frac{1}{\tilde{\sigma}_j^3} \end{bmatrix} \begin{bmatrix} E_{F_j}(y^0) - E_{G_j}(y^0) \\ E_{F_j}(y) - E_{G_j}(y) \\ E_{F_j}(y^2) - E_{G_j}(y^2) \end{bmatrix} \tag{10.21}$$

E is the expectation operator for $F_j = f_Y(y)\cdot g_j(y,\bar{\eta}_j)$ and $G_j = g_Y(y,\bar{\eta}_j)\cdot g_j(y,\bar{\eta}_j)$. The vector in (10.21) contains the zero-th, first and second non-central moments of F_j and G_j. Function F_j is expressed in terms of a sum of scaled Gaussian distributions.

$$F_j = \tilde{\omega}_j^2 \sum_{i=1}^{L} \omega_i \alpha_{ij} f_{N(\mu_{ij},\sigma_{ij}^2)}(y) \tag{10.22}$$

with,

$$\alpha_{ij} = f_{N(\tilde{\mu}_j,\sigma_i^2+\tilde{\sigma}_j^2)}(\mu_i) \tag{10.23}$$

$$\sigma_{ij}^2 = (1/\sigma_i^2 + 1/\tilde{\sigma}_j^2)^{-1} \tag{10.24}$$

$$\mu_{ij} = \sigma_{ij}^2(\mu_i/\sigma_i^2 + \tilde{\mu}_j/\tilde{\sigma}_j^2) \tag{10.25}$$

Therefore, the non-central moments of F_j are simply:

$$E_{F_j}\left(y^0\right) = \tilde{\omega}_j^2 \sum_{i=1}^{L} \omega_i \alpha_{ij} \tag{10.26}$$

$$E_{F_j}\left(y\right) = \tilde{\omega}_j^2 \sum_{i=1}^{L} \omega_i \alpha_{ij} \mu_{ij} \tag{10.27}$$

$$E_{F_j}\left(y^2\right) = \tilde{\omega}_j^2 \sum_{i=1}^{L} \omega_i \alpha_{ij} (\mu_{ij}^2 + \sigma_{ij}^2) \tag{10.28}$$

In terms of G_j, it is also expressed as scaled sum of Gaussian distributions:

$$G_j = \tilde{\omega}_j^2 \sum_{i=1}^{M} \tilde{\omega}_i^2 \tilde{\alpha}_{ij} f_{N(\tilde{\mu}_{ij},\tilde{\sigma}_{ij}^2)}(y) \tag{10.29}$$

with,

$$\tilde{\alpha}_{ij} = f_{N(\tilde{\mu}_j, \tilde{\sigma}_i^2 + \tilde{\sigma}_j^2)}(\tilde{\mu}_i) \tag{10.30}$$

$$\tilde{\sigma}_{ij}^2 = (1/\tilde{\sigma}_i^2 + 1/\tilde{\sigma}_j^2)^{-1} \tag{10.31}$$

$$\tilde{\mu}_{ij} = \tilde{\sigma}_{ij}^2 (\tilde{\mu}_i/\tilde{\sigma}_i^2 + \tilde{\mu}_j/\tilde{\sigma}_j^2) \tag{10.32}$$

Therefore, the non-central moments of G_j are:

$$E_{G_j}\left(y^0\right) = \tilde{\omega}_j^2 \sum_{i=1}^{M} \tilde{\omega}_i^2 \tilde{\alpha}_{ij} \tag{10.33}$$

$$E_{G_j}\left(y\right) = \tilde{\omega}_j^2 \sum_{i=1}^{M} \tilde{\omega}_i^2 \tilde{\alpha}_{ij} \tilde{\mu}_{ij} \tag{10.34}$$

$$E_{G_j}\left(y^2\right) = \tilde{\omega}_j^2 \sum_{i=1}^{M} \tilde{\omega}_i^2 \tilde{\alpha}_{ij} (\tilde{\mu}_{ij}^2 + \tilde{\sigma}_{ij}^2) \tag{10.35}$$

10.3.2 C.2: Solution of matrix $P(\cdot)$

Each of the elements in the 3×3 matrix $\mathbf{P}^{(i,j)}$ in (3.40) is as follows:

$$\begin{aligned} \mathbf{P}_{1,1}^{(i,j)} &= 4, \\ \mathbf{P}_{1,2}^{(i,j)} &= 2\tilde{\omega}_j \frac{\tilde{\mu}_i - \tilde{\mu}_j}{\tilde{\sigma}_i^2 + \tilde{\sigma}_j^2}, \\ \mathbf{P}_{1,3}^{(i,j)} &= 2\tilde{\omega}_j \tilde{\sigma}^2 \frac{(\tilde{\mu}_i - \tilde{\mu}_j)^2 - (\tilde{\sigma}_i^2 + \tilde{\sigma}_j^2)}{(\tilde{\sigma}_i^2 + \tilde{\sigma}_j^2)^2}, \end{aligned} \tag{10.36}$$

$$\begin{aligned} \mathbf{P}_{2,1}^{(i,j)} &= 2\tilde{\omega}_i \frac{\tilde{\mu}_j - \tilde{\mu}_i}{\tilde{\sigma}_i^2 + \tilde{\sigma}_j^2}, \\ \mathbf{P}_{2,2}^{(i,j)} &= \tilde{\omega}_i \tilde{\omega}_j \frac{(\tilde{\sigma}_i^2 + \tilde{\sigma}_j^2) - (\tilde{\mu}_i - \tilde{\mu}_j)^2}{(\tilde{\sigma}_i^2 + \tilde{\sigma}_j^2)^2}, \\ \mathbf{P}_{2,3}^{(i,j)} &= \tilde{\omega}_i \tilde{\omega}_j \tilde{\sigma}_j \frac{(\tilde{\mu}_j - \tilde{\mu}_i) \cdot \left((\tilde{\mu}_i - \tilde{\mu}_j)^2 - 3(\tilde{\sigma}_i^2 + \tilde{\sigma}_j^2) \right)}{(\tilde{\sigma}_i^2 + \tilde{\sigma}_j^2)^3}, \end{aligned} \tag{10.37}$$

$$\begin{aligned} \mathbf{P}_{3,1}^{(i,j)} &= 2\tilde{\omega}_i \tilde{\sigma}_i \frac{(\tilde{\mu}_i - \tilde{\mu}_j)^2 - (\tilde{\sigma}_i^2 + \tilde{\sigma}_j^2)}{(\tilde{\sigma}_i^2 + \tilde{\sigma}_j^2)^2}, \\ \mathbf{P}_{3,2}^{(i,j)} &= \tilde{\omega}_i \tilde{\omega}_j \tilde{\sigma}_i \frac{(\tilde{\mu}_i - \tilde{\mu}_j) \cdot \left((\tilde{\mu}_i - \tilde{\mu}_j)^2 - 3(\tilde{\sigma}_i^2 + \tilde{\sigma}_j^2) \right)}{(\tilde{\sigma}_i^2 + \tilde{\sigma}_j^2)^3}, \\ \mathbf{P}_{3,3}^{(i,j)} &= \tilde{\omega}_i \tilde{\omega}_j \tilde{\sigma}_i \tilde{\sigma}_j \frac{(\tilde{\mu}_i - \tilde{\mu}_j)^4 + 3(\tilde{\sigma}_i^2 + \tilde{\sigma}_j^2)\left((\tilde{\sigma}_i^2 + \tilde{\sigma}_j^2) - 2(\tilde{\mu}_i - \tilde{\mu}_j)^2 \right)}{(\tilde{\sigma}_i^2 + \tilde{\sigma}_j^2)^4} \end{aligned} \tag{10.38}$$

10.4 Appendix D

10.4.1 D.1: Power Flow Calculation in Radial Networks

Te power flow problem is solved when the current injection vector **I** and the voltage vector **V** satisfy:

$$S_i = \overline{V}_i \cdot \overline{I}_i^*, \quad i = 1, \ldots, N, \tag{10.39}$$

$$\overline{\mathbf{I}} = \mathbf{Y}_{bus}\overline{\mathbf{V}}, \tag{10.40}$$

where $\mathbf{Y}_{bus}$ is the nodal admittance matrix and N is the number of buses. The iterative algorithm is as follows:

1. Factorize the nodal admittance matrix into its lower **L** and Upper **U** matrix components:

$$\mathbf{Y}_{bus} = \mathbf{LU}. \tag{10.41}$$

2. Set initial estimates of voltages and compute the initial currents from (10.40).
3. Advance the iteration counter, k.
4. Compute the voltage dependent injected powers:

$$S_i^{sched} = P_i^{sched} + jQ_i^{sched}, \tag{10.42}$$

with

$$P_i^{sched} = P_i^0(\alpha_Z V_i^{k_{PZ}} + \alpha_I V_i^{k_{PI}} + \alpha_P V_i^{k_{PP}}), \tag{10.43}$$

$$Q_i^{sched} = Q_i^0(\beta_Z V_i^{k_{QZ}} + \beta_I V_i^{k_{QI}} + \beta_P V_i^{k_{QP}}). \tag{10.44}$$

The elements P_i^0 and Q_i^0 are the nominal load powers (i.e. the loading conditions at nominal voltage). The exponents can be defined accordingly to characteristic values $k_{PZ} = k_{QZ} = 2$, $k_{PI} = k_{QI} = 1$ and $k_{PP} = k_{QP} = 0$. The coefficients α and β indicate the proportion of the respective load type (*Z-constant impedance, I-constant current or P-constant power*) with respect to the total power consumption at bus i.

5. Compute the injected complex power for iteration (k)

$$S_i^{(k)} = \overline{V}_i^{(k-1)} \cdot \left(\overline{I}_i^{(k-1)}\right)^*, \quad i = 1, \ldots N \tag{10.45}$$

6. Compute the complex power mismatches using :

$$\Delta S_i^{(k)} = S_i^{(k)} - S_i^{sched}, \quad i = 1, \ldots N \tag{10.46}$$

7. Check if solution is converged within tolerances:

$$\left|\Delta P_i^{(k)}\right| \le \varepsilon_P, \quad \left|\Delta Q_i^{(k)}\right| \le \varepsilon_Q \tag{10.47}$$

8. If convergence is achieved stop here, otherwise:

9. Compute the complex incremental current injection vector:

$$\Delta \overline{I}_i^{(k)} = \frac{\Delta S_i^{(k)}}{\overline{V}_i^{(k-1)}}, \quad i = 1, \ldots N \tag{10.48}$$

10. Compute the total current vector to be used in the next iteration:

$$\overline{\mathbf{I}}^{(k)} = \overline{\mathbf{I}}^{(k-1)} + \Delta \overline{\mathbf{I}}^{(k)} \tag{10.49}$$

11. Solve for the complex incremental voltage vector (forward/backward substitution):

$$\Delta \overline{\mathbf{V}}^{(k)} = \mathbf{U}^{-1} \mathbf{L}^{-1} \Delta \overline{\mathbf{I}}^{(k)} \tag{10.50}$$

12. Update the complex voltage vector:

$$\overline{\mathbf{V}}^{(k)} = \overline{\mathbf{V}}^{(k-1)} + \Delta \overline{\mathbf{V}}^{(k)} \tag{10.51}$$

13. Go to step 3.

10.5 Appendix E

10.5.1 E.1: The Kalman Filter

Suppose the linear system:

$$\mathbf{x}_k = \mathbf{F}\mathbf{x}_{k-1} + \mathbf{B}\mathbf{u}_{k-1} + \mathbf{q}_{k-1} \tag{10.52}$$
$$\mathbf{z}_k = \mathbf{H}\mathbf{x}_k + \mathbf{e}_k \tag{10.53}$$

where $\mathbf{x}$ is the vector of states, $\mathbf{u}_{k-1}$ is the set of input variables and $\mathbf{z}_k$ is the set of measurements. Matrix **F** and **B** relate the previous state and system inputs with the new state $\mathbf{x}_k$ and matrix **H** relates the measurements with the state variables. The first equation is the transition of states model (prediction) whereas the second is the measurement model (correction).

Vectors $\mathbf{e}_k$ and $\mathbf{q}_{k-1}$ represent the measurement and system error, respectively. These errors are assumed to have zero mean and they are uncorrelated. The covariance matrix of $\mathbf{q}_{k-1}$ is defined by:

$$\mathbf{Q}_{k-1} = E[\mathbf{q}_{k-1}\mathbf{q}_{k-1}^T]. \tag{10.54}$$

The problem consists of estimating the state vector $\mathbf{x}$, given the prediction (10.52) and the correction (10.53) at instant *k*. The set of measurements is built up by the real-time measurements and the state predictions:

$$\tilde{\mathbf{z}}_k = \begin{bmatrix} \mathbf{z}_k \\ \bar{\mathbf{x}}_k \end{bmatrix} = \begin{bmatrix} \mathbf{z}_k \\ \mathbf{F}\hat{\mathbf{x}}_{k-1} + \mathbf{B}\mathbf{u}_{k-1} \end{bmatrix} \tag{10.55}$$

Where $\bar{\mathbf{x}}_k$ denotes the predicted state at time *k* according to the transition of states presented in (10.52). The error of the augmented measurement vector $\tilde{\mathbf{z}}_k$ is defined as:

$$\tilde{\mathbf{e}}_k = \begin{bmatrix} \mathbf{e}_k \\ \boldsymbol{\varepsilon}_k \end{bmatrix} = \begin{bmatrix} \mathbf{z}_k - \mathbf{H}\mathbf{x}_k \\ \bar{\mathbf{x}}_k - \mathbf{x}_k \end{bmatrix}. \tag{10.56}$$

while the prediction error has the following covariance matrix:

$$\mathbf{P}_{\bar{x}k} = \mathbf{F}\mathbf{P}_{\hat{x}k-1}\mathbf{F}^T + \mathbf{Q}_{k-1}. \tag{10.57}$$

Thus, the covariance matrix of the augmented measurement vector is:

$$\mathbf{R}_{\tilde{z}k} = \begin{bmatrix} \mathbf{R}_{zk} & 0 \\ 0 & \mathbf{P}_{\bar{x}k} \end{bmatrix} \tag{10.58}$$

where $\boldsymbol{R}_{zk}$ is the error covariance matrix of the real-time measurements, i.e. $\boldsymbol{R}_{zk} = E[\mathbf{e}_k\mathbf{e}_k^T]$. In addition, the augmented Jacobian matrix is defined as:

$$\tilde{\mathbf{H}}_k = \begin{bmatrix} \mathbf{H}_k \\ \mathbf{I} \end{bmatrix}. \tag{10.59}$$

Now, in order to estimate the value of $\mathbf{x}$ at time k, it is necessary to minimise the augmented objective function:

$$J(\mathbf{x}_k) = \frac{1}{2}\left[\mathbf{z}_k - \mathbf{H}_k\mathbf{x}_k\right]^T \mathbf{R}_{zk}^{-1}\left[\mathbf{z}_k - \mathbf{H}_k\mathbf{x}_k\right] + \frac{1}{2}\left[\bar{\mathbf{x}}_k - \mathbf{x}_k\right]^T \mathbf{P}_{\bar{x}k}^{-1}\left[\bar{\mathbf{x}}_k - \mathbf{x}_k\right]. \tag{10.60}$$

Note that this objective function has the same structure as a linear WLS problem. Hence, the WLS solution of (10.60) is:

$$\hat{\mathbf{x}}_k = [\tilde{\mathbf{H}}_k^T\mathbf{R}_{\tilde{z}k}^{-1}\tilde{\mathbf{H}}_k]^{-1}\tilde{\mathbf{H}}_k^T\mathbf{R}_{\tilde{z}k}^{-1}\tilde{\mathbf{z}}_k, \tag{10.61}$$

In view of (10.55)-(10.59), this equation can be rewritten as:

$$\hat{\mathbf{x}}_k = \left[(\mathbf{H}_k^T \quad \mathbf{I})\begin{pmatrix} \mathbf{R}_{zk}^{-1} & 0 \\ 0 & \mathbf{P}_{\bar{x}k}^{-1} \end{pmatrix}\begin{pmatrix} \mathbf{H}_k \\ \mathbf{I} \end{pmatrix}\right]^{-1} (\mathbf{H}_k^T \quad \mathbf{I})\begin{pmatrix} \mathbf{R}_{zk}^{-1} & 0 \\ 0 & \mathbf{P}_{\bar{x}k}^{-1} \end{pmatrix}\begin{pmatrix} \mathbf{z}_k \\ \bar{\mathbf{x}}_k \end{pmatrix}. \tag{10.62}$$

From (10.62), the state vector is also expressed by:

$$\hat{\mathbf{x}}_k = \left(\mathbf{P}_{\bar{x}k}^{-1} + \mathbf{H}_k^T\mathbf{R}_{zk}^{-1}\mathbf{H}_k\right)^{-1}\left(\mathbf{H}_k^T\mathbf{R}_{zk}^{-1}\mathbf{z}_k + \mathbf{P}_{\bar{x}k}^{-1}\bar{\mathbf{x}}_k\right). \tag{10.63}$$

This expression can be simplified even more. From the matrix inversion lemma, it is possible to demonstrate that [45]:

$$\left(\mathbf{P}_{\bar{x}k}^{-1} + \mathbf{H}_k^T\mathbf{R}_{zk}^{-1}\mathbf{H}_k\right)^{-1} = \mathbf{P}_{\bar{x}k} - \mathbf{P}_{\bar{x}k}\mathbf{H}_k^T\left(\mathbf{R}_{zk} + \mathbf{H}_k\mathbf{P}_{\bar{x}k}\mathbf{H}_k^T\right)^{-1}\mathbf{H}_k\mathbf{P}_{\bar{x}k}, \tag{10.64}$$

Hence, equation (10.63) is equivalent to:

$$\hat{\mathbf{x}}_k = \bar{\mathbf{x}}_k + \left(\mathbf{P}_{\bar{x}k}\mathbf{H}_k^T\mathbf{R}_{zk}^{-1} - \mathbf{P}_{\bar{x}k}\mathbf{H}_k^T(\mathbf{R}_{zk} + \mathbf{H}_k\mathbf{P}_{\bar{x}k}\mathbf{H}_k^T)^{-1}\mathbf{H}_k\mathbf{P}_{\bar{x}k}\mathbf{H}_k^T\mathbf{R}_{zk}^{-1}\right)^{-1}\mathbf{z}_k$$
$$-\mathbf{P}_{\bar{x}k}\mathbf{H}_k^T\left(\mathbf{R}_{zk} + \mathbf{H}_k\mathbf{P}_{\bar{x}k}\mathbf{H}_k^T\right)^{-1}\mathbf{H}_k\bar{\mathbf{x}}_k \tag{10.65}$$

The coefficient of $\mathbf{z}_k$ in the expression above can be rewritten as follows [45]:

$$\left(\mathbf{P}_{\bar{x}k}\mathbf{H}_k^T\mathbf{R}_{zk}^{-1} - \mathbf{P}_{\bar{x}k}\mathbf{H}_k^T(\mathbf{R}_{zk} + \mathbf{H}_k\mathbf{P}_{\bar{x}k}\mathbf{H}_k^T)^{-1}\mathbf{H}_k\mathbf{P}_{\bar{x}k}\mathbf{H}_k^T\mathbf{R}_{zk}^{-1}\right)^{-1} = \mathbf{P}_{\bar{x}k}\mathbf{H}_k^T\left(\mathbf{R}_{zk} + \mathbf{H}_k\mathbf{P}_{\bar{x}k}\mathbf{H}_k^T\right)^{-1} \tag{10.66}$$

This resulting matrix is known as the filter's Gain matrix $\mathbf{K}_k$:

$$\mathbf{K}_k = \mathbf{P}_{\bar{x}k}\mathbf{H}_k^T(\mathbf{R}_{zk} + \mathbf{H}_k\mathbf{P}_{\bar{x}k}\mathbf{H}_k^T)^{-1} \tag{10.67}$$

By including (10.67) in (10.65), one obtains:

$$\hat{\mathbf{x}}_k = \bar{\mathbf{x}}_k + \mathbf{K}_k(\mathbf{z}_k - \mathbf{H}_k\bar{\mathbf{x}}_k) \tag{10.68}$$

This is the updated state estimate at *k*, note that it is made of the predicted state and the correction from set of measurements $\mathbf{z}_k$.

Based on the classical WLS formulation, the covariance matrix of the updated state estimate is the inverse of the Gain matrix for the augmented system:

$$\mathbf{P}_{\hat{x}k} = \mathbf{G}_k^{-1} = \left(\tilde{\mathbf{H}}_k^T\mathbf{R}_{\tilde{z}k}^{-1}\tilde{\mathbf{H}}_k\right)^{-1} = \left(\mathbf{P}_{\bar{x}k}^{-1} + \mathbf{H}_k^T\mathbf{R}_{zk}^{-1}\mathbf{H}_k\right)^{-1} \tag{10.69}$$

which is equivalent to (matrix inversion lemma) [45]:

$$\mathbf{P}_{\hat{x}k} = (\mathbf{I} - \mathbf{K}_k\mathbf{H}_k)\mathbf{P}_{\bar{x}k} \tag{10.70}$$

10.6 Appendix F

10.6.1 F.1: Holt's Initialization

The initialization of the Holt's technique (introduced in Chapter 7) was carried out by using the first two samples (at $k = 0$ and $k = 1$) of voltage magnitudes and angles taken from the previous estimations. Based on this, $\mathbf{x}_0$ and $\mathbf{x}_1$ are known.

In order to initialize the Holts method, equations (7.44) and (7.45) are used:

$$\mathbf{a}_k = \alpha_k \hat{\mathbf{x}}_k + (1-\alpha_k)\overline{\mathbf{x}}_k \tag{10.71}$$

$$\mathbf{b}_k = \beta_k(\mathbf{a}_k - \mathbf{a}_{k\text{-}1}) + (1-\beta_k)\mathbf{b}_{k\text{-}1} \tag{10.72}$$

As it is desired to estimate the state vector $\mathbf{x}$ at $k = 2$, it is necessary to calculate a_k and b_k for $k = 0$ and $k = 1$. First, set $\mathbf{a}_0 = \mathbf{x}_0$ and $\mathbf{b}_0 = \mathbf{0}$ and assume that the prediction at $k = 1$ was very accurate, i.e. $\overline{\mathbf{x}}_1 = \hat{\mathbf{x}}_1$. Now calculate $\mathbf{a}_1$ and $\mathbf{b}_1$:

$$\mathbf{a}_1 = \alpha\hat{\mathbf{x}}_1 + (1-\alpha)\overline{\mathbf{x}}_1 \tag{10.73}$$

$$\mathbf{b}_1 = \beta(\mathbf{a}_1 - \mathbf{a}_0) + (1-\beta)\mathbf{b}_0 \tag{10.74}$$

Then calculate $\mathbf{F}_1$ and $\mathbf{g}_1$:

$$\mathbf{F}_1 = \alpha(1+\beta)\mathbf{I} \tag{10.75}$$

$$\mathbf{g}_1 = (1+\beta)(1-\alpha)\overline{\mathbf{x}}_1 - \beta\mathbf{a}_0 + (1-\beta)\mathbf{b}_0 \tag{10.76}$$

From the UKF or EKF, obtain the prediction at $k = 2$:

$$\overline{\mathbf{x}}_2 = \mathbf{F}_1\mathbf{x}_1 + \mathbf{g}_1 \tag{10.77}$$

After some steps in the UKF (or EKF), obtain the updated state vector $\hat{\mathbf{x}}_2$.

When the new set of measurements is received at $k = 3$, one has to calculate $\mathbf{a}_k$ and $\mathbf{b}_k$ for $k = 2$:

$$\mathbf{a}_2 = \alpha\hat{\mathbf{x}}_2 + (1-\alpha)\overline{\mathbf{x}}_2 \tag{10.78}$$

$$\mathbf{b}_2 = \beta(\mathbf{a}_2 - \mathbf{a}_1) + (1-\beta)\mathbf{b}_1 \tag{10.79}$$

Note that for $k = 2, 3, \ldots, k_{\max}$, the prediction vector $\overline{\mathbf{x}}_k$ is calculated from the UKF (or EKF).

10.7 Appendix G

10.7.1 G.1: 14-bus IEEE Test System Data

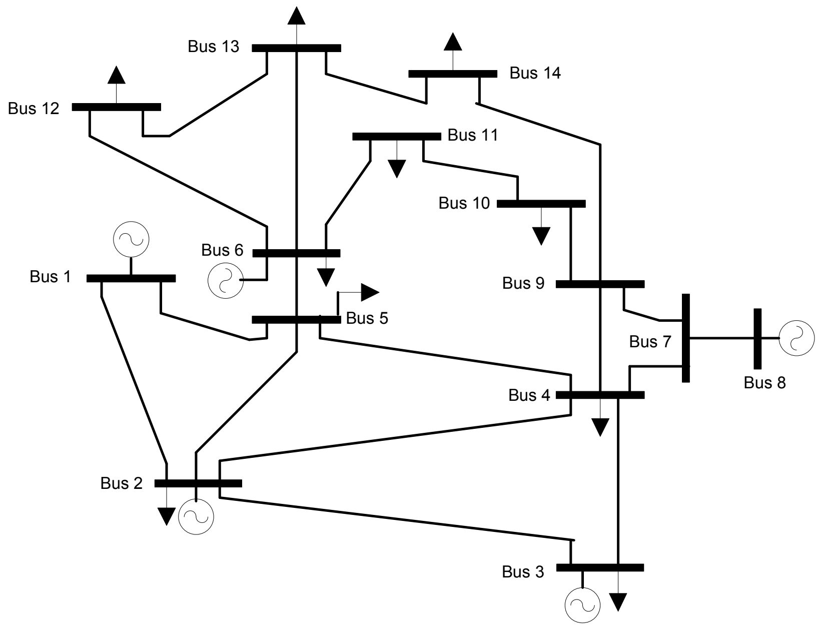

Figure 10.1: One Line Diagram 14-bus System

Table 10.1: 14-bus System: Buses Data

Bus	Voltage		Generation		Demand		Shunt Elements	
#	Mag(pu)	Ang(deg)	P (MW)	Q (MVAr)	P (MW)	Q (MVAr)	Gs (MW)	Bs (MVAr.)
1	1.060	0.000	232.39	-16.55	-	-	-	-
2	1.045	-4.983	40.00	43.56	21.70	12.70	-	-
3	1.010	-12.725	0.00	25.08	94.20	19.00	-	-
4	1.018	-10.313	-	-	47.80	-3.90	-	-
5	1.020	-8.774	-	-	7.60	1.60	-	-
6	1.070	-14.221	0.00	12.73	11.20	7.50	-	-
7	1.062	-13.360	-	-	-	-	-	-
8	1.090	-13.360	0.00	17.62	-	-	-	-
9	1.056	-14.939	-	-	29.50	16.60	-	-
10	1.051	-15.097	-	-	9.00	5.80	-	-
11	1.057	-14.791	-	-	3.50	1.80	-	-
12	1.055	-15.076	-	-	6.10	1.60	-	-
13	1.050	-15.156	-	-	13.50	5.80	-	-
14	1.036	-16.034	-	-	14.90	5.00	-	-

Table 10.2: 14-bus System: Branch Data

From Bus	To Bus	R p.u.	X p.u.	B p.u.	Tap p.u.
1	2	0.01938	0.05917	0.05280	1.0000
1	5	0.05403	0.22304	0.04920	1.0000
2	3	0.04699	0.19797	0.04380	1.0000
2	4	0.05811	0.17632	0.03400	1.0000
2	5	0.05695	0.17388	0.03460	1.0000
3	4	0.06701	0.17103	0.01280	1.0000
4	5	0.01335	0.04211	0.00000	1.0000
4	7	0.00000	0.20912	0.00000	0.9780
4	9	0.00000	0.55618	0.00000	0.9690
5	6	0.00000	0.25202	0.00000	0.9320
6	11	0.09498	0.19890	0.00000	1.0000
6	12	0.12291	0.25581	0.00000	1.0000
6	13	0.06615	0.13027	0.00000	1.0000
7	8	0.00000	0.17615	0.00000	1.0000
7	9	0.00000	0.11001	0.00000	1.0000
9	10	0.03181	0.08450	0.00000	1.0000
9	14	0.12711	0.27038	0.00000	1.0000
10	11	0.08205	0.19207	0.00000	1.0000
12	13	0.22092	0.19988	0.00000	1.0000
13	14	0.17093	0.34802	0.00000	1.0000

10.7.2 G.2: 57-bus IEEE Test System Data

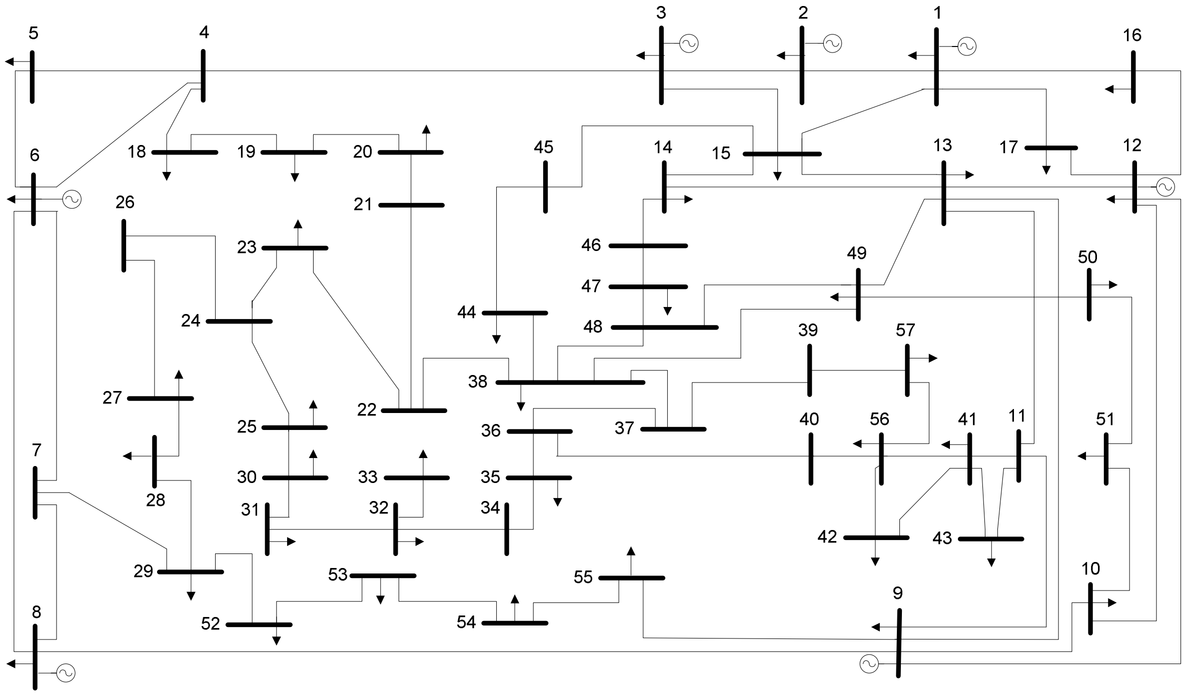

Figure 10.2: One Line Diagram 57-bus System

Table 10.3: 57-bus System: Buses Data

Bus	Voltage		Generation		Demand		Shunt Elements	
#	Mag(pu)	Ang(deg)	P (MW)	Q (MVAr)	P (MW)	Q (MVAr)	Gs (MW)	Bs (MVAr)
1	1.040	0.000	478.66	128.85	55.00	17.00	-	-
2	1.010	-1.188	0.00	-0.75	3.00	88.00	-	-
3	0.985	-5.988	40.00	-0.90	41.00	21.00	-	-
4	0.981	-7.337	-	-	-	-	-	-
5	0.976	-8.546	-	-	13.00	4.00	-	-
6	0.980	-8.674	0.00	0.87	75.00	2.00	-	-
7	0.984	-7.601	-	-	-	-	-	-
8	1.005	-4.478	450.00	62.10	150.00	22.00	-	-
9	0.980	-9.585	0.00	2.29	121.00	26.00	-	-
10	0.986	-11.450	-	-	5.00	2.00	-	-
11	0.974	-10.193	-	-	-	-	-	-
12	1.015	-10.471	310.00	128.63	377.00	24.00	-	-
13	0.979	-9.804	-	-	18.00	2.30	-	-
14	0.970	-9.350	-	-	10.50	5.30	-	-
15	0.988	-7.190	-	-	22.00	5.00	-	-
16	1.013	-8.859	-	-	43.00	3.00	-	-
17	1.017	-5.396	-	-	42.00	8.00	-	-
18	1.001	-11.730	-	-	27.20	9.80	-	10.00
19	0.970	-13.227	-	-	3.30	0.60	-	-

20	0.964	-13.444	-	-	2.30	1.00	-	-
21	1.008	-12.929	-	-	-	-	-	-
22	1.010	-12.874	-	-	-	-	-	-
23	1.008	-12.940	-	-	6.30	2.10	-	-
24	0.999	-13.292	-	-	-	-	-	-
25	0.983	-18.173	-	-	6.30	3.20	-	5.90
26	0.959	-12.981	-	-	-	-	-	-
27	0.982	-11.514	-	-	9.30	0.50	-	-
28	0.997	-10.482	-	-	4.60	2.30	-	-
29	1.010	-9.772	-	-	17.00	2.60	-	-
30	0.963	-18.720	-	-	3.60	1.80	-	-
31	0.936	-19.384	-	-	5.80	2.90	-	-
32	0.950	-18.512	-	-	1.60	0.80	-	-
33	0.948	-18.552	-	-	3.80	1.90	-	-
34	0.959	-14.149	-	-	-	-	-	-
35	0.966	-13.906	-	-	6.00	3.00	-	-
36	0.976	-13.635	-	-	-	-	-	-
37	0.985	-13.446	-	-	-	-	-	-
38	1.013	-12.735	-	-	14.00	7.00	-	-
39	0.983	-13.491	-	-	-	-	-	-
40	0.973	-13.658	-	-	-	-	-	-
41	0.996	-14.077	-	-	6.30	3.00	-	-
42	0.967	-15.533	-	-	7.10	4.40	-	-
43	1.010	-11.354	-	-	2.00	1.00	-	-
44	1.017	-11.856	-	-	12.00	1.80	-	-
45	1.036	-9.270	-	-	-	-	-	-
46	1.060	-11.116	-	-	-	-	-	-
47	1.033	-12.512	-	-	29.70	11.60	-	-
48	1.027	-12.611	-	-	-	-	-	-
49	1.036	-12.936	-	-	18.00	8.50	-	-
50	1.023	-13.413	-	-	21.00	10.50	-	-
51	1.052	-12.533	-	-	18.00	5.30	-	-
52	0.980	-11.498	-	-	4.90	2.20	-	-
53	0.971	-12.253	-	-	20.00	10.00	-	6.30
54	0.996	-11.710	-	-	4.10	1.40	-	-
55	1.031	-10.801	-	-	6.80	3.40	-	-
56	0.968	-16.065	-	-	7.60	2.20	-	-
57	0.965	-16.584	-	-	6.70	2.00	-	-

Table 10.4: 57-bus System: Branch Data

From Bus	To Bus	R p.u.	X p.u.	B p.u.	Tap p.u.
1	2	0.00830	0.02800	0.12900	1.0000
2	3	0.02980	0.08500	0.08180	1.0000
3	4	0.01120	0.03660	0.03800	1.0000
4	5	0.06250	0.13200	0.02580	1.0000
4	6	0.04300	0.14800	0.03480	1.0000
6	7	0.02000	0.10200	0.02760	1.0000

6	8	0.03390	0.17300	0.04700	1.0000
8	9	0.00990	0.05050	0.05480	1.0000
9	10	0.03690	0.16790	0.04400	1.0000
9	11	0.02580	0.08480	0.02180	1.0000
9	12	0.06480	0.29500	0.07720	1.0000
9	13	0.04810	0.15800	0.04060	1.0000
13	14	0.01320	0.04340	0.01100	1.0000
13	15	0.02690	0.08690	0.02300	1.0000
1	15	0.01780	0.09100	0.09880	1.0000
1	16	0.04540	0.20600	0.05460	1.0000
1	17	0.02380	0.10800	0.02860	1.0000
3	15	0.01620	0.05300	0.05440	1.0000
4	18	0.00000	0.55500	0.00000	0.9700
4	18	0.00000	0.43000	0.00000	0.9780
5	6	0.03020	0.06410	0.01240	1.0000
7	8	0.01390	0.07120	0.01940	1.0000
10	12	0.02770	0.12620	0.03280	1.0000
11	13	0.02230	0.07320	0.01880	1.0000
12	13	0.01780	0.05800	0.06040	1.0000
12	16	0.01800	0.08130	0.02160	1.0000
12	17	0.03970	0.17900	0.04760	1.0000
14	15	0.01710	0.05470	0.01480	1.0000
18	19	0.46100	0.68500	0.00000	1.0000
19	20	0.28300	0.43400	0.00000	1.0000
21	20	0.00000	0.77670	0.00000	1.0430
21	22	0.07360	0.11700	0.00000	1.0000
22	23	0.00990	0.01520	0.00000	1.0000
23	24	0.16600	0.25600	0.00840	1.0000
24	25	0.00000	1.18200	0.00000	1.0000
24	25	0.00000	1.23000	0.00000	1.0000
24	26	0.00000	0.04730	0.00000	1.0430
26	27	0.16500	0.25400	0.00000	1.0000
27	28	0.06180	0.09540	0.00000	1.0000
28	29	0.04180	0.05870	0.00000	1.0000
7	29	0.00000	0.06480	0.00000	0.9670
25	30	0.13500	0.20200	0.00000	1.0000
30	31	0.32600	0.49700	0.00000	1.0000
31	32	0.50700	0.75500	0.00000	1.0000
32	33	0.03920	0.03600	0.00000	1.0000
34	32	0.00000	0.95300	0.00000	0.9750
34	35	0.05200	0.07800	0.00320	1.0000
35	36	0.04300	0.05370	0.00160	1.0000
36	37	0.02900	0.03660	0.00000	1.0000
37	38	0.06510	0.10090	0.00200	1.0000
37	39	0.02390	0.03790	0.00000	1.0000
36	40	0.03000	0.04660	0.00000	1.0000
22	38	0.01920	0.02950	0.00000	1.0000
11	41	0.00000	0.74900	0.00000	0.9550

41	42	0.20700	0.35200	0.00000	1.0000
41	43	0.00000	0.41200	0.00000	1.0000
38	44	0.02890	0.05850	0.00200	1.0000
15	45	0.00000	0.10420	0.00000	0.9550
14	46	0.00000	0.07350	0.00000	0.9000
46	47	0.02300	0.06800	0.00320	1.0000
47	48	0.01820	0.02330	0.00000	1.0000
48	49	0.08340	0.12900	0.00480	1.0000
49	50	0.08010	0.12800	0.00000	1.0000
50	51	0.13860	0.22000	0.00000	1.0000
10	51	0.00000	0.07120	0.00000	0.9300
13	49	0.00000	0.19100	0.00000	0.8950
29	52	0.14420	0.18700	0.00000	1.0000
52	53	0.07620	0.09840	0.00000	1.0000
53	54	0.18780	0.23200	0.00000	1.0000
54	55	0.17320	0.22650	0.00000	1.0000
11	43	0.00000	0.15300	0.00000	0.9580
44	45	0.06240	0.12420	0.00400	1.0000
40	56	0.00000	1.19500	0.00000	0.9580
56	41	0.55300	0.54900	0.00000	1.0000
56	42	0.21250	0.35400	0.00000	1.0000
39	57	0.00000	1.35500	0.00000	0.9800
57	56	0.17400	0.26000	0.00000	1.0000
38	49	0.11500	0.17700	0.00300	1.0000
38	48	0.03120	0.04820	0.00000	1.0000
9	55	0.00000	0.12050	0.00000	0.9400

10.7.3 G.3: 69-bus IEEE Test System Data

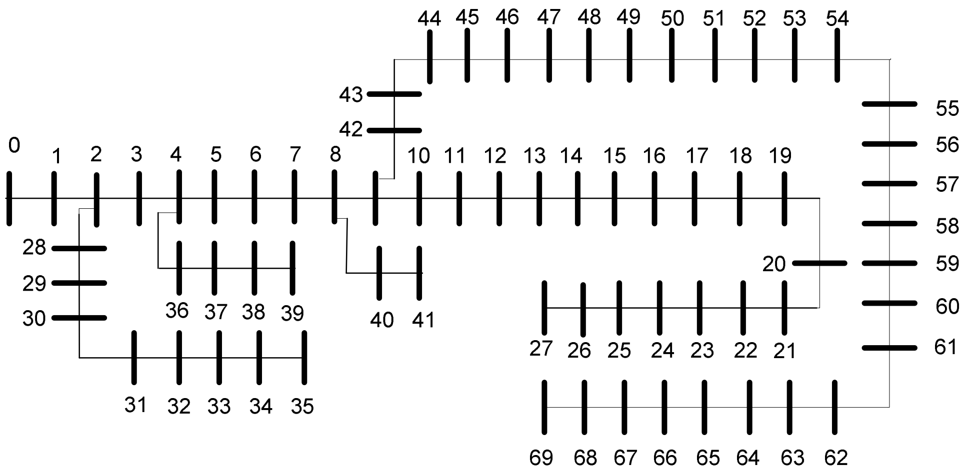

Figure 10.3: One Line Diagram 69-bus System

Table 10.5: 69-bus System: Buses Data

Bus	Voltage		Generation		Demand		Shunt Elements	
#	Mag(pu)	Ang(deg)	P (kW)	Q (kVAr)	P (kW)	Q (kVAr)	Gs (kW)	Bs (kVAr)
1	1.000	-0.001	-	-	-	-	-	-
2	1.000	-0.001	-	-	-	-	-	-
3	1.000	-0.002	-	-	-	-	-	-
4	1.000	-0.004	-	-	-	-	-	-
5	0.999	-0.009	-	-	-	-	-	-
6	0.993	0.083	-	-	2.60	2.20	-	-
7	0.987	0.180	-	-	40.40	30.00	-	-
8	0.986	0.204	-	-	75.00	54.00	-	-
9	0.985	0.214	-	-	30.00	22.00	-	-
10	0.981	0.278	-	-	28.00	19.00	-	-
11	0.980	0.293	-	-	145.00	104.00	-	-
12	0.978	0.333	-	-	145.00	104.00	-	-
13	0.976	0.368	-	-	8.00	5.50	-	-
14	0.973	0.402	-	-	8.00	5.50	-	-
15	0.971	0.437	-	-	-	-	-	-
16	0.971	0.443	-	-	45.50	30.00	-	-
17	0.970	0.454	-	-	60.00	35.00	-	-
18	0.970	0.454	-	-	60.00	35.00	-	-
19	0.970	0.460	-	-	-	-	-	-
20	0.969	0.465	-	-	1.00	0.60	-	-
21	0.969	0.471	-	-	114.00	81.00	-	-
22	0.969	0.471	-	-	5.30	3.50	-	-
23	0.969	0.472	-	-	0.00	0.00	-	-
24	0.969	0.474	-	-	28.00	20.00	-	-
25	0.969	0.477	-	-	0.00	0.00	-	-
26	0.969	0.478	-	-	14.00	10.00	-	-

27	0.969	0.478	-	-	14.00	10.00	-	-
28	1.000	-0.002	-	-	26.00	18.60	-	-
29	1.000	-0.004	-	-	26.00	18.60	-	-
30	1.000	-0.002	-	-	-	-	-	-
31	1.000	-0.002	-	-	-	-	-	-
32	1.000	0.000	-	-	-	-	-	-
33	1.000	0.003	-	-	14.00	10.00	-	-
34	0.999	0.008	-	-	19.50	14.00	-	-
35	0.999	0.008	-	-	6.00	4.00	-	-
36	1.000	-0.006	-	-	-	-	-	-
37	0.999	-0.040	-	-	79.00	56.40	-	-
38	0.996	-0.147	-	-	384.70	274.50	-	-
39	0.995	-0.162	-	-	384.70	274.50	-	-
40	0.986	0.204	-	-	40.50	28.30	-	-
41	0.986	0.204	-	-	3.60	2.70	-	-
42	0.983	0.250	-	-	4.30	3.50	-	-
43	0.981	0.293	-	-	26.40	19.00	-	-
44	0.978	0.352	-	-	24.00	17.20	-	-
45	0.976	0.410	-	-	-	-	-	-
46	0.962	0.847	-	-	-	-	-	-
47	0.956	1.067	-	-	-	-	-	-
48	0.953	1.154	-	-	100.00	72.00	-	-
49	0.950	1.264	-	-	-256.00	84.14	-	-
50	0.945	1.340	-	-	1244.00	888.00	-	-
51	0.945	1.348	-	-	32.00	23.00	-	-
52	0.945	1.358	-	-	-208.00	68.00	-	-
53	0.943	1.371	-	-	227.00	162.00	-	-
54	0.943	1.375	-	-	59.00	42.00	-	-
55	0.980	0.294	-	-	18.00	13.00	-	-
56	0.980	0.294	-	-	18.00	13.00	-	-
57	0.977	0.337	-	-	28.00	20.00	-	-
58	0.977	0.337	-	-	28.00	20.00	-	-
59	1.000	-0.003	-	-	26.00	18.50	-	-
60	1.000	-0.008	-	-	26.00	19.00	-	-
61	1.000	-0.010	-	-	-	-	-	-
62	1.000	-0.010	-	-	24.00	17.00	-	-
63	1.000	-0.010	-	-	24.00	17.00	-	-
64	0.999	-0.019	-	-	1.20	1.00	-	-
65	0.999	-0.022	-	-	0.00	0.00	-	-
66	0.999	-0.023	-	-	6.00	4.30	-	-
67	0.999	-0.023	-	-	-	-	-	-
68	0.999	-0.024	-	-	39.20	26.30	-	-
69	0.999	-0.024	-	-	39.20	26.30	-	-

Table 10.6: 69-bus System: Branch Data

From Bus	To Bus	R p.u.	X p.u.	B p.u.	Tap p.u.
0	1	0.000003	0.000007	0.0000	1.0000
1	2	0.000003	0.000007	0.0000	1.0000
2	3	0.000000	0.000006	0.0000	1.0000
3	4	0.000009	0.000022	0.0000	1.0000
4	5	0.000157	0.000183	0.0000	1.0000
5	6	0.002284	0.001163	0.0000	1.0000
6	7	0.002378	0.001211	0.0000	1.0000
7	8	0.000575	0.000293	0.0000	1.0000
8	9	0.000308	0.000175	0.0000	1.0000
9	10	0.005110	0.001689	0.0000	1.0000
10	11	0.001168	0.000386	0.0000	1.0000
11	12	0.004439	0.001467	0.0000	1.0000
12	13	0.006426	0.002121	0.0000	1.0000
13	14	0.006514	0.002153	0.0000	1.0000
14	15	0.006601	0.002181	0.0000	1.0000
15	16	0.001227	0.000406	0.0000	1.0000
16	17	0.002336	0.000772	0.0000	1.0000
17	18	0.000029	0.000010	0.0000	1.0000
18	19	0.002044	0.000676	0.0000	1.0000
19	20	0.001314	0.000434	0.0000	1.0000
20	21	0.002131	0.000704	0.0000	1.0000
21	22	0.000087	0.000029	0.0000	1.0000
22	23	0.000993	0.000328	0.0000	1.0000
23	24	0.002161	0.000714	0.0000	1.0000
24	25	0.004672	0.001544	0.0000	1.0000
25	26	0.001927	0.000637	0.0000	1.0000
26	27	0.001081	0.000357	0.0000	1.0000
2	28	0.000027	0.000067	0.0000	1.0000
28	29	0.000399	0.000976	0.0000	1.0000
29	30	0.002482	0.000820	0.0000	1.0000
30	31	0.000438	0.000145	0.0000	1.0000
31	32	0.002190	0.000724	0.0000	1.0000
32	33	0.005235	0.001757	0.0000	1.0000
33	34	0.010657	0.003523	0.0000	1.0000
34	35	0.009197	0.003040	0.0000	1.0000
4	36	0.000021	0.000052	0.0000	1.0000
36	37	0.000531	0.001300	0.0000	1.0000
37	38	0.001808	0.004424	0.0000	1.0000
38	39	0.000513	0.001255	0.0000	1.0000
8	40	0.000579	0.000295	0.0000	1.0000
40	41	0.002071	0.000695	0.0000	1.0000
9	42	0.001086	0.000553	0.0000	1.0000
42	43	0.001267	0.000645	0.0000	1.0000
43	44	0.001773	0.000903	0.0000	1.0000
44	45	0.001755	0.000894	0.0000	1.0000

45	46	0.009920	0.003330	0.0000	1.0000
46	47	0.004890	0.001641	0.0000	1.0000
47	48	0.001898	0.000628	0.0000	1.0000
48	49	0.002409	0.000731	0.0000	1.0000
49	50	0.003166	0.001613	0.0000	1.0000
50	51	0.000608	0.000309	0.0000	1.0000
51	52	0.000905	0.000460	0.0000	1.0000
52	53	0.004433	0.002258	0.0000	1.0000
53	54	0.006495	0.003308	0.0000	1.0000
11	55	0.001255	0.000381	0.0000	1.0000
55	56	0.000029	0.000009	0.0000	1.0000
12	57	0.004613	0.001525	0.0000	1.0000
57	58	0.000029	0.000010	0.0000	1.0000
3	59	0.000027	0.000067	0.0000	1.0000
59	60	0.000399	0.000976	0.0000	1.0000
60	61	0.000657	0.000767	0.0000	1.0000
61	62	0.000190	0.000221	0.0000	1.0000
62	63	0.000011	0.000013	0.0000	1.0000
63	64	0.004544	0.005309	0.0000	1.0000
64	65	0.001934	0.002260	0.0000	1.0000
65	66	0.000256	0.000298	0.0000	1.0000
66	67	0.000057	0.000072	0.0000	1.0000
67	68	0.000679	0.000857	0.0000	1.0000
68	69	0.000006	0.000007	0.0000	1.0000

10.7.4 G.4: 118-bus IEEE Test System Data

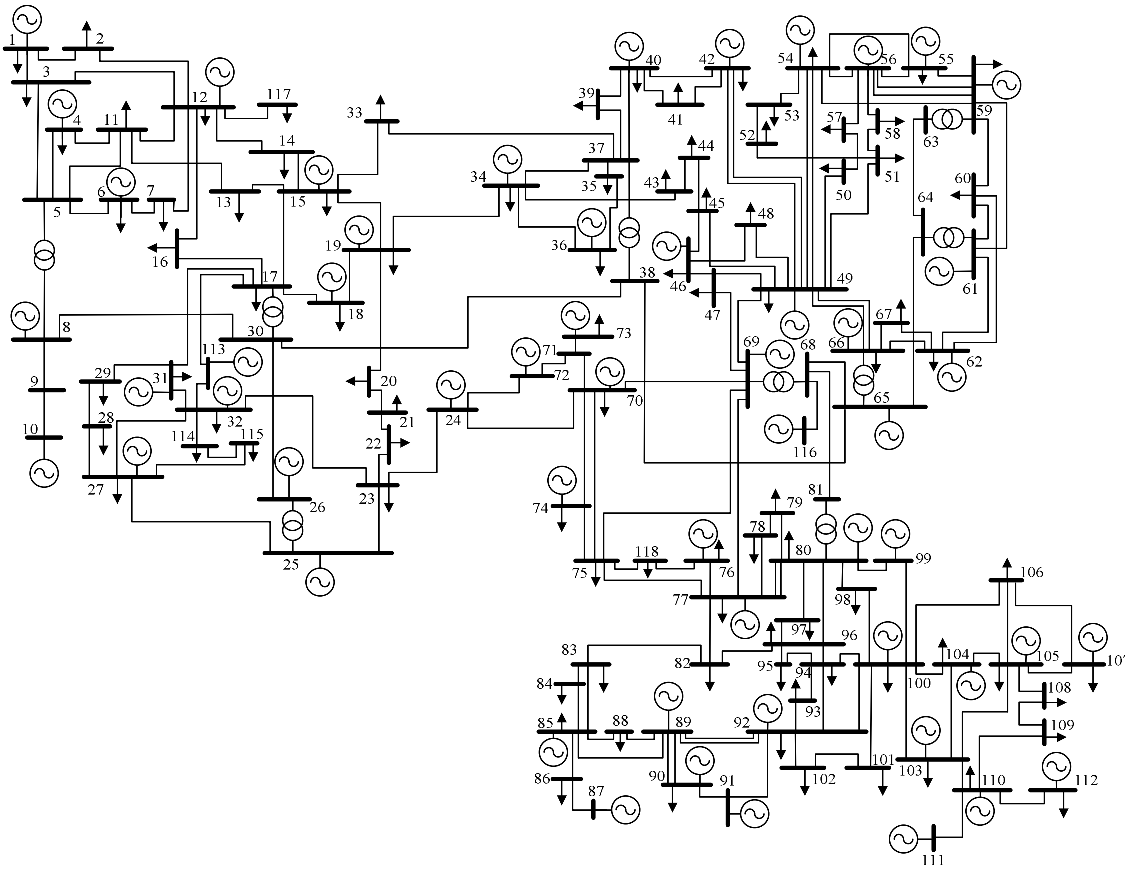

Figure 10.4: One Line Diagram 118-bus System

Table 10.7: 118-bus System: Buses Data

Bus	Voltage		Generation		Demand		Shunt Elements	
#	Mag(pu)	Ang(deg)	P (MW)	Q (MVAr)	P (MW)	Q (MVAr)	Gs (MW)	Bs (MVAr)
1	0.955	10.973	0.00	-3.10	51.00	27.00	-	-
2	0.971	11.513	-	-	20.00	9.00	-	-
3	0.968	11.856	-	-	39.00	10.00	-	-
4	0.998	15.574	0.00	-15.01	39.00	12.00	-	-
5	1.002	16.019	-	-	-	-	-	-40.00
6	0.990	13.292	0.00	15.93	52.00	22.00	-	-
7	0.989	12.847	-	-	19.00	2.00	-	-
8	1.015	21.041	0.00	63.14	28.00	0.00	-	-
9	1.043	28.295	-	-	-	-	-	-
10	1.050	35.876	450.00	-51.04	-	-	-	-
11	0.985	13.006	-	-	70.00	23.00	-	-
12	0.990	12.489	85.00	91.29	47.00	10.00	-	-
13	0.968	11.630	-	-	34.00	16.00	-	-
14	0.984	11.771	-	-	14.00	1.00	-	-

15	0.970	11.474	0.00	7.16	90.00	30.00	-	-
16	0.984	12.187	-	-	25.00	10.00	-	-
17	0.995	13.995	-	-	11.00	3.00	-	-
18	0.973	11.781	0.00	28.43	60.00	34.00	-	-
19	0.962	11.315	0.00	-14.27	45.00	25.00	-	-
20	0.957	12.191	-	-	18.00	3.00	-	-
21	0.958	13.778	-	-	14.00	8.00	-	-
22	0.969	16.332	-	-	10.00	5.00	-	-
23	0.999	21.249	-	-	7.00	3.00	-	-
24	0.992	21.114	0.00	-14.91	13.00	0.00	-	-
25	1.050	28.180	220.00	50.04	-	-	-	-
26	1.015	29.960	314.00	10.12	-	-	-	-
27	0.968	15.604	0.00	3.98	71.00	13.00	-	-
28	0.962	13.879	-	-	17.00	7.00	-	-
29	0.963	12.885	-	-	24.00	4.00	-	-
30	0.985	19.034	-	-	-	-	-	-
31	0.967	13.002	7.00	32.59	43.00	27.00	-	-
32	0.963	15.061	0.00	-16.28	59.00	23.00	-	-
33	0.971	10.854	-	-	23.00	9.00	-	-
34	0.984	11.511	0.00	-20.83	59.00	26.00	-	14.00
35	0.980	11.055	-	-	33.00	9.00	-	-
36	0.980	11.056	0.00	7.73	31.00	17.00	-	-
37	0.991	11.967	-	-	-	-	-	-25.00
38	0.961	17.108	-	-	-	-	-	-
39	0.970	8.577	-	-	27.00	11.00	-	-
40	0.970	7.496	0.00	28.45	66.00	23.00	-	-
41	0.967	7.052	-	-	37.00	10.00	-	-
42	0.985	8.653	0.00	41.03	96.00	23.00	-	-
43	0.977	11.460	-	-	18.00	7.00	-	-
44	0.984	13.943	-	-	16.00	8.00	-	10.00
45	0.986	15.773	-	-	53.00	22.00	-	10.00
46	1.005	18.576	19.00	-5.03	28.00	10.00	-	10.00
47	1.017	20.799	-	-	34.00	0.00	-	-
48	1.021	20.019	-	-	20.00	11.00	-	15.00
49	1.025	21.022	204.00	115.85	87.00	30.00	-	-
50	1.001	18.983	-	-	17.00	4.00	-	-
51	0.967	16.364	-	-	17.00	8.00	-	-
52	0.957	15.411	-	-	18.00	5.00	-	-
53	0.946	14.436	-	-	23.00	11.00	-	-
54	0.955	15.348	48.00	3.90	113.00	32.00	-	-
55	0.952	15.058	0.00	4.66	63.00	22.00	-	-
56	0.954	15.245	0.00	-2.29	84.00	18.00	-	-
57	0.971	16.449	-	-	12.00	3.00	-	-
58	0.959	15.592	-	-	12.00	3.00	-	-
59	0.985	19.448	155.00	76.83	277.00	113.00	-	-
60	0.993	23.230	-	-	78.00	3.00	-	-
61	0.995	24.121	160.00	-40.39	-	-	-	-
62	0.998	23.505	0.00	1.26	77.00	14.00	-	-

63	0.969	22.827	-	-	-	-	-	-
64	0.984	24.593	-	-	-	-	-	-
65	1.005	27.719	391.00	81.51	-	-	-	-
66	1.050	27.559	392.00	-1.96	39.00	18.00	-	-
67	1.020	24.919	-	-	28.00	7.00	-	-
68	1.003	27.598	-	-	-	-	-	-
69	1.035	30.000	513.86	-82.42	-	-	-	-
70	0.984	22.618	0.00	9.67	66.00	20.00	-	-
71	0.987	22.207	-	-	-	-	-	-
72	0.980	21.109	0.00	-11.13	12.00	0.00	-	-
73	0.991	21.995	0.00	9.65	6.00	0.00	-	-
74	0.958	21.669	0.00	-5.63	68.00	27.00	-	12.00
75	0.967	22.930	-	-	47.00	11.00	-	-
76	0.943	21.799	0.00	5.27	68.00	36.00	-	-
77	1.006	26.751	0.00	12.17	61.00	28.00	-	-
78	1.003	26.447	-	-	71.00	26.00	-	-
79	1.009	26.745	-	-	39.00	32.00	-	20.00
80	1.040	28.990	477.00	105.47	130.00	26.00	-	-
81	0.997	28.145	-	-	-	-	-	-
82	0.989	27.272	-	-	54.00	27.00	-	20.00
83	0.984	28.464	-	-	20.00	10.00	-	10.00
84	0.980	31.000	-	-	11.00	7.00	-	-
85	0.985	32.556	0.00	-5.61	24.00	15.00	-	-
86	0.987	31.186	-	-	21.00	10.00	-	-
87	1.015	31.445	4.00	11.02	-	-	-	-
88	0.987	35.690	-	-	48.00	10.00	-	-
89	1.005	39.748	607.00	-5.90	-	-	-	-
90	0.985	33.338	0.00	59.31	163.00	42.00	-	-
91	0.980	33.351	0.00	-13.09	10.00	0.00	-	-
92	0.990	33.881	0.00	-13.96	65.00	10.00	-	-
93	0.985	30.849	-	-	12.00	7.00	-	-
94	0.990	28.682	-	-	30.00	16.00	-	-
95	0.980	27.710	-	-	42.00	31.00	-	-
96	0.992	27.543	-	-	38.00	15.00	-	-
97	1.011	27.916	-	-	15.00	9.00	-	-
98	1.024	27.433	-	-	34.00	8.00	-	-
99	1.010	27.067	0.00	-17.54	42.00	0.00	-	-
100	1.017	28.059	252.00	95.55	37.00	18.00	-	-
101	0.991	29.647	-	-	22.00	15.00	-	-
102	0.989	32.365	-	-	5.00	3.00	-	-
103	1.010	24.318	40.00	75.42	23.00	16.00	-	-
104	0.971	21.748	0.00	2.39	38.00	25.00	-	-
105	0.965	20.644	0.00	-18.33	31.00	26.00	-	20.00
106	0.961	20.383	-	-	43.00	16.00	-	-
107	0.952	17.583	0.00	6.56	50.00	12.00	-	6.00
108	0.966	19.443	-	-	2.00	1.00	-	-
109	0.967	18.991	-	-	8.00	3.00	-	-
110	0.973	18.144	0.00	0.28	39.00	30.00	-	6.00

111	0.980	19.789	36.00	-1.84	-	-	-	-
112	0.975	15.045	0.00	41.51	68.00	13.00	-	-
113	0.993	13.993	0.00	6.75	6.00	0.00	-	-
114	0.960	14.726	-	-	8.00	3.00	-	-
115	0.960	14.718	-	-	22.00	7.00	-	-
116	1.005	27.163	0.00	51.32	184.00	0.00	-	-
117	0.974	10.948	-	-	20.00	8.00	-	-
118	0.949	21.942	-	-	33.00	15.00	-	-

Table 10.8: 118-bus System: Branch Data

From Bus	To Bus	R p.u.	X p.u.	B p.u.	Tap p.u.
1	2	0.03030	0.09990	0.02540	1.0000
1	3	0.01290	0.04240	0.01082	1.0000
4	5	0.00176	0.00798	0.00210	1.0000
3	5	0.02410	0.10800	0.02840	1.0000
5	6	0.01190	0.05400	0.01426	1.0000
6	7	0.00459	0.02080	0.00550	1.0000
8	9	0.00244	0.03050	1.16200	1.0000
8	5	0.00000	0.02670	0.00000	0.9850
9	10	0.00258	0.03220	1.23000	1.0000
4	11	0.02090	0.06880	0.01748	1.0000
5	11	0.02030	0.06820	0.01738	1.0000
11	12	0.00595	0.01960	0.00502	1.0000
2	12	0.01870	0.06160	0.01572	1.0000
3	12	0.04840	0.16000	0.04060	1.0000
7	12	0.00862	0.03400	0.00874	1.0000
11	13	0.02225	0.07310	0.01876	1.0000
12	14	0.02150	0.07070	0.01816	1.0000
13	15	0.07440	0.24440	0.06268	1.0000
14	15	0.05950	0.19500	0.05020	1.0000
12	16	0.02120	0.08340	0.02140	1.0000
15	17	0.01320	0.04370	0.04440	1.0000
16	17	0.04540	0.18010	0.04660	1.0000
17	18	0.01230	0.05050	0.01298	1.0000
18	19	0.01119	0.04930	0.01142	1.0000
19	20	0.02520	0.11700	0.02980	1.0000
15	19	0.01200	0.03940	0.01010	1.0000
20	21	0.01830	0.08490	0.02160	1.0000
21	22	0.02090	0.09700	0.02460	1.0000
22	23	0.03420	0.15900	0.04040	1.0000
23	24	0.01350	0.04920	0.04980	1.0000
23	25	0.01560	0.08000	0.08640	1.0000
26	25	0.00000	0.03820	0.00000	0.9600
25	27	0.03180	0.16300	0.17640	1.0000
27	28	0.01913	0.08550	0.02160	1.0000
28	29	0.02370	0.09430	0.02380	1.0000

30	17	0.00000	0.03880	0.00000	0.9600
8	30	0.00431	0.05040	0.51400	1.0000
26	30	0.00799	0.08600	0.90800	1.0000
17	31	0.04740	0.15630	0.03990	1.0000
29	31	0.01080	0.03310	0.00830	1.0000
23	32	0.03170	0.11530	0.11730	1.0000
31	32	0.02980	0.09850	0.02510	1.0000
27	32	0.02290	0.07550	0.01926	1.0000
15	33	0.03800	0.12440	0.03194	1.0000
19	34	0.07520	0.24700	0.06320	1.0000
35	36	0.00224	0.01020	0.00268	1.0000
35	37	0.01100	0.04970	0.01318	1.0000
33	37	0.04150	0.14200	0.03660	1.0000
34	36	0.00871	0.02680	0.00568	1.0000
34	37	0.00256	0.00940	0.00984	1.0000
38	37	0.00000	0.03750	0.00000	0.9350
37	39	0.03210	0.10600	0.02700	1.0000
37	40	0.05930	0.16800	0.04200	1.0000
30	38	0.00464	0.05400	0.42200	1.0000
39	40	0.01840	0.06050	0.01552	1.0000
40	41	0.01450	0.04870	0.01222	1.0000
40	42	0.05550	0.18300	0.04660	1.0000
41	42	0.04100	0.13500	0.03440	1.0000
43	44	0.06080	0.24540	0.06068	1.0000
34	43	0.04130	0.16810	0.04226	1.0000
44	45	0.02240	0.09010	0.02240	1.0000
45	46	0.04000	0.13560	0.03320	1.0000
46	47	0.03800	0.12700	0.03160	1.0000
46	48	0.06010	0.18900	0.04720	1.0000
47	49	0.01910	0.06250	0.01604	1.0000
42	49	0.07150	0.32300	0.08600	1.0000
42	49	0.07150	0.32300	0.08600	1.0000
45	49	0.06840	0.18600	0.04440	1.0000
48	49	0.01790	0.05050	0.01258	1.0000
49	50	0.02670	0.07520	0.01874	1.0000
49	51	0.04860	0.13700	0.03420	1.0000
51	52	0.02030	0.05880	0.01396	1.0000
52	53	0.04050	0.16350	0.04058	1.0000
53	54	0.02630	0.12200	0.03100	1.0000
49	54	0.07300	0.28900	0.07380	1.0000
49	54	0.08690	0.29100	0.07300	1.0000
54	55	0.01690	0.07070	0.02020	1.0000
54	56	0.00275	0.00955	0.00732	1.0000
55	56	0.00488	0.01510	0.00374	1.0000
56	57	0.03430	0.09660	0.02420	1.0000
50	57	0.04740	0.13400	0.03320	1.0000
56	58	0.03430	0.09660	0.02420	1.0000
51	58	0.02550	0.07190	0.01788	1.0000

54	59	0.05030	0.22930	0.05980	1.0000
56	59	0.08250	0.25100	0.05690	1.0000
56	59	0.08030	0.23900	0.05360	1.0000
55	59	0.04739	0.21580	0.05646	1.0000
59	60	0.03170	0.14500	0.03760	1.0000
59	61	0.03280	0.15000	0.03880	1.0000
60	61	0.00264	0.01350	0.01456	1.0000
60	62	0.01230	0.05610	0.01468	1.0000
61	62	0.00824	0.03760	0.00980	1.0000
63	59	0.00000	0.03860	0.00000	0.9600
63	64	0.00172	0.02000	0.21600	1.0000
64	61	0.00000	0.02680	0.00000	0.9850
38	65	0.00901	0.09860	1.04600	1.0000
64	65	0.00269	0.03020	0.38000	1.0000
49	66	0.01800	0.09190	0.02480	1.0000
49	66	0.01800	0.09190	0.02480	1.0000
62	66	0.04820	0.21800	0.05780	1.0000
62	67	0.02580	0.11700	0.03100	1.0000
65	66	0.00000	0.03700	0.00000	0.9350
66	67	0.02240	0.10150	0.02682	1.0000
65	68	0.00138	0.01600	0.63800	1.0000
47	69	0.08440	0.27780	0.07092	1.0000
49	69	0.09850	0.32400	0.08280	1.0000
68	69	0.00000	0.03700	0.00000	0.9350
69	70	0.03000	0.12700	0.12200	1.0000
24	70	0.00221	0.41150	0.10198	1.0000
70	71	0.00882	0.03550	0.00878	1.0000
24	72	0.04880	0.19600	0.04880	1.0000
71	72	0.04460	0.18000	0.04444	1.0000
71	73	0.00866	0.04540	0.01178	1.0000
70	74	0.04010	0.13230	0.03368	1.0000
70	75	0.04280	0.14100	0.03600	1.0000
69	75	0.04050	0.12200	0.12400	1.0000
74	75	0.01230	0.04060	0.01034	1.0000
76	77	0.04440	0.14800	0.03680	1.0000
69	77	0.03090	0.10100	0.10380	1.0000
75	77	0.06010	0.19990	0.04978	1.0000
77	78	0.00376	0.01240	0.01264	1.0000
78	79	0.00546	0.02440	0.00648	1.0000
77	80	0.01700	0.04850	0.04720	1.0000
77	80	0.02940	0.10500	0.02280	1.0000
79	80	0.01560	0.07040	0.01870	1.0000
68	81	0.00175	0.02020	0.80800	1.0000
81	80	0.00000	0.03700	0.00000	0.9350
77	82	0.02980	0.08530	0.08174	1.0000
82	83	0.01120	0.03665	0.03796	1.0000
83	84	0.06250	0.13200	0.02580	1.0000
83	85	0.04300	0.14800	0.03480	1.0000

84	85	0.03020	0.06410	0.01234	1.0000
85	86	0.03500	0.12300	0.02760	1.0000
86	87	0.02828	0.20740	0.04450	1.0000
85	88	0.02000	0.10200	0.02760	1.0000
85	89	0.02390	0.17300	0.04700	1.0000
88	89	0.01390	0.07120	0.01934	1.0000
89	90	0.05180	0.18800	0.05280	1.0000
89	90	0.02380	0.09970	0.10600	1.0000
90	91	0.02540	0.08360	0.02140	1.0000
89	92	0.00990	0.05050	0.05480	1.0000
89	92	0.03930	0.15810	0.04140	1.0000
91	92	0.03870	0.12720	0.03268	1.0000
92	93	0.02580	0.08480	0.02180	1.0000
92	94	0.04810	0.15800	0.04060	1.0000
93	94	0.02230	0.07320	0.01876	1.0000
94	95	0.01320	0.04340	0.01110	1.0000
80	96	0.03560	0.18200	0.04940	1.0000
82	96	0.01620	0.05300	0.05440	1.0000
94	96	0.02690	0.08690	0.02300	1.0000
80	97	0.01830	0.09340	0.02540	1.0000
80	98	0.02380	0.10800	0.02860	1.0000
80	99	0.04540	0.20600	0.05460	1.0000
92	100	0.06480	0.29500	0.04720	1.0000
94	100	0.01780	0.05800	0.06040	1.0000
95	96	0.01710	0.05470	0.01474	1.0000
96	97	0.01730	0.08850	0.02400	1.0000
98	100	0.03970	0.17900	0.04760	1.0000
99	100	0.01800	0.08130	0.02160	1.0000
100	101	0.02770	0.12620	0.03280	1.0000
92	102	0.01230	0.05590	0.01464	1.0000
101	102	0.02460	0.11200	0.02940	1.0000
100	103	0.01600	0.05250	0.05360	1.0000
100	104	0.04510	0.20400	0.05410	1.0000
103	104	0.04660	0.15840	0.04070	1.0000
103	105	0.05350	0.16250	0.04080	1.0000
100	106	0.06050	0.22900	0.06200	1.0000
104	105	0.00994	0.03780	0.00986	1.0000
105	106	0.01400	0.05470	0.01434	1.0000
105	107	0.05300	0.18300	0.04720	1.0000
105	108	0.02610	0.07030	0.01844	1.0000
106	107	0.05300	0.18300	0.04720	1.0000
108	109	0.01050	0.02880	0.00760	1.0000
103	110	0.03906	0.18130	0.04610	1.0000
109	110	0.02780	0.07620	0.02020	1.0000
110	111	0.02200	0.07550	0.02000	1.0000
110	112	0.02470	0.06400	0.06200	1.0000
17	113	0.00913	0.03010	0.00768	1.0000
32	113	0.06150	0.20300	0.05180	1.0000

32	114	0.01350	0.06120	0.01628	1.0000
27	115	0.01640	0.07410	0.01972	1.0000
114	115	0.00230	0.01040	0.00276	1.0000
68	116	0.00034	0.00405	0.16400	1.0000
12	117	0.03290	0.14000	0.03580	1.0000
75	118	0.01450	0.04810	0.01198	1.0000
76	118	0.01640	0.05440	0.01356	1.0000

10.7.5 G.5: 300-bus IEEE Test System Data

Table 10.9: 300-bus System: Buses Data

Bus	Voltage		Generation		Demand		Shunt Elements		Area
#	Mag(pu)	Ang(deg)	P (MW)	Q (MVAr)	P (MW)	Q (MVAr)	Gs (MW)	Bs (MVAr)	#
1	1.028	5.967	-	-	90.00	49.00	-	-	1
2	1.035	7.755	-	-	56.00	15.00	-	-	1
3	0.997	6.657	-	-	20.00	0.00	-	-	1
4	1.031	4.728	-	-	-	-	-	-	1
5	1.019	4.701	-	-	353.00	130.00	-	-	1
6	1.031	7.006	-	-	120.00	41.00	-	-	1
7	0.993	6.206	-	-	-	-	-	-	1
8	1.015	2.415	0.00	9.85	63.00	14.00	-	-	1
9	1.003	2.871	-	-	96.00	43.00	-	-	1
10	1.021	1.363	0.00	20.01	153.00	33.00	-	-	1
11	1.006	2.481	-	-	83.00	21.00	-	-	1
12	0.997	5.230	-	-	-	-	-	-	1
13	0.998	-0.537	-	-	58.00	10.00	-	-	1
14	0.999	-4.796	-	-	160.00	60.00	-	-	1
15	1.034	-8.567	-	-	126.70	23.00	-	-	1
16	1.032	-2.622	-	-	-	-	-	-	1
17	1.065	-13.085	-	-	561.00	220.00	-	-	1
19	0.982	1.089	-	-	-	-	-	-	2
20	1.001	-2.447	0.00	20.30	605.00	120.00	-	-	2
21	0.975	1.634	-	-	77.00	1.00	-	-	2
22	0.996	-1.960	-	-	81.00	23.00	-	-	2
23	1.050	3.951	-	-	21.00	7.00	-	-	2
24	1.006	6.033	-	-	-	-	-	-	2
25	1.023	1.453	-	-	45.00	12.00	-	-	2
26	0.999	-1.721	-	-	28.00	9.00	-	-	2
27	0.975	-4.883	-	-	69.00	13.00	-	-	2
33	1.025	-12.002	-	-	55.00	6.00	-	-	1
34	1.041	-7.901	-	-	-	-	-	-	1
35	0.976	-25.682	-	-	-	-	-	-	1
36	1.001	-22.519	-	-	-	-	-	-	1
37	1.020	-11.214	-	-	85.00	32.00	-	-	1
38	1.020	-12.539	-	-	155.00	18.00	-	-	1
39	1.054	-5.773	-	-	-	-	-	-	1
40	1.022	-12.761	-	-	46.00	-21.00	-	-	1
41	1.029	-10.425	-	-	86.00	0.00	-	-	1
42	1.045	-7.407	-	-	-	-	-	-	1
43	1.001	-16.763	-	-	39.00	9.00	-	-	1
44	1.009	-17.431	-	-	195.00	29.00	-	-	1
45	1.022	-14.690	-	-	-	-	-	-	1
46	1.035	-11.697	-	-	-	-	-	-	1
47	0.978	-23.163	-	-	58.00	11.80	-	-	1
48	1.002	-16.121	-	-	41.00	19.00	-	-	1
49	1.047	-2.945	-	-	92.00	26.00	-	-	1
51	1.025	-8.135	-	-	-5.00	5.00	-	-	1
52	0.998	-11.839	-	-	61.00	28.00	-	-	1

53	0.996	-17.579	-	-	69.00	3.00	-	-	1
54	1.005	-16.222	-	-	10.00	1.00	-	-	1
55	1.015	-12.187	-	-	22.00	10.00	-	-	1
57	1.033	-7.966	-	-	98.00	20.00	-	-	1
58	0.992	-5.959	-	-	14.00	1.00	-	-	1
59	0.979	-5.252	-	-	218.00	106.00	-	-	1
60	1.025	-9.515	-	-	-	-	-	-	1
61	0.991	-3.433	-	-	227.00	110.00	-	-	1
62	1.016	-1.062	-	-	-	-	-	-	1
63	0.958	-17.589	0.00	24.97	70.00	30.00	-	-	1
64	0.948	-12.936	-	-	-	-	-	-	1
69	0.963	-26.472	-	-	-	-	-	-	1
70	0.951	-35.124	-	-	56.00	20.00	-	-	1
71	0.979	-29.845	-	-	116.00	38.00	-	-	1
72	0.970	-27.441	-	-	57.00	19.00	-	-	1
73	0.978	-25.737	-	-	224.00	71.00	-	-	1
74	0.996	-21.943	-	-	-	-	-	-	1
76	0.963	-26.503	0.00	34.26	208.00	107.00	-	-	1
77	0.984	-24.911	-	-	74.00	28.00	-	-	1
78	0.990	-24.035	-	-	-	-	-	-	1
79	0.982	-25.011	-	-	48.00	14.00	-	-	1
80	0.987	-24.817	-	-	28.00	7.00	-	-	1
81	1.034	-18.757	-	-	-	-	-	-	1
84	1.025	-17.148	375.00	132.92	37.00	13.00	-	-	1
85	0.987	-17.765	-	-	-	-	-	-	2
86	0.991	-14.248	-	-	-	-	-	-	2
87	0.992	-7.793	-	-	-	-	-	-	2
88	1.015	-20.867	-	-	-	-	-	-	1
89	1.032	-11.143	-	-	44.20	0.00	-	-	1
90	1.027	-11.235	-	-	66.00	0.00	-	-	1
91	1.052	-9.437	155.00	44.03	17.40	0.00	-	-	1
92	1.052	-6.244	290.00	30.96	15.80	0.00	-	-	2
94	0.993	-9.449	-	-	60.30	0.00	-	-	2
97	1.018	-13.287	-	-	39.90	0.00	-	-	2
98	1.000	-14.665	68.00	-10.69	66.70	0.00	-	-	2
99	0.989	-20.375	-	-	83.50	0.00	-	-	2
100	1.006	-14.503	-	-	-	-	-	-	2
102	1.001	-15.293	-	-	77.80	0.00	-	-	2
103	1.029	-12.118	-	-	32.00	0.00	-	-	2
104	0.996	-17.402	-	-	8.60	0.00	-	-	2
105	1.022	-13.002	-	-	49.60	0.00	-	-	2
107	1.009	-16.082	-	-	4.60	0.00	-	-	2
108	0.990	-20.363	117.00	20.64	112.10	0.00	-	-	2
109	0.975	-26.292	-	-	30.70	0.00	-	-	2
110	0.973	-24.932	-	-	63.00	0.00	-	-	2
112	0.974	-29.274	-	-	19.60	0.00	-	-	2
113	0.970	-25.447	-	-	26.20	0.00	-	-	2
114	0.977	-29.209	-	-	18.20	0.00	-	-	2
115	0.960	-13.548	-	-	-	-	-	-	3
116	1.025	-12.667	-	-	-	-	-	-	3
117	0.935	-4.699	-	-	-	-	-	325.00	3
118	0.930	-4.102	-	-	14.10	650.00	-	-	3

119	1.044	5.187	1930.00	1050.70	-	-	-	-	3
120	0.958	-8.749	-	-	777.00	215.00	-	55.00	3
121	0.987	-12.615	-	-	535.00	55.00	-	-	3
122	0.973	-14.343	-	-	229.10	11.80	-	-	3
123	1.001	-17.613	-	-	78.00	1.40	-	-	3
124	1.023	-13.464	240.00	119.95	276.40	59.30	-	-	3
125	1.010	-18.407	0.00	199.84	514.80	82.70	-	-	3
126	0.998	-12.843	-	-	57.90	5.10	-	-	3
127	1.000	-10.502	-	-	380.80	37.00	-	-	3
128	1.002	-4.756	-	-	-	-	-	-	3
129	1.003	-4.377	-	-	-	-	-	-	3
130	1.019	5.578	-	-	-	-	-	-	3
131	0.986	6.074	-	-	-	-	-	-	3
132	1.005	3.064	-	-	-	-	-	-	3
133	1.002	-5.439	-	-	-	-	-	-	3
134	1.022	-8.022	-	-	-	-	-	-	3
135	1.019	-6.734	-	-	169.20	41.60	-	-	3
136	1.048	1.563	-	-	55.20	18.20	-	-	4
137	1.047	-1.432	-	-	273.60	99.80	-	-	4
138	1.055	-6.331	0.00	228.61	1019.20	135.20	-	-	4
139	1.012	-3.545	-	-	595.00	83.30	-	-	4
140	1.043	-3.412	-	-	387.70	114.70	-	-	4
141	1.051	0.074	281.00	65.10	145.00	58.00	-	-	4
142	1.016	-2.742	-	-	56.50	24.50	-	-	4
143	1.044	4.062	696.00	123.78	89.50	35.50	-	-	4
144	1.016	-0.661	-	-	-	-	-	-	4
145	1.008	-0.130	-	-	24.00	14.00	-	-	4
146	1.053	4.347	84.00	35.00	-	-	-	-	4
147	1.053	8.389	217.00	-49.96	-	-	-	-	4
148	1.058	0.306	-	-	63.00	25.00	-	-	4
149	1.073	5.257	103.00	49.97	-	-	-	-	4
150	0.987	6.355	-	-	-	-	-	-	3
151	1.005	4.150	-	-	-	-	-	-	3
152	1.053	9.264	372.00	-49.93	17.00	9.00	-	-	4
153	1.044	10.484	216.00	-23.84	-	-	-	-	4
154	0.966	-1.776	-	-	70.00	5.00	-	34.50	4
155	1.018	6.774	-	-	200.00	50.00	-	-	4
156	0.963	5.169	0.00	15.03	75.00	50.00	-	-	4
157	0.984	-11.905	-	-	123.50	-24.30	-	-	3
158	0.999	-11.381	-	-	-	-	-	-	3
159	0.987	-9.798	-	-	33.00	16.50	-	-	3
160	1.000	-12.530	-	-	-	-	-	-	3
161	1.036	8.867	-	-	35.00	15.00	-	-	4
162	0.992	18.524	-	-	85.00	24.00	-	-	4
163	1.041	2.929	-	-	0.00	0.40	-	-	4
164	0.984	9.684	-	-	-	-	-	-212.00	4
165	1.000	26.332	-	-	-	-	-	-	4
166	0.997	30.244	-	-	-	-	-	-103.00	4
167	0.971	-6.885	-	-	299.90	95.70	-	-	3
168	1.002	-4.779	-	-	-	-	-	-	3
169	0.988	-6.657	-	-	-	-	-	-	3
170	0.929	0.108	205.00	90.21	481.80	205.00	-	-	3

171	0.983	-9.914	0.00	150.09	763.60	291.10	-	-	3
172	1.024	-6.200	-	-	26.50	0.00	-	-	4
173	0.984	-12.729	-	-	163.50	43.00	-	53.00	4
174	1.062	-2.667	-	-	-	-	-	-	4
175	0.973	-7.180	-	-	176.00	83.00	-	-	4
176	1.052	4.691	228.00	39.72	5.00	4.00	-	-	4
177	1.008	0.646	84.00	34.99	28.00	12.00	-	-	4
178	0.940	-6.537	-	-	427.40	173.60	-	-	4
179	0.970	-9.338	-	-	74.00	29.00	-	45.00	4
180	0.979	-3.065	-	-	69.50	49.30	-	-	4
181	1.052	-1.303	-	-	73.40	0.00	-	-	4
182	1.045	-4.165	-	-	240.70	89.00	-	-	4
183	0.972	7.145	-	-	40.00	4.00	-	-	4
184	1.039	-6.824	-	-	136.80	16.60	-	-	3
185	1.052	-4.310	200.00	33.26	-	-	-	-	3
186	1.065	2.194	252.00	237.27	59.80	24.30	-	-	4
187	1.065	1.419	252.00	278.32	59.80	24.30	-	-	4
188	1.053	-0.701	-	-	182.60	43.60	-	-	4
189	1.003	-26.013	-	-	7.00	2.00	-	-	5
190	1.055	-20.417	475.00	-66.91	-	-	-	-150.00	6
191	1.044	12.452	1973.00	692.07	489.00	53.00	-	-	6
192	0.937	-10.978	-	-	800.00	72.00	-	-	6
193	0.998	-27.470	-	-	-	-	-	-	5
194	1.049	-19.045	-	-	-	-	-	-	5
195	1.036	-20.581	-	-	-	-	-	-	5
196	0.974	-24.229	-	-	10.00	3.00	-	-	5
197	0.992	-23.062	-	-	43.00	14.00	-	-	5
198	1.015	-20.094	424.00	93.42	64.00	21.00	-	-	5
199	0.954	-25.446	-	-	35.00	12.00	-	-	5
200	0.956	-25.367	-	-	27.00	12.00	-	-	5
201	0.974	-29.233	-	-	41.00	14.00	-	-	1
202	0.991	-24.969	-	-	38.00	13.00	-	-	5
203	1.003	-21.926	-	-	42.00	14.00	-	-	5
204	0.967	-29.549	-	-	72.00	24.00	-	-	5
205	0.986	-28.516	-	-	0.00	-5.00	-	-	5
206	1.004	-28.473	-	-	12.00	2.00	-	-	5
207	1.019	-28.295	-	-	-21.00	-14.20	-	-	2
208	0.999	-26.998	-	-	7.00	2.00	-	-	5
209	1.005	-25.614	-	-	38.00	13.00	-	-	5
210	0.980	-23.603	-	-	-	-	-	-	5
211	1.002	-22.971	-	-	96.00	7.00	-	-	5
212	1.013	-22.203	-	-	-	-	-	-	5
213	1.010	-11.379	272.00	44.08	-	-	-	-	5
214	0.992	-17.238	-	-	22.00	16.00	-	-	5
215	0.987	-19.951	-	-	47.00	26.00	-	-	6
216	0.975	-22.271	-	-	176.00	105.00	-	-	6
217	1.022	-21.987	-	-	100.00	75.00	-	-	6
218	1.008	-22.422	-	-	131.00	96.00	-	-	6
219	1.055	-20.947	-	-	-	-	-	-	6
220	1.008	-21.520	100.00	35.72	285.00	100.00	-	-	6
221	1.000	-22.285	450.00	160.31	171.00	70.00	-	-	6
222	1.050	-22.964	250.00	161.39	328.00	188.00	-	-	6

223	0.997	-22.496	-	-	428.00	232.00	-	-	6
224	1.000	-21.350	-	-	173.00	99.00	-	-	6
225	0.945	-11.142	-	-	410.00	40.00	-	-	6
226	1.018	-21.405	-	-	-	-	-	-	6
227	1.000	-27.016	303.00	262.96	538.00	369.00	-	-	6
228	1.042	-20.737	-	-	223.00	148.00	-	-	6
229	1.050	-19.741	-	-	96.00	46.00	-	-	6
230	1.040	-13.620	345.00	42.53	-	-	-	-	6
231	1.054	-21.020	-	-	159.00	107.00	-	-300.00	6
232	1.041	-22.994	-	-	448.00	143.00	-	-	6
233	1.000	-25.696	300.00	132.53	404.00	212.00	-	-	6
234	1.039	-20.691	-	-	572.00	244.00	-	-	6
235	1.010	-20.823	-	-	269.00	157.00	-	-	6
236	1.017	-15.195	600.00	300.23	-	-	-	-	6
237	1.056	-20.898	-	-	-	-	-	-	6
238	1.010	-20.735	250.00	164.08	255.00	149.00	-	-150.00	6
239	1.000	-15.657	550.00	68.38	-	-	-	-	6
240	1.024	-19.934	-	-	-	-	-	-140.00	6
241	1.050	-16.304	575.43	-35.44	-	-	-	-	6
242	0.993	-17.226	170.00	51.76	-	-	-	-	5
243	1.010	-18.949	84.00	52.20	8.00	3.00	-	-	5
244	0.992	-19.888	-	-	-	-	-	-	5
245	0.971	-20.577	-	-	61.00	30.00	-	-	5
246	0.965	-21.416	-	-	77.00	33.00	-	-	5
247	0.969	-21.330	-	-	61.00	30.00	-	-	5
248	0.977	-24.810	-	-	29.00	14.00	-	45.60	5
249	0.976	-25.233	-	-	29.00	14.00	-	-	5
250	1.021	-23.379	-	-	-23.00	-17.00	-	-	5
281	1.025	-19.861	-	-	-33.10	-29.40	-	-	6
319	1.015	1.488	-	-	115.80	-24.00	-	-	2
320	1.015	-2.221	-	-	2.40	-12.60	-	-	2
322	1.000	-17.690	-	-	2.40	-3.90	-	-	2
323	0.981	-13.748	-	-	-14.90	26.50	-	-	2
324	0.975	-23.522	-	-	24.70	-1.20	-	-	2
526	0.943	-34.277	-	-	145.30	-34.90	-	-	1
528	0.972	-37.543	-	-	28.10	-20.50	-	-	1
531	0.960	-29.064	-	-	14.00	2.50	-	-	1
552	1.001	-23.330	-	-	-11.10	-1.40	-	-	1
562	0.978	-27.944	-	-	50.50	17.40	-	-	1
609	0.958	-28.760	-	-	29.60	0.60	-	-	1
664	1.031	-16.833	-	-	-113.70	76.70	-	-	5
251	1.013	3.925	-	-	100.31	29.17	-	-	3
252	1.024	-7.503	-	-	-100.00	34.17	-	-	3
253	1.012	-15.156	-	-	-	-	-	-	3
254	0.969	-24.701	-	-	-	-	-	-	5
255	1.051	10.809	467.00	139.61	-	-	-	-	1
256	1.051	12.502	623.00	93.42	-	-	-	-	1
257	1.032	13.774	1210.00	420.02	-	-	-	-	1
258	1.015	5.009	234.00	51.81	-	-	-	-	1
259	1.051	11.589	372.00	200.25	-	-	-	-	1
260	1.051	-10.451	330.00	348.05	-	-	-	-	1
261	1.051	6.162	185.00	6.32	-	-	-	-	2

262	1.029	12.608	410.00	106.67	-	-	-	-	2
263	1.050	2.146	500.00	153.35	-	-	-	-	1
264	1.015	-13.881	37.00	41.56	-	-	-	-	1
265	1.051	0.000	455.95	38.84	-	-	-	-	1
266	0.997	-7.476	45.00	25.01	-	-	-	-	1
267	1.021	-3.411	165.00	89.91	-	-	-	-	1
268	1.014	2.002	400.00	120.64	-	-	-	-	1
269	1.002	5.831	400.00	150.01	-	-	-	-	1
270	0.989	-25.315	116.00	86.93	-	-	-	-	1
271	1.051	19.044	1292.00	324.37	-	-	-	-	3
272	1.051	2.769	700.00	283.93	-	-	-	-	4
273	1.015	35.072	553.00	136.92	-	-	-	-	4
274	1.012	-11.235	-	-	-	-	-	-	7
275	0.994	-18.844	0.00	2.00	4.20	0.00	-	-	7
276	0.983	-19.673	-	-	2.71	0.94	0.14	2.40	7
277	0.977	-19.810	-	-	0.86	0.28	-	-	7
278	1.012	-11.308	-	-	-	-	-	-	7
279	1.003	-17.412	-	-	-	-	-	-	7
280	0.991	-18.673	-	-	-	-	-	-	7
282	1.002	-17.253	-	-	-	-	-	-	7
283	0.989	-19.064	-	-	4.75	1.56	-	-	7
284	0.965	-21.637	-	-	1.53	0.53	0.08	-	7
285	0.975	-19.374	-	-	-	-	-	-	7
286	0.971	-21.410	-	-	1.35	0.47	0.07	-	7
287	0.965	-20.435	-	-	0.45	0.16	0.02	-	7
288	0.966	-20.345	-	-	0.45	0.16	0.02	-	7
289	0.932	-25.016	-	-	1.84	0.64	0.10	-	7
290	0.944	-23.827	-	-	1.39	0.48	0.07	-	7
291	0.929	-25.331	-	-	1.89	0.65	0.10	-	7
292	0.997	-21.087	-	-	1.55	0.54	0.08	1.72	7
293	0.950	-23.172	-	-	1.66	0.58	0.09	-	7
294	0.960	-22.658	-	-	3.03	1.00	-	-	7
295	0.957	-22.579	-	-	1.86	0.64	0.10	-	7
296	0.939	-24.411	-	-	2.58	0.89	0.14	-	7
297	0.964	-21.312	-	-	1.01	0.35	0.05	-	7
298	0.950	-22.476	-	-	0.81	0.28	0.04	-	7
299	0.965	-21.414	-	-	1.60	0.52	-	-	7
300	0.979	-19.770	-	-	-	-	-	-	7
301	1.000	-19.381	0.00	12.20	35.81	0.00	-	-	7
302	0.979	-17.233	-	-	30.00	23.00	-	-	7
303	1.000	-17.668	0.00	11.17	26.48	0.00	-	-	7
304	1.000	-6.812	50.00	22.00	-	-	-	-	7
305	1.000	-7.523	8.00	4.07	-	-	-	-	7
306	0.975	-20.459	-	-	1.02	0.35	0.05	-	7
307	0.980	-19.905	-	-	1.02	0.35	0.05	-	7
308	0.980	-19.277	-	-	3.80	1.25	-	-	7
309	1.041	-18.182	-	-	1.19	0.41	0.10	-	7

Table 10.10: 300-bus System: Branch Data

From Bus	To Bus	R p.u.	X p.u.	B p.u.	Tap p.u.
37	274	0.00006	0.00046	0.00000	1.0082
274	278	0.00080	0.00348	0.00000	1.0000
274	279	0.02439	0.43682	0.00000	0.9668
274	282	0.03624	0.64898	0.00000	0.9796
278	301	0.01578	0.37486	0.00000	1.0435
278	302	0.01578	0.37486	0.00000	0.9391
278	303	0.01602	0.38046	0.00000	1.0435
278	304	0.00000	0.15200	0.00000	1.0435
278	305	0.00000	0.80000	0.00000	1.0435
279	280	0.05558	0.24666	0.00000	1.0000
279	276	0.11118	0.49332	0.00000	1.0000
279	276	0.11118	0.49332	0.00000	1.0000
282	275	0.07622	0.43286	0.00000	1.0000
282	275	0.07622	0.43286	0.00000	1.0000
275	283	0.05370	0.07026	0.00000	1.0000
283	285	1.10680	0.95278	0.00000	1.0000
283	284	0.44364	2.81520	0.00000	1.0000
275	286	0.50748	3.22020	0.00000	1.0000
285	287	0.66688	3.94400	0.00000	1.0000
285	288	0.61130	3.61520	0.00000	1.0000
280	306	0.44120	2.96680	0.00000	1.0000
280	307	0.30792	2.05700	0.00000	1.0000
280	276	0.05580	0.24666	0.00000	1.0000
276	289	0.73633	4.67240	0.00000	1.0000
276	290	0.76978	4.88460	0.00000	1.0000
276	291	0.75732	4.80560	0.00000	1.0000
276	300	0.07378	0.06352	0.00000	1.0000
300	277	0.03832	0.02894	0.00000	1.0000
277	297	0.36614	2.45600	0.00000	1.0000
277	298	1.05930	5.45360	0.00000	1.0000
277	299	0.15670	1.69940	0.00000	1.0000
276	292	0.13006	1.39120	0.00000	1.0000
276	293	0.54484	3.45720	0.00000	1.0000
276	294	0.15426	1.67290	0.00000	1.0000
276	295	0.38490	2.57120	0.00000	1.0000
276	296	0.44120	2.96680	0.00000	1.0000
282	308	0.23552	0.92940	0.00000	1.0000
303	309	0.00000	0.75000	0.00000	0.9583
1	5	0.00100	0.00600	0.00000	1.0000
2	6	0.00100	0.00900	0.00000	1.0000
2	8	0.00600	0.02700	0.05400	1.0000
3	7	0.00000	0.00300	0.00000	1.0000
3	19	0.00800	0.06900	0.13900	1.0000
3	150	0.00100	0.00700	0.00000	1.0000
4	16	0.00200	0.01900	1.12700	1.0000
5	9	0.00600	0.02900	0.01800	1.0000
7	12	0.00100	0.00900	0.07000	1.0000
7	131	0.00100	0.00700	0.01400	1.0000
8	11	0.01300	0.05950	0.03300	1.0000

8	14	0.01300	0.04200	0.08100	1.0000
9	11	0.00600	0.02700	0.01300	1.0000
11	13	0.00800	0.03400	0.01800	1.0000
12	21	0.00200	0.01500	0.11800	1.0000
13	20	0.00600	0.03400	0.01600	1.0000
14	15	0.01400	0.04200	0.09700	1.0000
15	37	0.06500	0.24800	0.12100	1.0000
15	89	0.09900	0.24800	0.03500	1.0000
15	90	0.09600	0.36300	0.04800	1.0000
16	42	0.00200	0.02200	1.28000	1.0000
19	21	0.00200	0.01800	0.03600	1.0000
19	87	0.01300	0.08000	0.15100	1.0000
20	22	0.01600	0.03300	0.01500	1.0000
20	27	0.06900	0.18600	0.09800	1.0000
21	24	0.00400	0.03400	0.28000	1.0000
22	23	0.05200	0.11100	0.05000	1.0000
23	25	0.01900	0.03900	0.01800	1.0000
24	319	0.00700	0.06800	0.13400	1.0000
25	26	0.03600	0.07100	0.03400	1.0000
26	27	0.04500	0.12000	0.06500	1.0000
26	320	0.04300	0.13000	0.01400	1.0000
33	34	0.00000	0.06300	0.00000	1.0000
33	38	0.00250	0.01200	0.01300	1.0000
33	40	0.00600	0.02900	0.02000	1.0000
33	41	0.00700	0.04300	0.02600	1.0000
34	42	0.00100	0.00800	0.04200	1.0000
35	72	0.01200	0.06000	0.00800	1.0000
35	76	0.00600	0.01400	0.00200	1.0000
35	77	0.01000	0.02900	0.00300	1.0000
36	88	0.00400	0.02700	0.04300	1.0000
37	38	0.00800	0.04700	0.00800	1.0000
37	40	0.02200	0.06400	0.00700	1.0000
37	41	0.01000	0.03600	0.02000	1.0000
37	49	0.01700	0.08100	0.04800	1.0000
37	89	0.10200	0.25400	0.03300	1.0000
37	90	0.04700	0.12700	0.01600	1.0000
38	41	0.00800	0.03700	0.02000	1.0000
38	43	0.03200	0.08700	0.04000	1.0000
39	42	0.00060	0.00640	0.40400	1.0000
40	48	0.02600	0.15400	0.02200	1.0000
41	42	0.00000	0.02900	0.00000	1.0000
41	49	0.06500	0.19100	0.02000	1.0000
41	51	0.03100	0.08900	0.03600	1.0000
42	46	0.00200	0.01400	0.80600	1.0000
43	44	0.02600	0.07200	0.03500	1.0000
43	48	0.09500	0.26200	0.03200	1.0000
43	53	0.01300	0.03900	0.01600	1.0000
44	47	0.02700	0.08400	0.03900	1.0000
44	54	0.02800	0.08400	0.03700	1.0000
45	60	0.00700	0.04100	0.31200	1.0000
45	74	0.00900	0.05400	0.41100	1.0000
46	81	0.00500	0.04200	0.69000	1.0000

47	73	0.05200	0.14500	0.07300	1.0000
47	113	0.04300	0.11800	0.01300	1.0000
48	107	0.02500	0.06200	0.00700	1.0000
49	51	0.03100	0.09400	0.04300	1.0000
51	52	0.03700	0.10900	0.04900	1.0000
52	55	0.02700	0.08000	0.03600	1.0000
53	54	0.02500	0.07300	0.03500	1.0000
54	55	0.03500	0.10300	0.04700	1.0000
55	57	0.06500	0.16900	0.08200	1.0000
57	58	0.04600	0.08000	0.03600	1.0000
57	63	0.15900	0.53700	0.07100	1.0000
58	59	0.00900	0.02600	0.00500	1.0000
59	61	0.00200	0.01300	0.01500	1.0000
60	62	0.00900	0.06500	0.48500	1.0000
62	64	0.01600	0.10500	0.20300	1.0000
62	144	0.00100	0.00700	0.01300	1.0000
63	526	0.02650	0.17200	0.02600	1.0000
69	211	0.05100	0.23200	0.02800	1.0000
69	79	0.05100	0.15700	0.02300	1.0000
70	71	0.03200	0.10000	0.06200	1.0000
70	528	0.02000	0.12340	0.02800	1.0000
71	72	0.03600	0.13100	0.06800	1.0000
71	73	0.03400	0.09900	0.04700	1.0000
72	77	0.01800	0.08700	0.01100	1.0000
72	531	0.02560	0.19300	0.00000	1.0000
73	76	0.02100	0.05700	0.03000	1.0000
73	79	0.01800	0.05200	0.01800	1.0000
74	88	0.00400	0.02700	0.05000	1.0000
74	562	0.02860	0.20130	0.37900	1.0000
76	77	0.01600	0.04300	0.00400	1.0000
77	78	0.00100	0.00600	0.00700	1.0000
77	80	0.01400	0.07000	0.03800	1.0000
77	552	0.08910	0.26760	0.02900	1.0000
77	609	0.07820	0.21270	0.02200	1.0000
78	79	0.00600	0.02200	0.01100	1.0000
78	84	0.00000	0.03600	0.00000	1.0000
79	211	0.09900	0.37500	0.05100	1.0000
80	211	0.02200	0.10700	0.05800	1.0000
81	194	0.00350	0.03300	0.53000	1.0000
81	195	0.00350	0.03300	0.53000	1.0000
85	86	0.00800	0.06400	0.12800	1.0000
86	87	0.01200	0.09300	0.18300	1.0000
86	323	0.00600	0.04800	0.09200	1.0000
89	91	0.04700	0.11900	0.01400	1.0000
90	92	0.03200	0.17400	0.02400	1.0000
91	94	0.10000	0.25300	0.03100	1.0000
91	97	0.02200	0.07700	0.03900	1.0000
92	103	0.01900	0.14400	0.01700	1.0000
92	105	0.01700	0.09200	0.01200	1.0000
94	97	0.27800	0.42700	0.04300	1.0000
97	100	0.02200	0.05300	0.00700	1.0000
97	102	0.03800	0.09200	0.01200	1.0000

97	103	0.04800	0.12200	0.01500	1.0000
98	100	0.02400	0.06400	0.00700	1.0000
98	102	0.03400	0.12100	0.01500	1.0000
99	107	0.05300	0.13500	0.01700	1.0000
99	108	0.00200	0.00400	0.00200	1.0000
99	109	0.04500	0.35400	0.04400	1.0000
99	110	0.05000	0.17400	0.02200	1.0000
100	102	0.01600	0.03800	0.00400	1.0000
102	104	0.04300	0.06400	0.02700	1.0000
103	105	0.01900	0.06200	0.00800	1.0000
104	108	0.07600	0.13000	0.04400	1.0000
104	322	0.04400	0.12400	0.01500	1.0000
105	107	0.01200	0.08800	0.01100	1.0000
105	110	0.15700	0.40000	0.04700	1.0000
108	324	0.07400	0.20800	0.02600	1.0000
109	110	0.07000	0.18400	0.02100	1.0000
109	113	0.10000	0.27400	0.03100	1.0000
109	114	0.10900	0.39300	0.03600	1.0000
110	112	0.14200	0.40400	0.05000	1.0000
112	114	0.01700	0.04200	0.00600	1.0000
115	122	0.00360	0.01990	0.00400	1.0000
116	120	0.00200	0.10490	0.00100	1.0000
117	118	0.00010	0.00180	0.01700	1.0000
118	119	0.00000	0.02710	0.00000	1.0000
118	253	0.00000	0.61630	0.00000	1.0000
253	120	0.00000	-0.36970	0.00000	1.0000
118	121	0.00220	0.29150	0.00000	1.0000
119	120	0.00000	0.03390	0.00000	1.0000
119	121	0.00000	0.05820	0.00000	1.0000
122	123	0.08080	0.23440	0.02900	1.0000
122	125	0.09650	0.36690	0.05400	1.0000
123	124	0.03600	0.10760	0.11700	1.0000
123	125	0.04760	0.14140	0.14900	1.0000
125	126	0.00060	0.01970	0.00000	1.0000
126	127	0.00590	0.04050	0.25000	1.0000
126	129	0.01150	0.11060	0.18500	1.0000
126	132	0.01980	0.16880	0.32100	1.0000
126	157	0.00500	0.05000	0.33000	1.0000
126	158	0.00770	0.05380	0.33500	1.0000
126	169	0.01650	0.11570	0.17100	1.0000
127	128	0.00590	0.05770	0.09500	1.0000
127	134	0.00490	0.03360	0.20800	1.0000
127	168	0.00590	0.05770	0.09500	1.0000
128	130	0.00780	0.07730	0.12600	1.0000
128	133	0.00260	0.01930	0.03000	1.0000
129	130	0.00760	0.07520	0.12200	1.0000
129	133	0.00210	0.01860	0.03000	1.0000
130	132	0.00160	0.01640	0.02600	1.0000
130	151	0.00170	0.01650	0.02600	1.0000
130	167	0.00790	0.07930	0.12700	1.0000
130	168	0.00780	0.07840	0.12500	1.0000
133	137	0.00170	0.01170	0.28900	1.0000

133	168	0.00260	0.01930	0.03000	1.0000
133	169	0.00210	0.01860	0.03000	1.0000
133	171	0.00020	0.01010	0.00000	1.0000
134	135	0.00430	0.02930	0.18000	1.0000
134	184	0.00390	0.03810	0.25800	1.0000
135	136	0.00910	0.06230	0.38500	1.0000
136	137	0.01250	0.08900	0.54000	1.0000
136	152	0.00560	0.03900	0.95300	1.0000
137	140	0.00150	0.01140	0.28400	1.0000
137	181	0.00050	0.00340	0.02100	1.0000
137	186	0.00070	0.01510	0.12600	1.0000
137	188	0.00050	0.00340	0.02100	1.0000
139	172	0.05620	0.22480	0.08100	1.0000
140	141	0.01200	0.08360	0.12300	1.0000
140	142	0.01520	0.11320	0.68400	1.0000
140	145	0.04680	0.33690	0.51900	1.0000
140	146	0.04300	0.30310	0.46300	1.0000
140	147	0.04890	0.34920	0.53800	1.0000
140	182	0.00130	0.00890	0.11900	1.0000
141	146	0.02910	0.22670	0.34200	1.0000
142	143	0.00600	0.05700	0.76700	1.0000
143	145	0.00750	0.07730	0.11900	1.0000
143	149	0.01270	0.09090	0.13500	1.0000
145	146	0.00850	0.05880	0.08700	1.0000
145	149	0.02180	0.15110	0.22300	1.0000
146	147	0.00730	0.05040	0.07400	1.0000
148	178	0.05230	0.15260	0.07400	1.0000
148	179	0.13710	0.39190	0.07600	1.0000
152	153	0.01370	0.09570	0.14100	1.0000
153	161	0.00550	0.02880	0.19000	1.0000
154	156	0.17460	0.31610	0.04000	1.0000
154	183	0.08040	0.30540	0.04500	1.0000
155	161	0.01100	0.05680	0.38800	1.0000
157	159	0.00080	0.00980	0.06900	1.0000
158	159	0.00290	0.02850	0.19000	1.0000
158	160	0.00660	0.04480	0.27700	1.0000
162	164	0.00240	0.03260	0.23600	1.0000
162	165	0.00180	0.02450	1.66200	1.0000
163	164	0.00440	0.05140	3.59700	1.0000
165	166	0.00020	0.01230	0.00000	1.0000
167	169	0.00180	0.01780	0.02900	1.0000
172	173	0.06690	0.48430	0.06300	1.0000
172	174	0.05580	0.22100	0.03100	1.0000
173	174	0.08070	0.33310	0.04900	1.0000
173	175	0.07390	0.30710	0.04300	1.0000
173	176	0.17990	0.50170	0.06900	1.0000
175	176	0.09040	0.36260	0.04800	1.0000
175	179	0.07700	0.30920	0.05400	1.0000
176	177	0.02510	0.08290	0.04700	1.0000
177	178	0.02220	0.08470	0.05000	1.0000
178	179	0.04980	0.18550	0.02900	1.0000
178	180	0.00610	0.02900	0.08400	1.0000

181	138	0.00040	0.02020	0.00000	1.0000
181	187	0.00040	0.00830	0.11500	1.0000
184	185	0.00250	0.02450	0.16400	1.0000
186	188	0.00070	0.00860	0.11500	1.0000
187	188	0.00070	0.00860	0.11500	1.0000
188	138	0.00040	0.02020	0.00000	1.0000
189	208	0.03300	0.09500	0.00000	1.0000
189	209	0.04600	0.06900	0.00000	1.0000
190	231	0.00040	0.00220	6.20000	1.0000
190	240	0.00000	0.02750	0.00000	1.0000
191	192	0.00300	0.04800	0.00000	1.0000
192	225	0.00200	0.00900	0.00000	1.0000
193	205	0.04500	0.06300	0.00000	1.0000
193	208	0.04800	0.12700	0.00000	1.0000
194	219	0.00310	0.02860	0.50000	1.0000
194	664	0.00240	0.03550	0.36000	1.0000
195	219	0.00310	0.02860	0.50000	1.0000
196	197	0.01400	0.04000	0.00400	1.0000
196	210	0.03000	0.08100	0.01000	1.0000
197	198	0.01000	0.06000	0.00900	1.0000
197	211	0.01500	0.04000	0.00600	1.0000
198	202	0.33200	0.68800	0.00000	1.0000
198	203	0.00900	0.04600	0.02500	1.0000
198	210	0.02000	0.07300	0.00800	1.0000
198	211	0.03400	0.10900	0.03200	1.0000
199	200	0.07600	0.13500	0.00900	1.0000
199	210	0.04000	0.10200	0.00500	1.0000
200	210	0.08100	0.12800	0.01400	1.0000
201	204	0.12400	0.18300	0.00000	1.0000
203	211	0.01000	0.05900	0.00800	1.0000
204	205	0.04600	0.06800	0.00000	1.0000
205	206	0.30200	0.44600	0.00000	1.0000
206	207	0.07300	0.09300	0.00000	1.0000
206	208	0.24000	0.42100	0.00000	1.0000
212	215	0.01390	0.07780	0.08600	1.0000
213	214	0.00250	0.03800	0.00000	1.0000
214	215	0.00170	0.01850	0.02000	1.0000
214	242	0.00150	0.01080	0.00200	1.0000
215	216	0.00450	0.02490	0.02600	1.0000
216	217	0.00400	0.04970	0.01800	1.0000
217	218	0.00000	0.04560	0.00000	1.0000
217	219	0.00050	0.01770	0.02000	1.0000
217	220	0.00270	0.03950	0.83200	1.0000
219	237	0.00030	0.00180	5.20000	1.0000
220	218	0.00370	0.04840	0.43000	1.0000
220	221	0.00100	0.02950	0.50300	1.0000
220	238	0.00160	0.00460	0.40200	1.0000
221	223	0.00030	0.00130	1.00000	1.0000
222	237	0.00140	0.05140	0.33000	1.0000
224	225	0.01000	0.06400	0.48000	1.0000
224	226	0.00190	0.00810	0.86000	1.0000
225	191	0.00100	0.06100	0.00000	1.0000

226	231	0.00050	0.02120	0.00000	1.0000
227	231	0.00090	0.04720	0.18600	1.0000
228	229	0.00190	0.00870	1.28000	1.0000
228	231	0.00260	0.09170	0.00000	1.0000
228	234	0.00130	0.02880	0.81000	1.0000
229	190	0.00000	0.06260	0.00000	1.0000
231	232	0.00020	0.00690	1.36400	1.0000
231	237	0.00010	0.00060	3.57000	1.0000
232	233	0.00170	0.04850	0.00000	1.0000
234	235	0.00020	0.02590	0.14400	1.0000
234	237	0.00060	0.02720	0.00000	1.0000
235	238	0.00020	0.00060	0.80000	1.0000
241	237	0.00050	0.01540	0.00000	1.0000
240	281	0.00030	0.00430	0.00900	1.0000
242	245	0.00820	0.08510	0.00000	1.0000
242	247	0.01120	0.07230	0.00000	1.0000
243	244	0.01270	0.03550	0.00000	1.0000
243	245	0.03260	0.18040	0.00000	1.0000
244	246	0.01950	0.05510	0.00000	1.0000
245	246	0.01570	0.07320	0.00000	1.0000
245	247	0.03600	0.21190	0.00000	1.0000
246	247	0.02680	0.12850	0.00000	1.0000
247	248	0.04280	0.12150	0.00000	1.0000
248	249	0.03510	0.10040	0.00000	1.0000
249	250	0.06160	0.18570	0.00000	1.0000
3	1	0.00000	0.05200	0.00000	0.9470
3	2	0.00000	0.05200	0.00000	0.9560
3	4	0.00000	0.00500	0.00000	0.9710
7	5	0.00000	0.03900	0.00000	0.9480
7	6	0.00000	0.03900	0.00000	0.9590
10	11	0.00000	0.08900	0.00000	1.0460
12	10	0.00000	0.05300	0.00000	0.9850
15	17	0.01940	0.03110	0.00000	0.9561
16	15	0.00100	0.03800	0.00000	0.9710
21	20	0.00000	0.01400	0.00000	0.9520
24	23	0.00000	0.06400	0.00000	0.9430
36	35	0.00000	0.04700	0.00000	1.0100
45	44	0.00000	0.02000	0.00000	1.0080
45	46	0.00000	0.02100	0.00000	1.0000
62	61	0.00000	0.05900	0.00000	0.9750
63	64	0.00000	0.03800	0.00000	1.0170
73	74	0.00000	0.02440	0.00000	1.0000
81	88	0.00000	0.02000	0.00000	1.0000
85	99	0.00000	0.04800	0.00000	1.0000
86	102	0.00000	0.04800	0.00000	1.0000
87	94	0.00000	0.04600	0.00000	1.0150
114	207	0.00000	0.14900	0.00000	0.9670
116	124	0.00520	0.01740	0.00000	1.0100
121	115	0.00000	0.02800	0.00000	1.0500
122	157	0.00050	0.01950	0.00000	1.0000
130	131	0.00000	0.01800	0.00000	1.0522
130	150	0.00000	0.01400	0.00000	1.0522

132	170	0.00100	0.04020	0.00000	1.0500
141	174	0.00240	0.06030	0.00000	0.9750
142	175	0.00240	0.04980	-0.08700	1.0000
143	144	0.00000	0.08330	0.00000	1.0350
143	148	0.00130	0.03710	0.00000	0.9565
145	180	0.00050	0.01820	0.00000	1.0000
151	170	0.00100	0.03920	0.00000	1.0500
153	183	0.00270	0.06390	0.00000	1.0730
155	156	0.00080	0.02560	0.00000	1.0500
159	117	0.00000	0.01600	0.00000	1.0506
160	124	0.00120	0.03960	0.00000	0.9750
163	137	0.00130	0.03840	-0.05700	0.9800
164	155	0.00090	0.02310	-0.03300	0.9560
182	139	0.00030	0.01310	0.00000	1.0500
189	210	0.00000	0.25200	0.00000	1.0300
193	196	0.00000	0.23700	0.00000	1.0300
195	212	0.00080	0.03660	0.00000	0.9850
200	248	0.00000	0.22000	0.00000	1.0000
201	69	0.00000	0.09800	0.00000	1.0300
202	211	0.00000	0.12800	0.00000	1.0100
204	254	0.02000	0.20400	-0.01200	1.0500
209	198	0.02600	0.21100	0.00000	1.0300
211	212	0.00300	0.01220	0.00000	1.0000
218	219	0.00100	0.03540	-0.01000	0.9700
223	224	0.00120	0.01950	-0.36400	1.0000
229	230	0.00100	0.03320	0.00000	1.0200
234	236	0.00050	0.01600	0.00000	1.0700
238	239	0.00050	0.01600	0.00000	1.0200
196	254	0.00010	0.02000	0.00000	1.0000
119	251	0.00100	0.02300	0.00000	1.0223
120	252	0.00000	0.02300	0.00000	0.9284
256	2	0.00100	0.01460	0.00000	1.0000
257	3	0.00000	0.01054	0.00000	1.0000
268	61	0.00000	0.02380	0.00000	1.0000
269	62	0.00000	0.03214	0.00000	0.9500
273	166	0.00000	0.01540	0.00000	1.0000
262	24	0.00000	0.02890	0.00000	1.0000
255	1	0.00000	0.01953	0.00000	1.0000
271	130	0.00000	0.01930	0.00000	1.0000
258	11	0.00000	0.01923	0.00000	1.0000
261	23	0.00000	0.02300	0.00000	1.0000
265	49	0.00000	0.01240	0.00000	1.0000
272	139	0.00000	0.01670	0.00000	1.0000
259	12	0.00000	0.03120	0.00000	1.0000
260	17	0.00000	0.01654	0.00000	0.9420
263	39	0.00000	0.03159	0.00000	0.9650
267	57	0.00000	0.05347	0.00000	0.9500
264	44	0.00000	0.18181	0.00000	0.9420
266	55	0.00000	0.19607	0.00000	0.9420
270	71	0.00000	0.06896	0.00000	0.96

10.8 Appendix H

10.8.1 H.1 Published Journal Papers

Paper 1. G. Valverde and V. Terzija; “Unscented kalman filter for power system dynamic state estimation”, *IET Generation, Transmission & Distribution*, vol. 5, no.1, pp: 29-37, Jan. 2011.

Paper 2. G. Valverde, S. Chakrabarti, E. Kyriakides and V. Terzija; “A Constrained Formulation for Hybrid State Estimation” *IEEE Transactions on Power Systems*, vol. 26, no.3, pp. 1102-1109, Aug. 2011.

Paper 3. G. Valverde, E. Kyriakides, G. Heydt and V. Terzija, “Non-linear Estimation of Synchronous Machine Parameters using Operating Data”, *IEEE Transactions on Energy Conversion,* vol. 26, no.3, pp: 831-839. Sept. 2011.

Paper 4. G. Valverde, A. Saric and V. Terzija: “Probabilistic Load Flow with non-Gaussian Correlated Random Variables using Gaussian Mixture Models”, accepted for publication in *IET Generation, Transmission & Distribution*, Jan. 2012.

10.8.2 H.2 Submitted Journal Papers

Paper 5. G. Valverde, A. Saric and V. Terzija: “Stochastic Monitoring of Distribution Networks with Correlated Input Variables” submitted to *IEEE Transactions on Power Systems* (under 2nd revision), Dec. 2011.

10.8.3 H.3 Published Conference Papers

Paper 6. G. Valverde and V. Terzija, “PMU-based multi-area state estimation with low data exchange” IEEE Conference on *Innovative Smart Grid Technologies Europe*. Gothenburg, Oct. 2010.

Paper 7. G. Valverde, A. Saric and V. Terzija “Iterative Load Re-allocation for Distribution State Estimation,” *IEEE PowerTech* in Trondheim, Norway, Jun. 2011.

Paper 8. G. Valverde, E. Kyriakides and V. Terzija, “A Non-linear Approach for On-line Parameter Estimation of Synchronous Machines,” *17th Power Systems Computation Conference (PSCC 2011)*, Stockholm, Sweden, paper no. 189, pp. 1-7, Aug. 2011.

Paper 9. G. Valverde, J. Quiros Tortos and V. Terzija: “Comparison of Gaussian Mixture Reductions for Probabilistic Studies in Power Systems” accepted for publication in *IEEE PES General Meeting*, San Diego, 2012.